Department of Materials

Graphene/Carbon Nanotube based Conductive Materials

By

Suaad AlSawafi

A doctoral thesis submitted in partial fulfilment of the requirements for the award of

Doctor of Philosophy (Materials Engineering)

of Loughborough University

November 2016

Supervision: Prof. Mo Song

ACKNOWLEDGMENT

First of all, I would like to thank Al-WAHAB for helping me through all the trials and tribulation in getting to successfully complete this thesis. As well as getting me to where I am today, Loughborough, United kingdom.

I would like to express my sincere gratitude to everyone who gave me the possibility to complete this thesis. Extraordinary thanks to my supervisor Professor Mo Song for all his unlimited efforts in supporting and guiding me during all my way from the moment of beginning until the end of this project. Also, I would like to thank Dr. Jie Jin for her valuable time and unconditional help in experimental works and laboratory procedures.

Special and deep thanks to my brothers and sisters (Taher, Jamal, Kawthar, Ahlam, Nada & Abir) for their moral and financial support during my study. I would like also to give my sincere thanks to all friends who have contributed to and help me in order to reach the success beach of the world especially Eman Al-Abri, Sabrina Al-Asmi and Shatha Al-Amri.

Dedication

This work is dedicated to my parents for their

Love and selfless support.

To

My Paradise

MAMAN

''Maryam''

ABSTRACT

This project is basically an investigation of graphene and carbon nanotube (CNT) based material's electrical properties. In its first part, graphene (G) and graphene oxide (GO)/carbon nanotubes (CNTs) hybrid films were successfully fabricated as high-performance electrode materials for an energy storage application using a simple water solution casting method and with an assistance of strong ultra-sonication. This was done with different contents of G, GO, single-wall CNT (SWCNT), multi-wall CNT (MWCNT) and multi-wall CNT with a hydroxyl group (MWCNT-OH). The films with MWCNTs showed well interconnected layered structures at the nanoscale range where GO worked as support insulated plates for the CNTs.

The electrical properties were investigated in an alternating circuit (AC) which revealed a linear relationship between the dielectric constant and the weight percent of the CNTs. By increasing the CNT contents, the dielectric constant of the G/MWCNT and GO/MWCNT films raised almost linearly and their resistivity reduced. On the other hand, the dielectric constant was found to be decreased as the frequency went up. The maximum special capacitance reached 142 F/g in G (40wt %) /MWCNTs (60wt %) in which the dielectric constant reached 9.98 $x10^7$/g in the same film.

In comparison, GO/SWCNT and G/SWCNT were found to be not applicable to be used as a capacitor system using the water solution casting method which resulted in a bad dispersion. G/SWCNT and GO/SWCNT films did not form layered structures leading to a very low dielectric constant. On the other hand, the dimension and the thickness of the film influence the capacitor performance and the conductivity. Shorter and thicker film can make a huge difference.

Nonlinear behaviour of the dielectric constant with voltage was observed in both of G/CNT or GO/CNT hybrid films. At some voltages, the dielectric constant reached to peak or valley. Obviously, it is quite dependent on the voltage loaded.

In the second part, a well-dispersed MWCNT/HDPE nanocomposite powder was successfully prepared by coating the MWCNTs on the surface of the matrix particles (HDPE). The volume resistivity of the nanocomposites was investigated relating to the

temperature and stress influences. Besides, the reproducibility of the nanocomposites was studied in this project and several conclusions could be drawn:

Firstly, the average electrical resistivity for the MWCNT/HDPE nanocomposite sheets with the MWCNT contents of 0.1 wt%, 0.5 wt%, and 1.0 wt% were 792.64 kΩ.mm, 111.67 kΩ.mm, and 9.953 kΩ.mm respectively, which indicated that the 1.0 wt% MWCNT/HDPE nanocomposite showed the best electrical conductivity.

Furthermore, the results of the temperature electrical conductivity measurements revealed that with rising of temperature, the electrical resistivity for the MWCNT/HDPE nanocomposites increases due to the widening of the distances between the conductive nanofillers. In addition, the heat treatment could effectively improve the reproducibility of the MWCNT/HDPE nanocomposites, especially the nanocomposite with the MWCNT content of 1.0 wt%, as it has been found that the voids in the nanocomposite sheets were excluded during the heat treatment.

Finally, the results of the tensional electrical resistivity measurements showed that the initial electrical resistivity for the MWCNT/HDPE nanocomposites increased with the increase of the applied tensional stress which caused the widening of the distances between the conductive nanofillers and some conductive networks to be damaged. Additionally, the reproducibility of the 1.0 wt% MWCNT/HDPE nanocomposites was better than that of the 0.5 wt% MWCNT/HDPE nanocomposite. It was found that the MWCNT/HDPE nanocomposite sheets exhibited “viscoelastic” behaviour of the electrical recovery in which the electrical resistivity could not totally recover after relaxation.

TABLE OF CONTENTS

LIST OF FIGURES

LIST OF TABLES

Introduction and Aim of the Project

1. Introduction

Currently, energy storage applications are considered to be a fundamental demand in life. Researchers are still looking for environmentally friendly, cheap and highly efficient storage resources as much as possible.

Decades ago, carbon nanotubes (CNTs) with their wonderful properties such as ultra-high surface area, high conductivity, excellent temperature stability, good corrosion resistance and percolated pore structure have been regarded as the next-generation electrode materials for energy devices [1]-[3]. Huge considerable efforts have been concluded by using CNTs in various electrochemical energy storage applications. This included Li-ion secondary batteries [4], [5], hydrogen fuel cells [6] and super-capacitor (ultra-capacitors)[1], [2] which has the ability to store and release a huge amount of charges in a short period of time within its cycles compared with the conventional capacitors. Therefore, they can be identified as the most remarkable power density at this time. The incorporation of the pore structures with the CNTs increases the energy density (capacitance) of a capacitor compared to the standard ones [7].

Accordingly, preparation of reliable CNTs films (high surface area, high conductivity and good electrolyte accessibility of the nano-porous structures) is a critical first step to elevating the excellent performance of the CNTs based capacitor. Quite a few different methods have been published for fabrication of the CNT films as electrodes since their discovery [2],[8],[9].Some of these techniques are the electrophoretic deposition (EPD) and the chemical vapour deposition (CVD) techniques which have mostly been applied to nano- thin films fabrication[9],[10].

Besides the carbon nanotubes (CNTs), graphene demonstrates an important part of the nanomaterial's world in various energy and power applications due to their excellent thermal, optical, mechanical, and electrical properties [11]-[15]. This make them suitable for wide applications that started from field-effect transistor [16], batteries [17], solar cells [18], fuel cells[19] and actuators [20], [21] to supercapacitors[22]-,[25]. Graphene-

based materials have been considered as the era subject in most of the current research since graphene discovery in 2004 [26]-[31].

Recently, hybrid nanostructures materials that focused on graphene (G) and carbon nanotubes (CNT) based material hybrid films have received a great deal of attention in different studies. The functionalized hybrid material can complement the deficiencies of graphene pure film [32]-[34]. Accordingly, graphene and CNTs hybrid films have been developed with excellent electronic properties to work in their various potential applications, for instance, photoelectric films [35], electromagnetic interference shielding [36], electrodes [7] and micro-heaters [37].

Up to date, indium tin oxide (ITO) has usually been used as a transparent electrode (TE) in solar cells, organic light emitting diode panels and touch panels because of its high optical transparency and low sheet resistance. However, sustainability and price concerns give the need to be replaced by new transparent conductive materials with a high mechanical flexible material but low-cost one [38]. Thus, there are daily efforts to fabricate transparent, conductive and flexible graphene-based material electrodes (TEs) and field effect transistors electrodes (FETs) [22], [25], [39]-[53]. For example, graphene and silver or copper nanowire hybrid films [54]-[58] attracted enormous interest to be investigated as possible replacements in particular transparent and flexible electrodes [38], [53]. Xu reported the use of graphene /silver nanowire hybrid films as an electrode for transparent and flexible acoustic devices [59]. In which the AgNWs linked the grain boundaries in graphene and the empty spaces in AgNWs network are filled by graphene. It presented some properties which are better than ITO with a sheet resistances as low as 16 Ω/m and a high optical transparency of 91.1% at 550 nm. It also showed excellent mechanical flexibility and superb stability against thermal oxidation. Iskandar, on the other hand, claimed in how reduced graphene oxide /Copper nanowire hybrid films can be used as transparent electrodes in Prussian blue based electrochromic apparatus [53]. Their performances came with improved adhesion, electrical conductivity, oxidation resistance and stability in harsh environments which makes them better than the pure metal nanowires.

Alternatively, graphene and CNTs hybrid films have been developed with enhanced electronic properties to work as electrodes. Sung Ho Kim reported the high-performance FETs and TEs by using the single wall carbon nanotube SWCNTs / graphene films [38].

He approved some improvements in the sheet resistance performance, which reached 300Ω/m with 96.4% transparency.

Very recently, a simple and practical solution-casting method has been used to prepare the graphene-based electrodes (G/CNTs hybrid thin films) [60]. It is a mixing of graphene-based powders with CNT powder in water or in an organic solution such as polytetrafluoroethylene [45]-[47]. This can solve some other technique's drawbacks such as EPD and CVD [8], [61].

To date, the main focused issues in all studies and papers of G/CNTs hybrid films were in the wonderful electronic properties that make outstanding willing materials which are used in different electrical devices and applications. Nevertheless, the impact of the hybrid film own nanostructure has never been considered. In this project, the electronic properties of the electrode such as conductivity and specific capacitance were measured and investigated with altered film's contents and dimensions. This study exposed some important contribution of the electrode structure and how much impacts can it has on the hybrid film final electrical properties. This may result in causing some damages to devices if they are ignored or underestimated.

Conversely, electrical conductive polymer nanocomposites become as a life requirement in many sensing materials areas such as nano-electric devices [62], electromagnetic interference (EMI) shielding [63], temperature sensors [64] and deformation sensors [65]. In fact, materials development in science and technology is influenced by the dimension of the component system as much as by the chemical bonding and composition. As some unique physical and chemical characteristics arise only when the size moves to nano–scale, novel properties appear from nanomaterials which have attracted scientists and engineers [66]. One interesting example of these nano-materials in the polymer nanocomposites field is the carbon nanotubes (CNTs).

CNTs have been considered as a superb candidate for conductive nanofillers in the development of conductive polymer nanocomposites since its discovery in 1991[67]. It is used to improve the electrical properties of polymers [68] due to its physical properties such as electronic structure [68]-[70], mechanical properties [71]-[73], electrical and thermal transport properties [74]-[76]. CNTs possess a one-dimensional electrical band structure, which gives these amazing electrical and thermal properties. Moreover, the

electrical conductivity of MWCNT has been reported to be in the range of 1000 to 200,000 S/cm [77]. In addition, the percolation threshold of the CNTs based nanocomposites can be achieved at very low filler contents because of its high aspect ratio and surface areas [78]. Hence, the sensitive electronic structure gives CNTs a great potential to develop new strain and temperature sensing material [74].

How to obtain electrically conductive CNTs based nanocomposites without losing the amazing electrical property of the CNT is an important question at this stage. The CNTs needs to be dispersed into polymer matrices to form conductive networks of CNTs all through the whole nanocomposites. The surface areas and the high aspect ratio of the CNTs are resulting in some difficulties of having a uniform dispersion of the CNTs in the polymer. This may interrupt with the total conductivity of the conductive polymer nanocomposites [79]. Hence, the preparation of well-dispersed CNTs/polymer nanocomposites is critical. Different methods have been reported to combine CNTs with the polymer matrices, including solution mixing, in-situ polymerization, melt compounding and latex technology [80]. In previous research works, a well-dispersed CNTs/nylon 12 nanocomposite powders have successfully been prepared using a patent method, where the CNT was coated on the nylon 12 particles surfaces [81], [82].

Beside the dispersion state of the CNTs, some factors such as external force; pressure, and temperature still have strong influences on the electrical conductivity of the conductive polymer nanocomposites. Jie et al. reported that the electrical conductivity is mainly determined by the distance between neighbouring nanofillers [83]. She concluded that the electrical conductivity decreases with the increasing of this distance. Consequently, when the conductive nanofillers are in quite large apart from each other, electrical conductivity of the conductive polymer nanocomposites could be hardly detected [83]. In addition, this electrical conductivity can also be affected by the changes of conductive networks or the conductive pathways in the nanocomposite. The relationship between the temperature or external force and the electrical conductivity of the conductive polymer nanocomposites has been carried out by several researchers [84]-[87]. These investigations lead to the hypothesis of which the temperature can induce thermal expansion, leading to the decrease of the electrical conductivity.

Although many efforts have contributed to study the effects of the temperature or external force on the electrical conductivity, the knowledge of the reproducibility of the

conductive polymer nanocomposites is still limited. Thus, the investigation of the conductive polymer nanocomposites reproducibility will be one of this study aims.

2. Aim of the Project

This project intends to prepare and studies some graphene/carbon nanotube based conductive materials. The main aims are as follows:

Part One: Conductive behaviour of graphene/carbon nanotube and graphene oxide/ carbon nanotube hybrid materials.

1. Preparation and characterization of graphene/carbon nanotube and graphene oxide /carbon nanotube hybrid films.
2. Study the conductive behaviour of graphene/carbon nanotube and graphene oxide /carbon nanotube hybrid materials.

Part Two: Carbon nanotube/polyethylene nanocomposites as strain and temperature sensing materials.

1. Preparation and characterization of carbon nanotube/ polyethylene composites.
2. Study of the temperature-conductivity behaviour in carbon nanotube/polyethylene composites.
3. Study of the strain-conductivity behaviour in carbon nanotube/polyethylene composites.

References

[1] K. H. An, W. S. Kim, Y. S. Park, Y. C. Choi, S. M. Lee, D. C. Chung, D. J. Bae, S. C. Lim, and Y. H. Lee, "Supercapacitors Using Single-Walled Carbon Nanotube Electrodes," *Adv. Mater.*, Vol. 13, No. 7, pp. 497–500, Apr. 2001.

[2] C. Du and N. Pan, "High power density supercapacitor electrodes of carbon nanotube films by electrophoretic deposition," *Nanotechnology*, Vol. 17, No. 21, pp. 5314–5318, Nov. 2006.

[3] M. Hughes, M. S. P. S. P. Shaffer, A. C. C. Renouf, C. Singh, G. Z. Z. Chen, D. J. J. Fray, and A. H. H. Windle, "Electrochemical Capacitance of Nanocomposite Films Formed by Coating Aligned Arrays of Carbon Nanotubes with Polypyrrole," *Adv. Mater.*, Vol. 14, No. 5, p. 382, Mar. 2002.

[4] A. S. Claye, J. E. Fischer, C. B. Huffman, A. G. Rinzler, and R. E. Smalley, "Solid-State Electrochemistry of the Li Single Wall Carbon Nanotube System," *J. Electrochem. Soc.*,Vol. 147, No. 8, p. 2845, 2000.

[5] B. Gao, A. Kleinhammes, X. P. Tang, C. Bower, L. Fleming, Y. Wu, and O. Zhou, "Electrochemical intercalation of single-walled carbon nanotubes with lithium," *Chem. Phys. Lett.*, Vol. 307, No. 3–4, pp. 153–157, Jul. 1999.

[6] S. M. Khantimerov, E. F. Kukovitsky, N. a Sainov, and N. M. Suleimanov, "Fuel Cell Electrodes Based on Carbon Nanotube / Metallic Nanoparticles Hybrids Formed on Porous Stainless Steel Pellets," Vol. 2013, 2013.

[7] C. Niu, E. K. Sichel, R. Hoch, D. Moy, and H. Tennent, "High power electrochemical capacitors based on carbon nanotube electrodes," *Appl. Phys. Lett.*, Vol. 70, No. 11, p. 1480, Mar. 1997.

[8] B.-J. Yoon, S.-H. Jeong, K.-H. Lee, H. Seok Kim, C. Gyung Park, and J. Hun Han, "Electrical properties of electrical double layer capacitors with integrated carbon nanotube electrodes," *Chem. Phys. Lett.*, Vol. 388, No. 1–3, pp. 170–174, Apr. 2004.

[9] M. Kumar and Y. Ando, "Chemical vapor deposition of carbon nanotubes: a review on growth mechanism and mass production.," *J. Nanosci. Nanotechnol.*,

Vol. 10, No. 6, pp. 3739–58, Jun. 2010.

[10] A. Fraczek-Szczypta, E. Dlugon, A. Weselucha-Birczynska, M. Nocun, and M. Blazewicz, "Multi walled carbon nanotubes deposited on metal substrate using EPD technique. A spectroscopic study," *J. Mol. Struct.*, Vol. 1040, pp. 238–245, May 2013.

[11] A. Javey, J. Guo, Q. Wang, M. Lundstrom, and H. Dai, "Ballistic carbon nanotube field-effect transistors," V. 424, No. August, pp. 7–10, 2003.

[12] T. Dürkop, S. a. Getty, E. Cobas, and M. S. Fuhrer, "Extraordinary Mobility in Semiconducting Carbon Nanotubes," *Nano Lett.*, Vol. 4, No. 1, pp. 35–39, Jan. 2004.

[13] K. S. Novoselov, A. K. Geim, S. V Morozov, D. Jiang, Y. Zhang, S. V Dubonos, I. V Grigorieva, and A. A. Firsov, "Electric field effect in atomically thin carbon films.," *Science*, Vol. 306, No. 5696, pp. 666–9, Oct. 2004.

[14] K. S. Novoselov, Z. Jiang, Y. Zhang, S. V Morozov, H. L. Stormer, U. Zeitler, J. C. Maan, G. S. Boebinger, P. Kim, and A. K. Geim, "Room-temperature quantum Hall effect in graphene.," *Science*, Vol. 315, No. 5817, p. 1379, Mar. 2007.

[15] R. B. Sharma, D. J. Late, D. S. Joag, A. Govindaraj, and C. N. R. Rao, "Field emission properties of boron and nitrogen doped carbon nanotubes," *Chem. Phys. Lett.*, Vol. 428, No. 1–3, pp. 102–108, Sep. 2006.

[16] Q. He, H. G. Sudibya, Z. Yin, S. Wu, H. Li, F. Boey, W. Huang, P. Chen, and H. Zhang, "Centimeter-long and large-scale micropatterns of reduced graphene oxide films: fabrication and sensing applications.," *ACS Nano*, Vol. 4, No. 6, pp. 3201–8, Jul. 2010.

[17] Y. Si and E. T. Samulski, "Exfoliated Graphene Separated by Platinum Nanoparticles," *Chem. Mater.*, Vol. 20, No. 21, pp. 6792–6797, Nov. 2008.

[18] E. Yoo, J. Kim, E. Hosono, H. Zhou, T. Kudo, and I. Honma, "Large reversible Li storage of graphene nanosheet families for use in rechargeable lithium ion batteries.," *Nano Lett.*, Vol. 8, No. 8, pp. 2277–82, Aug. 2008.

[19] C. Wang, D. Li, C. O. Too, and G. G. Wallace, "Electrochemical Properties of Graphene Paper Electrodes Used in Lithium Batteries," *Chem. Mater.*, Vol. 21, No. 13, pp. 2604–2606, Jul. 2009.

[20] Z. Yin, S. Wu, X. Zhou, X. Huang, Q. Zhang, F. Boey, and H. Zhang, "Electrochemical deposition of ZnO nanorods on transparent reduced graphene oxide electrodes for hybrid solar cells.," *Small*, Vol. 6, No. 2, pp. 307–12, Jan. 2010.

[21] S. Park, J. An, J. W. Suk, and R. S. Ruoff, "Graphene-based actuators.," *Small*, Vol. 6, No. 2, pp. 210–2, Jan. 2010.

[22] M. D. Stoller, S. Park, Y. Zhu, J. An, R. S. Ruoff, Z. Yanwu, J. An, R. S. Ruoff, and Y. Zhu, "Graphene-based ultracapacitors.," *Nano Lett.*, Vol. 8, No. 10, pp. 3498–502, Oct. 2008.

[23] X. Zhao, H. Tian, M. Zhu, K. Tian, J. J. Wang, F. Kang, and R. A. Outlaw, "Carbon nanosheets as the electrode material in supercapacitors," *J. Power Sources*, Vol. 194, No. 2, pp. 1208–1212, Dec. 2009.

[24] Y. Wang, Z. Shi, Y. Huang, Y. Ma, C. Wang, M. Chen, and Y. Chen, "Supercapacitor Devices Based on Graphene Materials," *J. Phys. Chem. C*, Vol. 113, No. 30, pp. 13103–13107, Jul. 2009.

[25] S. R. C. Vivekchand, C. S. Rout, K. S. Subrahmanyam, A. Govindaraj, and C. N. R. Rao, "Graphene-based electrochemical supercapacitors," *J. Chem. Sci.*, Vol. 120, No. 1, pp. 9–13, Mar. 2008.

[26] K. V Emtsev, A. Bostwick, K. Horn, J. Jobst, G. L. Kellogg, L. Ley, J. L. McChesney, T. Ohta, S. A. Reshanov, J. Röhrl, E. Rotenberg, A. K. Schmid, D. Waldmann, H. B. Weber, and T. Seyller, "Towards wafer-size graphene layers by atmospheric pressure graphitization of silicon carbide.," *Nat. Mater.*, Vol. 8, No. 3, pp. 203–7, Mar. 2009.

[27] S. C. Xu, B. Y. Man, S. Z. Jiang, C. S. Chen, C. Yang, M. Liu, X. G. Gao, Z. C. Sun, and C. Zhang, "Direct synthesis of graphene on SiO2 substrates by chemical vapor deposition," *CrystEngComm*, Vol. 15, No. 10, p. 1840, Feb. 2013.

[28] V. Yong and H. T. Hahn, "Graphene growth with giant domains using chemical vapor deposition," *CrystEngComm*, Vol. 13, No. 23, Oct. 2011.

[29] X. Li, W. Cai, J. An, S. Kim, J. Nah, D. Yang, R. Piner, A. Velamakanni, I. Jung, E. Tutuc, S. K. Banerjee, L. Colombo, and R. S. Ruoff, "Large-area synthesis of high-quality and uniform graphene films on copper foils.," *Science*, Vol. 324, No. 5932, pp. 1312–4, Jun. 2009.

[30] Y. Zhu, Z. Sun, Z. Yan, Z. Jin, and J. M. Tour, "Rational design of hybrid graphene films for high-performance transparent electrodes.," *ACS Nano*, Vol. 5, No. 8, pp. 6472–9, Aug. 2011.

[31] C. Xu, J.-H. Lee, J.-C. Lee, B.-S. Kim, S. W. Hwang, and D. Whang, "Electrochemical growth of vertically aligned ZnO nanorod arrays on oxidized bi-layer graphene electrode," *CrystEngComm*, Vol. 13, No. 20, p. 6036, Sep. 2011.

[32] V. Jousseaume, J. Cuzzocrea, N. Bernier, V. Renard, V. Jousseaume, J. Cuzzocrea, N. Bernier, V. Renard, and F. Graphene, "Few Graphene layer / Carbon-Nanotube composite Grown at CMOS-compatible Temperature To cite this version :," *Appl. Phys. Lett.*, Vol. 98, p. 123103, 2011.

[33] T. Pei, H. Xu, Z. Zhang, Z. Wang, Y. Liu, Y. Li, S. Wang, and L.-M. Peng, "Electronic transport in single-walled carbon nanotube/graphene junction," *Appl. Phys. Lett.*, Vol. 99, No. 11, p. 113102, Sep. 2011.

[34] D. H. Lee, J. E. Kim, T. H. Han, J. W. Hwang, S. Jeon, S.-Y. Choi, S. H. Hong, W. J. Lee, R. S. Ruoff, and S. O. Kim, "Versatile carbon hybrid films composed of vertical carbon nanotubes grown on mechanically compliant graphene films.," *Adv. Mater.*, Vol. 22, No. 11, pp. 1247–52, Mar. 2010.

[35] R. Könenkamp, K. Boedecker, M. C. Lux-Steiner, M. Poschenrieder, F. Zenia, C. Levy-Clement, and S. Wagner, "Thin film semiconductor deposition on free-standing ZnO columns," *Appl. Phys. Lett.*, Vol. 77, No. 16, p. 2575, Oct. 2000.

[36] D. D. . Chung, "Electromagnetic interference shielding effectiveness of carbon materials," *Carbon N. Y.*, Vol. 39, No. 2, pp. 279–285, 2001.

[37] O. C. Jeong and S. Konishi, “Three-dimensionally combined carbonized polymer sensor and heater,” *Sensors Actuators A Phys.*, Vol. 143, No. 1, pp. 97–105, May 2008.

[38] S. H. Kim, W. Song, M. W. Jung, M.-A. Kang, K. Kim, S.-J. Chang, S. S. Lee, J. Lim, J. Hwang, S. Myung, and K.-S. An, “Carbon nanotube and graphene hybrid thin film for transparent electrodes and field effect transistors.,” *Adv. Mater.*, Vol. 26, No. 25, pp. 4247–52, Jul. 2014.

[39] L. L. Zhang, R. Zhou, and X. S. Zhao, “Graphene-based materials as supercapacitor electrodes,” *J. Mater. Chem.*, Vol. 20, No. 29, p. 5983, Jul. 2010.

[40] W. Lv, D.-M. Tang, Y.-B. He, C.-H. You, Z.-Q. Shi, X.-C. Chen, C.-M. Chen, P.-X. Hou, C. Liu, and Q.-H. Yang, “Low-temperature exfoliated graphenes: vacuum-promoted exfoliation and electrochemical energy storage.,” *ACS Nano*, Vol. 3, No. 11, pp. 3730–6, Nov. 2009.

[41] A. V. Murugan, T. Muraliganth, and A. Manthiram, “Rapid, Facile Microwave-Solvothermal Synthesis of Graphene Nanosheets and Their Polyaniline Nanocomposites for Energy Strorage,” *Chem. Mater.*, Vol. 21, No. 21, pp. 5004–5006, Nov. 2009.

[42] K. Zhang, L. L. Zhang, X. S. Zhao, and J. Wu, “Graphene/Polyaniline Nanofiber Composites as Supercapacitor Electrodes,” *Chem. Mater.*, Vol. 22, No. 4, pp. 1392–1401, Feb. 2010.

[43] D.-W. Wang, F. Li, Z.-S. Wu, W. Ren, and H.-M. Cheng, “Electrochemical interfacial capacitance in multilayer graphene sheets: Dependence on number of stacking layers,” *Electrochem. commun.*, Vol. 11, No. 9, pp. 1729–1732, Sep. 2009.

[44] Y. Chen, X. Zhang, P. Yu, and Y. Ma, “Electrophoretic deposition of graphene nanosheets on nickel foams for electrochemical capacitors,” *J. Power Sources*, Vol. 195, No. 9, pp. 3031–3035, May 2010.

[45] D.-W. Wang, F. Li, J. Zhao, W. Ren, Z.-G. Chen, J. Tan, Z.-S. Wu, I. Gentle, G. Q. Lu, and H.-M. Cheng, “Fabrication of Graphene/Polyaniline Composite Paper

via In Situ Anodic Electropolymerization for High-Performance Flexible Electrode.," *ACS Nano*, Vol. 3, No. 7, pp. 1745–52, Jul. 2009.

[46] G. G. Wallace, J. Chen, D. Li, S. E. Moulton, and J. M. Razal, "Nanostructured carbon electrodes," *J. Mater. Chem.*, Vol. 20, No. 18, p. 3553, Apr. 2010.

[47] H. Wang, Q. Hao, X. Yang, L. Lu, and X. Wang, "Graphene oxide doped polyaniline for supercapacitors," *Electrochem. commun.*, Vol. 11, No. 6, pp. 1158–1161, Jun. 2009.

[48] H.-K. Jeong, M. Jin, E. J. Ra, K. Y. Sheem, G. H. Han, S. Arepalli, and Y. H. Lee, "Enhanced electric double layer capacitance of graphite oxide intercalated by poly(sodium 4-styrensulfonate) with high cycle stability.," *ACS Nano*, Vol. 4, No. 2, pp. 1162–6, Feb. 2010.

[49] J. Yan, T. Wei, Z. Fan, W. Qian, M. Zhang, X. Shen, and F. Wei, "Preparation of graphene nanosheet/carbon nanotube/polyaniline composite as electrode material for supercapacitors," *J. Power Sources*, Vol. 195, No. 9, pp. 3041–3045, May 2010.

[50] D. Yu and L. Dai, "Self-Assembled Graphene/Carbon Nanotube Hybrid Films for Supercapacitors," *J. Phys. Chem. Lett.*, Vol. 1, No. 2, pp. 467–470, Jan. 2010.

[51] C.-P. Tien and H. Teng, "Polymer/graphite oxide composites as high-performance materials for electric double layer capacitors," *J. Power Sources*, Vol. 195, No. 8, pp. 2414–2418, Apr. 2010.

[52] X. Zhou, X. Huang, X. Qi, S. Wu, C. Xue, F. Y. C. Boey, Q. Yan, P. Chen, and H. Zhang, "In Situ Synthesis of Metal Nanoparticles on Single-Layer Graphene Oxide and Reduced Graphene Oxide Surfaces," *J. Phys. Chem. C*, Vol. 113, No. 25, pp. 10842–10846, Jun. 2009.

[53] I. N. Kholmanov, S. H. Domingues, H. Chou, X. Wang, C. Tan, J. Kim, H. Li, R. Piner, A. J. G. Zarbin, and R. S. Ruoff, "Reduced Graphene Oxide / Copper Nanowire Hybrid Films as High-Performance Transparent Electrodes," No. 2, pp. 1811–1816, 2013.

[54] C. Wang, Y. Hu, C. M. Lieber, and S. Sun, "Ultrathin Au nanowires and their transport properties.," *J. Am. Chem. Soc.*, Vol. 130, No. 28, pp. 8902–3, Jul. 2008.

[55] S. De, T. M. Higgins, P. E. Lyons, E. M. Doherty, P. N. Nirmalraj, W. J. Blau, J. J. Boland, and J. N. Coleman, "Silver Nanowire Networks as Flexible, Transparent, Conducting Films: Extremely High DC to Optical Conductivity Ratios.," *ACS Nano*, Vol. 3, No. 7, pp. 1767–74, Jul. 2009.

[56] D. Wang and C. M. Lieber, "Inorganic materials: nanocrystals branch out.," *Nat. Mater.*, Vol. 2, No. 6, pp. 355–6, Jun. 2003.

[57] L. Yang, T. Zhang, H. Zhou, S. C. Price, B. J. Wiley, and W. You, "Solution-processed flexible polymer solar cells with silver nanowire electrodes.," *ACS Appl. Mater. Interfaces*, Vol. 3, No. 10, pp. 4075–84, Oct. 2011.

[58] W. Hu, X. Niu, L. Li, S. Yun, Z. Yu, and Q. Pei, "Intrinsically stretchable transparent electrodes based on silver-nanowire-crosslinked-polyacrylate composites.," *Nanotechnology*, Vol. 23, No. 34, p. 344002, Aug. 2012.

[59] S. Xu, B. Man, S. Jiang, M. Liu, C. Yang, C. Chen, and C. Zhang, "Graphene–silver nanowire hybrid films as electrodes for transparent and flexible loudspeakers," *CrystEngComm*, Vol. 16, No. 17, p. 3532, 2014.

[60] S. Stankovich, R. D. Piner, X. Chen, N. Wu, S. T. Nguyen, and R. S. Ruoff, "Stable aqueous dispersions of graphitic nanoplatelets via the reduction of exfoliated graphite oxide in the presence of poly(sodium 4-styrenesulfonate)," *J. Mater. Chem.*, Vol. 16, No. 2, p. 155, Dec. 2006.

[61] Y.-H. Li, Y. M. Zhao, M. Roe, D. Furniss, Y. Q. Zhu, S. R. P. Silva, J. Q. Wei, D. H. Wu, and C. H. P. Poa, "In-plane large single-walled carbon nanotube films: in situ synthesis and field-emission properties.," *Small*, Vol. 2, No. 8–9, pp. 1026–30, Aug. 2006.

[62] P. Thori, P. Sharma, and M. Bhargava, "an Approach of Composite Materials in Industrial Machinery : Advantages , Disadvantages and Applications," pp. 350–355, 2013.

[63] Alamusi, N. Hu, H. Fukunaga, S. Atobe, Y. Liu, and J. Li, "Piezoresistive strain sensors made from carbon nanotubes based polymer nanocomposites.," *Sensors (Basel).*, Vol. 11, No. 11, pp. 10691–723, Jan. 2011.

[64] M. Knite, V. Teteris, B. Polyakov, and D. Erts, "Electric and Elastic Properties of Conductive Polymeric Nanocomposites on Macro- and Nanoscales," *publication.editionName*, Vol. C 19, pp. 15–19, 2002.

[65] T. Chelidze and Y. Gueguen, "Pressure-induced percolation transitions in composites," *J. Phys. D. Appl. Phys.*, Vol. 31, No. 20, pp. 2877–2885, 1999.

[66] a Dowling, R. Clift, N. Grobert, D. Hutton, R. Oliver, O. O'neill, J. Pethica, N. Pidgeon, J. Porritt, J. Ryan, and Et Al., "Nanoscience and nanotechnologies : opportunities and uncertainties," *London R. Soc. R. Acad. Eng. Rep.*, Vol. 46, No. July, pp. 618–618, 2004.

[67] S. Iijima, "Helical microtubules of graphitic carbon," *Nature*, Vol. 354, No. 6348, pp. 56–58, Nov. 1991.

[68] E. Kymakis, I. Alexandou, and G. A. . Amaratunga, "Single-walled carbon nanotube–polymer composites: electrical, optical and structural investigation," *Synth. Met.*, Vol. 127, No. 1–3, pp. 59–62, Mar. 2002.

[69] R. H. Baughman, A. A. Zakhidov, and W. A. de Heer, "Carbon nanotubes--the route toward applications.," *Science*, vol. 297, no. 5582, pp. 787–92, Aug. 2002.

[70] L. Yang and J. Han, "Electronic Structure of Deformed Carbon Nanotubes," *Phys. Rev. Lett.*, Vol. 85, No. 1, pp. 154–157, Jul. 2000.

[71] M. Damnjanović, T. Vuković, and I. Milošević, "Fermi level quantum numbers and secondary gap of conducting carbon nanotubes," *Solid State Commun.*, Vol. 116, No. 5, pp. 265–267, Sep. 2000.

[72] C. L. Kane and E. J. Mele, "Size, Shape, and Low Energy Electronic Structure of Carbon Nanotubes," *Phys. Rev. Lett.*, Vol. 78, No. 10, pp. 1932–1935, 1997.

[73] J.-C. Charlier and S. Roche, "Electronic and transport properties of nanotubes," *Rev. Mod. Phys.*, Vol. 79, No. 2, pp. 677–732, May 2007.

[74] P. Dharap, Z. Li, S. Nagarajaiah, and E. V Barrera, “Nanotube film based on single-wall carbon nanotubes for strain sensing,” *Nanotechnology*, Vol. 15, No. 3, pp. 379–382, Mar. 2004.

[75] P. J. F. Harris, “C AR B ON NANO TUBES AND RELATED STRUCTURES New Materials for the Twenty-first Century.”

[76] S. Reich and C. Thomsen, “Chirality dependence of the density-of-states singularities in carbon nanotubes,” *Phys. Rev. B*, Vol. 62, No. 7, pp. 4273–4276, Aug. 2000.

[77] T. W. Ebbesen, H. J. Lezec, H. Hiura, J. W. Bennett, H. F. Ghaemi, and T. Thio, “Electrical conductivity of individual carbon nanotubes,” *Nature*, Vol. 382, No. 6586, pp. 54–56, Jul. 1996.

[78] M. O. Lisunova, Y. P. Mamunya, N. I. Lebovka, and A. V. Melezhyk, “Percolation behaviour of ultrahigh molecular weight polyethylene/multi-walled carbon nanotubes composites,” *Eur. Polym. J.*, Vol. 43, No. 3, pp. 949–958, Mar. 2007.

[79] N. Grossiord, M. E. L. Wouters, H. E. Miltner, K. Lu, J. Loos, B. Van Mele, and C. E. Koning, “Isotactic polypropylene/carbon nanotube composites prepared by latex technology: Electrical conductivity study,” *Eur. Polym. J.*, Vol. 46, pp. 1833–43, 2010.

[80] O. Regev, P. ElKati, J. Loos, and C. Koning, “Preparation of conductive nanotube-polymer composites using latex technology,” *Adv. Mater.*, Vol. 16, No. 3, pp. 248–251, 2004.

[81] J. Bai, R. D. Goodridge, R. J. M. Hague, M. Song, and M. Okamoto, “Influence of carbon nanotubes on the rheology and dynamic mechanical properties of polyamide-12 for laser sintering,” *Polym. Test.*, Vol. 36, pp. 95–100, Jun. 2014.

[82] D. Cai and M. Song, “Latex technology as a simple route to improve the thermal conductivity of a carbon nanotube/polymer composite,” *Carbon N. Y.*, Vol. 46, No. 15, pp. 2107–2112, Dec. 2008.

[83] J. Jin, Y. Lin, M. Song, C. Gui, and S. Leesirisan, “Enhancing the electrical conductivity of polymer composites,” *Eur. Polym. J.*, Vol. 49, No. 5, pp. 1066–1072, May 2013.

[84] M. S. Xinxin Sun, “Conductive Behaviour of Carbon Nanotube Based Composites,” *Dr. thesis Loughbrgh. Univ.*, 2009.

[85] L. Flandin, Y. Bréchet, and J.-Y. Cavaillé, “Electrically conductive polymer nanocomposites as deformation sensors,” *Compos. Sci. Technol.*, Vol. 61, No. 6, pp. 895–901, May 2001.

[86] B. Lundberg and B. Sundqvist, “Resistivity of a composite conducting polymer as a function of temperature, pressure, and environment: Applications as a pressure and gas concentration transducer,” *J. Appl. Phys.*, Vol. 60, No. 3, p. 1074, Aug. 1986.

[87] C. Zhang, C.-A. Ma, P. Wang, and M. Sumita, “Temperature dependence of electrical resistivity for carbon black filled ultra-high molecular weight polyethylene composites prepared by hot compaction,” *Carbon N. Y.*, Vol. 43, No. 12, pp. 2544–2553, 2005.

Part One: Conductive Behaviour of Graphene/Carbon Nanotube and Graphene Oxide/ Carbon Nanotube Hybrid Materials.

ChapterI-1: Literature Review

1.1 Introduction

Many scientific efforts have been involved in developing alternative materials to replace the demand of the graphene material's larger scale with fully perfect structure and properties. Thus, researchers have begun to incorporate graphene or graphene derivatives with other carbon-based materials to get graphene-based hybrid films that may replace the pure graphene in future applications such as the energy storage one. The motivation after the previous year's works is to develop a new approach whereby to combine the two different carbon allotropic (G and CNT) and to report on the electrical properties and conductive behaviour of graphene/CNT and graphene oxide (GO) / CNT hybrid materials.

This chapter introduces the background of the nanoscale materials which includes the graphene (G), carbon nanotubes (CNTs) with their properties and applications. Section 1.2 reviewed a brief induction of the graphene history. In section 1.3 the structure, physical properties and fabrication methods of graphene were summarized. Characterization of graphene was covered in section 1.4. The graphene oxide production was summarized in 1.5. Then, section 1.6 briefly goes through the different storage energy application. To sum up, section 1.7 provided a summary of this chapter.

1.2 History of Graphene

Years ago, only two carbon forms are well known; diamond which is the hardest natural carbon substance that has a tetrahedral structure with each atom connects to other four carbon neighbours in a pyramid shaped lattice [1], the graphite which has hexagonal sheets and each carbon atom connects to other three atoms in a hexagonal lattice [2] as in figure 1-1. Different forms lead to different properties, while the diamond is electrically insulating and hard, graphite is an electrical soft conductor [3].

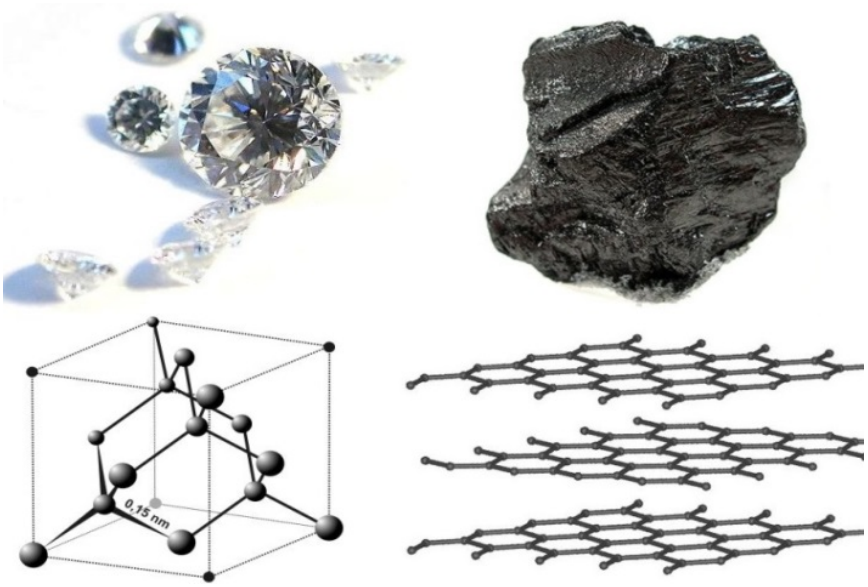

Figure 1-1: Diamond and graphite structure [2].

Later on, other different carbon allotropes, different forms of the same elements in new binding arrangements between atoms resulting in structures that have another altered chemical and physical properties, have been discovered as illustrated in figure 1-2. In another word, the way that atoms are connected in solid material has a huge impact on the overall properties. Carbons with less than 20 atoms can form a stable chain with an alternative triple and single carbon bonds. That was discovered in 1970, however, the discovery of 1-dimensional (1D) carbon nanotubes was in 1991. It is a tube of hexagonal carbons structure with double and single bonds. After that, in 1995, zero-dimensional (0D) fullerene C^{60} has shown up with cages that are formed with more than 20 carbon atoms. The Noble Prize has been given to this discovery in 1996. For a very large numbers of atoms, stable graphite sheets or diamond can be formed. Amorphous of carbon, which is a combined of graphite and carbon cages, is another carbons forms that are available by nature[4].

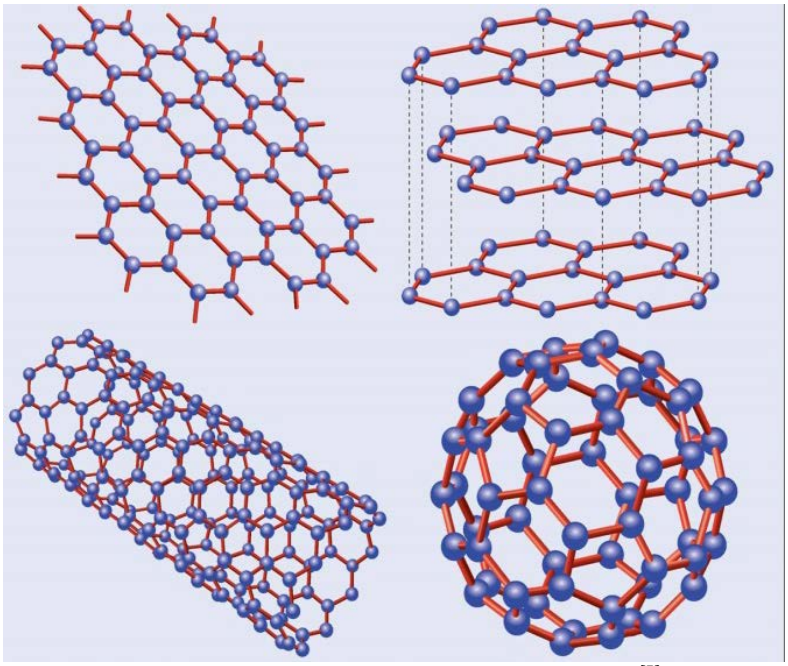

Figure 1-2: Different carbon forms (allotropes) [5]

1.3 Graphene Structure, Physical Properties, and Fabrication Methods

1.3.1 Graphene Structure

In 2004, two scientists prepared the graphene from a single planar layer of graphite, which has double carbon atom's bonds. Each carbon atom joins other three atoms by strong σ covalent bonds, the strong carbon-carbon bonding granted graphene as a rigid structure. Carbon has four electrons in the valence band; π bonds are formed above the plane of the carbon sheet by the contribution of each atom with one unbounded electron.

Graphene layers arrange as hexagons and every hexagon is completely surrounded by other hexagons that are packed in a honeycomb crystal lattice as shown in figure 1-3. Their thickness is about one atom thick [6] and their bond-length in the range of 0.142nm [7],[8]. Thus, in 1 mm thick graphite, there are about three millions of graphene sheets[9]. The 2010 Nobel Prize in physics has been awarded to Andre Geim and Konstantin Novoselov from University of Manchester (UK) for their discovery of graphene.

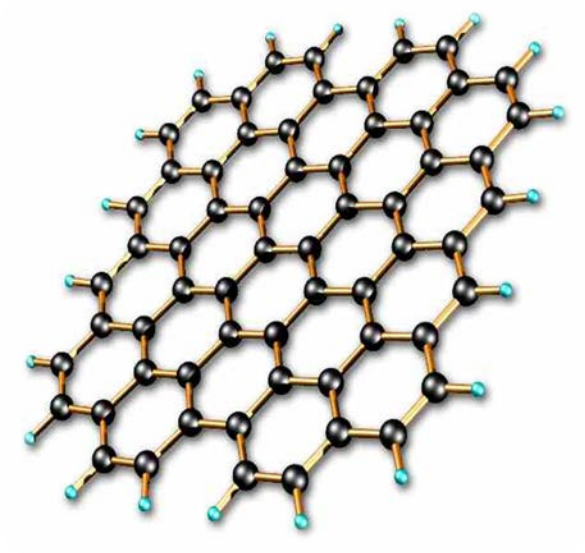

Figure 1-3: Graphene honeycomb crystal lattice [10]

The graphene sheet is the most interesting form of carbon allotropes which promises to be a super-material due to its fabulous properties. Graphene is the mother of other carbon allotropes as shown in figure 1-4 [11]. The sheets of graphene in graphite are held together via Van der Waals electrostatic force [12]. Also, the surface area of the graphene single sheet was found to be 2630 m^2/g [13]

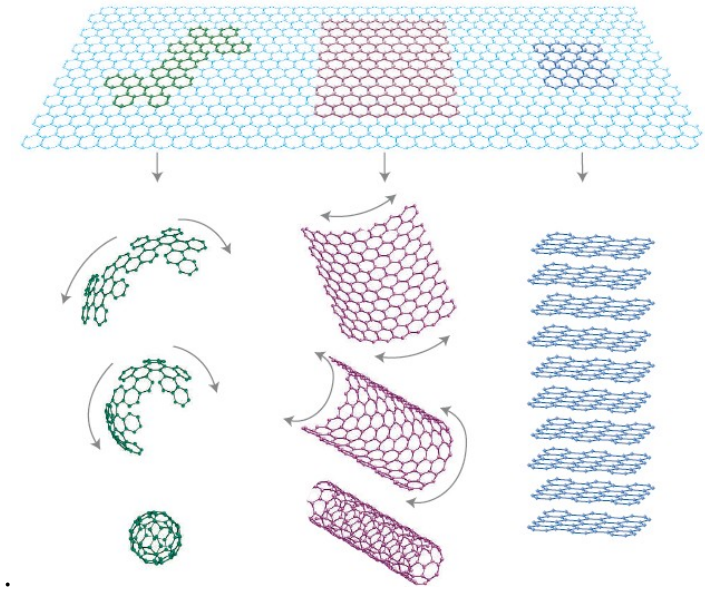

Figure 1-4: Carbon allotropes Graphene is a 2D building material for carbon materials of all the other dimensionalities. It can be wrapped up into 0D Buckyballs, rolled into 1D nanotube or stacked into 3D graphite [14].

1.3.2 Physical Properties of Graphene

1.3.2.1 Electrical Properties

While graphene is usually defined as being a monolayer of carbon atoms, the term few-layer graphene also exists [15]. Mono and few-layer graphene possess many fascinating properties. Although graphene is two-dimensional material, it has the full fixed three-dimensional properties of this material. In the electronic part view, graphene has super electrical properties [16]. Basically, Graphene can be considered as a semiconductor but with a zero band gap as shown in figure 1-5. Therefore, due to its perfectly crystallized atoms that are packed together in a regular array, the best electrical conductivity ever known in the world has been verified.

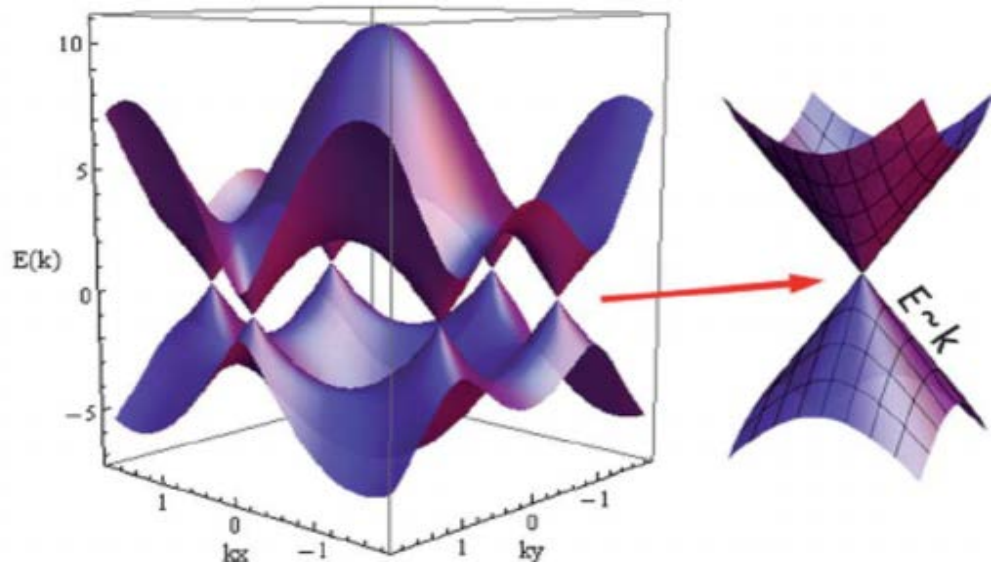

Figure 1-5: The graphene zero band gap [17].

Thus, charges flow through graphene sheet much faster than any other substance. Furthermore, graphene is considered to be the lowest resistivity material known at room temperature which attracts physicists, chemists, and engineers. The graphene's electron mobility is extremely high which can reach 150,000 $cm^2V^{-1}s^{-1}$ at room temperature [14]. Moreover, phenomena like quantum Hall effect [18] and ambipolar electric properties [19] have been verified in graphene. Graphene resistivity is 10^{-6} Ω.cm which is less than silver [20]. However, as the graphene is too thin and needs a substrate like silicon, this can trap electrical charges and reduce the electron mobility in graphene to 40,000 $cm^2V^{-1}s^{-1}$ [21]. Basically, the currently used graphene sample has a mobility of about

10,000 $cm^2V^{-1}s^{-1}$ [22]. Some material's electrical conductivities are presented in table 1-1:

Table 1-1: Different materials with their electrical conductivities[23].

Material	**Electrical Conductivity ($S \cdot m^{-1}$)**
Graphene	$\sim 10^8$
Silver	63.0×10^6
Copper	59.6×10^6
Annealed Copper	58.0×10^6
Gold	45.2×10^6
Aluminium	37.8×10^6
Sea water	4.8
Drinking water	$5x10^{-4}$ - $5x10^{-2}$
Deionized water	5.5×10^{-6}
Jet A-1 Kerosene	$50 - 450 \times 10^{-12}$
n-hexane	100×10^{-12}
Air	$0.3 - 0.8 \times 10^{-14}$

1.3.2.2 Thermal Properties

Graphene can allow heat dissipation rapidly because of its good thermal conductivity. Its ballistic thermal conductivity is in all directions i.e. (isotropic) [24]. It has a thermal conductivity up to 5000 $Wm^{-1}K^{-1}$[25], which is about 5 times higher than graphite (1000 $Wm^{-1}K^{-1}$). That is because of the presence of elastic waves (phonons) in the graphene lattice. Table 1-2 shows this value excess of those of diamond as well as carbon

nanotubes [24], [25]. The room temperature thermal conductivity of graphene can be as high as 5.30×10^{3} $Wm^{-1}K^{-1}$, which is even superior to MWCNT [25].

Table 1-2: Materials thermal conductivity values [26].

Material	**Thermal conductivity** $Wm^{-1}K^{-1}$
Silica Aerogel	0.004 - 0.04
Air	0.025
Wood	0.04 - 0.4
Water (liquid)	0.6
Thermal grease	0.7 - 3
Thermal epoxy	1 - 7
Glass	1.1
Soil	1.5
Concrete, stone	1.7
Ice	2
Aluminium	237 (pure) 120—180 (alloys)
Gold	318
Copper	401
Silver	429
Diamond	900 - 2320
MWCNT	3000
Graphene	(4840±440) - (5300±480)

1.3.2.3 Mechanical Properties

Although graphene is the thinnest and lightest known material, one atom thick, it is one hundred times stronger than steel and harder than diamond. It is the strongest material ever known [27], [11]. Graphene is similar to single-wall carbon nanotubes (SWNTs) in some electronic properties such as Young's modulus of 1 TPa and intrinsic strength of 130 GPa [27]-[29]. Measurements from Lee et al. showed that the intrinsic breaking stress for a single defect-free graphene sheet is about 42 Nm^{-2} while Young's modulus is 1.0 TPa, which makes graphene the strongest measured material [28].

1.3.2.4 Optical Properties:

The research by Nair et al. showed that graphene sheet (monolayer) has the ability to absorb a percentage of $\pi\alpha \approx 2.3\%$ from the white light, where α is the fine-structure constant. That makes 97.7% of white light transmittances through the graphene. [15].

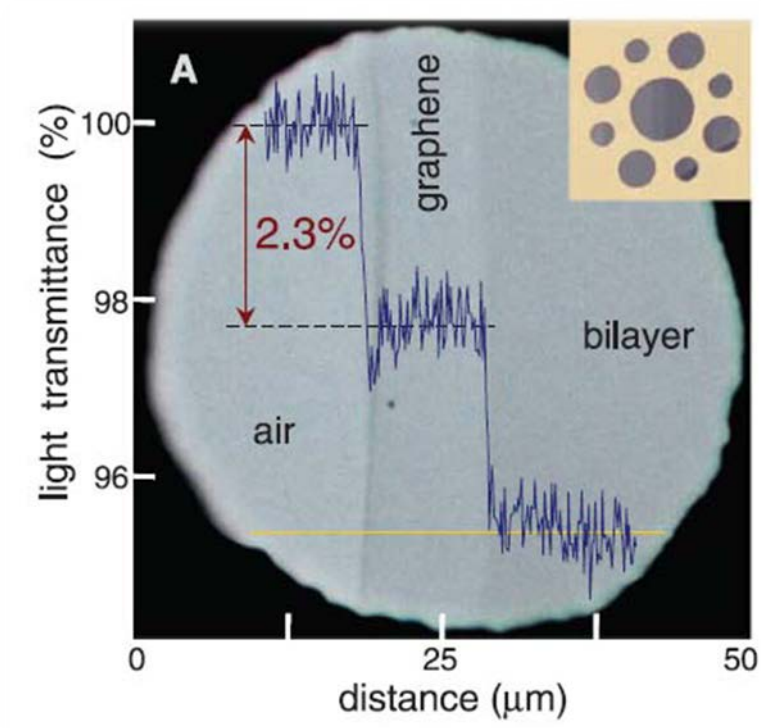

Figure 1-6: Transparency of the graphene [15].

1.3.2.5 Chemical Properties:

Graphene surface acts in a similar manner to the surface of graphite which can adsorb and desorb various atoms or molecules. Also, graphene can be functionalized by several chemical groups. (-OH) is one example that can react with the G and form the graphene oxide. In addition, the different types of defects within the graphene sheet lead to increase the chemical reactivity [30]. It has been proved that a single layer of graphite (graphene) is much more reactive than two or more [31]. Furthermore, it has been revealed that the edge of graphene has higher reactive agents than those on the surface. Compared to another similar material such as carbon nanotubes, it has the highest ratio of edgy carbons. However, in harsh reaction conditions, it works as an inert material and does not react [32], [33].

1.3.3 Graphene Applications

New horizons have been exposed to physical, optical, electronic and high-energy research for future application technology. For starters, the graphene special electronic spectrum makes a new ‘relativistic’ model of physics condensed-matter. Normally, the physics that describes solids is quantum physics like tunnelling particle that are tunnelled through other particles because the electrons travel very fast through this material. Graphene can help to mimic the quantum phenomena and test them in laboratory experiments [18], [19]. Another important application is the graphene-based electronic devices and integrated circuits. Very small devices can be made from graphene-based materials which allow electrical signals to pass and cross them quickly. As a result, super-fast computers and transistors can be manufactured from them [34]. Although graphene may be only one layer thick, it is impermeable to common gasses such as helium; this can be useful in the making atomic-scale membrane-based devices [35]. An alternative application is the slandered size batteries that hold a longer charged which can be manufactured and the electric car batteries that can be enhanced. Additionally, graphene can be utilized in nanoelectromechanical system’s (NEM) applications like pressure sensors, resonators, and single molecule gas detection, which could be useful for detecting microbes [36]. Graphene can conduct heat better than diamond and conduct electricity better than silver and as it is two-dimensional material, it can be used to detect single molecules of a gas. When a gas molecule sticks to a sheet of graphene, a local change in the electrical resistivity can be found [36]. Kim et al. demonstrated the

possibility of producing both stretchable and transparent graphene electrodes as shown in figure 1-7 [37]. It is applicable for bendable electronic devices fabrication. On the other hand, besides graphene sheets are almost transparent and they can be bending easily, they have a very good permeability control in which they allow nothings to pass them except water. Thus, another application is to be used as the greatest filter for the clean drinking water, in which salt is easily separated from seawater [38]. Bolotin et al. achieved an extremely high electron mobility of over 200,000 $cm^2\ V^{-1}\ s^{-1}$ with monolayer graphene suspended above Si/SiO_2 gate electrode [39]. This makes graphene attractive for the production of electronic devices. Combined with the transparency, graphene could prove to be a good replacement for indium tin oxide (ITO) materials in the production of organic photovoltaic cells [40].

Similarly, properties like thin and flexible may be integrated for using graphene in bionic planted devices which implanted into living tissues. Bionic devices which are made up of graphene were found to hold for a longer time than others. That is because of the graphene higher resistance in a salt-ionic solution of living tissue. Thus, graphene can conduct electrical signals and connected to the neuron to carry the electrical signals from one cell to another inside the body [41]. Besides, graphene can be utilized in electronics as in communications and imaging technologies which require ultrafast transistors [34]. Therefore, if a line transistor made of graphene along a damage spinner core, this graphene could transfer and deliver nerve pulses from an undamaged section of the spinner core and pass the damaged part and the muscles easily and fast [34]. Moreover, touch screens in cell phones work by carrying the electrical charges. As the screen being touched, some of those charges transfer to the human body and so decrease on the screen. Each corner of the screen has a sensor to measure this decrease. Then information transmits to the processor which determines the action needs to take. If the touch screen can be prepared from graphene as its conductive element, then the cell phone may be printed out on a thin plastic instead of glass [42].

Figure 1-7: Transparency and flexibility of graphene [43].

1.3.4 Preparation of Graphene

1.3.4.1 Mechanical Cleavage

It is the method introduced by Geim and Novoselov 2004 to produce graphene in its first time as shown in figure 1-8. This method involves using an adhesive tape to repeatedly peel off highly oriented pyrolytic graphite (HOPG), which in turn resulted in films of few-layered graphene with a maximum size of 10μm. However, creating larger but thicker films is also possible with a thickness of over 3nm and size around 100μm [19]. Therefore, the resulting graphene varies in thickness. While the quality of the graphene sheets was high, the long processing time and the relatively small size of sheets produced limited the use of this method in the large-scale production of graphene [44].

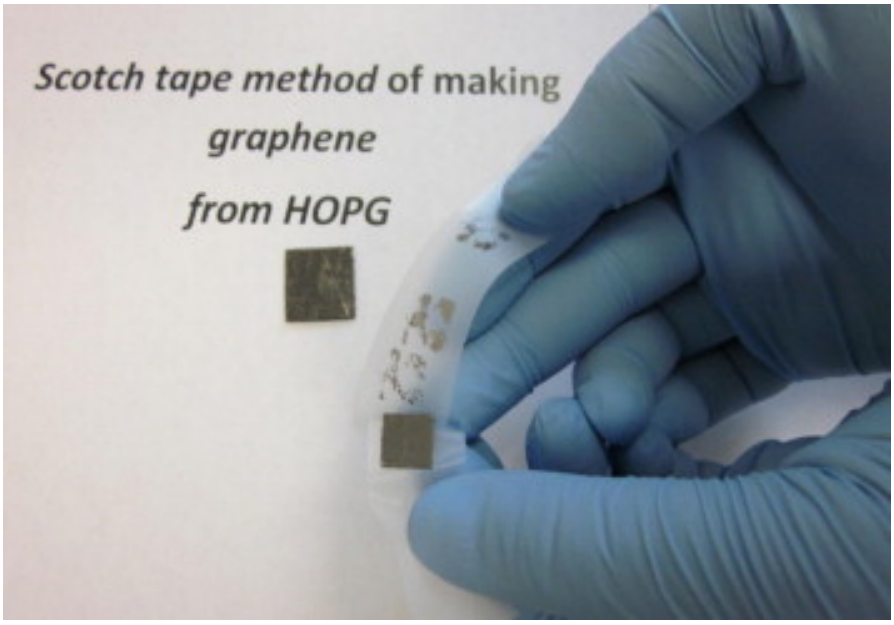

Figure 1-8: Mechanical cleavage method of preparing graphene from HOPG [45].

1.3.4.2 Electrochemical Exfoliation

The basis of current electrochemical exfoliation approaches as demonstrated in figure 1-9 is to use the graphite as an electrode and expand the layers of graphite in-situ; after expanding, the electrode is exfoliated by the means of sonication to form monolayer graphene [44]. Wang et al. used lithium ions (Li^+) to form graphite intercalation compounds, which can be inserted between the graphite layers and cause expansion of the layers due to their large dimensions [46]. In this approach, the high electrical potential is applied to the lithium-propylene carbonate solution in order to activate the intercalation. Under a high current density, the Li^+/PC complexes showed exceptionally high potential in expanding the graphite electrode. The final exfoliation procedure is done with high-intensity ultrasound in N, N-dimethylformamide solution. The Li^+/PC remainder is washed away with water and acid. It was also found by Wang et al. that while exfoliation of graphite is possible in the absence of Li ions, the percentage of exfoliation and quality of the product is inferior. This approach is able to produce a few layers graphene up to 70% with a considerable quality. Huang et al., on the other side, proposed an altered approach where they used lithium ions from a molten Li-OH to form intercalation compounds with 80% yield [47].

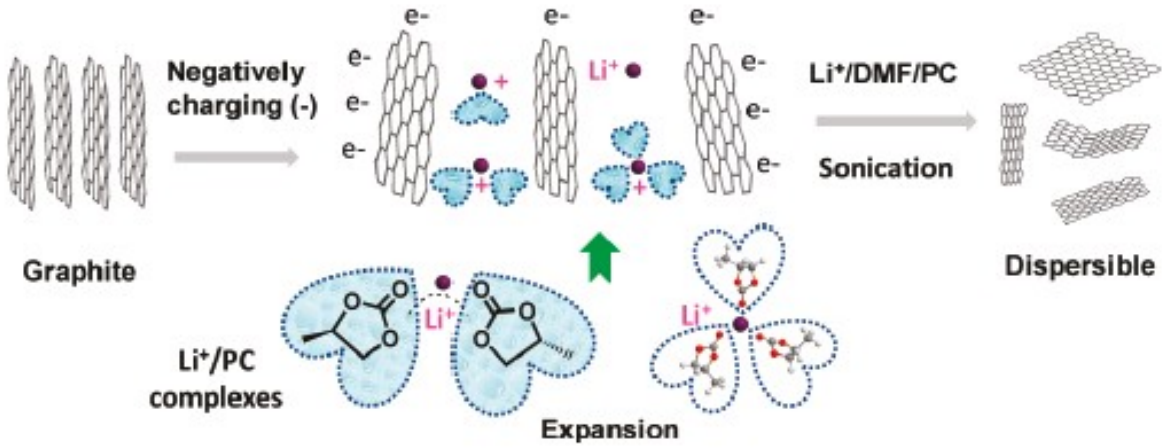

Figure 1-9: Preparation of graphene by the means of electrochemical exfoliation [46].

1.3.4.3 Arc Discharge

Arc discharge as shown in figure 1-10 is the method of using graphite as electrodes inside a hydrogen atmosphere where a direct current (DC) is applied to evaporate different gasses from graphite, which then deposit on the cathode [48]. The cathode deposition contains both multi-wall carbon nanotubes and graphene that are difficult to be separated. However, as it has been found out by Subrahmanyam et al., the deposition on the inner wall of the reaction chamber contains only graphene flakes of 2-4 layers [49]. A steel reaction chamber can be filled with hydrogen and helium and used to produce graphene. While the helium is to provide the inert gas environment, the hydrogen is used in the termination of dangling carbon bonds during the arc discharge. This is believed to be important in avoidance the rolling up of graphene sheets [50]. Two high purity graphite rods are used as the anode and the cathode with a discharge current of (100 - 150) A and a maximum voltage of 60V. It was found that high current, voltage, and hydrogen percentage are desired for high yield of graphene. This approach yields up to 20% of the anode weight, with relatively to simple procedures that are suitable for large-scale production [50].

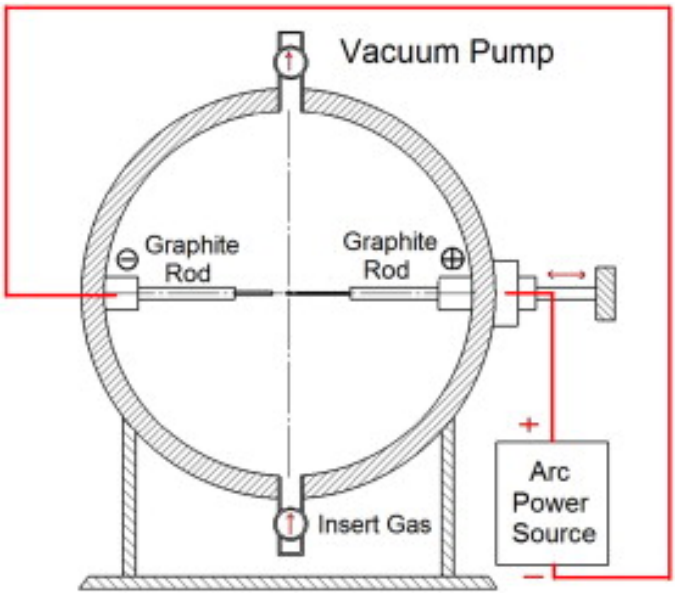

Figure 1-10: Schematic of the apparatus designed for the preparation of graphene by the means of arc discharge [50].

1.3.4.4 Unzipping Carbon Nanotubes

Since the carbon nanotubes is a "rolled up" graphene sheet, then 2D graphene sheet can be obtained from nanotubes by cutting the nanotube along its length as shown in figure 1-11. The approach of unzipping CNT can be applied to single or multi-walled (MWCNT) to produce graphene. Jiao et al. [51] unzipped MWCNTs by the mean of plasma etching. MWCNTs are first deposited on a silicon substrate. Then, a thin film of poly (methyl methacrylate) (PMMA) is coated on top of them. After heating, the MWCNTs are partially embedded in the PMMA layers. When the PMMA layer is peeled off, the MWCNTs stay embedded in that PMMA layer. The embedded MWCNTs are then subjected to Ar plasma in which the top parts are etched away much faster than the embedded lower part during the exposure. By controlling the time of MWCNTs etching, the numbers of graphene layers that left in the PMMA layer can be altered. The PMMA layers along with the embedded graphene are transferred to the substrate and the PMMA layer is removed, leaving the graphene on the substrate. On the other hand, Kosynkin et al. [52] also suggested a different approach that employs $KMnO_4$ to cut the MWNT and obtain oxidized graphene. The difficulties with this approach are the graphene morphology which cannot be well controlled and they are considerably complicated.

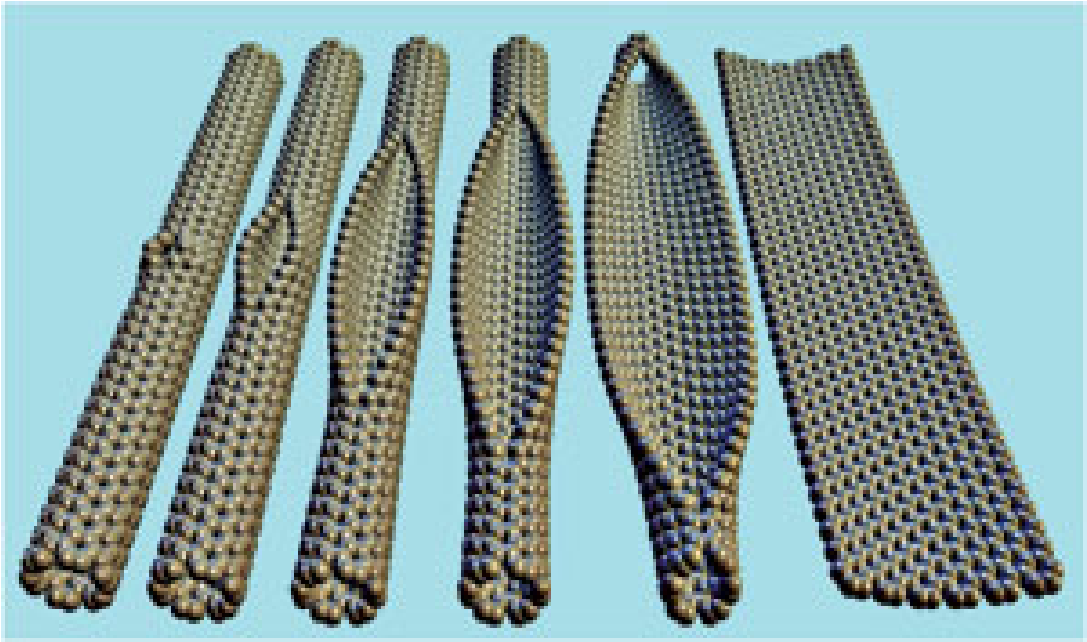

Figure 1-11: Principle of graphene preparation by the means of unzipping nanotubes [52].

1.3.4.5 Reduction of Graphitic Oxide

This method requires the production of graphene oxide (GO) from graphite as a first stage (figure 1-12) [53]. Tung et al. projected a graphene monolayer production method, where GO is first dispersed in pure hydrazine [54]. The reducing effect of hydrazine removed the oxygen of GO. The monolayer morphology of graphene is also achieved using this process. The result, as suggested, is a suspension of negatively charged monolayer graphene with surrounding $N_2H_4^+$ counter ions. The static repulsion of counter ion pairs causes the suspension to remain stable for months with limited agglomeration. Moreover, the morphology of the graphene sheets can be controlled by varying the composition and concentration of the suspension. Graphene sheets that prepared by this approach can reach $20\times40\mu m^2$ in size. The problem with this reduced GO is that the oxidation may cause changes in the chemical and physical properties of graphene, which subsequently causes a drop in the final performance. However, this approach is appropriate for industrial production due to its fast and simple nature.

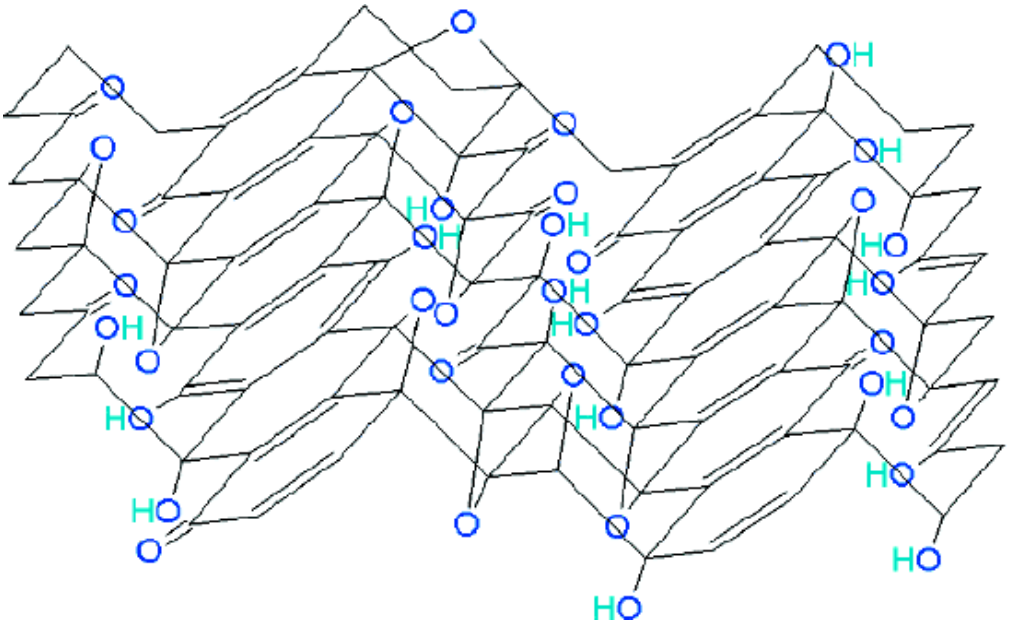

Figure 1-12: Structure of GO proposed by Szabo et al. [55].

1.3.4.6 Exfoliation of Graphene

During the preparation of GO, graphite cannot be fully oxidized and thus defects may exist in the GO sheets. After reduction, the electrical conductivity is found to be lower than pristine graphene. To control this problem, Li et al. proposed an exfoliation-reintercalation-expansion approach in preparing graphene sheets [56] as shown in figure 1-13. Graphite is first exfoliated by a brief heating and then grounded. Then, the ground graphite is re-intercalated by oleum treating for a day. After the graphite is fully intercalated, an N, N-dimethylformamide solution of tetrabutylammonium hydroxide (TBA) is added, and the suspension goes under a brief sonication. Then, it has been left to stand for three days to allow the TBA to be fully inserted into the graphite layers. The final procedure is to acquire a stable suspension of monolayer graphene sheets by sonication in 2-Distearoyl-sn-Glycero-3-Phosphoethanolamine (DSPE) conjugated Polyethylene Glycol. The graphene sheet that is prepared by this method exhibits a higher electrical conductance than the GO reduction methods.

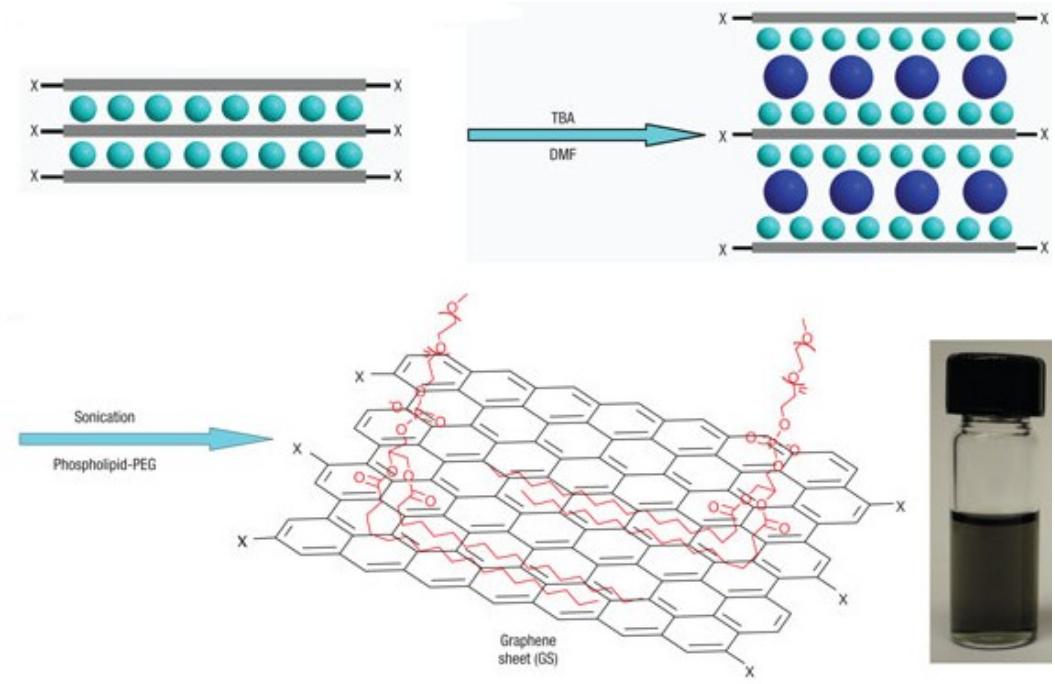

Figure 1-13: The prepared graphene suspension and its route of preparation by the means of exfoliation-reintercalation-expansion [56].

1.3.4.7 Epitaxial Growth

Epitaxial growth allows the graphene (G) sheets to be formed on the surface of a carbon-containing substrate under definite conditions. Pan et al. used thermal annealing to grow the graphene layers on a Ruthenium Ru (0001) surface successfully as illustrated in figure 1-14 [57]. In this process, a chemically cleaned Ru crystal surface with a roughness of less than 0.03μm is required. The Ru sample containing carbon is subjected to Argon-ion sputtering under high vacuum conditions and around 1000K which then cooled to room temperature slowly. During the treatment, highly ordered graphene crystal would gradually form on the surface of the Ru crystal. This results in graphene sheets with continuous excellent long range order to a few millimeters. However, the thickness of graphene sheets that are produced by this method is inconsistent; the adhesion between the graphene sheets and the Ru crystal will also affect the product.

Epitaxial growth of graphene on silicon carbide is an alternative approach. Srivastava, Feenstra, and Fisher used SiC (0001) surface as a substrate for the G formation [58]. The basis of this approach is that at high temperatures the silicon would sublimate preferentially, leaving the carbon to form graphene sheets on the surface. Prior to the treatment, the (0001) surface of the SiC wafers requires mechanical polishing and

chemical cleaning. Further etching of hydrogen is also required to form a step-terrace structure on the surface which is preferred for graphene growth. Different to epitaxial growth on Ru crystals, annealing in an atmosphere of 1 atm of argon is applied. The sublimation rate of silicon in an argon atmosphere is reduced. This allows higher temperatures to be used for graphene production in superior quality. The problem with this approach is that the continuity and the consistency of the film are limited, which reduces the large scale quality of the product [59].

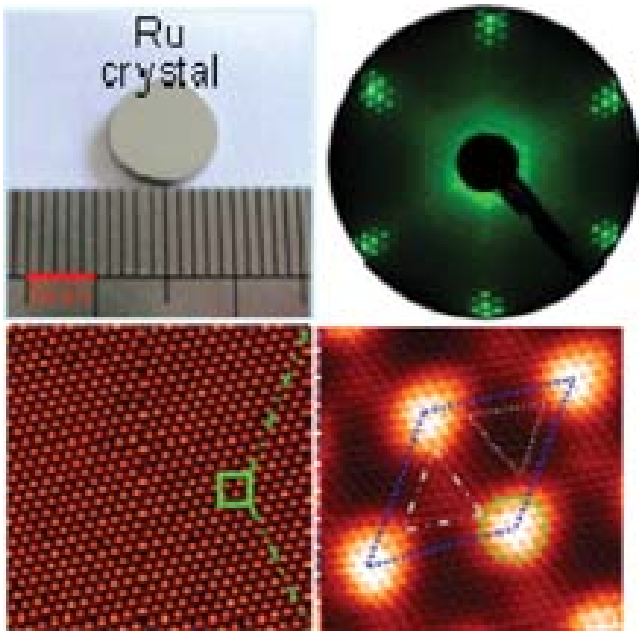

Figure 1-14: A single-crystalline graphene monolayer is grown on a Ru (0001) surface by thermal annealing of a ruthenium single crystal containing carbon [57].

1.3.4.8 Chemical Vapour Deposition

Chemical vapour deposition (CVD) is another method to prepare graphene films. It is the process of depositing graphene films on metal substrates [44]. While the CVD technique has long been known as a possible approach to the production of thin graphene layers on Ni substrate, the Ni substrate tends to absorb more carbon than the amount required to form thin graphene layers, which results in thick graphene crystals [60]. In response to this problem, Kim et al. [37] refined the process by using thin layers of nickel and rapid cooling process as shown in figure 1-15. In their approach, a Ni layer of less than 300 nm thick is first deposited on SiO_2/Si substrates by the means of electron-beam evaporation. The sample is then placed in a quartz tube and heated to 1000°C in the argon atmosphere. A mixture of gasses (CH_4: H_2: Ar-20: 65: 200) is pumped through the

tube and the sample is rapidly cooled down to room temperature by argon flows. The graphene films that formed on the substrate were separated by etching away the Ni layer underneath. Kim found out that the key to suppressing the increase in thickness of the graphene films is the rapid cooling by argon flows. The graphene films that are manufactured by this technique have not exposed to a mechanical or chemical treatment; therefore, the crystal stability comes relatively high. It was also found that by altering the growth time and the thickness of the Ni substrate, the average number of graphene sheets that are produced by this approach can be controlled to meet the different application requirements.

Wei et al. correspondingly succeeded in the preparation of few layers graphene with controlled morphologies by applying ZnS ribbons as templates [61]. The problem with CVD approaches on metal substrates is the procedures have some requiring conditions such as high temperature and ultra-high vacuum [44]. Improving these conditions may prove vital in the industrialization of CVD approaches.

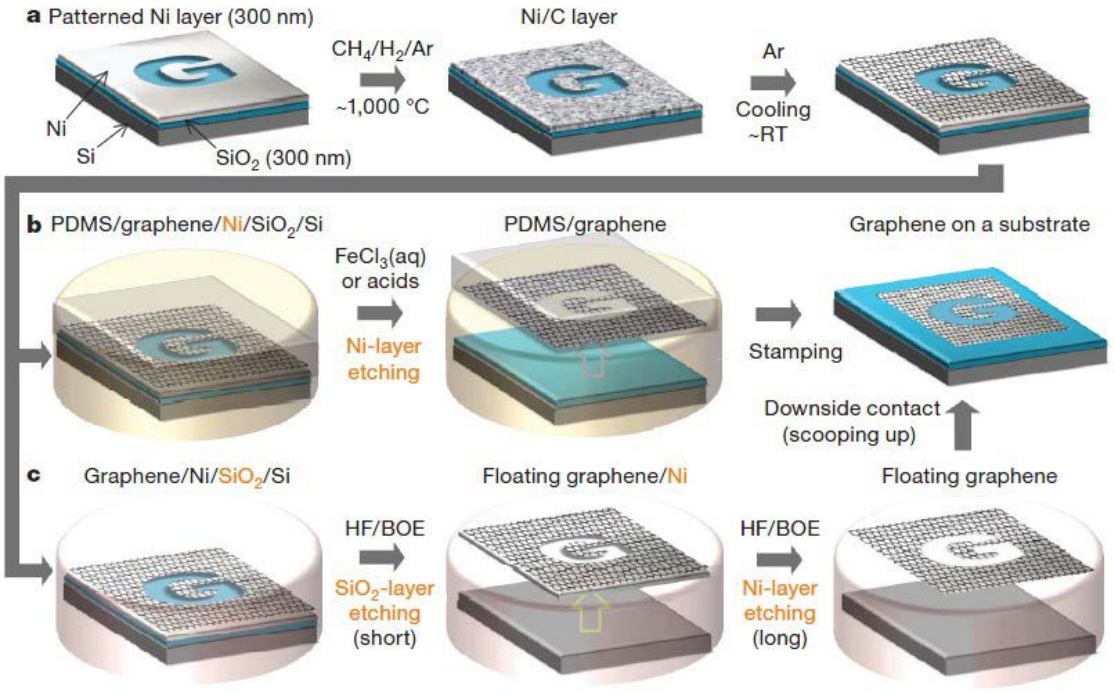

Figure 1-15: Preparation of patterned graphene sheets by the means of CVD [37].

1.3.4.9 Ball-Milling

This technique takes an advantage of the strong shear force that is created during the milling operations to exfoliate graphite platelets. Zhao et al. [62] used graphite nanosheets (GN) as a starting material and dimethylformamide (DMF) as a liquid medium. Multi-layered GN was dispensed into DMF and underwent a wet ball-milling. The resulting material was a mixture of graphene and partially exfoliated GN. This mixture was then centrifuged to separate the graphene products. They reported acquiring irregular single and few layers of graphene that less than 2nm thick. Another similar approach was suggested by Leon et al. [63] which was without any liquid medium during the ball-milling. Instead, melamine was mixed with graphite and underwent dry ball-milling in air or nitrogen atmosphere. The ball-milled mixture was dispersed into DMF to produce a suspension of graphene as shown in figure 1-16.

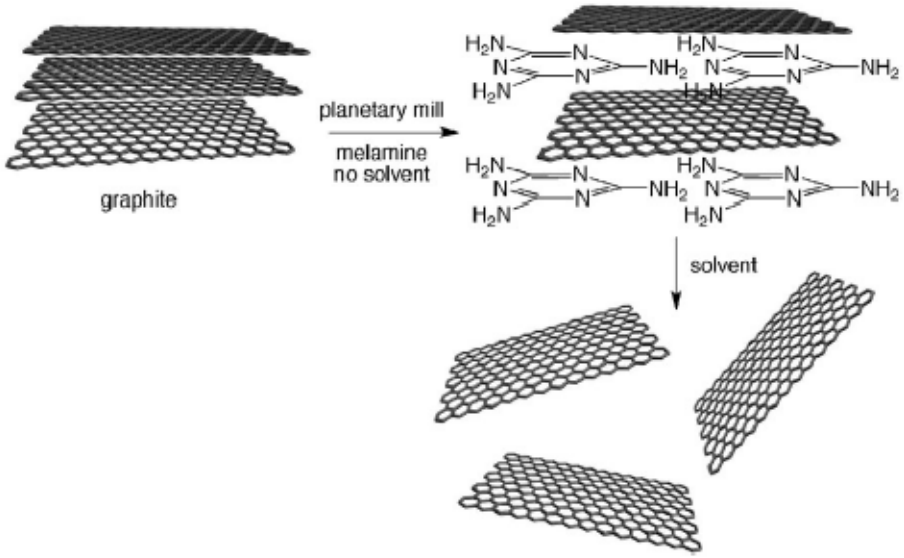

Figure 1-16: Schematic illustration for the exfoliation of graphite by the means of ball-milling [63].

1.4 Characterization of Graphene

Various methods of characterization have been used to analyse the properties of mono and few layers of graphene such as Optical Imaging, Scanning Electron Microscopy (SEM), Transmission Electron Microscopy (TEM), Energy Dispersive X-ray Spectroscopy (EDS), Raman Spectroscopy and X-ray Diffraction (XRD).

1.4.1 Optical Imaging

Optical imaging (shown in figure 1-17) is the most commonly used one due to the fast and inexpensive nature of its process. It is also non-destructive, which further decreases the cost and simplifies the procedures. The difficulty with optical imaging is that the thin nature of graphene layers requires a SiO_2 substrate to act as a background for better contrast. Overcoming this problem is the key to improving the optical imaging of graphene layers [45].

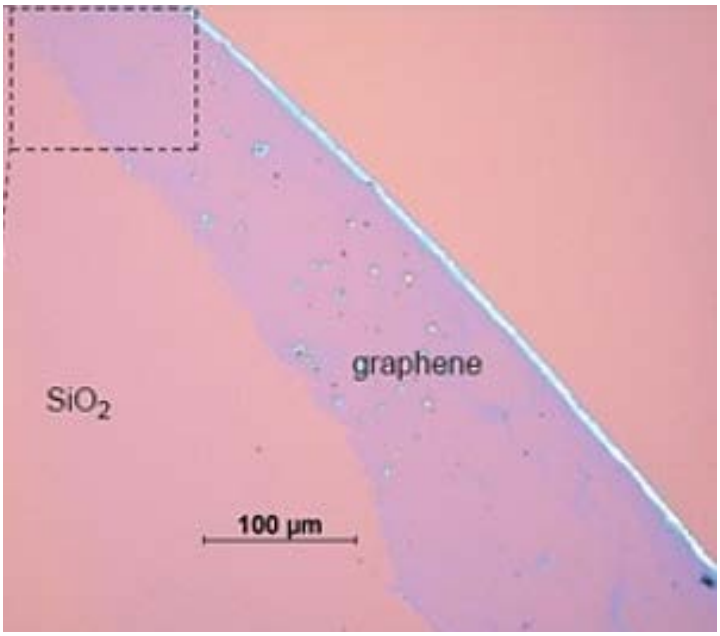

Figure 1-17: Optical images of graphene layers deposited on SiO2 substrates [64].

1.4.2 Atomic Force Microscopy (AFM)

AFM is a straightforward technique to determine the structure of the graphene layers on a nano-meter scale. Atomic force microscopy generates 3D images of the specimen surface by using an extremely fine tip to probe the surface (shown in figure 1-18). The position of the tip is recorded by both piezo-electric crystals and laser beam paired with a photodetector [65]. However, it is still considered as a time-consuming for a large area image of graphene sheets. Moreover, the graphene sheets can't be distinguishable from the graphene oxide one [66].

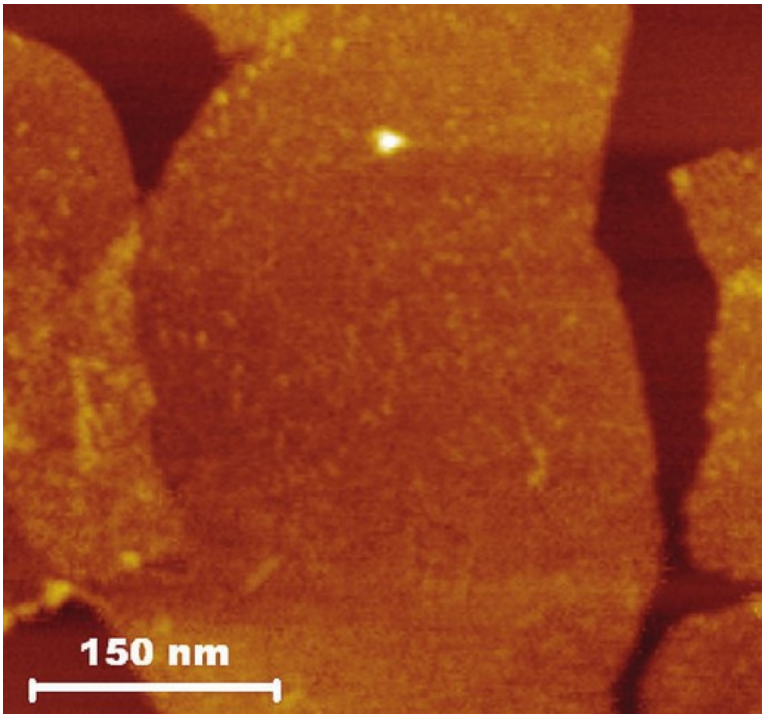

Figure 1-18: Detailed tapping mode AFM height image for chemically reduced graphene oxide nanosheets [66].

1.4.3 Transmission Electron Microscopy (TEM)

On the other hand, TEM is another common tool for the atomic level characterization of materials. It forms an image due to the interaction of the electrons that transmitted through the samples which are usually (ultra-thin sample). An image is formed from this interaction, which is magnified and focused onto an imaging device such as a fluorescent screen. The traditional TEM is unsuitable for the characterization of monolayer graphene as the resolution at a low operating voltage is incompatible while high voltage causes damage to the monolayer. Meyer et al. have successfully resolved every carbon atom in the field of view, where the 1Å resolution was achieved at an acceleration voltage of only 80 kV (figure 1-19). That was by combining the aberration correction with a monochromator in their experiment [67].

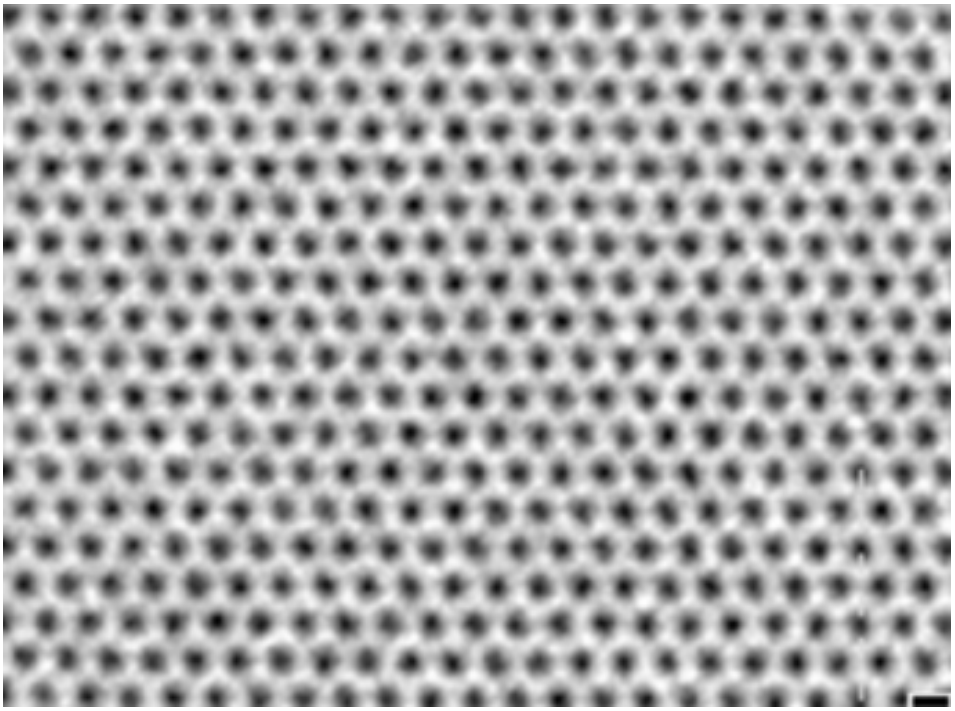

Figure 1-19: TEM image of single-layer graphene membrane, the scale bar is 2Å [67].

1.4.4 Raman Spectroscopy

It is commonly used in chemistry to identify molecules. It operates by collecting the light from a specimen that has been illuminated by a laser. Then, by analyzing the scattering light and the molecular vibrations, the substance can be determined. The G band at 1582cm^{-1}, the 2D band at 2685cm^{-1} and the D band at 1350cm^{-1} (figure 1-20) are the three promising bands exist in the graphene Raman spectrum. The G band can be used to distinguish between graphite and graphene due to the shifts to lower energy when the layer thickness increases. The 2D band, on contrary, can also be used to determine layer thickness as it is always present in graphene but not in graphite [68].

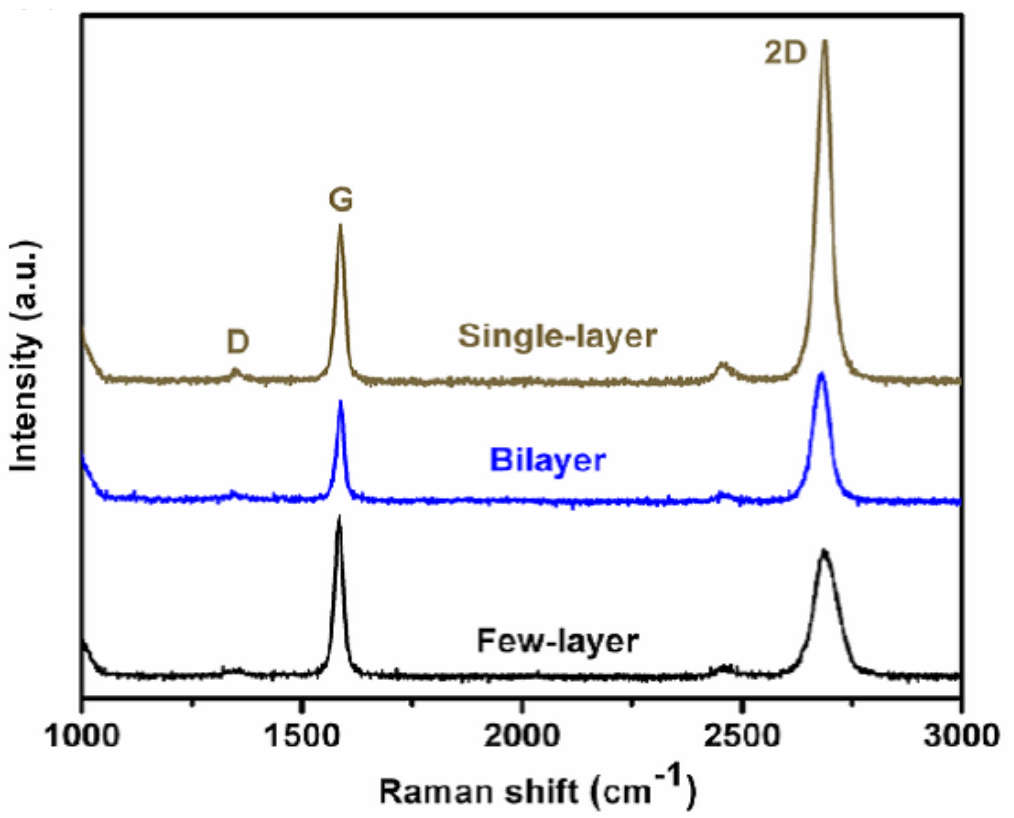

Figure 1-20: Raman spectra for graphene flakes. 2D bands change in position and shape according to the number of layers [68].

1.4.5 X-ray Photoelectron Spectroscopy

XPS is X-ray electron spectroscopy that is used to measure the element composition; empirical formulas, chemical state and electronic state of different elements exist within a material. The principle of XPS is to excite the sample by a beam of X-ray, which causes the electrons to escape from the inner layer atoms. The energy spectrum of the electrons is recorded, which reflect the electronic state of the material. The chemical content of graphene can be determined by wide scan XPS to show the purity of the sample. Also, the state of carbon atoms can be determined to assess the quality of the graphene sheets, especially in the reduction GO, where the amount of sp3 hybridised carbon with C-O bonding should be kept to a minimum [69]. An example of C1s XPS spectra for expandable graphite oxide is shown in figure 1-21.

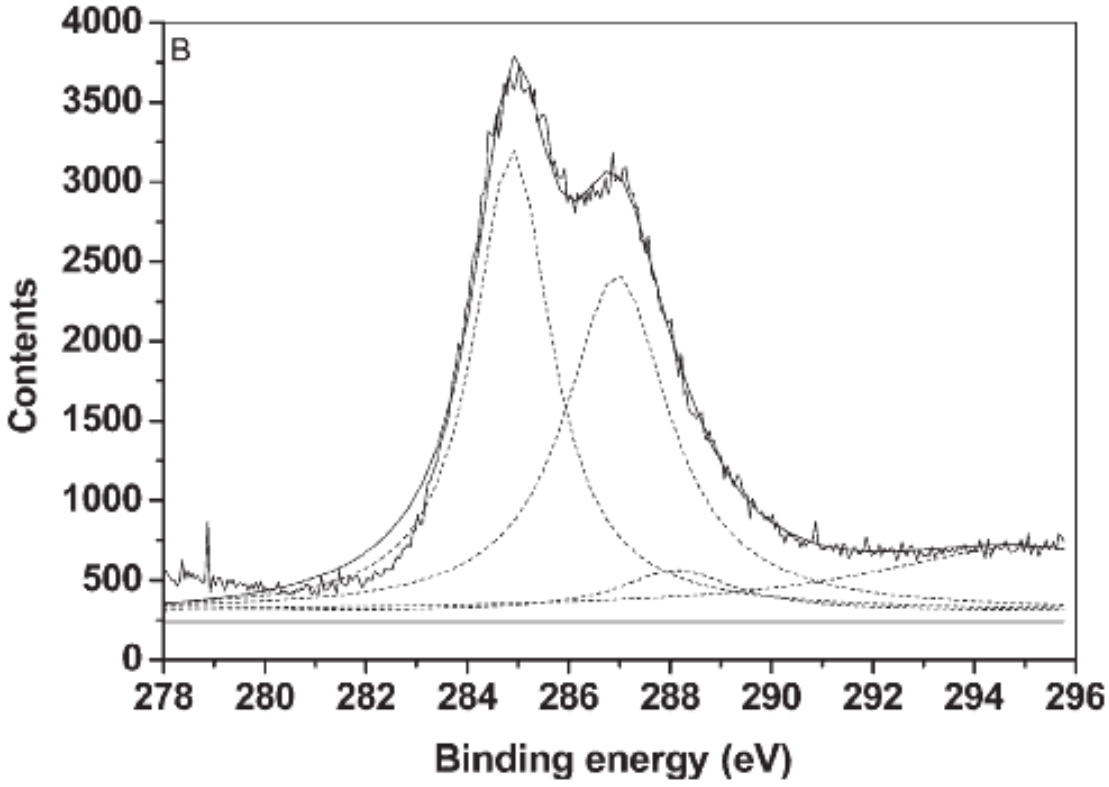

Figure 1-21: C 1s XPS spectra for expandable graphite oxide [70].

1.4.6 Scanning Electron Microscopy (SEM)

It is used for inspecting the topography and morphology, chemistry, crystallography and the grains orientation of specimens at very high magnifications. Thus, cracks and fractured surfaces, bond failures, and physical defects on the die or the package surface can be analysed. Magnifications in SEM can go to more than 300,000 X, but most semiconductor manufacturing applications require magnifications of only less than 3,000X.

SEM images can be obtained by scanning the sample with a high-energy beam of electrons. The electrons interact with the atoms and the reflecting electrons (secondary electrons) which are translated into signals after attracted and collected by a detector. They contain information about the sample's composition, surface topography, and other properties such as electrical conductivity. To produce the SEM image, the electron beam is swept across the area being inspected, producing many such signals. These signals are then amplified, analysed, and translated into images of the topography being inspected. Figure 1-22 shows SEM images of graphene on copper grown by CVD.

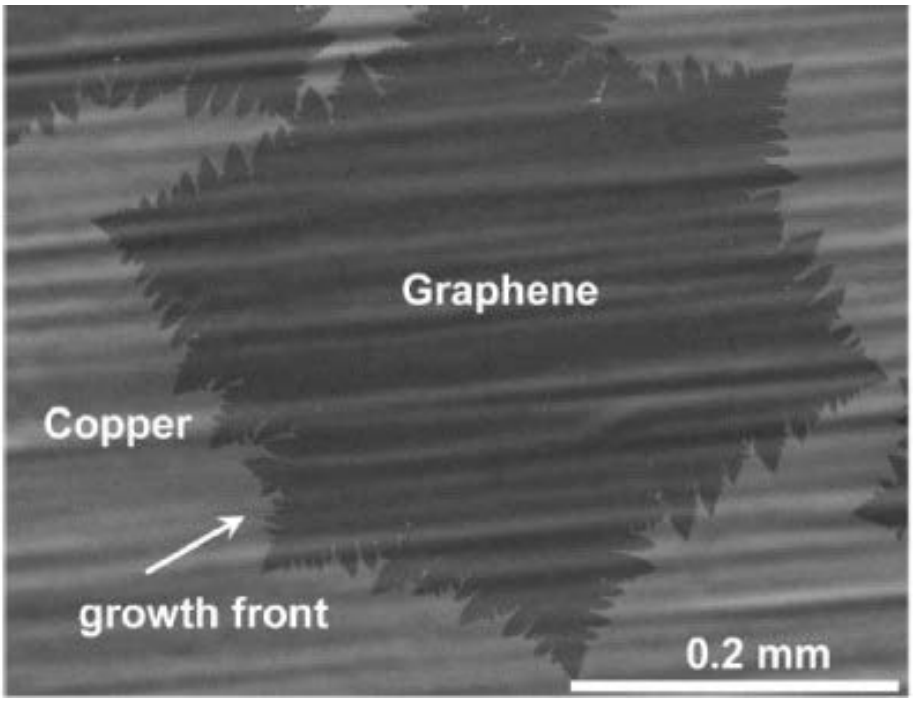

Figure 1-22: SEM images of graphene on copper grew by CV [71].

1.5 Graphene Derivatives

1.5.1 Graphene Functionalization

Essentially, it has been found that some new graphene features or properties can be enhanced and developed by several methodologies. This is called functionalization which includes both hydrogenation and fluorination. Thus, various graphene derivatives with unusual properties, structure, and composition can be created using small organic molecules and polymer [72]-[75]. Recently, graphene derivatives are considered to be the critical route towards practical applications in a number of different fields, especially in biomedical performance [76]. Graphene oxide will be highlighted in here.

1.5.2 Graphene Oxide (GO)

Graphene oxide consists of different hydrophilic oxidized groups on its plane and edges. It is electrically an insulator which is known to contain the epoxide functional group =O along the basal plane and the hydroxyl -OH and carboxyl -OOH functional groups along the edges [77] GO is the probable common route for graphene as shown in figure 1-23. Graphene oxide is a sheet of the graphite oxide, which can be fabricated from graphite

oxide without any assistance of chemical treatment [70]. However, the difficulty comes in forming the graphite oxide itself. That is because of the strong bonds between graphene sheets in the graphite which make sheets difficult to be stripped out. Though by introducing of hydroxyl or carboxyl into graphite (functionalized groups), the binding energy between sheets will be reduced and oxidation can take place.

Expandable flake graphite (EG) is a form of intercalated graphite in which the natural flake graphite has been treated chemically [70]. Intercalation is a process of inserting an intercalant material such as sulfuric acid between the layers of graphite crystal which resulting in different cryptographic structure, density and electronic properties [70]. It has been reported that expandable graphite d-spacing can be increased because after intercalation and so, expandable graphene be able to expand in volume up to 100 times more than the natural one at high temperature [78]. Also, the new physical and chemical properties like the expand of the surface area and edge's size will allow much more functional groups to be introduced between the graphite layers and make the oxidization happens easier with a higher reactivity and at a faster rate[78].

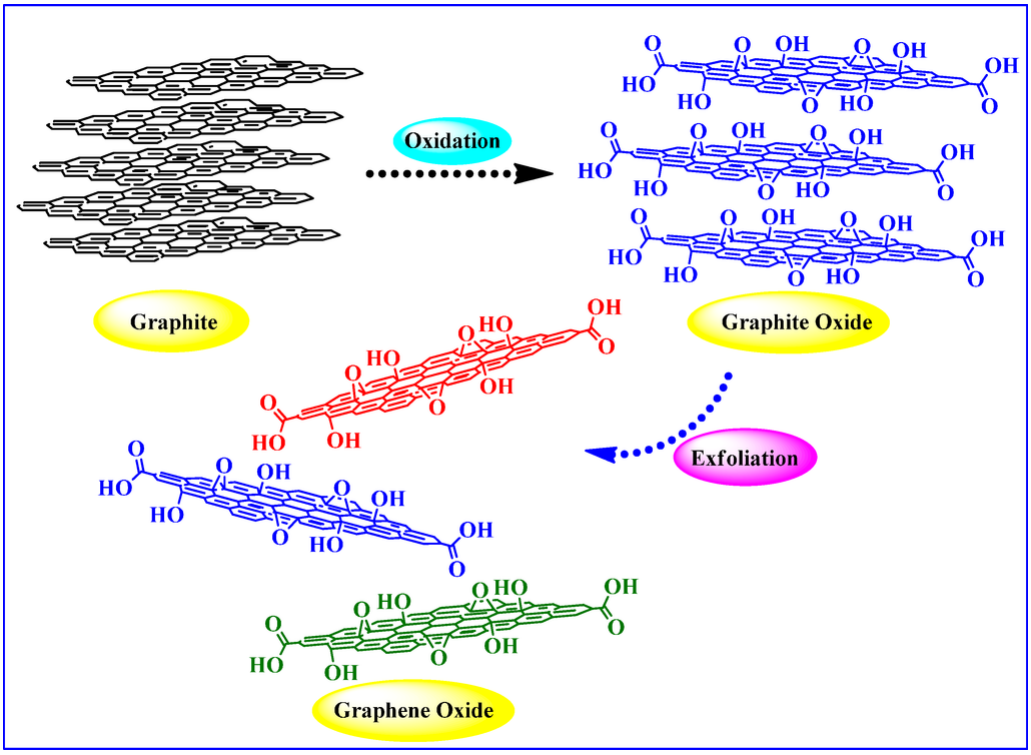

Figure 1-23: Synthesis of graphite oxide and graphene oxide (GO) from natural graphite [79].

1.5.2.1 Graphene Oxide Preparation

The oxidation chemistry can be done using different methods such as Hummer method which is a faster and efficient process for oxidization using a mixture of sulfuric acid H_2SO_4, potassium permanganate $KMnO_4$ and sodium nitrate $NaNO_3$[53],[80]. Another technique is Staudenmeier method which uses potassium chlorate as an oxidizer [81, 82]. In addition, Wei et al. [83] reported another successful way to produce GO by using Au molecular templates (AUP) to assemble graphite oxide sheets. On the other hand, Dikin et al. [77] prepared GO via anodising the filter membrane. Then, graphite oxide can be exfoliated to graphene oxide in water due to the strong hydrophilicity of graphite oxide [84] which happens easily with the assistance of ultra-sonication. Basically, organic solvents such as DMF can be also used as well as water for exfoliation [70].

1.6 Carbon Nanotubes (CNTs)

CNT literature review has been covered in part II-1

1.7 Energy Storage Applications

Energy production and storage are both critical research domains where the demand for improved energy device's performance is high.

1.7.1 Capacitors

The capacitor is a well-known energy storage component that is used in timer electronic circuits to store electrical charges or in a relay to smooth a current [85]. It is also widely used in electronic circuits for blocking the direct current and allowing alternating current to pass [85,86] based on the nature of the capacitor. Basically, the capacitor is composed of a pair of conductors that are separated by an insulator which is called (dielectric). When a power is supplied across the conductors of a capacitor, the capacitor charges up and an electric field exists in the insulator. This leads to the accumulation of opposite electric charges on each conductor and so, energy being stored. Then, the capacitor discharges its electrical charges slowly when the power is turned off [85]-[87]. The intrinsic constant of a capacitor is called capacitance.(C) which is defined as the ratio of charges ±Q on each conductor to the voltage V between them as in equation 1-1:

$$C = \frac{Q}{V} \qquad (1\text{-}1)$$

The capacitance is directly proportional to the area of the conductor and inversely proportional to the separated distance [88] as presented in equation 1-2 and illustrated in figure 1-24.

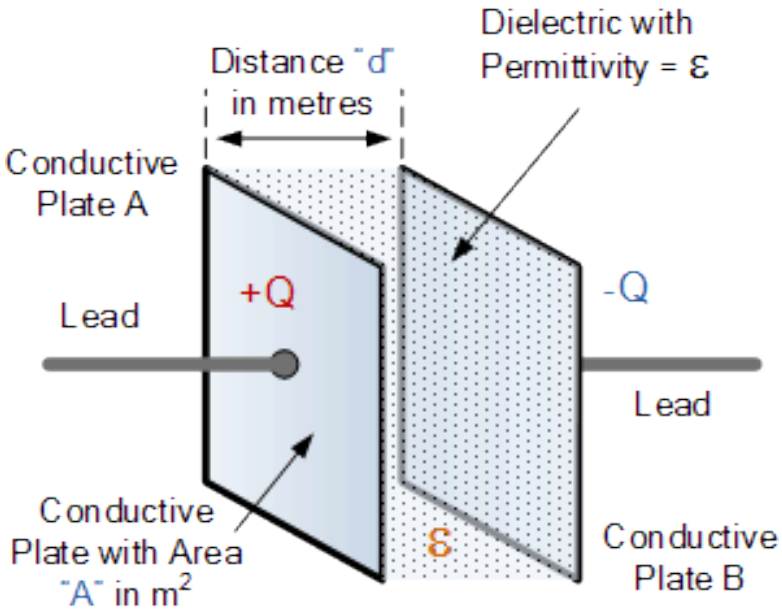

Figure 1-24: Capacitor dimensions [86].

The dielectric is placed between two conducting plates, each of area A and with a separation of distance d as in equation 1-2:

$$C = \frac{A\varepsilon}{d} \qquad (1\text{-}2)$$

Where,

$\varepsilon = \varepsilon_r \times \varepsilon_o$ and εr is the relative dielectric constant, ε_o is the vacuum permittivity

Essentially, the dielectric in the capacitor leaks a small amount of current and has an electric field strength limit. This is called the breakdown voltage which breaks down the capacitor system [89].

1.7.1.1 Types of Capacitors

Capacitors can be sorted by different categories such as the type of dielectric, capacitance and properties.

1.7.1.1.1 Types of Insulators (dielectric)

Among these several categories, distinguish between capacitors kinds by its insulator type is the most common one. mica, ceramic, cellulose, porcelain, mylar, teflon and even air are some of the non-conductive substance used. In theory, the insulator can be any non-conductive material, nevertheless, specific materials are used which suit the capacitor's function for particular application needs. Examples of dielectric constants for various materials are presented in table 1-3. Some capacitors are suitable for high-frequency applications, whereas others are good for high voltage usages. This depends on the insulator size and type [88]-[90].

Table 1-3: Dielectric Constants for Various Materials[93].

constants (at 20°C)		
Material	**Dielectric constant K**	**Dielectric strength (V/m)**
Vacuum	1.0000	
Air (1 atm)	1.0006	3×10^6
Paraffin	2.2	10×10^6
Polystyrene	2.6	24×10^6
Vinyl (plastic)	2–4	50×10^6
Paper	3.7	15×10^6
Quartz	4.3	8×10^6
Oil	4	12×10^6
Glass, Pyrex	5	14×10^6
Rubber, neoprene	6.7	12×10^6
Porcelain	6–8	5×10^6
Mica	7	150×10^6
Water (liquid)	80	
Strontium titanate	300	8×10^6

1.7.1.1.2 Type of Capacitance

Capacitors also can be sorted as fixed capacitance and variable capacitance in their application manner. Variable capacitance can be used in radio tuning circuits where the dielectric for it is the air. Its capacitance is changed by turning the shaft at one end to vary the area of the movable and fixed plates [90].

1.7.1.1.3 Types based on Properties

From another point of view, properties can be used to divide the capacitors into conventional capacitor and ultra-capacitor (supercapacitor) which is also called (electrochemical capacitor). It provides a huge amount of energy in a short period rather than the conventional one. In a normal capacitor, most of the surface area is full with microspores which fail in supporting the electrical double layer which results in weak frequency responses [94]. Figure 1-25 shows the schematic of the conventional and electrochemical capacitor.

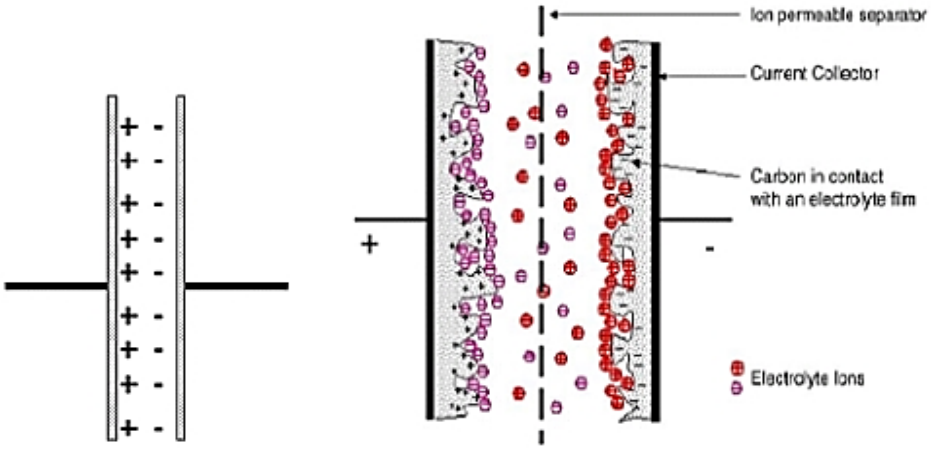

Figure 1-25: Schematic representation of an electrochemical capacitor [95].

1.7.1.2 Capacitor Applications

As mention in a previous section, capacitors are generally used in a number of different ways such as blocking DC voltage while allowing alternating current to pass in electronic circuits. In analogy filter networks, they smooth the output of power supplies. Moreover, capacitors are used to store charges for high-speed use. It has been also used

in resonant circuits to tune radios in particular frequencies. Moreover, they are used in electric power transmission systems as a stabilizer for voltage and power flow [96].

1.7.2 Ultra-capacitors

As it is stated previously, a supercapacitor or ultracapacitor can be defined as an energy storage device that stores unusually high energy density comparing to the normal capacitors [97]. It is also called an electrochemical capacitor because most of them currently are based on electrochemical double layer capacitance (EDLC). Figure 1-26 illustrates the principle of the electrochemical double layer capacitance. In other words, it is a double-layer technology with electrodes such as activated carbon (carbon cloth, carbon black, aerogel carbon, particulate from SiC, particulate from TiC) and an electrolyte such as KOH, organic solutions or sulfuric acid.

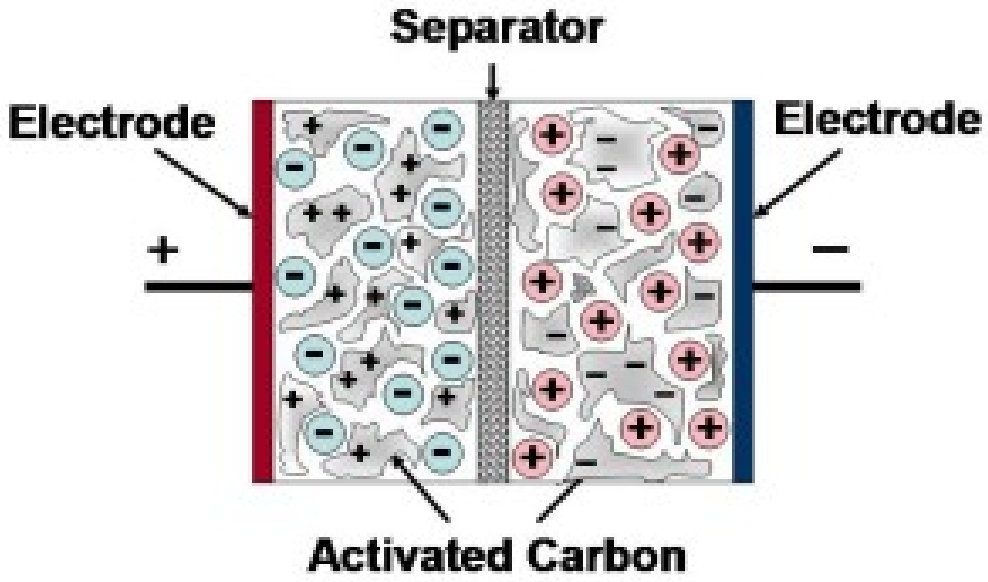

Figure 1-26: Schematic representation of an electrochemical capacitor [95].

Electrochemical capacitor is an electrical energy storage device, but different from batteries. There is no chemical reaction taken place when the energy is being stored or released. Charging and discharging energy occur in nanoscale by the separation of charges at the electrochemical interface between an electrolyte and an electrode [98]. The key principle is that as the area is increased, the distance is decreased [99] as shown in figure 1-27. Thus, ultra-capacitors can undergo through hundreds of charging cycles without a noticeable degradation. The mechanism of EDLCs is non-Faradic and the electrodes are usually the porous carbon [100]. On the other hand, pseudo-capacitor is

another class of ultra-capacitor which involves a faradic mechanism and redox reaction. The electrode is often a metal oxide or any electrically conducting polymer. This type has a higher energy density, but lower power density and shorter lifetime than EDLCs [101].

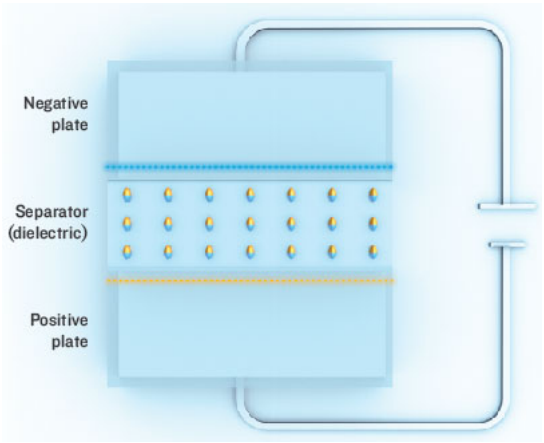

(A)

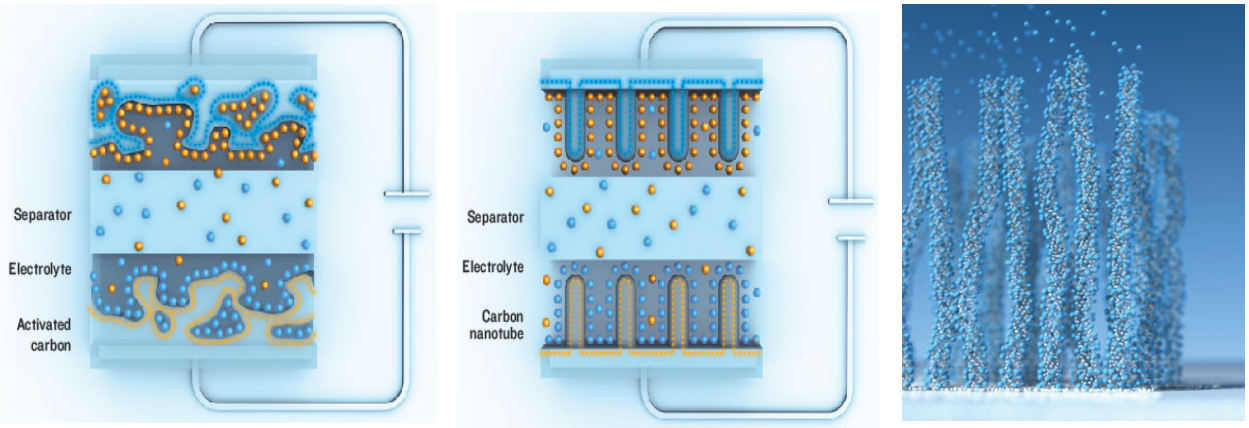

(B)

Figure 1-27: A. In a typical capacitor, electrons are removed from one plate and deposited on the other. B. An ultra-capacitor can store more charge than a capacitor can, because the activated carbon has a pocked interior, much like a sponge. This means that ions in the electrolyte can cling to more surface area. However, with finer dimensions and more uniform distribution, carbon nanotubes enable greater energy storage in ultra-capacitors than activated carbon does[97].

1.8 Graphene-Based Hybrid Nanostructures

Although Carbon nanotubes and graphene have been used in quite a few applications as revealed formerly, many of them, such as supercapacitors, field-emission devices, sensor devices and others relay in thin film technology in such applications [102]-[105]. Therefore, several approaches have been developed for thin film fabrication from G or CNT suspensions this including dip coating, electrophoretic deposition [106], filtration [107], [108] and others. Kim, K. S. et al. [109] reported that although the large-scale and low-cost manufacturing using such techniques, graphene films were still produced with lower electrical conductivities than its theoretical value. This serious drawback apparently can be due to the high interlayer junction resistance.

A suggested solution to this problem is the hybrid nanostructure films which have received a great deal of attention in different studies. Recently, many of them focused on graphene-based material hybrid films especially, the graphene/CNT hybrids. The CNTs can connect the graphene flakes by forming conductive paths between them [110], [111] leading to a higher electrical conductivities than the pure graphene films [107], [112]-[115]. This hybrid film enhances the properties of both graphene and CNT films. Additionally, it was found that the graphene/CNT hybrids also have higher electrical conductivities than pure CNT films [113]-[115]. King et al. suggested that the space between the CNTs layers are filled by the graphene particles filling which causing the conductivity to increase thereby providing a lower junction resistance between the graphene and the CNTs. Moreover, the graphene films coated with CNTs were found to have much lower electrical conductivities than graphene/ CNT films with graphene and CNTs mixed and dispersed in the same layer [113].

1.9 Conclusion

In this chapter, the fundamental of the graphene (G), GO and MWCNTs with their physical properties, fabrication methods and applications were reviewed. Different methods for graphene characterization were summarized. A brief introduction to storage energy application and how graphene-based hybrid film materials can make a difference was discussed.

References

[1] S. Iijima, “Helical microtubules of graphitic carbon,” *Nature*, Vol. 354, No. 6348, pp. 56–58, Nov. 1991.

[2] G. Davies and INSPEC (Information service), *Properties and growth of diamond*. INSPEC, the Institution of Electrical Engineers, 1994.

[3] A. Yu, H. W. Park, A. Davies, D. C. Higgins, Z. Chen, and X. Xiao, “Free-standing layer-by-layer hybrid thin film of graphene-MnO2 nanotube as anode for lithium ion batteries,” *J. Phys. Chem. Lett.*, Vol. 2, No. 15, pp. 1855–1860, Aug. 2011.

[4] H.-G. Lu and S. Li, “Two-dimensional carbon allotropes from graphene to graphyne,” *J. Mater. Chem. C*, Vol. 1, No. 23, p. 3677, 2013.

[5] N. Papasimakis, Z. Luo, Z. X. Shen, F. De Angelis, E. Di Fabrizio, A. E. Nikolaenko, and N. I. Zheludev, “Graphene in a photonic metamaterial.,” *Opt. Express*, Vol. 18, No. 8, pp. 8353–9, 2010.

[6] M. S. Arnold, A. A. Green, J. F. Hulvat, S. I. Stupp, and M. C. Hersam, “Sorting carbon nanotubes by electronic structure using density differentiation,” *Nat. Nanotechnol.*, Vol. 1, No. 1, pp. 60–65, Oct. 2006.

[7] R. Heyrovska, “Atomic Structures of Graphene, Benzene and Methane with Bond Lengths as Sums of the Single, Double and Resonance Bond Radii of Carbon,” *arXiv Prepr. arXiv0804.4086*, pp. 1–4, Apr. 2008.

[8] M. H. Gass, U. Bangert, A. L. Bleloch, P. Wang, R. R. Nair, and A. K. Geim, “Free-standing graphene at atomic resolution.,” *Nat. Nanotechnol.*, Vol. 3, No. 11, pp. 676–81, Nov. 2008.

[9] J. H. Warner, F. Schaffel, M. Rummeli, A. Bachmatiuk, F. Schäffel, A. Bachmatiuk, and M. H. Rümmeli, *Graphene Fundamentals and emergent applications*, vol. 17. Elsevier, 2013.

[10] F. Mark, O. Goerbig, and L. Notes, “Introduction to the Physical Properties of Graphene,” *Carbon N. Y.*, Vol. 472, No. 1860, pp. 8539–8539, 2008.

[11] S. Iijima and T. Ichihashi, “Single-shell carbon nanotubes of 1-nm diameter,” *Nature*, Vol. 363, No. 6430, pp. 603–605, 1993.

[12] R. H. Baughman, A. A. Zakhidov, and W. A. de Heer, “Carbon nanotubes --- the route toward applications,” *Science (80-.).*, Vol. 297, No. 5582, pp. 787–92, Aug. 2002.

[13] M. D. Stoller, S. Park, Y. Zhu, J. An, and R. S. Ruoff, “Graphene-Based Ultracapacitors,” 2008.

[14] A. K. Geim and K. S. Novoselov, “The rise of graphene,” *Nat. Mater.*, Vol. 6, No. 3, pp. 183–191, Mar. 2007.

[15] R. R. Nair, A. N. Grigorenko, P. Blake, K. S. Novoselov, T. J. Booth, N. M. R. Peres, T. Stauber, and A. K. Geim, “Fine structure constant defines visual transparency of graphene.,” *Science (80-.).*, Vol. 320, No. 5881, p. 1308, Jun. 2008.

[16] S. V. Morozov, K. S. Novoselov, M. I. Katsnelson, F. Schedin, D. C. Elias, J. A. Jaszczak, and A. K. Geim, “Giant intrinsic carrier mobilities in graphene and its bilayer,” *Phys. Rev. Lett.*,Vol. 100, No. 1, p. 16602, Jan. 2008.

[17] M. K. Pati, S. K. Sarangi, P. Pattojoshi, and G. S. Roy, “RESEARCH ARTICLE NANOSCALE BASED GRAPHENE : A REVIEW OF ITS PROPERTIES FOR ELECTRONIC AND PHOTONIC APPLICATIONS,” Vol. 6, No. Figure 2, pp. 3267–3271, 2015.

[18] K. S. Novoselov, Z. Jiang, Y. Zhang, S. V. Morozov, H. L. Stormer, U. Zeitler, J. C. Maan, G. S. Boebinger, P. Kim, and A. K. Geim, “Room-temperature quantum Hall effect in graphene.,” *Science*, Vol. 315, No. 5817, p. 1379, Feb. 2007.

[19] K. S. Novoselov, A. K. Geim, S. V Morozov, D. Jiang, Y. Zhang, S. V Dubonos, I. V Grigorieva, and A. A. Firsov, “Electric field effect in atomically thin carbon films.,” *Science (80-.).*, Vol. 306, No. 5696, pp. 666–669, Oct. 2004.

[20] W. Choi and J. Lee, *Graphene : synthesis and applications*. CRC Press, 2012.

[21] Klaus D. Sattler, *Carbon Nanomaterials Sourcebook: Graphene, Fullerenes,*

Nanotubes, and Nanodiamonds, Volume I. 2016.

[22] L.-F. Mao, H. Ning, and X. Li, "Effects of Energy Relaxation via Quantum Coupling Among Three-Dimensional Motion on the Tunneling Current of Graphene Field-Effect Transistors," *Nanoscale Res. Lett.*, Vol. 10, No. 1, p. 322, Dec. 2015.

[23] Group NanoXplore Inc, "From Graphite to Graphene UNLEASHING THE POWER OF GRAPHENE."2014. [Online]. Available: http://www.fotocatproject.eu/files/2%20meeting/10.%20NXE-%20%20Soroush%20Nazarpour-%20Canada.pdf

[24] K. Saito, J. Nakamura, and A. Natori, "Ballistic thermal conductance of a graphene sheet," *Phys. Rev. B - Condens. Matter Mater. Phys.*, Vol. 76, No. 11, p. 115409, Sep. 2007.

[25] A. A. Balandin, S. Ghosh, W. Bao, I. Calizo, D. Teweldebrhan, F. Miao, and C. N. Lau, "Superior thermal conductivity of single-layer graphene," *Nano Lett.*, Vol. 8, No. 3, pp. 902–907, Mar. 2008.

[26] T. M. Tritt, *Thermal Conductivity*. 2014.

[27] I. W. Frank, D. M. Tanenbaum, A. M. van der Zande, and P. L. McEuen, "Mechanical properties of suspended graphene sheets," *J. Vac. Sci. Technol. B Microelectron. Nanom. Struct.*, Vol. 25, No. 2007, p. 2558, 2007.

[28] S. Stankovich, D. A. Dikin, G. H. Dommett, K. M. Kohlhaas, E. J. Zimney, E. A. Stach, R. D. Piner, S. T. Nguyen, and R. S. Ruoff, "Graphene-based composite materials," *Nature*, Vol. 442, No. 7100, pp. 282–286, Jul. 2006.

[29] C. Lee, X. Wei, J. W. Kysar, J. Hone, and =, "Measurement of the Elastic Properties and Intrinsic Strength of Monolayer Graphene," *Science (80-.).*, Vol. 321, No. 18 July 2008, pp. 385–388, Jul. 2008.

[30] P. A. Denis and F. Iribarne, "Comparative study of defect reactivity in graphene," *J. Phys. Chem. C*, Vol. 117, No. 37, pp. 19048–19055, Sep. 2013.

[31] V. K. Thakur and M. K. Thakur, *Eco-friendly Polymer Nanocomposites:*

Chemistry and Applications. 2015.

[32] A. Ashjaran, "Some Properties and Applications of Graphene as High Performance Material," *Int. J. Curr. Trends Eng. Technol.*, pp. 67–71, 2015.

[33] M. J. O'Connell, P. Boul, L. M. Ericson, C. Huffman, Y. Wang, E. Haroz, C. Kuper, J. Tour, K. D. Ausman, and R. E. Smalley, "Reversible water-solubilization of single-walled carbon nanotubes by polymer wrapping," *Chem. Phys. Lett.*, Vol. 342, No. 3–4, pp. 265–271, 2001.

[34] J. H. Chen, M. Ishigami, C. Jang, D. R. Hines, M. S. Fuhrer, and E. D. Williams, "Printed graphene circuits," *Adv. Mater.*, Vol. 19, No. 21, pp. 3623–3627, Nov. 2007.

[35] J. S. Bunch, S. S. Verbridge, J. S. Alden, A. M. Van Der Zande, J. M. Parpia, H. G. Craighead, and P. L. McEuen, "Impermeable atomic membranes from graphene sheets," *Nano Lett.*, Vol. 8, No. 8, pp. 2458–2462, Aug. 2008.

[36] F. Schedin, A. K. Geim, S. V. Morozov, E. W. Hill, P. Blake, M. I. Katsnelson, and K. S. Novoselov, "Detection of individual gas molecules adsorbed on graphene," *Nat. Mater.*, Vol. 6, No. 9, pp. 652–655, Sep. 2007.

[37] K. S. Kim, Y. Zhao, H. Jang, S. Y. Lee, J. M. Kim, J.-H. Ahn, P. Kim, J.-Y. Choi, and B. H. Hong, "Large-scale pattern growth of graphene films for stretchable transparent electrodes," *Nature*, Vol. 457, No. 7230, pp. 706–710, Feb. 2009.

[38] R. K. Joshi, P. Carbone, F. C. Wang, V. G. Kravets, Y. Su, I. V Grigorieva, H. A. Wu, A. K. Geim, and R. R. Nair, "Precise and Ultrafast Molecular Sieving Through Graphene Oxide Membranes," *Science (80-.).*, Vol. 343, No. 6172, pp. 752–754, Feb. 2014.

[39] K. I. Bolotin, K. J. Sikes, Z. Jiang, M. Klima, G. Fudenberg, J. Hone, P. Kim, and H. L. Stormer, "Ultrahigh electron mobility in suspended graphene," *Solid State Commun.*, Vol. 146, No. 9–10, pp. 351–355, 2008.

[40] L. Gomez De Arco, Y. Zhang, C. W. Schlenker, K. Ryu, M. E. Thompson, and C. Zhou, "Continuous, highly flexible, and transparent graphene films by chemical

vapor deposition for organic photovoltaics," *ACS Nano*, Vol. 4, No. 5, pp. 2865–2873, May 2010.

[41] S. Akca, A. Foroughi, D. Frochtzwajg, and H. W. C. Postma, "Competing interactions in dna assembly on graphene," *PLoS One*, Vol. 6, No. 4, p. e18442, 2011.

[42] B. H. Nguyen and V. H. Nguyen, "Promising applications of graphene and graphene-based nanostructures," *Adv. Nat. Sci. Nanosci. Nanotechnol.*, Vol. 7, No. 2, p. 23002, 2016.

[43] K. Sanderson, "Graphene electrode promises stretchy circuits," *Nature*. Nature Publishing Group, 14-Jan-2009.

[44] R. S. Edwards and K. S. Coleman, "Graphene synthesis: relationship to applications," *Nanoscale*, Vol. 5, No. 1, pp. 38–51, Jan. 2013.

[45] V. Singh, D. Joung, L. Zhai, S. Das, S. I. Khondaker, and S. Seal, "Graphene based materials: Past, present and future," *Prog. Mater. Sci.*,Vol. 56, No. 8, pp. 1178–1271, 2011.

[46] J. Wang, K. K. Manga, Q. Bao, and K. P. Loh, "High-yield synthesis of few-layer graphene flakes through electrochemical expansion of graphite in propylene carbonate electrolyte," *J. Am. Chem. Soc.*, Vol. 133, No. 23, pp. 8888–8891, Jun. 2011.

[47] H. Huang, Y. Xia, X. Tao, J. Du, J. Fang, Y. Gan, and W. Zhang, "Highly efficient electrolytic exfoliation of graphite into graphene sheets based on Li ions intercalation–expansion–microexplosion mechanism," *J. Mater. Chem.*, Vol. 22, No. 21, p. 10452, 2012.

[48] X. Zhao, M. Ohkohchi, H. Shimoyama, and Y. Ando, "Morphology of carbon allotropes prepared by hydrogen arc discharge," *J. Cryst. Growth*, Vol. 198–199, No. pt 2, pp. 934–938, 1999.

[49] K. S. Subrahmanyam, L. S. Panchakarla, A. Govindaraj, and C. N. R. Rao, "Simple method of preparing graphene flakes by an arc-discharge method," *J.*

Phys. Chem. C, Vol. 113, No. 11, pp. 4257–4259, Mar. 2009.

[50] Y. Chen, H. Zhao, L. Sheng, L. Yu, K. An, J. Xu, Y. Ando, and X. Zhao, "Mass-production of highly-crystalline few-layer graphene sheets by arc discharge in various H2–inert gas mixtures," *Chem. Phys. Lett.*, Vol. 538, pp. 72–76, Jun. 2012.

[51] L. Jiao, L. Zhang, X. Wang, G. Diankov, and H. Dai, "Narrow graphene nanoribbons from carbon nanotubes," *Nature*, Vol. 458, No. 7240, pp. 877–880, Apr. 2009.

[52] D. V Kosynkin, A. L. Higginbotham, A. Sinitskii, J. R. Lomeda, A. Dimiev, B. K. Price, and J. M. Tour, "Longitudinal unzipping of carbon nanotubes to form graphene nanoribbons.," *Nature*, Vol. 458, No. 7240, pp. 872–876, Apr. 2009.

[53] W. S. Hummers and R. E. Offeman, "Preparation of Graphitic Oxide," *J. Am. Chem. Soc.*, Vol. 80, No. 6, pp. 1339–1339, Mar. 1958.

[54] V. C. Tung, M. J. Allen, Y. Yang, and R. B. Kaner, "High-throughput solution processing of large-scale graphene," *Nat. Nanotechnol.*, Vol. 4, No. 1, pp. 25–29, Jan. 2009.

[55] T. Szab, O. Berkesi, P. Forg, K. Josepovits, Y. Sanakis, D. Petridis, and I. Dkny, "Evolution of Surface Functional Groups in a Series of Progressively Oxidized Graphite Oxides Evolution of Surface Functional Groups in a Series of Progressively Oxidized Graphite Oxides," *Chem. Mater.*, Vol. 18, No. 11, pp. 2740–2749, May 2006.

[56] X. Li, G. Zhang, X. Bai, X. Sun, X. Wang, E. Wang, and H. Dai, "Highly conducting graphene sheets and Langmuir-Blodgett films," *Nat. Nanotechnol.*, Vol. 3, No. 9, pp. 538–542, Sep. 2008.

[57] Y. Pan, H. Zhang, D. Shi, J. Sun, S. Du, F. Liu, and H. J. Gao, "Highly ordered, millimeter-scale, continuous,single-crystalline graphene monolayer formed on Ru (0001)," *Adv. Mater.*, Vol. 21, No. 27, pp. 2777–2780, Jul. 2009.

[58] Luxmi, N. Srivastava, R. M. Feenstra, and P. J. Fisher, "Formation of epitaxial graphene on SiC(0001) using vacuum or argon environments," *J. Vac. Sci.*

Technol. B Microelectron. Nanom. Struct., Vol. 28, No. 4, p. C5C1, 2010.

[59] K. V Emtsev, A. Bostwick, K. Horn, J. Jobst, G. L. Kellogg, L. Ley, J. L. McChesney, T. Ohta, S. A. Reshanov, J. Röhrl, E. Rotenberg, A. K. Schmid, D. Waldmann, H. B. Weber, and T. Seyller, "Towards wafer-size graphene layers by atmospheric pressure graphitization of silicon carbide.," *Nat. Mater.*, Vol. 8, No. 3, pp. 203–207, Mar. 2009.

[60] A. N. Obraztsov, E. A. Obraztsova, A. V. Tyurnina, and A. A. Zolotukhin, "Chemical vapor deposition of thin graphite films of nanometer thickness," *Carbon N. Y.*, Vol. 45, No. 10, pp. 2017–2021, Sep. 2007.

[61] D. Wei, Y. Liu, H. Zhang, L. Huang, B. Wu, J. Chen, and G. Yu, "Scalable synthesis of few-layer graphene ribbons with controlled morphologies by a template method and their applications in nanoelectromechanical switches," *J. Am. Chem. Soc.*, Vol. 131, No. 31, pp. 11147–11154, Aug. 2009.

[62] W. Zhao, M. Fang, F. Wu, H. Wu, L. Wang, and G. Chen, "Preparation of graphene by exfoliation of graphite using wet ball milling," *J. Mater. Chem.*, Vol. 20, No. 28, p. 5817, 2010.

[63] V. León, M. Quintana, M. A. Herrero, J. L. G. Fierro, A. D. La Hoz, M. Prato, and E. Vázquez, "Few-layer graphenes from ball-milling of graphite with melamine," *Chem. Commun.*, Vol. 47, No. 39, p. 10936, Oct. 2011.

[64] P. D. W. and D. G. N. Dr Monica Craciun, "Graphene devices Engineering University of Exeter." .

[65] S. Chatterjee, S. S. Gadad, and T. K. Kundu, "Atomic force microscopy," *Resonance*, Vol. 15, No. 7, pp. 622–642, Jul. 2010.

[66] J. I. Paredes, S. Villar-Rodil, P. Solís-Fernández, A. Martínez-Alonso, and J. M. D. Tascón, "Atomic force and scanning tunneling microscopy imaging of graphene nanosheets derived from graphite oxide," *Langmuir*, Vol. 25, No. 10, pp. 5957–5968, May 2009.

[67] J. C. Meyer, C. Kisielowski, R. Erni, M. D. Rossell, M. F. Crommie, and A. Zettl,

"Direct imaging of lattice atoms and topological defects in graphene membranes," *Nano Lett.*, Vol. 8, No. 11, pp. 3582–3586, 2008.

[68] Benphysics, "Graphene gets serious," real science. [Online]. Available: https://quantumfrontiers.com/2013/09/06/graphene-gets-serious/. [Accessed: 26-Jan-2017].

[69] A. Bagri, C. Mattevi, M. Acik, Y. J. Chabal, M. Chhowalla, and V. B. Shenoy, "Structural evolution during the reduction of chemically derived graphene oxide.," *Nat. Chem.*, Vol. 2, No. 7, pp. 581–587, Jul. 2010.

[70] D. Cai and M. Song, "Preparation of fully exfoliated graphite oxide nanoplatelets in organic solvents," *J. Mater. Chem.*, Vol. 17, No. 35, p. 3678, 2007.

[71] L. P. Biro and P. Lambin, "Grain boundaries in graphene grown by chemical vapor deposition," *New J. Phys.*, Vol. 15, No. 3, p. 35024, Mar. 2013.

[72] J. Shen, Y. Hu, C. Li, C. Qin, and M. Ye, "Synthesis of amphiphilic graphene nanoplatelets," *Small*, Vol. 5, No. 1, pp. 82–85, Jan. 2009.

[73] M. Fang, K. Wang, H. Lu, Y. Yang, and S. Nutt, "Covalent polymer functionalization of graphene nanosheets and mechanical properties of composites," *J. Mater. Chem.*, Vol. 19, No. 38, p. 7098, 2009.

[74] Y. Xu, Z. Liu, X. Zhang, Y. Wang, J. Tian, Y. Huang, Y. Ma, X. Zhang, and Y. Chen, "A graphene hybrid material covalently functionalized with porphyrin: Synthesis and optical limiting property," *Adv. Mater.*, Vol. 21, No. 12, pp. 1275–1279, Mar. 2009.

[75] Y. Liu, J. Zhou, X. Zhang, Z. Liu, X. Wan, J. Tian, T. Wang, and Y. Chen, "Synthesis, characterization and optical limiting property of covalently oligothiophene-functionalized graphene material," *Carbon N. Y.*, Vol. 47, No. 13, pp. 3113–3121, 2009.

[76] H. W. Ch Postma, "Rapid sequencing of individual DNA molecules in graphene nanogaps," *Nano Lett.*, Vol. 10, No. 2, pp. 420–425, Feb. 2010.

[77] D. A. Dikin, S. Stankovich, E. J. Zimney, R. D. Piner, G. H. B. Dommett, G.

Evmenenko, S. T. Nguyen, and R. S. Ruoff, “Preparation and characterization of graphene oxide paper.,” *Nature*, Vol. 448, No. 7152, pp. 457–60, Jul. 2007.

[78] B. Z. Jang and A. Zhamu, “Processing of nanographene platelets (NGPs) and NGP nanocomposites: A review,” *J. Mater. Sci.*, Vol. 43, No. 15, pp. 5092–5101, Aug. 2008.

[79] B. Garg, T. Bisht, and Y. C. Ling, “Graphene-based nanomaterials as heterogeneous acid catalysts: A comprehensive perspective,” *Molecules*, Vol. 19, No. 9, pp. 14582–14614, Sep. 2014.

[80] W. Zhongqing, D. E. Barlow, and P. E. Sheehan, “The assembly of single-laye oxide and graphene oxide and graphene using molecular templates,” *Nano Lett.*, Vol. 8, No. 10, pp. 3141–3145, 2008.

[81] L. Staudenmaier, “Verfahren zur Darstellung der Graphitsäure,” *Berichte der Dtsch. Chem. Gesellschaft*, Vol. 31, No. 2, pp. 1481–1487, May 1898.

[82] H. C. Schniepp, J. L. Li, M. J. McAllister, H. Sai, M. Herrera-Alonson, D. H. Adamson, R. K. Prud'homme, R. Car, D. A. Seville, and I. A. Aksay, “Functionalized single graphene sheets derived from splitting graphite oxide,” *J. Phys. Chem. B*, Vol. 110, No. 17, pp. 8535–8539, May 2006.

[83] Z. Wei, D. E. Barlow, and P. E. Sheehan, “The Assembly of Single-Layer Graphene Oxide and Graphene Using Molecular Templates,” *Nano Lett.*, Vol. 8, No. 10, pp. 3141–3145, Oct. 2008.

[84] G. I. Titelman, V. Gelman, S. Bron, R. L. Khalfin, Y. Cohen, and H. Bianco-Peled, “Characteristics and microstructure of aqueous colloidal dispersions of graphite oxide,” *Carbon N. Y.*, Vol. 43, No. 3, pp. 641–649, 2005.

[85] “Types of capacitors and their circuit applications.” [Online]. Available: http://www.howtoguide4windows.com/resources/electronics/component/what-is-a-capacitor.php.

[86] “Introduction to Capacitors, Capacitance and Charge.” [Online]. Available: http://www.electronics-tutorials.ws/capacitor/cap_1.html.

[87] "Capacitors."[Online].Available: http://www.technologystudent.com/elec1/capac1.htm.

[88] "Capacitance and Charge on a Capacitors Plates." [Online]. Available: http://www.electronics-tutorials.ws/capacitor/cap_4.html.

[89] T. Longland, T. W. Hunt, and W. A. Brecknell, *Power capacitor handbook*. Butterworths, 1984.

[90] "ACU Capacitors." [Online]. Available: http://ian.r.scott.tripod.com/acu_capacitors.htm.

[91] "Types of Capacitor and their Construction."[Online].Available: http://www.electronics-tutorials.ws/capacitor/cap_2.html.

[92] E. Flux, "Capacitance And Dielectrics," *Fizika?*, p. 232, 1996.

[93] "Copyright © 2007, Pearson Education, Inc., Publishing as Pearson Addison-Wesley. Electric potential energy Electric potential Conservation of energy Chapter.-ppt download."[Online]. Available: http://slideplayer.com/slide/9507100/.

[94] M. Jayalakshmi and K. Balasubramanian, "Simple capacitors to supercapacitors-an overview," *Int. J. Electrochem. Sci*, vol. 3, pp. 1196–1217, 2008.

[95] C. Hu, "FLUID COKE DERIVED ACTIVATED CARBON AS ELECTRODE MATERIAL FOR ELECTROCHEMICAL Fluid coke Derived Activated Carbon as Electrode Material for Electrochemical Double Layer Capacitor," *Chem. Eng.*, 2008.

[96] "Capacitor Uses | Capacitor Applications | Electronics+Radio." [Online]. Available: http://www.electronics radio.com/articles/electronic_components/capacitors/capacitor-uses.php.

[97] "Enerize Corporation." [Online]. Available: http://www.enerize.com/superCap.php.

[98] B. E. Conway, "Electrochemical Supercapacitors Scientific Fundamentals and

Technological Applications.” Springer US, Boston, MA, p. 736, 1999.

[99] J. Schindall, “THE CHARGE OF THE Ultra: Capacitors,” *IEEE Spectr.*, vol. 44, no. 11, p. 42–46 %U http://search.ebscohost.com.proxy.grenobl, 2007.

[100] J. Z. Pei Kang Shen, Chao-Yang Wang, San Ping Jiang, Xueliang Sun, *Electrochemical Energy: Advanced Materials and Technologies*. 2015.

[101] A. Venkataraman, “Pseudocapacitors for Energy Storage,” 2015.

[102] S. Iijima and T. Ichihashi, “Single-shell carbon nanotubes of 1-nm diameter,” *Nature*, vol. 363, no. 6430, pp. 603–605, Jun. 1993.

[103] M. Zhang, “Strong, Transparent, Multifunctional, Carbon Nanotube Sheets,” *Science (80-.).*, vol. 309, no. 5738, pp. 1215–1219, Aug. 2005.

[104] Z. Wu, Z. Chen, X. Du, J. M. Logan, J. Sippel, M. Nikolou, K. Kamaras, J. R. Reynolds, D. B. Tanner, A. F. Hebard, and A. G. Rinzler, “Transparent, conductive carbon nanotube films.,” *Science*, Vol. 305, No. 5688, pp. 1273–6, Aug. 2004.

[105] J. Kong, M. G. Chapline, H. Dai, F. C. Nanotubes, and M. H. Sensors, “Functionalized Carbon Nanotubes for Molecular Hydrogen Sensors,” *Adv. Mater.*, Vol. 13, No. 18, pp. 1384–1386, Sep. 2001.

[106] M. Jung de Andrade, M. Dias Lima, V. Skákalová, C. Pérez Bergmann, and S. Roth, “Electrical properties of transparent carbon nanotube networks prepared through different techniques,” *Phys. status solidi – Rapid Res. Lett.*, Vol. 1, No. 5, pp. 178–180, Oct. 2007.

[107] D. Cai, M. Song, and C. Xu, “Highly conductive carbon-nanotube/graphite-oxide hybrid films,” *Adv. Mater.*, Vol. 20, No. 9, pp. 1706–1709, May 2008.

[108] Y. Xu, H. Bai, G. Lu, C. Li, and G. Shi, “Flexible graphene films via the filtration of water-soluble noncovalent functionalized graphene sheets,” *J. Am. Chem. Soc.*, Vol. 130, No. 18, pp. 5856–5857, May 2008.

[109] K. S. K. S. Kim, Y. Zhao, H. Jang, S. Y. Lee, J. M. Kim, K. S. K. S. Kim, J.-H.

Ahn, P. Kim, J.-Y. Choi, and B. H. Hong, “Large-scale pattern growth of graphene films for stretchable transparent electrodes.,” *Nature*, Vol. 457, No. 7230, pp. 706–10, Feb. 2009.

[110] C. Li, Z. Li, H. Zhu, K. Wang, J. Wei, X. Li, P. Sun, H. Zhang, and D. Wu, “Graphene nano-‘patches’ on a carbon nanotube network for highly transparent/conductive thin film applications,” *J. Phys. Chem. C*, Vol. 114, No. 33, pp. 14008–14012, Aug. 2010.

[111] V. C. Tung, L. M. Chen, M. J. Allen, J. K. Wassei, K. Nelson, R. B. Kaner, and Y. Yang, “Low-Temperature solution processing of graphene-carbon nanotube hybrid materials for high-performance transparent conductors,” *Nano Lett.*, Vol. 9, No. 5, pp. 1949–1955, May 2009.

[112] Y. K. Kim and D. H. Min, “Durable large-area thin films of graphene/carbon nanotube double layers as a transparent electrode,” *Langmuir*, Vol. 25, No. 19, pp. 11302–11306, Oct. 2009.

[113] S. H. Kim, W. Song, M. W. Jung, M. A. Kang, K. Kim, S. J. Chang, S. S. Lee, J. Lim, J. Hwang, S. Myung, and K. S. An, “Carbon nanotube and graphene hybrid thin film for transparent electrodes and field effect transistors,” *Adv. Mater.*, Vol. 26, No. 25, pp. 4247–4252, Jul. 2014.

[114] I. N. Kholmanov, C. W. Magnuson, R. Piner, J.-Y. Kim, A. E. Aliev, C. Tan, T. Y. Kim, A. A. Zakhidov, G. Sberveglieri, R. H. Baughman, and R. S. Ruoff, “Optical, Electrical, and Electromechanical Properties of Hybrid Graphene/Carbon Nanotube Films,” *Adv. Mater.*, Vol. 27, No. October, p. n/a-n/a, May 2015.

[115] Z. Yan, Z. Peng, G. Casillas, J. Lin, C. Xiang, H. Zhou, Y. Yang, G. Ruan, A. R. O. Raji, E. L. G. Samuel, R. H. Hauge, M. J. Yacaman, and J. M. Tour, “Rebar graphene,” *ACS Nano*, Vol. 8, No. 5, pp. 5061–5068, May 2014.

Part One: Conductive Behaviour of Graphene/Carbon Nanotube and Graphene Oxide/ Carbon Nanotube Hybrid Materials

Chapter I-2 Experimental

2.1 Introduction

Although CNTs and graphene-based electrodes have been developed with outstanding properties, drawbacks are still noticeable using some methods. EPD method, for example, commonly produces unsatisfied CNTs film strength. CVD technique, on the other hand, is costly. Moreover, graphene-based electrodes need lots of labour work which is costly and time-consuming. Hence, there are still some restrictions in controlling CNT and graphene film to get the large scale quality and the massive quantity [1], [2]. Very recently, a simple and practical solution-casting method has been used to prepare the graphene-based electrodes [3]-[8].

The motivation after the previous researcher works is to develop a new approach whereby to combine the two different carbon allotropic (G and CNT) and to report on the electrical properties and conductive behaviour of graphene/CNT and graphene oxide (GO) / CNT hybrid materials. So, a water solution casting method was used to fabricate graphene-based hybrid materials films with various CNT contents. The understanding of the hybrid thin film structure was carried out through some advanced material characterization instruments which involve the Scanning Electron Microscopy (SEM), Transmission Electron Microscopy (TEM) and X-Ray Photoelectron Spectroscopy (XPS).

This chapter is structured as follows: Section 2.2 presents the materials used in the experiments. Section 2.3 gives the preparation of GO, G, G/CNT and GO /CNT hybrid film samples. Section 2.4 and 2.5 provides the characterization and the measurements of the hybrid film samples. A summary of this chapter is provided in Sections 2.6.

2.2 Materials

The materials used in this experiment were: expandable graphite (EG), which is the natural flake graphite that has been treated chemically with sulphuric acid, was purchased from China Qing Dao Graphite Company. Single-walled carbon nanotubes (SWCNTs), multi-walled CNTs (MWCNTs), and MWCNTs-OH (with hydroxyl groups 3-5 wt%) were purchased from Chengdu Institute of Organic Chemistry, Chinese Academy of Sciences. Concentrated sulphuric acid (H_2SO_4, 98%) and other materials like Potassium permanganate ($KMnO_4$), hydrochloric acid (HCl, 36-38%) and barium chloride ($BaCl_2$) that were used for oxidation of graphite were obtained from Fisher Ltd (UK).

2.3 Sample Preparation

2.3.1 Preparation of Graphene Oxide (GO)

Expandable flake graphite (EG) is a form of intercalated graphite in which the natural flake graphite has been treated chemically [9]. Inserted an intercalant material such as (sulfuric acid) between the layers of graphite crystals is called intercalation, which resulting in different cryptographic structure, electronic properties and density [9]. It has been reported that expandable graphite d-spacing can be increased by intercalation process and the expandable graphene can be able to expand in volume up to 100 times than the natural one at high temperature [10], [11]. Also, the new physical and chemical properties like increasing the surface area and edges size will allow much more functional groups to be introduced between the graphite layers which make the oxidization happens easier and at a faster rate and higher reactivity [11]. Thus, to prepare a powder of the GO from graphite, Hummer method was used [12]. 57.5 ml of concentrated H_2SO_4 was mixed with 2.5g of expandable graphite flake in an ice bath for 30 minutes. Then, a 7.5 g of $KMnO_4$ was added slowly to the mixture for keeping the temperature of the mixture below 20^oC. Then, using a water bath, the mixture was heated to (35 ± 3) ^oC with continuous stirring for about 30 minutes (before heating, the water bath was changed to oil one and the magnetic stirring to a mechanical one). 115 ml of distilled and dropwise water was added into the mixture which increased the temperature until 98 ^oC. Then the mixture was kept for 15 minutes at this temperature (the temperature can be adjusted by heating). To terminate the oxidation reaction, 25 ml

of 30% hydrogen peroxide solution (H_2O_2) in 350 ml of distilled water was added. Lastly, graphite oxide was collected by filtering and was successively washed with 5% HCl aqueous solution. HCl washing was repeated until there was no sulphate detected by the $BaCl_2$ solution. After that, GO was collected and dried for one week at 50^{o}C and under a vacuum. GO sheet was prepared by carrying out ultra-sonication of a concentrated dispersion of GO in water or acetone. Ultrasonic machine (Fisher scientific Sonic Dismembrator Model 500, 300 W) with a power of 300 W for 1h at room temperature was used to get a good dispersion mixture. Figure 2-1 shows digital pictures of expandable graphite /acetone and expandable graphite oxide /acetone dispersions.

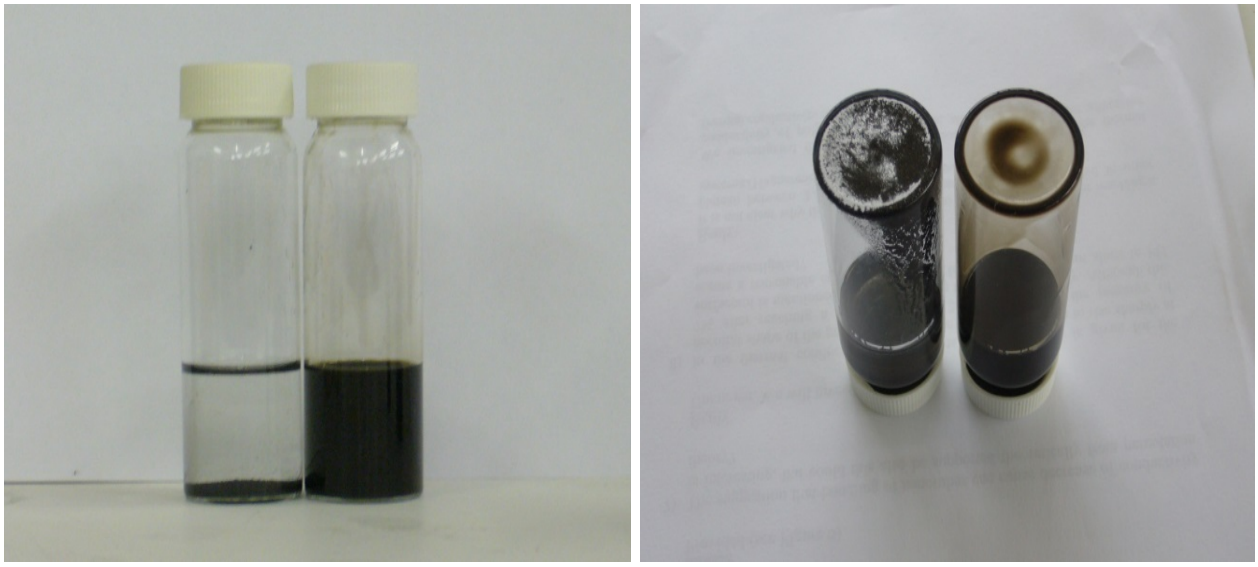

(a) (b)

Figure 2-1: (a) Digital pictures of expandable graphite /acetone (b) and expandable graphite oxide /acetone dispersions.

2.3.2 Preparation of Graphene

The used graphene was produced by mechanochemical method [13] from the expandable graphite in the lab. The preparation of graphene procedure is as follows: The expandable graphite was mixed with powder melamine in volume ratios of 1:1 and 1:3 to produce some different combinations as shown in table 2-1. The mixtures were

dispensed into the de-ionised water to make suspensions with a concentration of 1g/100ml. Then, these suspensions were then heated up and kept at 80°C for 1 hour with constant stirring. This is to allow the melamine to fully penetrate and expand the graphite spaces. Later, the suspensions were filtrated and dried for five hours at 80°C. The dried mixtures then underwent ball-milling to exfoliate the graphite layers and then distributed in de-ionised water. Then, they underwent further exfoliation with sonication handling for 1 hour using the ultrasonic machine (Fisher scientific Sonic Dismembrator Model 500, 300 W). Finally, to remove the melamine, hot water was used repeatedly to wash the mixtures. The prepared graphene is presented in figure 2-2.

Figure 2-2: Digital picture of final graphene sample (Left) and dispersion of graphene with water (Right).

As shown in table 2-1, six specimens were made with different specifications of preparation.

Table 2-1: Preparation specifications for graphene specimens

Specimens	Graphite to Melamine Volume Ratio	Ball-milling Revolutions	Exfoliation Method	Exfoliation Time (hours)
A	1:1	1000	Ultrasonic	1
B	1:1	1000	Mechanical	4
C	1:3	1000	Mechanical	4
D	1:3	1000	Ultrasonic	1
E	1:3	1000	Mechanical	1
F	1:3	1500	Mechanical	4

2.3.3 Preparation SWCNT and MWCNT Suspensions

For starters, 100 mg of MWCNT was dissolved and dispersed in 20 ml of distilled water using first: the magnetic stirring for around five minutes, then the assistance of the strong ultrasonic of 300 W for 1 hour using the ultrasonic machine (Fisher scientific Sonic Dismembrator Model 500, 300 W). Also, the same steps have been followed to prepare the SWCNT and MWCNT-OH suspensions with 5 mg/ml concentration.

2.3.4 Preparation of Graphene Oxide /Carbon Nanotube (GO/MWCNT) (GO/SWCNT) and (GO/MWCNT-OH) Hybrid Thin Films.

Preparation of (GO)/CNT) hybrid thin films: GO/distilled water dispersion was obtained via ultrasonic treatment for 30 min at room temperature. Each of SWCNTs, MWCNTs, and MWCNTs-OH was dissolved also in distilled water. The ultrasonic machine (Fisher scientific Sonic Dismembrator Model 500, 300 W) was used to conserve a good distribution of CNT in the solution. Then, the dispersion solution of the G/distilled water and SWCNTs, or MWCNTs, or MWCNTs-OH/distilled water were mixed. Different concentration can be reached by controlling the volume of the GO and CNT. All the mixtures were then treated by ultrasound separately for another 30 mins. After this, each mixture was dropped on a coverslip placed in a glass container as in figure 2-3. The

hybrid thin films were coated on the coverslips. The thickness of the films was controlled by the volume of the mixture dropped on the cover slip. The coated hybrid films were obtained after drying for one day at 40 °C and then in a vacuum oven at 60 °C for 3 days as shown in figure 2-4.

Figure 2-3: Digital picture of the samples of GO/MWCNT after casting.

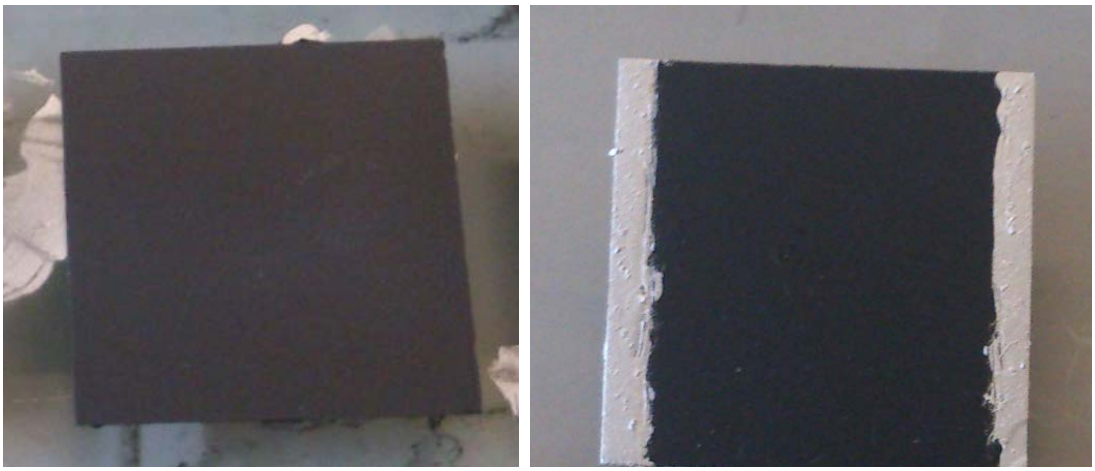

Figure 2-4: Digital picture of the sample of GO/MWCNT at final stage after drying and before measurements.

2.3.5 Preparation of Graphene /Carbon Nanotube (G/MWCNT) (G/SWCNT) and MWCNTs-OH Hybrid Thin Films.

Preparation of G /CNT hybrid thin films: Similar to GO/MWCNT preparation, G /distilled water dispersion was obtained via ultrasonic treatment for 30 mins at room

temperature. SWCNTs, or MWCNTS, or MWCNTs-OH was also dissolved in distilled water. With the assistance of ultra-sonication using (Fisher scientific Sonic Dismembrator Model 500, 300 W), a high degree of dispersion and distribution of carbon nanotubes was achieved. Then, the dispersion suspensions of the G/distilled water and SWCNTs, or MWCNTs, or MWCNTs-OH/distilled water were mixed. Different suspensions concentrations were obtained by controlling the volume of G and CNT used. All the mixtures were then treated with ultrasonic machine separately for another 30mins. After this, each mixture was dropped on a cover slip placed in a glass container as in figure 2-3. The hybrid thin films coated on the coverslips and the thickness of the films was controlled by the volume of the mixture dropped on the cover slip. The coated hybrid films were obtained after drying for one day at 40 °C and then in a vacuum oven at 60 °C for 3 days as shown in figure 2-5.

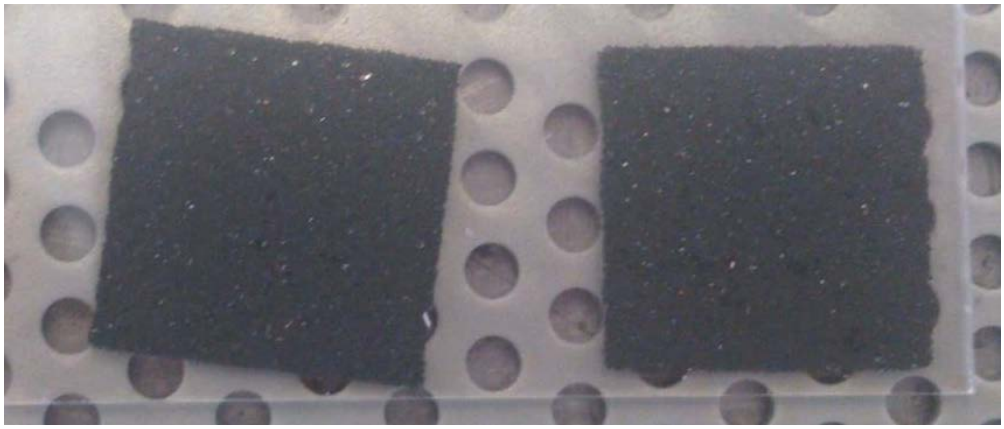

Figure 2-5: Digital picture of the G/MWCNT Film.

2.3.6 Preparation of G, SWCNT, and MWCNT, MWCNT-OH Suspensions

Repeating the same procedure with graphene but this time with acetone, 100 mg of graphene was dissolved in 20ml of acetone to get 5mg/ml concentrated suspension. Then, using the ultrasonic machine (Fisher scientific Sonic Dismembrator Model 500, 300 W) for a strong sonication of 300 W for one hour at room temperature, a stable dispersion of G in acetone was obtained. The next step was the dissolving of 100mg MWCNT in 20 ml of acetone. The MWCNT was dispersed using the magnetic stirring for around five minutes and then the ultrasonic machine of 300 W for 1 hour. The same procedures have

been followed to prepare the SWCNT and MWCNT-OH suspensions with 5 mg/ml concentration.

2.3.7 Preparation of Graphene /Carbon Nanotube (G/MWCNT) (G/SWCNT) and MWCNTs-OH Hybrid Thin Films.

The following step is the mixing of the dispersion G and CNT suspensions. This has been done with different percentage of CNT: G(40wt%)/SWCNT(60wt%), G(20wt%)/ MWCNTs-OH(80wt%), G(40wt%)/MWCNTs-OH(60wt%) , G(60wt%)/MWCNTs-OH(40wt%) and G (20wt%)/MWCNTs(80wt%), G(60wt%)/MWCNTs(40wt%), GO(80wt%)/MWCNTs(20wt%). As previously, the thickness of the hybrid film was adjusted by controlling the solution volume that is used during casting. After that, each mixture was treated by ultrasonic for 30mins. The casting has been done by pouring the solution on a glass coverslip inside with size of 18x18 mm and 22x22 mm, and 5 µm and 15 µm thicknesses. The coated hybrid films were obtained after drying for one day at 40 °C and then in a vacuum oven at 60 °C for 3 days.

2.4 Microstructure

2.4.1 Fourier Transforms Infrared Spectroscopy (FTIR)

FTIR spectroscopy is commonly used to investigate the material's chemical structure by measuring the frequencies of the molecules in that material [14]. As infrared radiations hit a material surface, some of the IR radiations are absorbed by the material and the other are transmitted through the material. This is due to the specific frequencies of molecules that rotate or vibrate corresponding to discrete energy levels (vibrational mode). These frequencies are unique for different molecules and can help to identify the complex functional groups in the substance.

FTIR spectra were recorded on Mattson 3000 FTIR spectrometer using transmission mode with a $4cm^{-1}$ resolution over 120 scans. Thin films of the samples were prepared on the KBr pellets. G, GO powders are grounded with KBr powders and pressed into thin films. FTIR spectra were recorded on a SHIMADZU FTIR-S400s spectrophotometer using ATR mode with a $4cm^{-1}$ resolution over 120 scans.

2.4.2 Raman Spectroscopy

Raman spectroscopy is the technique usually used in chemistry to identify molecules. It investigates the vibrational frequencies of molecules and provides spectroscopic fingerprints for each a material [15]. The principle of Raman spectroscopy is based on inelastic scattering of laser light. When it is interacting with the material, photons of the laser light are absorbed by the material and then emitted later on. Unlike the FTIR, the vibrational frequencies of molecules can be determined by the change in the frequency of the emitted photons in comparison with original monochromatic frequency. In FTIR, the vibrational frequencies of molecules are determined by the frequencies of infrared photons that are absorbed by a vibrating molecule.

In chapter I-3, Raman spectra of G and GO were recorded by scanning the 20-3000 cm^{-1} region with a total acquisition time of 3 mins on a Jobin Yvon Horiba high-resolution LabRam. Raman microscope system equipped with an optical microscope adapted to a double grating spectrograph and a CCD array detector. The laser excitation was provided by a Spectra-Physics model 127 helium-neon laser operating at 35 mW of 633 nm output. The laser power at the sample was nearly 8 mW and was focused to nearly 10μm. Calibration was carried out using the 520.5 cm^{-1} line of a silicon wafer. A spectrum of resolution of ~1 cm^{-1} was used. The sample can be scanned at glass substrate directly without any specific requirements for the sample preparation. Like graphite, three promising bands exist in the graphene Raman spectrum, the G band at 1582cm^{-1}, the 2D band at 2685cm^{-1} and the D band at 1350cm^{-1}. The G band shifts to lower energy when the layer thickness increases and can be used to distinguish between graphite and graphene. The layer thickness can be also determined by the 2D band. However, it presents in graphene but not in graphite [16].

2.4.3 Scanning Electron Microscopy (SEM)

As a type of electron microscopes, SEM is used for inspecting the topography of the specimens at a very high magnification for investigation of the topography and morphology, chemistry, crystallography and the orientation of the sample grains. Thus, cracks and fractured surfaces, bond failures, and physical defects on the die or package surface can be analysed by SEM. It works by scanning the sample with a high-energy electron beam emitted from an electron gun fitted with a filament cathode. The

interaction between the electron beam and the atoms of the sample generates a variety of signals that containing information. Secondary electrons and back-scattered electrons are two of them.

As secondary electrons mode is the most common imaging process, it is normally used to show morphology and topography of the specimen. Back -scattered electrons are elastically scattered from the specimen after electron beams interact with specimen atoms. It is well-known that stronger backscattering of electrons by heavy elements (high atomic number) than light elements (low atomic number). This results in a contrast between the areas with different chemical compositions in multiphase materials [17]. To produce the SEM image, the electron beam is swept across the area being inspected, producing many such signals. These signals of the topography being inspected are then amplified, analysed, and translated into digital images.

In this project, SEM images were taken by field emission gun scanning electron microscopy (FEGSEM) (LEO 1530VP instrument). The samples were fractured after gold coating. Then, they were placed on the specimen holder.

2.4.4 Transmission Electron Microscopy (TEM)

TEM is another common tool for the atomic level of material characterization. In principle, TEM detects the electron beam that passes through an ultra-thin sample to image the structure of the material. This electron has a significantly higher resolution than a normal light microscopy due to the small de Broglie wavelength of electrons. Basically, TEM image contrast is generated from the absorption of electrons in materials with the difference in the thickness and composition [18]. The traditional TEM is unsuitable for the characterization of monolayer graphene as the resolution at a low operating voltage is improper, while high voltage causes damage to the monolayer. Meyer et al. successfully resolved every carbon atom in the field of view by using aberration correction in combination with a monochromator, where 1Å resolution is achieved at an acceleration voltage of only 80 kV [19].

In this project, TEM analysis was conducted using a JEOL 2100 FX instrument. The GO and G dispersions were dropped on the copper grid for TEM imaging directly.

2.4.5 X-Ray Photoelectron Spectroscopy (XPS)

XPS is a spectroscopic technique that can quantitatively measure and characterise the chemical contents, the empirical formula of a pure material, and the chemical and electronic state of the element in the surface. The principle of XPS is to irradiate the sample with a beam of X-ray, which is in turn, causes the electrons to escape from the inner layer atoms. The energy spectrum of these electrons is recorded which reflects the electronic state of the material. To identify the electron, the binding energy of the electron (E_a) is specifically used which is in relation to its parent element and atomic energy level. The E_B of the emitted electrons can be determined by equation (2-1) as follows [20]:

$$E_B = E_{pho} - E_K - W \qquad (2\text{-}1)$$

Where E_{pho} is the photon energy,

W is the spectrometer work function.

In chapter I-3, XPS analysis of G and GO powders was performed on a VG ESCALAB 5 (VG Scientific Ltd., England) under 10^{-7} Torr vacuum with an AIKa X-Ray source using the power of 200 W.

2.4.6 Wide Angle X-ray Diffraction (WXRD)

X-rays are electromagnetic radiation with a short wavelength between $10^{-6}$and 10^{-10} cm. As X-ray photons interact with electrons in atoms, some photons from the radiation will be deflected away from their original pathway. The process is called elastic scattering if there is no energy loss by x-ray photons. However, some energy of X-ray photons may transfer into the electrons, these scattered x-ray photons will have a different wavelength from original photons. Thus, interference can take place among deflected waves and result in the distribution of intensity. Diffraction happens when the electromagnetic radiation interacts with the atoms arranged in a periodic structure i.e. (crystals) that results in sharp interference peaks called diffraction patterns. The crystal structures of a material can be determined by measuring the diffraction patterns. According to Bragg equation, the distance between crystals planes relates to the angles of incoming X-ray

beams [21]. The diffraction can be observed at some specific angles in an XRD spectrum, which provides the information of the crystalline structure in the material.

In chapter I-3, a Philip-X' Pert X-ray diffractometer (anode 40kV, the filament current 35 mA) with Nickel-filtered CuK_{α} (λ=0.1542 nm) radiation at a scan speed of 1^0/min for XRD analysis was performed.

2.5 Electrical Property

2.5.1 Measurement of the dielectric constant of GO/MWCNTs, GO/SWCNTs, and GO/MWCNT-OH Hybrid Films

The self-capacitance of the GO/MWCNT, GO/SWCNT and GO/MWCNT-OH hybrid films was measured using the programmable automatic RCL meter (Fluke PM6306) with SMD tweezers (Fluke PM9540/TWE). This was by scanning the voltage in (50 mV and 2V) and the frequency from (50Hz to 100 kHz) which are limited to the measuring range of the apparatus under AC condition. All the coverslips were painted with silver at two opposite edges in order to get steady readings. The tweezers were just touching the two painted edges during testing. The dielectric constant was calculated for each measurement.

The dialectic constant ($\mathcal{E}_r$) is

$$\varepsilon_r = \frac{\varepsilon}{\varepsilon_\circ} \tag{2-2}$$

Where; ε is the material permittivity and ε_o is the vacuum permittivity.

2.5.2 Measurement of the Resistivity of GO/MWCNTs, GO/SWCNTs, and GO/MWCNT-OH Hybrid Films

Fluke PM6306 has four-terminal sensing points that are used to amount the square resistance of a semiconductor material. This can be done by separating the current and the voltage electrodes which help to eliminate the contribution of wiring impedance and contacting resistance. As a constant current is passing through the outer probes, the voltage can be measured through the inner probes. Therefore, the electrical impedance of

the substrate R and capacitance can be measured. Each sample was painted with silver at two opposite edges in order to get steady readings during the test.

The resistivity in Ω.cm is reported using the equation:

$$\rho = \frac{\pi}{\ln 2}\, t\left(\frac{V}{I}\right) = 4.523t\left(\frac{V}{I}\right) \qquad (2\text{-}3)$$

Where t is the substrate thickness in cm. The conductivity is the resistivity inverse.

2.5.3 Measurement of dielectric constant of G/MWCNTs, G/SWCNTs, and GMWCNT-OH Hybrid Films

Similarly, programmable automatic RCL meters (Fluke PM6306) with SMD tweezers (Fluke PM9540/TWE) were used to measure the resistance and self-capacitance of the G/MWCNTS, G/SWCNTS and GMWCNT-OH hybrid films. The scanning voltage was (50 mV and 2V) with a frequency range of (50Hz to 100 kHz). The dielectric constant was calculated for each measurement using equation (2-2).

2.5.4 Measurement of Resistivity of G/MWCNTS, G/SWCNTS, and G/MWCNT-OH hybrid films

Fluke PM6306 has also been used to measure the resistance and to calculate the conductivity using equation (2-3).

2.6 Summary

High-performance electrodes were fabricated using (G)/MWCNT and (GO)/MWCNT with different contents of (MWCNT) and (MWCNT-OH) using a simple water solution casting method. Water casting solution technique was found to be not time or money consuming like any other techniques like CVD or EPD. The films were characterised using SEM, TEM, XPS, WXPD, and FTIR.

References

[1] B.-J. Yoon, S.-H. Jeong, K.-H. Lee, H. Seok Kim, C. Gyung Park, and J. Hun Han, "Electrical properties of electrical double layer capacitors with integrated carbon nanotube electrodes," *Chem. Phys. Lett.*, Vol. 388, No. 1–3, pp. 170–174, Apr. 2004.

[2] Y.-H. Li, Y. M. Zhao, M. Roe, D. Furniss, Y. Q. Zhu, S. R. P. Silva, J. Q. Wei, D. H. Wu, and C. H. P. Poa, "In-plane large single-walled carbon nanotube films: in situ synthesis and field-emission properties.," *Small*, Vol. 2, No. 8–9, pp. 1026–30, Aug. 2006.

[3] V. Jousseaume, J. Cuzzocrea, N. Bernier, V. Renard, V. Jousseaume, J. Cuzzocrea, N. Bernier, V. Renard, and F. Graphene, "Few Graphene layer / Carbon-Nanotube composite Grown at CMOS-compatible Temperature To cite this version :," *Appl. Phys. Lett.*, Vol. 98, p. 123103, 2011.

[4] D. H. Lee, J. E. Kim, T. H. Han, J. W. Hwang, S. Jeon, S.-Y. Choi, S. H. Hong, W. J. Lee, R. S. Ruoff, and S. O. Kim, "Versatile carbon hybrid films composed of vertical carbon nanotubes grown on mechanically compliant graphene films.," *Adv. Mater.*, Vol. 22, No. 11, pp. 1247–52, Mar. 2010.

[5] D.-W. Wang, F. Li, Z.-S. Wu, W. Ren, and H.-M. Cheng, "Electrochemical interfacial capacitance in multilayer graphene sheets: Dependence on number of stacking layers," *Electrochem. commun.*, Vol. 11, No. 9, pp. 1729–1732, Sep. 2009.

[6] J. Yan, T. Wei, Z. Fan, W. Qian, M. Zhang, X. Shen, and F. Wei, "Preparation of graphene nanosheet/carbon nanotube/polyaniline composite as electrode material for supercapacitors," *J. Power Sources*, Vol. 195, No. 9, pp. 3041–3045, May 2010.

[7] H. Wang, Q. Hao, X. Yang, L. Lu, and X. Wang, "Graphene oxide doped polyaniline for supercapacitors," *Electrochem. commun.*, Vol. 11, No. 6, pp. 1158–1161, Jun. 2009.

[8] S. Stankovich, D. a Dikin, G. H. B. Dommett, K. M. Kohlhaas, E. J. Zimney, E. a Stach, R. D. Piner, S. T. Nguyen, and R. S. Ruoff, "Graphene-based composite materials.," *Nature*, Vol. 442, No. 7100, pp. 282–286, Jul. 2006.

[9] S. Duquesne, M. Le Bras, S. Bourbigot, R. Delobel, H. Vezin, G. Camino, B. Eling, C. Lindsay, and T. Roels, "Expandable graphite: A fire retardant additive for polyurethane coatings," *Fire Mater.*, Vol. 27, No. 3, pp. 103–117, May 2003.

[10] F. Kang, T.-Y. Zhang, and Y. Leng, "Electrochemical behavior of graphite in electrolyte of sulfuric and acetic acid," *Carbon N. Y.*, Vol. 35, No. 8, pp. 1167–1173, 1997.

[11] F. M. Uhl, Q. Yao, H. Nakajima, E. Manias, and C. A. Wilkie, "Expandable graphite/polyamide-6 nanocomposites," *Polym. Degrad. Stab.*, Vol. 89, No. 1, pp. 70–84, 2005.

[12] W. S. Hummers and R. E. Offeman, "Preparation of Graphitic Oxide," *J. Am. Chem. Soc.*, Vol. 80, No. 6, pp. 1339–1339, Mar. 1958.

[13] W. Zhao, M. Fang, F. Wu, H. Wu, L. Wang, and G. Chen, "Preparation of graphene by exfoliation of graphite using wet ball milling," *J. Mater. Chem.*, Vol. 20, No. 28, p. 5817, Jul. 2010.

[14] Andrew Garton, *Infrared Spectroscopy of Polymer Blends, Composites and Surfaces*. 1992.

[15] J. R. Ferraro, K. Nakamoto, and C. W. Brown, *Introductory Raman Spectroscopy*. Academic Press, 2003.

[16] J. Hodkiewicz, "Characterizing Graphene with Raman Spectroscopy," *Whitepaper*, p. Application note: 51946, 2010.

[17] J. Goldstein, D. E. Newbury, D. Joy, and C. Lyman, *Scanning electron microscopy and x-ray microanalysis*. Boston, MA: Springer US, 2003.

[18] D. B. Williams and C. B. Carter, *Transmission electron microscopy: A textbook for materials science*. Boston, MA: Springer US, 2009.

[19] J. C. Meyer, C. Kisielowski, R. Erni, M. D. Rossell, M. F. Crommie, and A. Zettl, "Direct imaging of lattice atoms and topological defects in graphene membranes," *Nano Lett.*, Vol. 8, No. 11, pp. 3582–3586, 2008.

[20] J. F. Watts and J. Wolstenholme, *An introduction to surface analysis by XPS and AES*. J. Wiley, 2003.

[21] C. Suryanarayana and M. G. Norton, "X-Rays and Diffraction," in *X-Ray Diffraction*, Boston, MA: Springer US, 1998, pp. 3–19.

Part One: Conductive Behaviour of Graphene/Carbon Nanotube and Graphene Oxide/ Carbon Nanotube Hybrid Materials

Chapter I-3 Characterization of Graphene, Graphene Oxide, Graphene/Carbon Nanotube and Graphene Oxide /Carbon Nanotube Hybrid Films

3.1 Introduction

Graphene (G) and carbon nanotubes (CNTs) hybrid films have been already fabricated to be used as electrodes. The high-performance TEs and FETs have been reported by Kim et al. [1] using single wall (SWCNT)/ (G) hybrid films. The sheet resistance of the thin hybrid film has reached 300Ω/m with 96.4% transparency. Simple and practical solution-casting method has been reported recently to be used in preparing the graphene-based material electrodes [2]-[4].

In this chapter, the characterization results of the fabricated GO, G, G/CNT and GO/CNT films using the water casting method will be discussed. Then, the quality of these thin films will be investigated**.**

3.2 Results and Discussion

3.2.1 Characterization Graphene Oxide (GO)

The synthesis of a functionalized graphene (graphene oxide) by Hummer's method is always considered as an oxidation reaction in which the graphite is oxidized by the potassium permanganate. The characterization results of the prepared GO are as follows:

3.2.1.1 FTIR of GO

FTIR spectrum of GO is shown in figure 3-1.

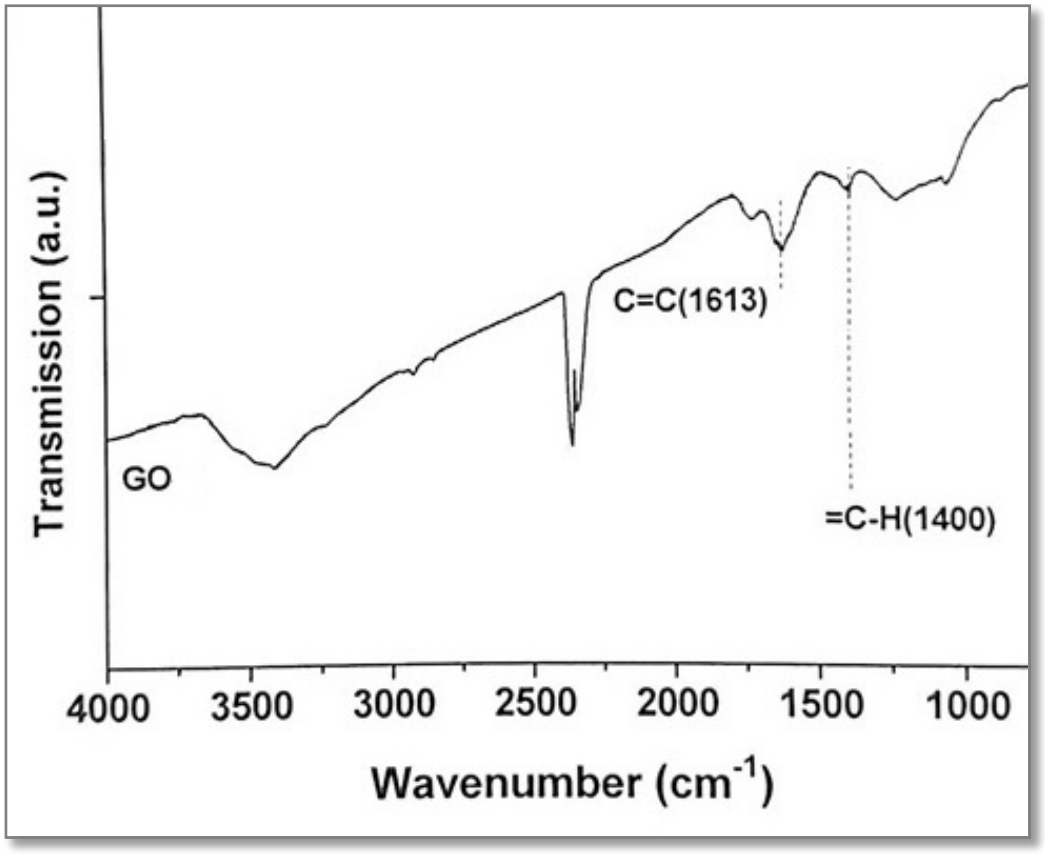

Figure 3-1: FTIR of GO.

This FTIR was applied to give some analysis about the chemical components of the sample. This spectrum has shifted in parallel for clarification. A very intensive peak has been detected in the GO spectrum between 2400 cm^{-1} which could be from the presence of CO_2 in the surrounding testing environment. The characteristic bands were detected at 3420cm^{1}, 1745 cm^{-1}, 1250 cm^{-1} in (-OH),(C=O) and (C-O-C) respectively which showed that hydroxyl, epoxide and carboxyl (-COOH) groups are the main functionalized groups of the 2D graphene sheets.

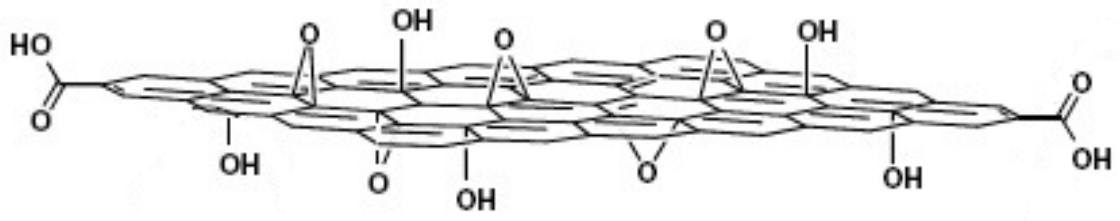

Figure 3-2: Chemical structure of graphene oxide [5].

Also, from the chemical structure of the GO in figure 3-2, additional functional groups presented as listed in table 3-1 which exposing the vibration of the aromatic ring in graphene.

Table 3-1: FTIR spectrum analysis of GO.

Peak position of =C-H/ cm^{-1}	1400
Peak position of C=C/ cm^{-1}	1613
Content ratio of (=C-H)/(C=C)	0.23

3.2.1.2 XPS of GO and Graphite

The XPS of graphite and GO are illustrated in figure 3-3 and their elements content are listed in table 3-2. It shows the massive increase of the Oxygen from (4.3 to 26.3) %, while the carbon content declines from (95.7 to 71.2) % and this accordingly matches the oxidation reaction effects which confirms that oxidation of EG was successfully conducted by the Hummers method. Some elements such as nitrogen, silicon and sulphur were found as a contamination from different sources in the GO sample.

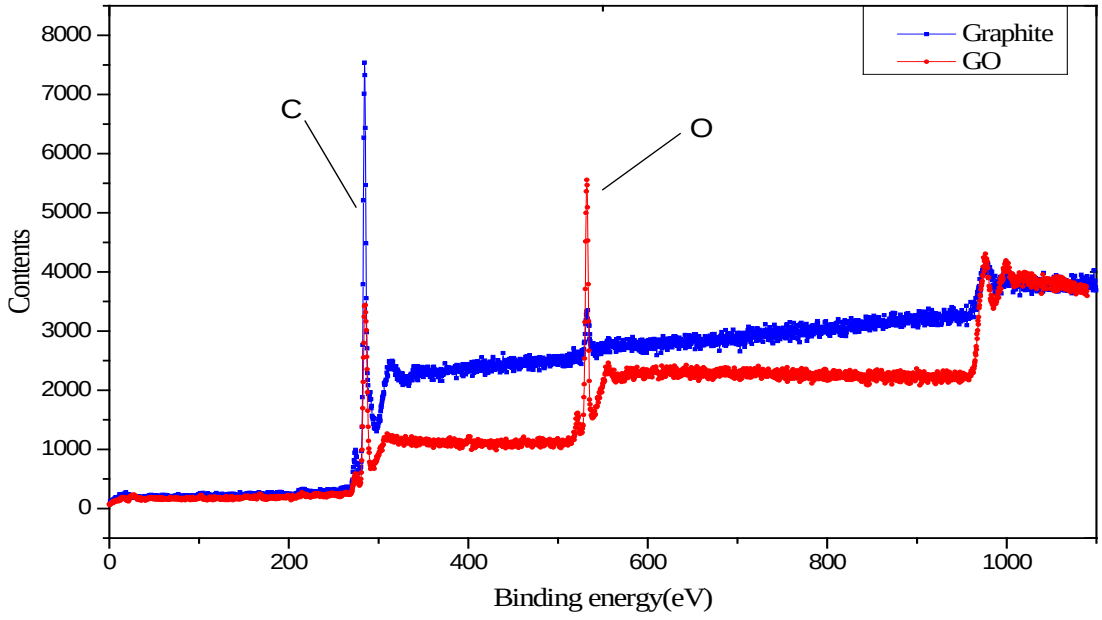

Figure 3-3: XPS plots of the contents of graphite and GO flakes synthesized by the Hummers method.

Table 3-2: Graphite and GO spectrum elements.

Sample	C	O	N	Si	S
Graphite Powder (%)	95.7	4.3	-	-	-
GO (%)	71.2	26.3	0.8	1.1	0.6

3.2.1.3 C1s XPS of Graphite and GO

The C1s XPS spectra of graphite and GO are demonstrated in figure 3-4 (A) and (B) respectively. Alternatively, this can similarly confirm the degree of oxidation which clearly can be seen from figure 3-4 (A). The C1s XPS spectrum of graphite splits into two peaks locating at 284.6 eV and 287 eV, respectively. These are the representative peaks that are attributed to carbon atoms with different functional groups such as non-oxygenated C, in the sample, with 284.6 eV and the carbon atoms in its C-O bond state. Similarly, the C 1s XPS spectrum of GO is divided into three peaks (284.6eV, 287eV, and 288eV). Those peaks are attributed to carbon in the non-oxygenated ring C, the C in C-O bond and carbonyl C in C=O bond correspondingly. Moreover, the weight percent of non-oxygenated C in GO was calculated to be (58%) while it is (90.1%) in graphite, which is also an oxidation indication.

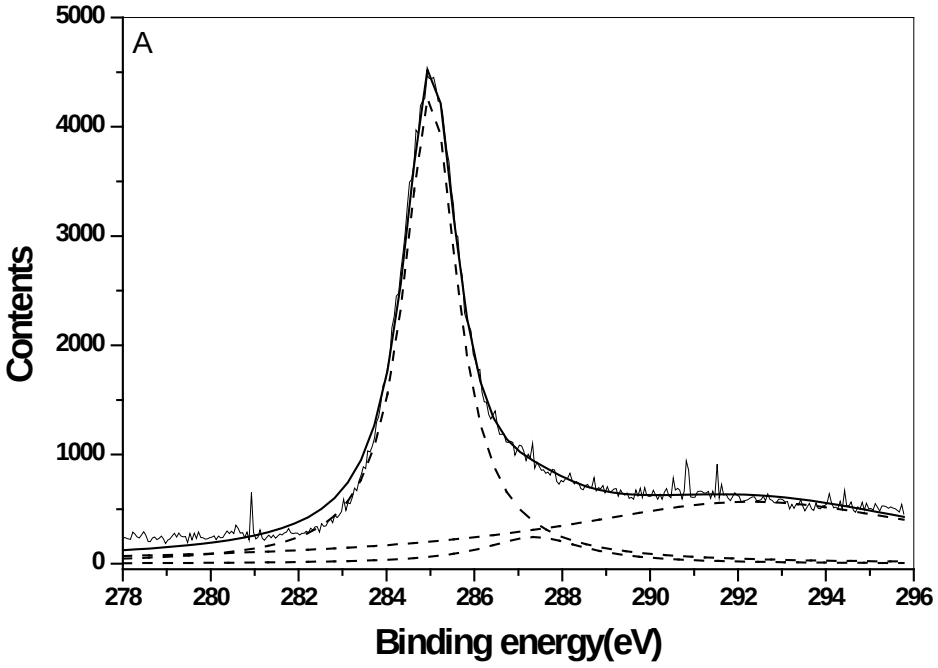

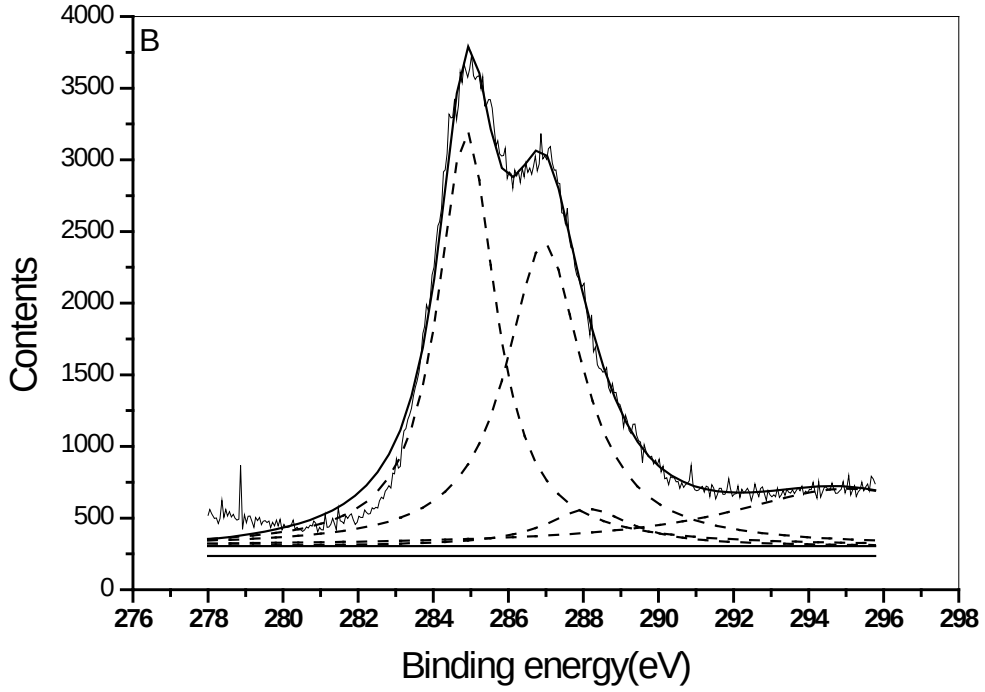

Figure 3-4: C 1s XPS spectra of Graphite (A) and GO (B).

3.2.1.4 Transmission Electron Microscopy (TEM)

TEM was employed to observe the existence of the GO in water. Since the presence of the functionalized groups can increase the sample hydrophilicity that makes the energy between graphite sheets decreases, the exfoliated GO in water can be occurred with the assistance of ultrasonic treatment, as shown in figure 3-5 and figure 3-6.

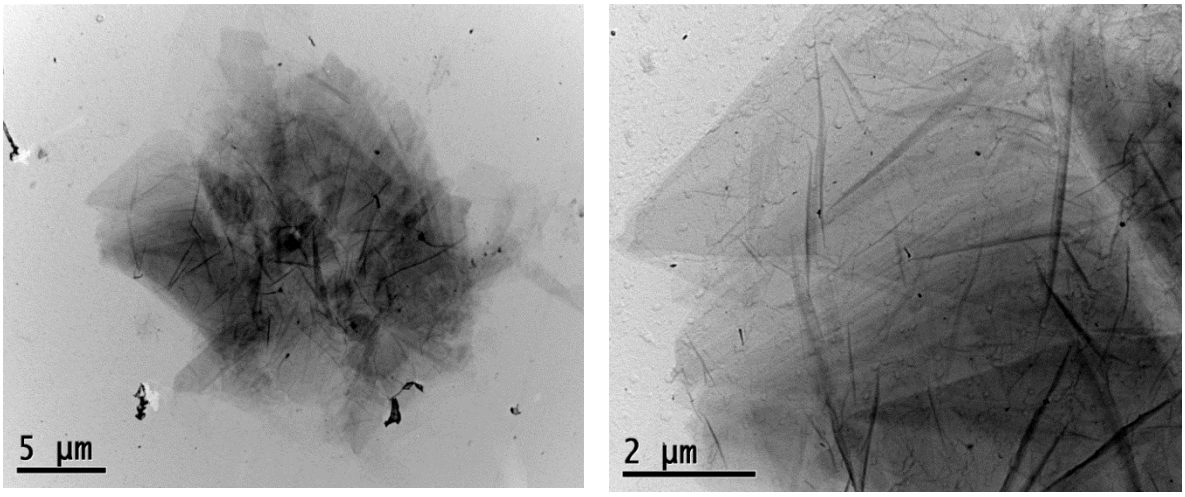

(a) **(b)**

Figure 3-5: TEM images of exfoliated GO flakes in distilled water with (a) low magnification and (b) higher magnification

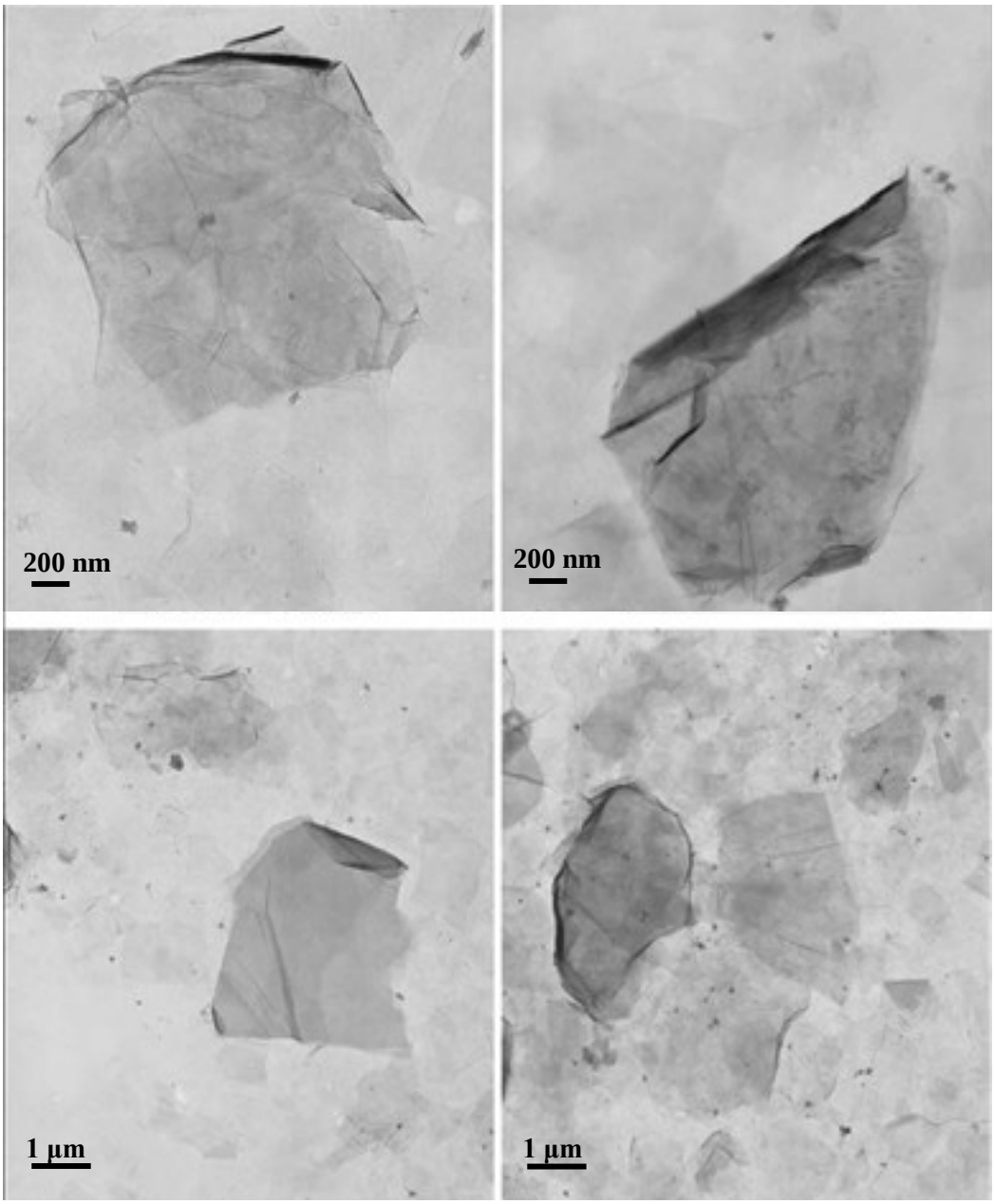

Figure 3-6: TEM images of GO.

It can be seen that the graphite oxide is fully exfoliated into the GO by ultrasonic treatment. In the TEM images, the thickness of the GO cannot be exactly measured but from the folded edge of the GO in the high magnification TEM images, the thickness of the GO can be estimated to be several nanometers. Interestingly, the structure of exfoliated GO is observed as well in TEM images. Since the edge of the GO layers is observed to be folded, the toughness of the GO is confirmed to be extremely high. Conversely, the wrinkled surface structure in the GO sheets can be clearly observed. This may affect the resulted film mechanical properties.

3.2.1.5 High-Resolution Transmission Electron Microscopy (HRTEM)

HRTEM technique was used to study the graphene-layered structure. Based on different GO edges observation, there were between 2 to 5 layers in each sample while the thickness was around 1 nm. Figure 3-7 illustrates the layer structure of the used GO.

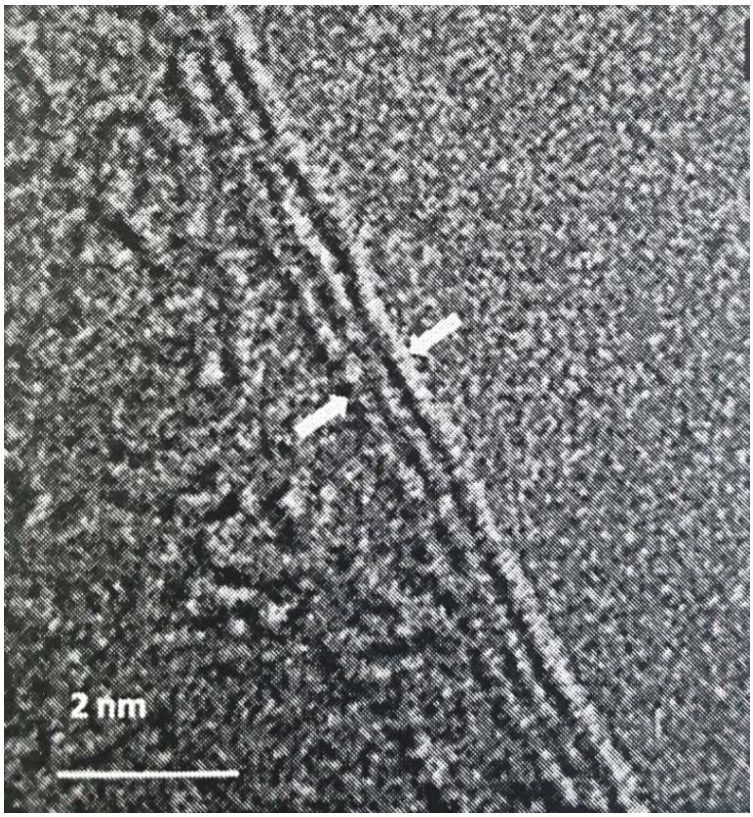

Figure 3-7: HRTEM image of a GO sheet edge.

Figure 3-8 shows the X-ray diffraction pattern of expanded graphite (EG) and the prepared graphene oxide specimens. It is clear that a distinctive peak presented the flake graphite at approximately at $2\Theta = 26^{\circ}$ which represents the crystallographic direction of graphite crystal (002) with a theoretical d spacing of 3.354 Å [6]. This peak is the strongest at the graphite standard XRD spectrum besides the other peak at about $2\Theta=10.9°$ corresponding to the (001) plane reflection of graphite oxide. The graphene oxide sample still retains the multi-layered structure of graphite, however, the GO peaks were found to be with lesser intensity compared to that of graphite oxide one which indicates that exfoliation disrupted the layered structures. Thus, effectively, with the lesser intensity of the (002) peak, the lesser layered structure is reserved and

better exfoliation is achieved. Although the assumption that graphene is present instead of graphite can be made, the average number of graphene layers cannot be precisely defined by XRD.

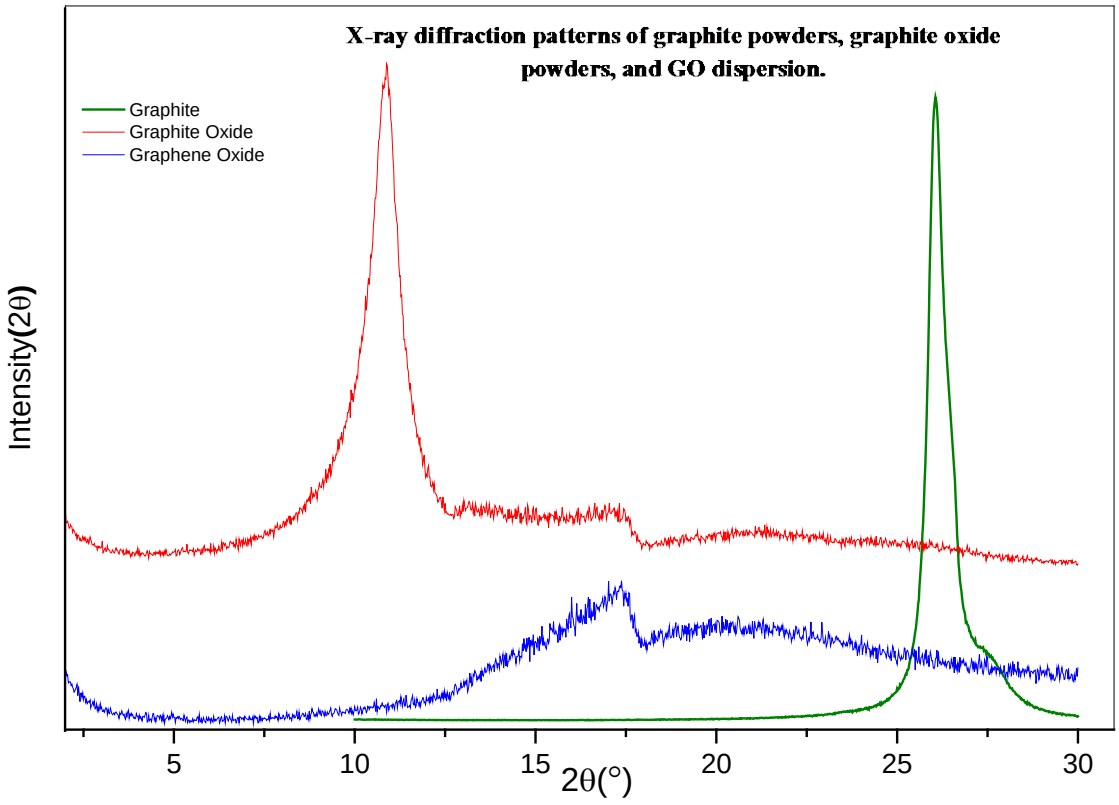

Figure 3-8: X-ray diffraction patterns of graphite powders, graphite oxide powders, and GO dispersion.

3.2.2 Characterization of Graphene

3.2.2.1 X-ray Diffraction

Exfoliation procedures effectiveness of graphite flake was determined by X-ray diffraction scans (XRD) on the D2 phaser (Brunker Corporation) from 1° to 30° (2Θ) with a step size of 0.02°. The spectra are illustrated in figure 3-9 and the peaks specifically in figure 3-10. The peak intensity in figure 3-9 (for samples A and D) shows them the weakest among others. This indicates that A and D have the lower numbers of layers that come from the higher level of exfoliation. since A and D samples are the only samples went through sonication exfoliation, thus, sonication could be much more

effective than the mechanical method in terms of exfoliating expanded graphite layers. Moreover, despite the different volume ratio of the graphite-melamine for the two mixtures (1:1 and 1:3 for sample A and D respectively), the peak intensity for both of them has a similar magnitude.

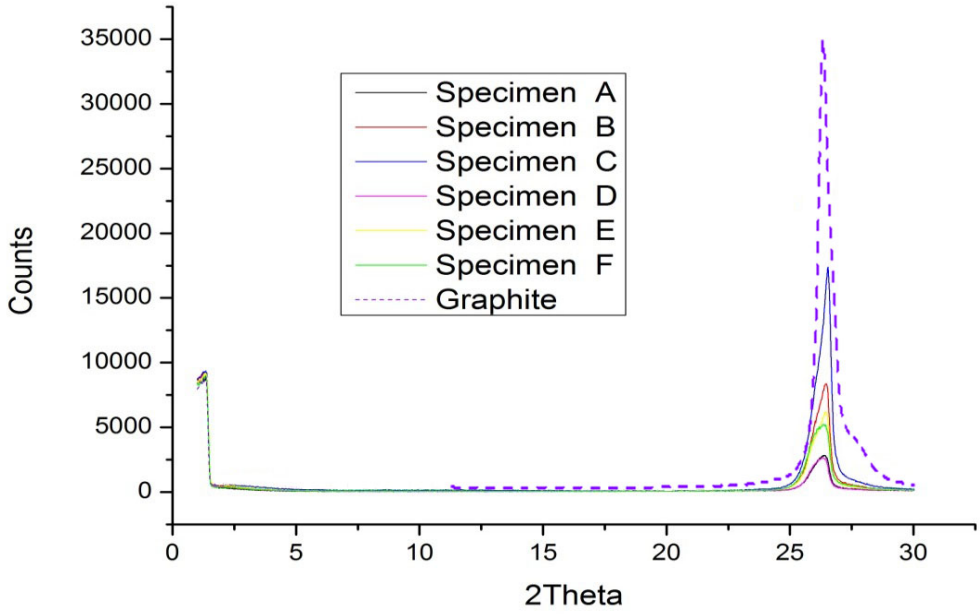

Figure 3-9: XRD spectra for the specimens and pristine graphite

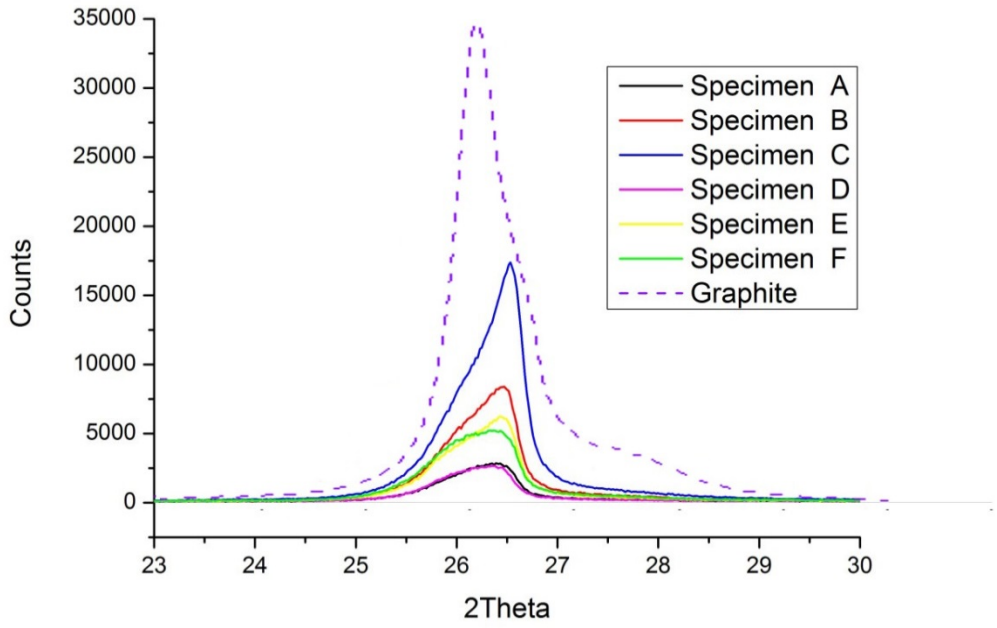

Figure 3-10: XRD spectra for the specimens and pristine graphite, from 2Θ= (23° to 30°).

As a result, the rise of melamine ratio does not contribute to the exfoliation of graphene layers in sonication method. Thus, using a higher percentage of melamine could increase the difficulty in the removal of the small molecules before the final stage of preparation which may reduce graphene purity and performance.

On the other hand, while the more milling revolutions and extended stirring had been considered as beneficial for exfoliation, the highest XRD peak intensity of sample C was indicated for ineffective exfoliation. Comparing it with sample E, it can be seen that underwent 4 hours of mechanical stirring for sample C instead of 1 hour as in sample E will not result in a well-exfoliated sample. Not even with extra 500 revolutions of ball-milling as comparing with sample F.

Apart from experimental errors that may occur during mixing graphene with melamine, there is also the possibility that mechanical stirring has no effect at exfoliating graphite. From the XRD peaks of specimens B and E, it can be seen that specimen B with extended stirring was, unexpectedly, less exfoliated. Therefore, it is possible that mechanical stirring does not largely affect the exfoliation of graphite for 1 hour. Nevertheless, independent of such speculations, the conclusion is that the mechanical stirring was much less effective compared to the sonication method.

3.2.2.2 Morphology by TEM

The graphene flakes morphologies were observed and characterized under the JEM-2000FX transmission electron microscope (TEM) (JEOL Limited. Figure 3-11 to figure 3-15 are the TEM images of selected graphene specimens. The low-magnification images of specimen A and F are shown in figure 3-11 and figure 3-12 respectively, are displaying a distribution of graphene flakes all over the image.

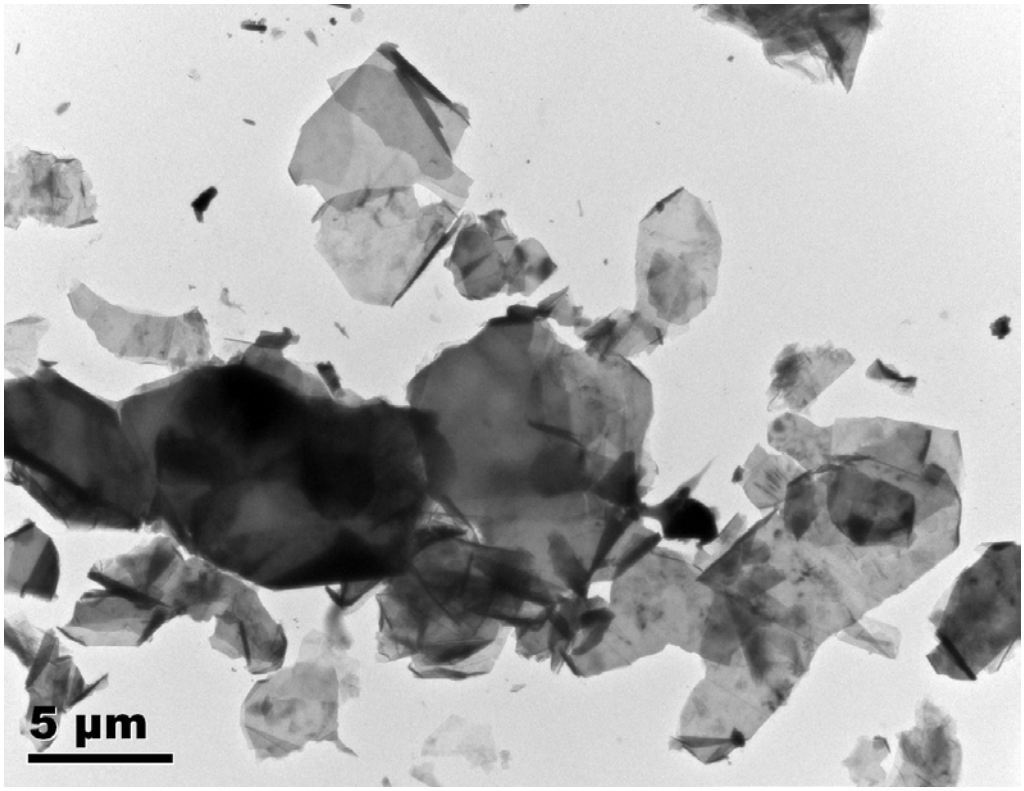

Figure 3-11: TEM image for specimen A.

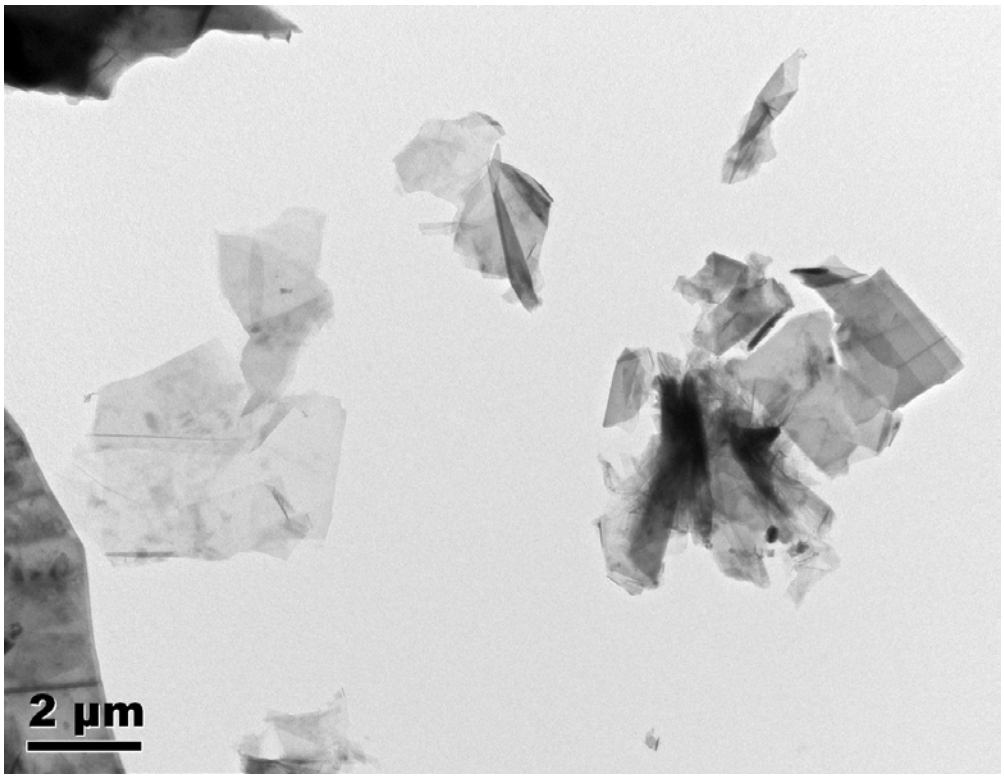

Figure 3-12: TEM image of graphene sample F.

Those flakes have variable thicknesses that were ranging approximately from 5 to 10 layers. They have different morphologies and their size varies from few microns to over 10 μm. Although the TEM image cannot provide a collective overview of the thickness and size distribution of the whole specimens, it can provide a general idea on the status of the prepared specimens.

It should be noted that while isolated graphene flakes were present, the number of flakes are overlapped or stacked together. Those are possibly resulting from incomplete exfoliation. This corresponds with the X-ray diffraction results, which shows that the current method of exfoliation may not be sufficient in producing dispersions with uniformly distributed flakes of fully exfoliated graphene. Therefore, extended sonication and mechanical exfoliation may be required, and possibly with higher intensity. On the other hand, excessive sonication may lead to the breaking down of graphene flakes [7].

Figure 3-13 shows the existence of small particles besides the graphene flakes. These could be the remains of graphene sheets that were broken down during the sonication process or mechanical stirring. This reduction in size can cause some changes in the specimen physical properties which may affect related applications. For example, as the length of graphene nano-ribbons reduced, thermo-conductivity decreased as well [8].

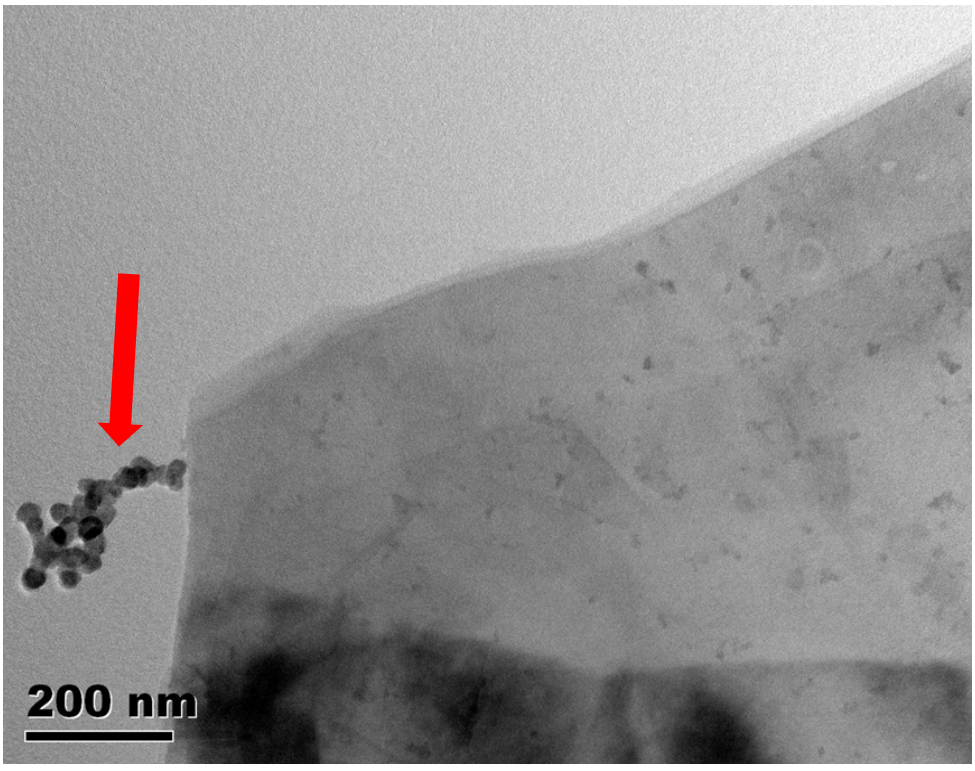

Figure 3-13: TEM image for specimen E. The impurities are indicated by the arrows.

Apart from incomplete exfoliation, the nature of graphene itself might cause this phenomenon. As the structure of single-layer graphene is a sheet with microns size or larger and thickness of a single atom, the specific surface area of graphene is considerable. This has combined with the strong van de Waals interactions between layers that cause the graphene flakes to possess the tendency to form aggregates [9]. The aggregation or restocking usually occurs in the graphene dry state and it is irreversible. It is effectively the reverse of the exfoliation process. Thus, the specific area of the graphene is reduced, causing losses in some application performance such as capacitance [10]. Since the graphene needs to be in a reasonable quality for electrical components usages such as electrodes, the aggregation, and the restocking effect should be prevented.

Regarding the chemical-mechanical approach, several methods have been suggested. Si and Samulski proposed an approach of graphene separation by applying platinum particles [11]. They deposited platinum nanoparticles on graphene flakes with reduction of chloric platinic acid. The metallic nanoparticles will prevent the layers from aggregating; while at the mean time they do not cause a reduction in electric properties. This method does not involve any special tool and only require reactions within water solution of graphene. Therefore, it is fully compatible with chemical-mechanical method. However, the cost will involve some extra metal nanoparticles price which may be unacceptable for commercial production.

Carbon nanotubes have been proposed as well to separate graphene layers. Cheng et al. used sonication in ethanol and vacuum filtration to produce graphene/carbon nanotube film [12]. The carbon nanotubes are positioned between the graphene layers in a direction parallel to the layers. As carbon nanotubes and graphene are of similar carbon nature, the nanotubes can provide enough conductivity while preventing the layers from restacking. While the interactions between the layers may affect the quality of the graphene prepared, it is also can be beneficial. As it can be seen from figure 3-14 and figure 3-15, the edges of the graphene flakes were folded and remained with this folded position because of the Van der Waals forces. These forces help to stabilize the layers against the elastic energies introduced by folding [13]. Zhang et al. have confirmed that high power sonication can produce graphene flakes with approximately ten layers, most of them with folded edges [14]. The presence of folded double or single layered graphene flakes has also been confirmed by TEM images that correlated with their

findings. Thus, while sonication may be detrimental in terms of morphology control, the folded graphene edges produced may become useful in certain applications.

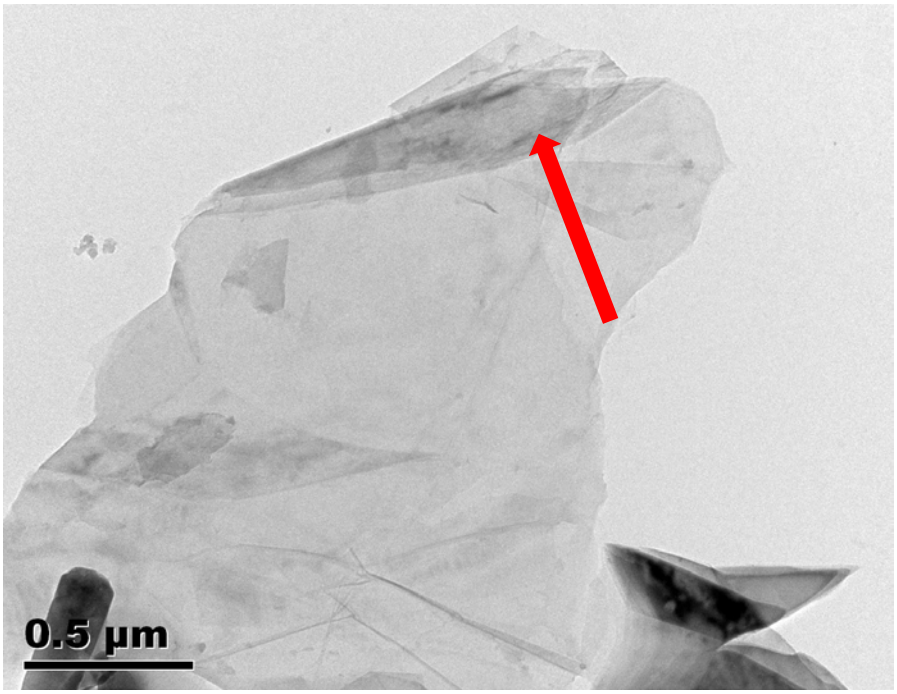

Figure 3-14: TEM image for specimen A. The folded edges are indicated by the arrow.

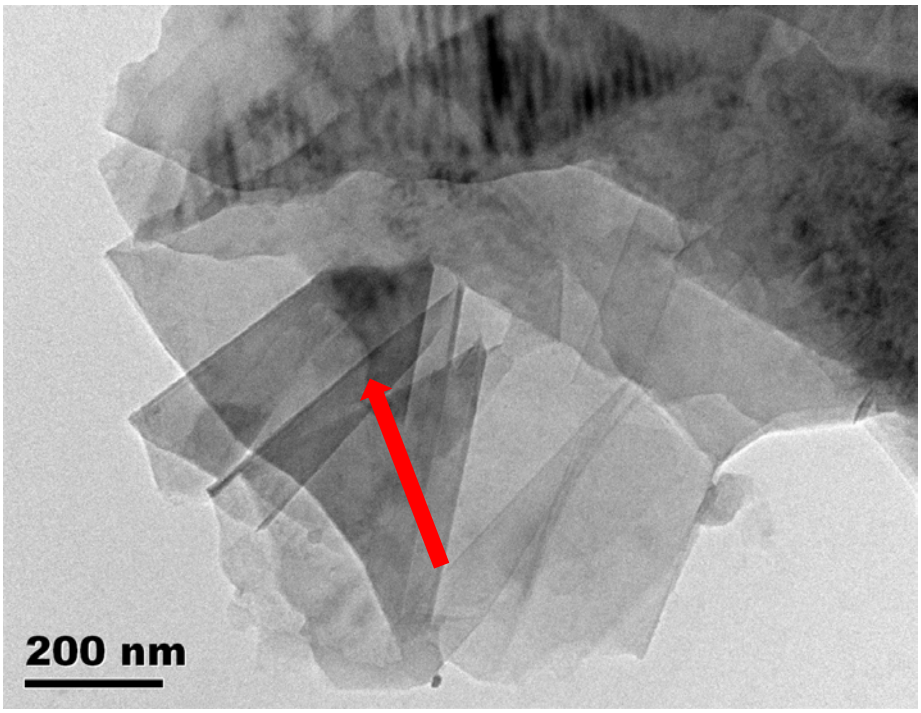

Figure 3-15: TEM image for specimen A. The folded edges are indicated by the arrow.

Figure 3-16, on the other hand, shows a set of parallel patterns that existed on some of the graphene flakes. This was suspected to be the crumpling of the flakes in the direction perpendicular to the surface of the flake. Such wrinkles of graphene have been reported before, however, the physics behind such phenomena is not yet completely known. These are thought to be related to the natural instability of graphene, where thermal fluctuations caused 2D crystalline structures to crumple in 3D space [15]. This effect is commonly seen in graphene prepared by methods such as CVD where transferring of graphene to another substrate is needed. The thermal stress involved with the thermos-expansion coefficient difference between graphene and metal substrates is believed to be the cause for the wrinkles [16]. Conversely, despite the absence of substrates, the flakes prepared by sonication or mechanical stirring still possess wrinkles. Suspended graphene flakes prepared by the micromechanical cleavage method are known to be not entirely flat [17]. In this case, the assumption is taken to make the exfoliation methods of higher intensity, such as ball-milling with subsequent sonication or mechanical stirring would surely create wrinkles on the product.

The presence of wrinkles, on the other side, may alter some of the graphene flakes properties, such as decreasing the carrier mobility [18] which might reduce the graphene effectiveness in electrical application. To control the formation of wrinkles, Wang et al. suggested that reducing the temperature can reduce wrinkling by stabilising the graphene flakes [19]. Increasing the layer number is another option to restrain individual graphene layers, hindering the formation of wrinkles. However, this will affect the final graphene properties. Thus, decreasing the temperature during the preparation of graphene is a realistic approach. Usually, the chemical-mechanical approach involves heat which coming from drying, ball-milling, and sonication. During the ball-milling stage, heat is generated by the kinetic energies related; this can be reduced by adding DMF during ball-milling. The common solvent can absorb the heat generated by vaporising, thus reduce the temperature within the mill. On the other hand, when ultrasound propagates through the liquid, a considerable amount of heat is generated. A simple water bath was used to compensate the heating. This can be improved by using ice bath which is exchanged regularly between sonication intervals or applying a circulating cooling system to the water bath. Also, the drying stage can be altered so that a lower temperature but longer dry time is applied.

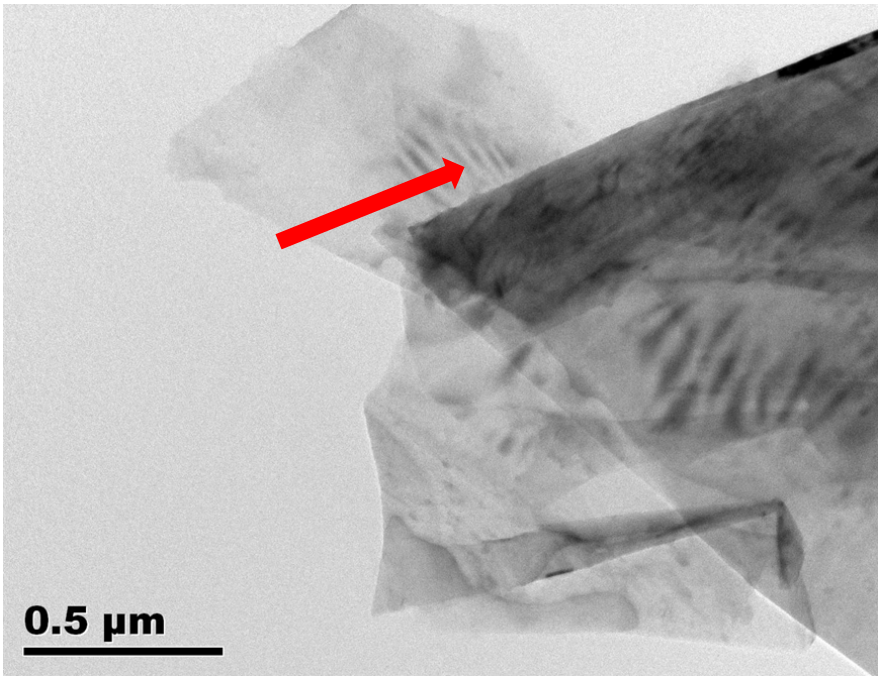

Figure 3-16: TEM image for specimen E. The wrinkles are indicated by the arrows.

Those unidentified particles that were shown previously in figure 3-13 and existed along with the graphene flakes are most likely to be the melamine added during the first stage of exfoliation. Although the hot water was used to wash the graphene flakes after sonication or mechanical stirring, complete removal cannot be expected. The purity of the specimens was further investigated by FTIR and wide-scan XPS in the next section.

3.2.2.3 Wide-Scan X-ray Photoelectron Spectroscopy XPS

Figure 3-17 illustrates the wide-scan XPS spectra of the specimen. There is a present of some elements beside the carbon that come from the graphene flakes as shown table 3-3. Those elements may come from different sources such as the substances that were added during the preparation of graphene. Moreover, the existing of impurities is predictable and some unwanted chemical contents may come from some experimental errors.

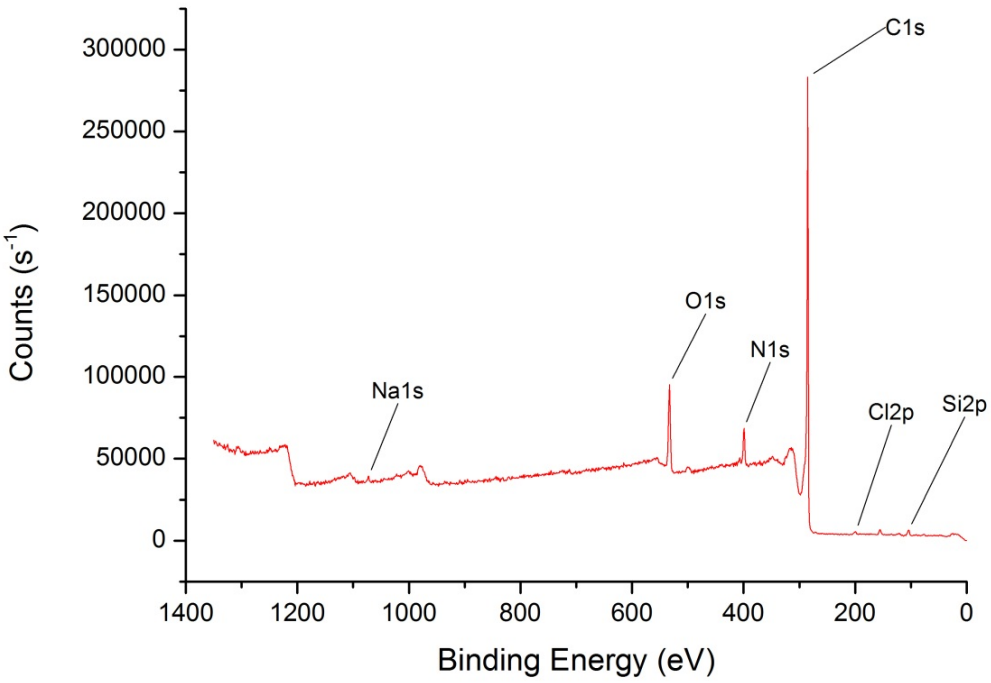

Figure 3-17: Wide-scan XPS spectra for specimen A.

Metallic contents such as calcium and magnesium were found within some of the specimens. This is likely to be in the form of salts. As the chlorine is found in every specimen, calcium chloride and magnesium chloride are commonly found in water, which may come from the various containers and equipment. The contamination of sodium is likely to be from sodium chloride. Another possible source of metallic particles is the surface of metal tools used during the production.

The silicone was found in every specimen but with various amounts. It might be related to the ball-milling process. Silicone is containing ceramic components that are commonly used within the ball-mill due to their hardness and abrasion resistance. Thus, contamination may occur to the specimens.

Nitrogen, on the other hand, was also found in all samples which varied from 2.59% to 8.97%. The absorption of nitrogen into the graphitic lattice is a well-known phenomenon; however, even with using nitrogen as a performance altering dopant, the solubility of nitrogen in graphene is believed to be as low as 2% [20]. In this case, as nitrogen impurities within the specimens were above this amount, extensive doping might be introduced.

Table 3-3: XPS determined atomic ratio of contained elements for each specimen

Element	**Atomic ratio (%) for each specimen**					
	A	B	C	D	E	F
C	84.33	77.32	81.34	73.55	80.08	83.14
O	8.77	12.11	9.55	12.21	9.62	10.72
N	4.5	6.95	5.93	8.97	6.39	2.59
Si	1.77	2.65	1.3	1.59	1.44	1.4
Na	0.28	0.46	0.18	0.3	0.23	-
Cl	0.35	0.51	0.37	0.5	0.52	0.73
Ca	-	-	0.53	1.15	0.76	0.65
Mg	-	-	0.55	1.34	0.96	0.54
S	-	-	-	0.38	-	-
P	-	-	0.24	-	-	-
Zn	-	-	-	-	-	0.24

The Fourier transform infrared (FTIR) spectra were done by the FTIR-8400S Fourier Transform Infrared Spectrophotometer (Shimadzu Corporation) with 4 cm^{-1} resolution over 64 scans to further investigation. There was a considerable oxygen amount within each specimen which is considered as a common impurity which could be from multi sources. One likely source for oxygen is the vapour absorbed by the specimen. There is also the possibility of getting oxygen containing ceramic particles or salts from equipment. Beside this contamination, attention must be paid to the oxidation of the graphene sheets. While the Hummers method makes extensive use of oxidizing agents to oxidize graphite, oxidation can occur to graphene without the presence of such agents. It has been established that after 200°C, graphene specimens with less than 3 layers would oxidize heavily, causing strong hole doping in the graphene sheets [21]. Thus, the temperatures that involved with the chemical-mechanical method were lower than 100°C.

Although the oxidation theoretically should not reach a considerable level, the possibility of oxidation does exist.

3.2.2.4 Infra-Red Spectroscopy

To analyze the structure of these compounds, infra-red spectroscopy was used. Infrared radiation (IR) is a form of electromagnetic radiation of slightly lower energy than visible light. When such radiation interacts with a covalent bond (has an electrical dipole), the energy is absorbed and the bond will start to oscillate. In fact, any vibration that causes a change in the dipole of the molecule should absorb IR radiation. IR spectroscopy measures this vibration of the atoms and based on this, the functional groups can be determined [22]. Therefore, IR spectrum of a chemical substance is the fingerprint for molecule identification. Summarized positions of these bands are shown in table 3-4.

The infra-red transmission spectra of the graphene A and B specimens are shown as examples in figure 3-18 and figure 3-19. The other specimens C to F spectra are with similar spectrum. It is clear from these figures that the peaks positions of each sample are similar to others but with variation in intensities. This might be due to the fact that graphene, in its powder state, is not the ideal material for IR examination. Potassium bromide is transparent from the range near to the ultraviolet to the long wavelength infrared without any significant optical absorption in this region. As the sample was simply grinding with powder KBr and placed inside a disk, the dark powder has a relatively low transmittance for visible light and IR, which increases the difficulty in the preparations of the KBr sample disc. In order to produce a KBr disc that is transparent, the amount of graphene powder was kept at a minimum, thus it was difficult to create complete homogeneous mixtures. Moreover, the nature of graphene also made it difficult to be fully ground, causing further inhomogeneity. Some wavy features can be seen in figure 3-18 and figure 3-19, especially after 3400cm^{-1}, this is due to the inhomogeneous nature of the prepared discs which had caused interference of the infra-red waves.

Comparing table 3-4 to figure 3-18 and figure 3-19, a broad peak at around 3421 cm^{-1} was present; this identifies the characteristic peak of –OH stretching, which confirms the presence of water within the discs. The peaks at around 1020cm^{-1} and 1060cm^{-1} were in the fingerprint region which might relate to C-O vibrations, indicating a possible oxidation.

Table 3-4: Functional groups absorbed at different and specific frequencies of IR radiation [23].

Bond type	**Frequency (cm^{-1})**
C-H alkane	2950 – 2850
C-H alkene	3080 – 3020
C-H aldehyde	~2900
C-H alkyne	~3300
alkyne triple bond	2250 – 2100 (s)
alkene double bond	1680 - 1620 (s)
carbonyl, ketone	1725 – 1700 (s)
carbonyl, aldehyde	1740 – 1720 (s)
carbonyl, ester	1750 – 1730 (s)
carbonyl, acid	1725 – 1700 (s)
carbonyl, amide	1690 – 1650 (s)
O-H, alcohol	3600 – 3200 (s, broad)
O-H, acid	3000 – 2500 (s, broad)
C-O, alcohol, ester, ether	1300 - 1000

The twin peaks that were found at around 2852cm^{-1} and 2924cm^{-1} are the stretching of -CH. The peaks at around 2314cm^{-1} and 2374cm^{-1} were assigned to the CO_2 fluctuations in the air. The C-C skeleton vibrations of the graphene carbon rings were found at around 669cm^{-1} and 777 cm^{-1}. The points 1385 cm^{-1}, 1580cm^{-1} and 1641cm^{-1}, where the later was hard to identify in figure 3-19 due to the neighbouring peak, were caused by the presence of melamine $C_3H_6N_6$.

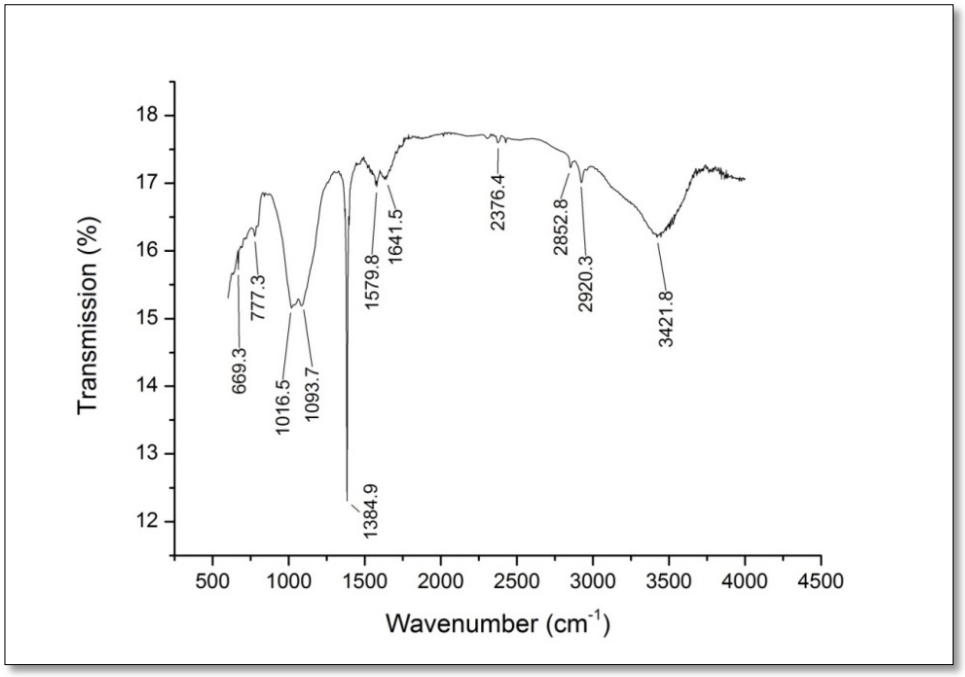

Figure 3-18: Infra-red transmission spectra for specimen A.

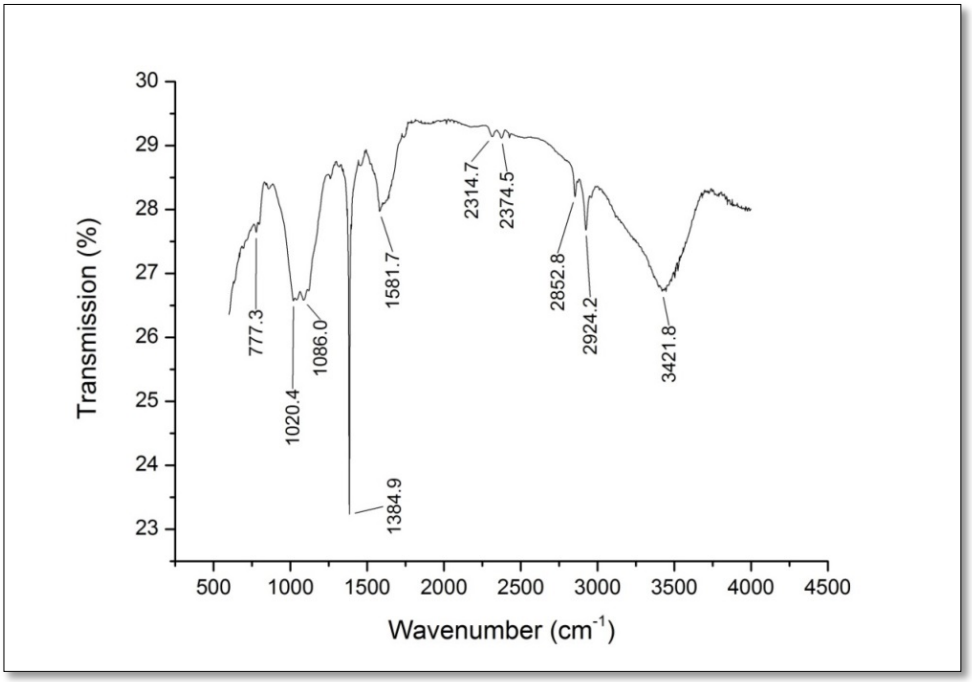

Figure 3-19: Infra-red transmission spectra for specimen B.

Despite the washing operations after sonication and stirring, the presence of melamine peaks confirms the results of wide-scan XPS that melamine was not completely removed from the graphene specimens. It is most likely to remain between the graphene galleries. This impurity may cause the deterioration of sample electrical performance.

The -CH peaks, on the other hand, were rather uncommon since the chemical content of graphene is predominately sp^2 hybridized carbon. Considering the structure of graphene, the zigzag and the armchair are two types of edge configuration with different magnetic and electronic properties as shown in figure 3-20 [35]. For both configurations, the carbon atoms at the edge of the layer possess only two C-C bonds, which would leave two free electrons. One of the free electrons forms π bond with free electrons from other carbon atoms. The other electron which is left forms C-H bond.

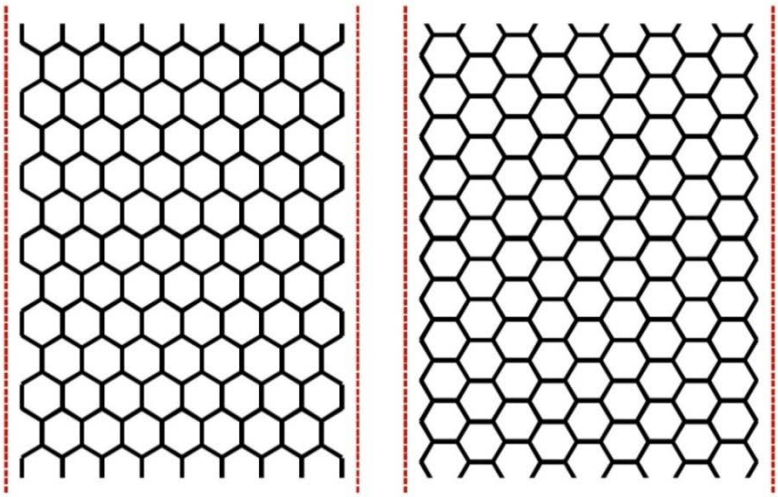

Zigzag **Armchair**

Figure 3-20: The zigzag and armchair configurations of graphene edges [24].

3.2.2.5 C1s X-ray Photoelectron Spectroscopy (XPS)

The C1s XPS spectra of graphene specimens A and B are illustrated in figure 3-21 and figure 3-22. It is clear that only a single peak at 284.68eV is visible for spectrum B while the spectrum of specimen A is splitting into four peaks which have located at 284eV, 285eV, 287eV, and 291eV. Despite the above, both A and B spectra are of a very similar shape, which shows that the specimens were identical in terms of the electronic state. Moreover, apart from the peak at 284eV, all three peaks found in figure 3-21 are in a very low intensity which leads to a limited contribution to the fitting peak. Vadahanmbi et al. revealed that the main peak at 284.6eV was attributed to the carbon atoms in non-oxygenated rings, which is the backbone of graphene [36]. Additionally, at 285eV, a weak peak for C-N bonds was spotted, which corresponded with the FTIR results, confirming the presence of residue melamine. The peak at 287eV represented the C-O

bonds which are an indication for oxidation. The peak at around 291eV is designated to the π - π^* configuration of sp^2 hybridized carbons.

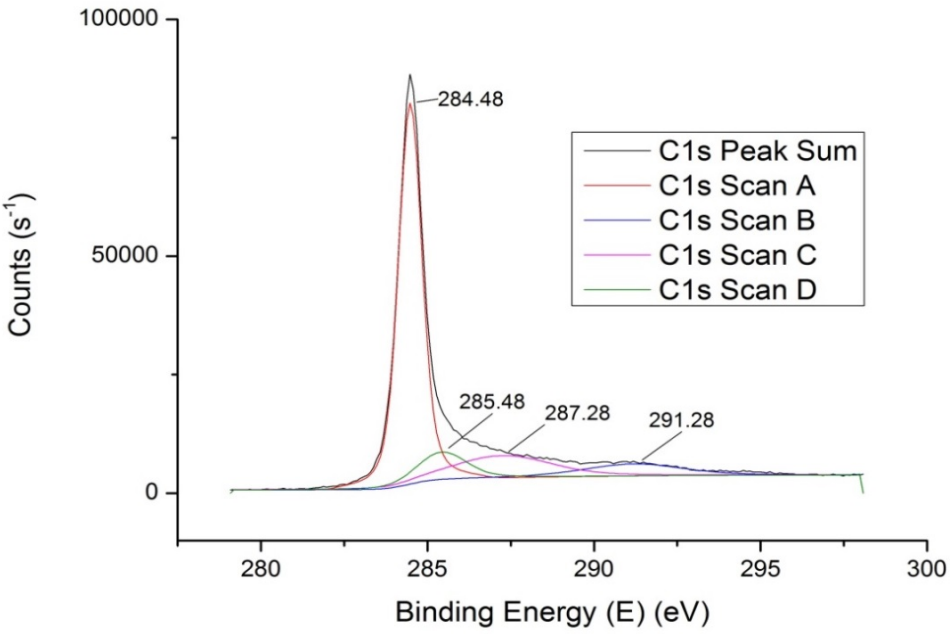

Figure 3-21: C 1s XPS spectra for graphene specimen A.

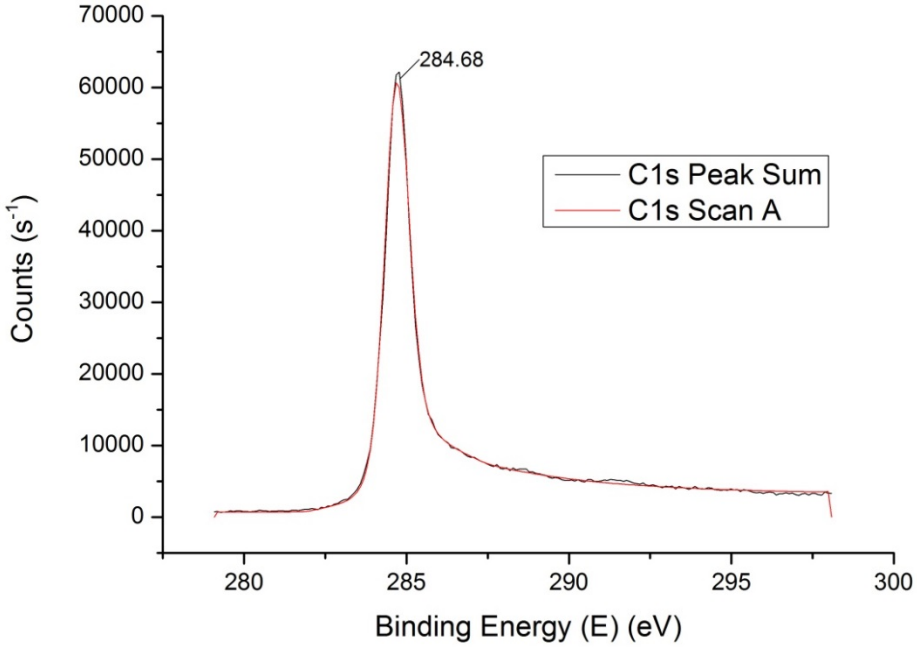

Figure 3-22: C 1s XPS spectra for graphene specimen B.

Thus, despite the existence of a minor level of oxidation in the specimen (A), graphene samples are generally not changed chemically. The oxidation process may change the carbon atoms in the graphene flake from sp^2 hybridized to sp^3 hybridized. In theory, these sp^3 hybridized carbons can cause a disturbance in carrier transport, forcing the carriers to hop over the sp^3 sites instead of near ballistic transport [37]. Hence, the conductance will be reduced. Since, there is no oxidizing agent deliberately added during the preparation, the only possible source of oxidation will be the heat involved during the drying process. The temperature used during drying was 80^oC, which is not exceptionally high for normal drying processes. Therefore, to reduce the chances of oxidation, lower temperature with extended drying time is suggested, which also can reduce the chance of wrinkling within the graphene layers.

3.2.3 Characterization of GO/MWCNT and GO/SWCNT and GO/MWCNT-OH Films

3.2.3.1 The Morphology of GO/GNT Hybrid Materials Using SEM

Figure 3-23 shows the cross-section SEM images for GO/MWCNTs and GO/MWCNT-OH hybrid films. These SEM images reveal the appearance of tilting layered structure in the thin films. This layered structure is well-arranged in where each the conductive CNT sandwich between two insulating layers of graphene oxide. This structure exhibits the information of the support of 2D graphene oxide for MWCNTs horizontally. GO layers act as strong holders to maintain the organization of the MWCNTs. Therefore; the film structure is conserved in a large area. This large contact area between CNTs and GO is able to store quite a lot of charges in the conductor's layers. As for energy storage, this layer structure exactly matches the nature of a capacitor. The GO sheets are just stacked as layers of insulators, while massive MWCNTs filaments are acting as conductors.

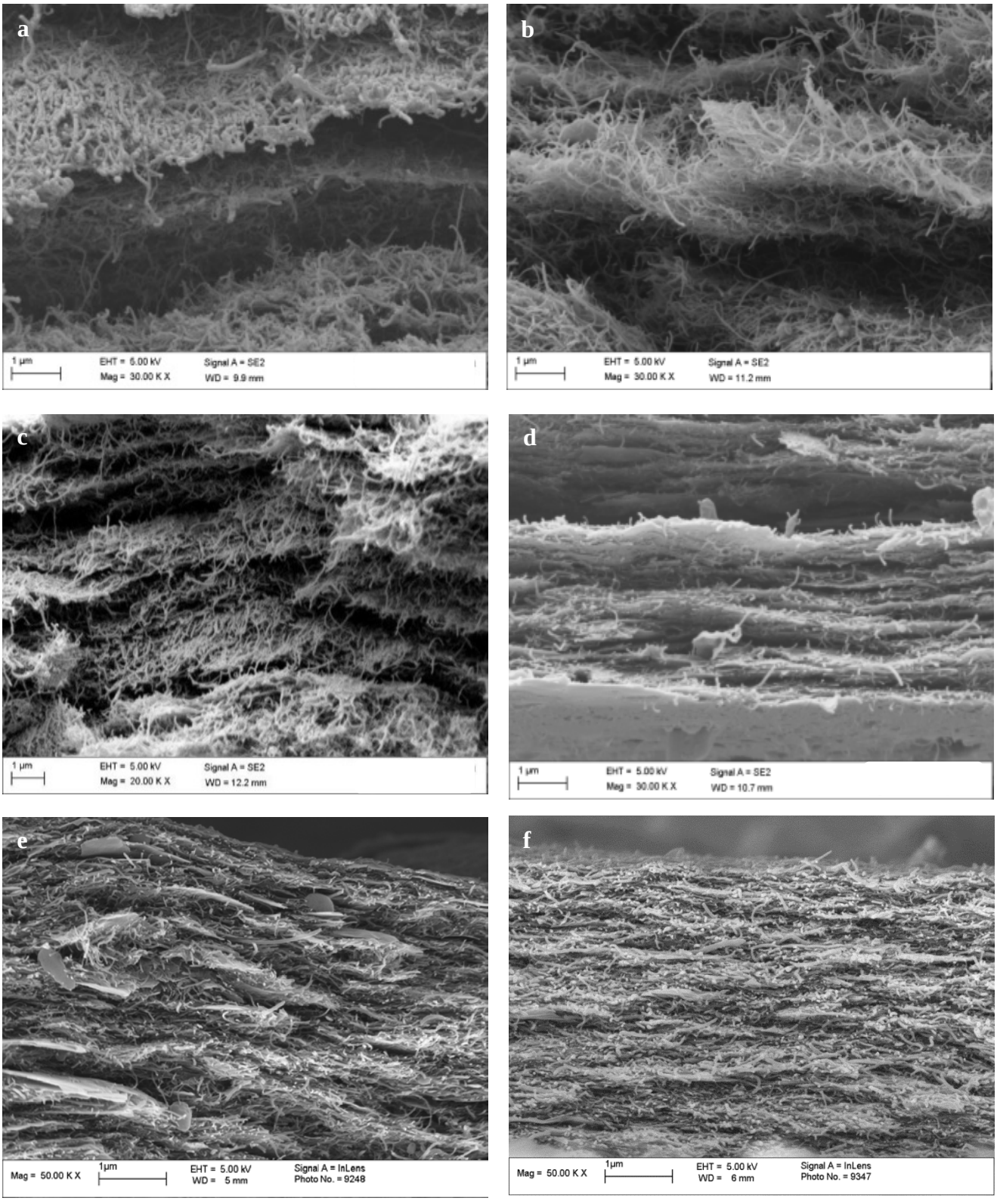

Figure 3-23: Cross section SEM images of the GO/CNT hybrid films. (a)GO(20wt%)/ MWCNTs (80wt%); (b) GO(40wt%) /MWCNTs (60wt%)); (c) GO(60wt%)/MWCNTs (40wt%); (d)GO(80wt%)/ MWCNTs (20wt%); (e) GO (50wt%)/MWCNT-OH (50wt%);(f) GO (50wt%)/MWCNT (50wt%).

The cross-sectional SEM images show that the morphology can be influenced by the quantity of each element in the film structure. As it is clear in figure 3-23, the images of GO (80 wt %) /MWCNTs (20wt %) has the smaller component of the MWCNTs in the film which is filled in between the GO layers. This forms a kind of straight layers that hold a smaller amount of charges than the one with GO (20 wt %) /MWCNTs (80wt %). The later has a fuzzy film structure that increases its capacitance to be capable of storing a high amount of charges.

On the other hand, It can be found that the layers of GO (50wt %) /MWCNTs-OH (50wt %) film stack more compactly and tightly with clear layer structures than GO (50wt %) /MWCNTs (50wt %). This probably results from the existence of the hydroxyl groups in MWCNTs-OH. The (–OH) is a very hydrophilic chemical group that could help MWCNTs to be well dispersed in distilled water. Also, in the GO/MWCNT-OH mixture, strong intermolecular forces such as hydrogen bonds might be formed between –OH of MWCNTs-OH and the functionalized groups on GO surface such as –COOH and -OH. These forces, thus, can further hold the GO and MWCNTs-OH together and condense the layer structures.

Figure 3-24 shows the SEM images of the surface of the GO/MWCNT hybrid films. The SEM images for different compositions of multiple walls of CNT (20 %, 40%, 60 % and 80 %) and GO hybrid thin films can provide a deep understand of the thin film surface structure and morphology. Obviously, as the weight percentage of MWCNT increases in the hybrid thin film from 20 % to 80%, the number of MWCNTs covering the surface is increased and a kind of percolated network are formed. This may reduce the film resistance and so the electrical conductivity increased. This incorporation of MWCNT may result in rising of the storing capacity of charges. These influences on the film electrical properties will be discussed in chapter I-4. The transparent sheets covered a larger area in these films with increasing GO content which leads to a percolated network. Unlike MWCNTs, figure 3-24 (f) shows that the networks are not noticeable even with 60 wt% of SWCNT, which shows poor percolated networks due to the poor dispersion of SWCNT in water.

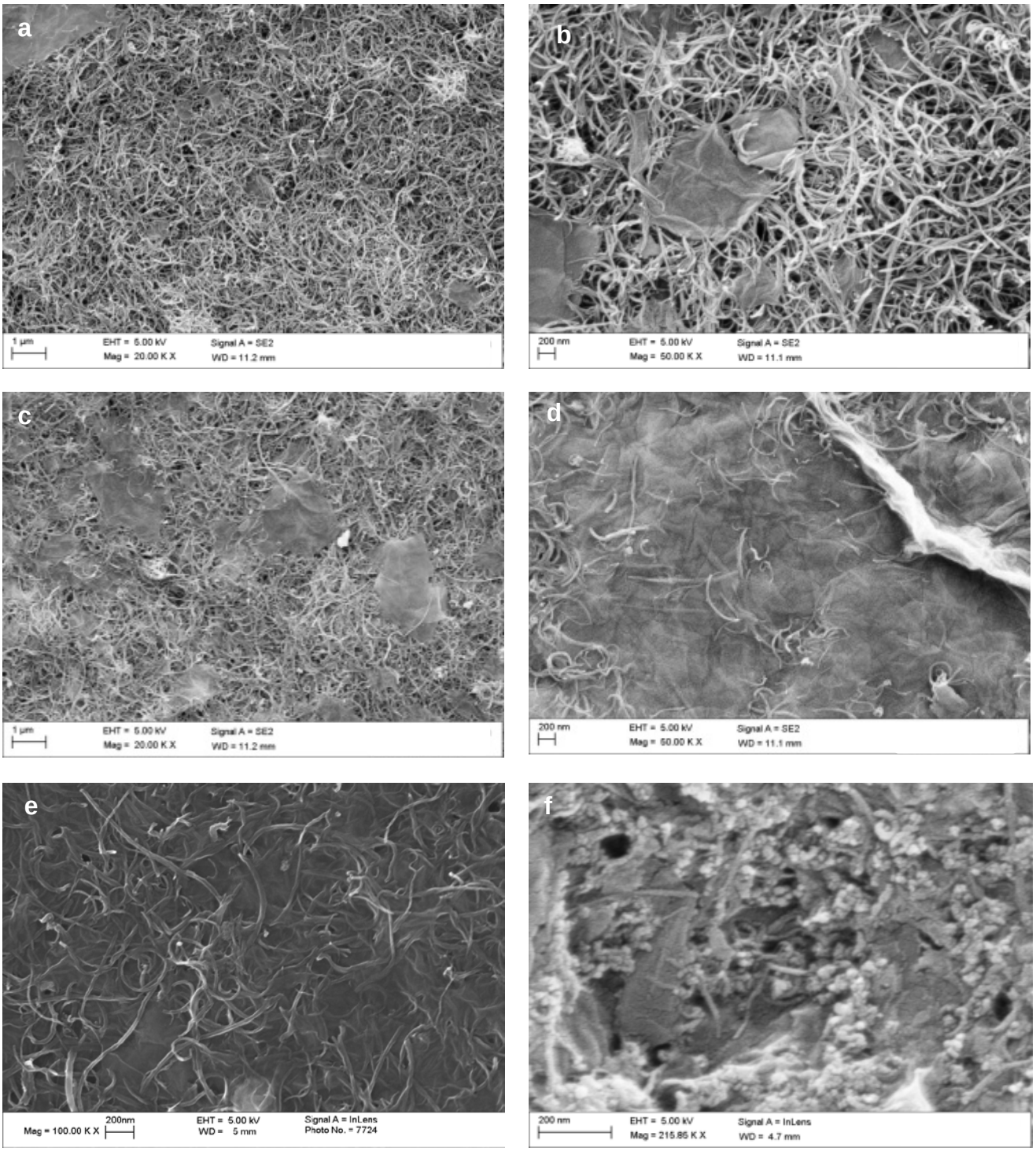

Figure 3-24: SEM images of the surface of the hybrid films. (a) GO(20wt%)/MWCNTs (80wt%); (b) GO(40wt%)/MWCNTs (60wt%); (c) GO(60wt%)/ MWCNTs (40wt%); (d) GO(80wt%)/MWCNTs(20wt%); (e) Surface SEM image of GO(wt%)/MWCNT-OH (50wt%); (f) GO(40wt%)/ SWCNTs (60wt%).

3.2.4 Characterization of G/MWCNT, G/SWCNT and G/MWCNT-OH Hybrid Films

3.2.4.1 The Morphology G/GNT Hybrid Materials Using SEM

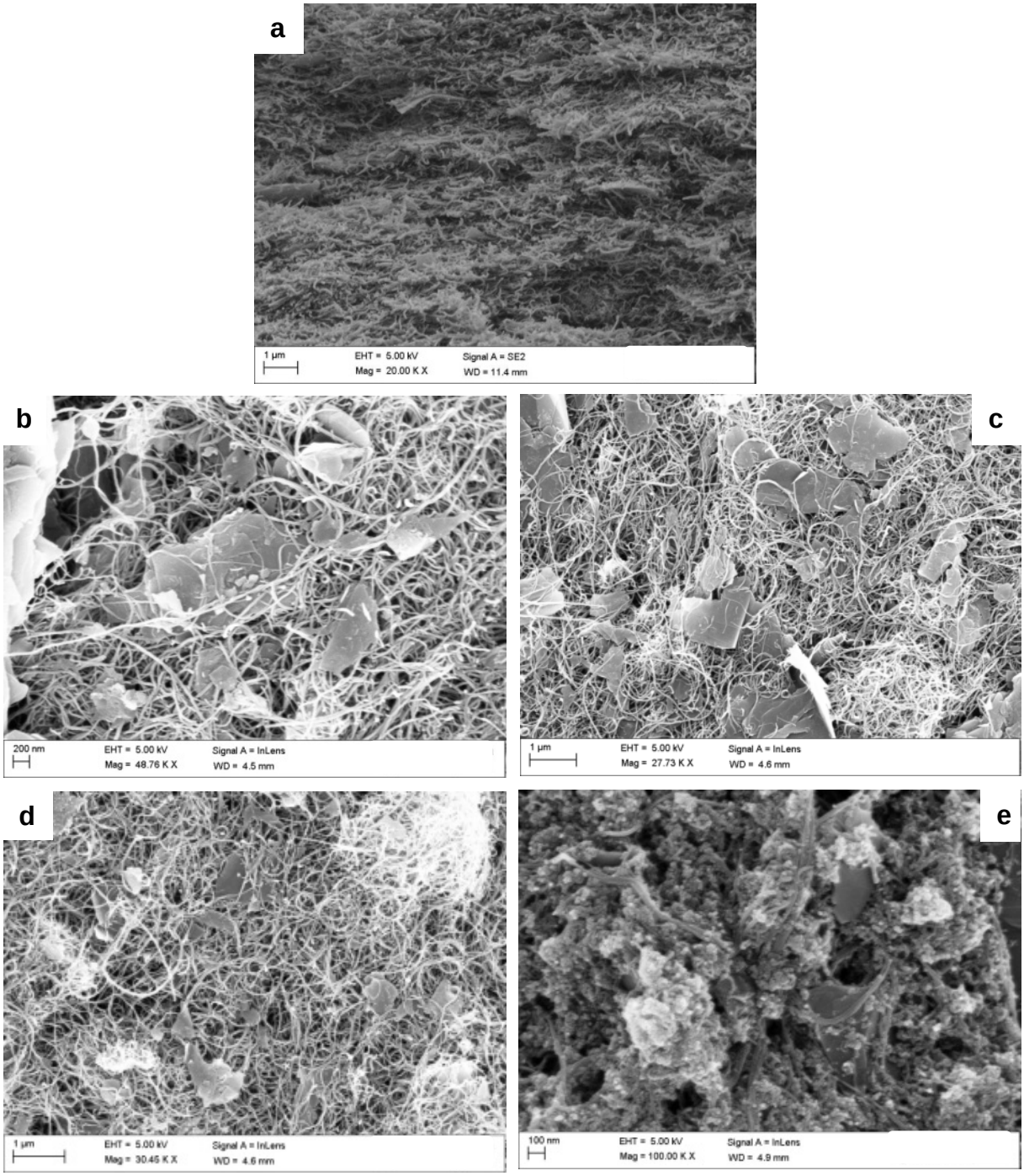

Figure 2-25: SEM images of the surface of the hybrid films. (a) cross sectional area of G (40wt%)/MWCNTs (60wt%) hybrid film; (b) surface of G(20wt%)/MWCNTs (80wt%); (c) surface of G(60wt%)/MWCNTs (40wt%); (d) surface of G(80wt%)/MWCNTs (40wt%); and (e) surface of

3.3 Summary

In this research, graphene (G) and graphene oxide (GO)/carbon nanotubes (CNTs) hybrid film materials were fabricated as high-performance electrodes with different contents of SWCNT, MWCNT and MWCNT-OH using a simple water solution casting method. Different from other fabricated techniques such as CVD or EPD, water casting solution method is not time or money consuming. The films with MWCNTs showed a consistent and well-entangled layered structure at nanometer scale. This layered structure of the thin film is obvious, especially in the film with 80% GO. This formed layered structure can procedure a self-capacitor for energy storage, which is well-arranged as insulating layers of graphene oxide are sandwiched between conductive CNT. The support of the 2D graphene oxide for the MWCNT horizontally can be conserved in a large area. This large contact area between the MWCNTs and GO as well as the small thickness of the GO (the insulators) can store quite a lot of charges in conductors layers results in a high capacitance.

The SEM pictures for different compositions of multiple walls from MWCNT (20 %, 40%, 60 % and 80 %) and GO hybrid thin films can provide a deep understanding of the thin film surface structure and morphology. Obviously, as the weight percentage of MWCNT increase in the hybrid thin film from 20 % to 80%, the number of MWCNTs covering the surface is increased and a kind of percolated network are formed. This reduces the film resistance and thus, the electrical conductivity increased. Therefore, the incorporation of MWCNT may result in rising of storing capacity of charges.

References

[1] S. H. Kim, W. Song, M. W. Jung, M. A. Kang, K. Kim, S. J. Chang, S. S. Lee, J. Lim, J. Hwang, S. Myung, and K. S. An, "Carbon nanotube and graphene hybrid thin film for transparent electrodes and field effect transistors," *Adv. Mater.*, Vol. 26, No. 25, pp. 4247–4252, Jul. 2014.

[2] T. Pei, H. Xu, Z. Zhang, Z. Wang, Y. Liu, Y. Li, S. Wang, and L. M. Peng, "Electronic transport in single-walled carbon nanotube/graphene junction," *Appl. Phys. Lett.*, Vol. 99, No. 11, p. 113102, 2011.

[3] V. Jousseaume, J. Cuzzocrea, N. Bernier, and V. T. Renard, "Few graphene layers/carbon nanotube composites grown at complementary-metal-oxide-semiconductor compatible temperature," *Appl. Phys. Lett.*, Vol. 98, No. 12, p. 123103, 2011.

[4] D. Yu and L. Dai, "Self-assembled graphene/carbon nanotube hybrid films for supercapacitors," *J. Phys. Chem. Lett.*, Vol. 1, No. 2, pp. 467–470, 2010.

[5] S. Stankovich, R. D. Piner, S. T. Nguyen, and R. S. Ruoff, "Synthesis and exfoliation of isocyanate-treated graphene oxide nanoplatelets," *Carbon N. Y.*, Vol. 44, No. 15, pp. 3342–3347, 2006.

[6] L. Meng and S. Park, "Preparation and Characterization of Reduced Graphene Nanosheets via Pre-exfoliation of Graphite Flakes.pdf," Vol. 33, No. 1, pp. 209–214, 2012.

[7] O. Monticelli, S. Bocchini, A. Frache, E. S. Cozza, O. Cavalleri, and L. Prati, "Simple Method for the Preparation of Composites Based on PA6 and Partially Exfoliated Graphite," *J. Nanomater.*, Vol. 2012, pp. 1–5, 2012.

[8] H.-Y. Cao, Z.-X. Guo, H. Xiang, and X.-G. Gong, "Layer and size dependence of thermal conductivity in multilayer graphene nanoribbons," *Phys. Lett. A*, Vol. 376, No. 4, pp. 525–528, Jan. 2012.

[9] J. Shen, Y. Hu, C. Li, C. Qin, and M. Ye, "Synthesis of amphiphilic graphene nanoplatelets.," *Small*, Vol. 5, No. 1, pp. 82–5, Jan. 2009.

[10] M. F. El-Kady, V. Strong, S. Dubin, and R. B. Kaner, "Laser scribing of high-performance and flexible graphene-based electrochemical capacitors.," *Science*, Vol. 335, No. 6074, pp. 1326–30, Mar. 2012.

[11] Y. Si and E. T. Samulski, "Exfoliated Graphene Separated by Platinum Nanoparticles," *Chem. Mater.*, Vol. 20, No. 21, pp. 6792–6797, Nov. 2008.

[12] Q. Cheng, J. Tang, J. Ma, H. Zhang, N. Shinya, and L. C. Qin, "Graphene and carbon nanotube composite electrodes for supercapacitors with ultra-high energy density," *Phys. Chem. Chem. Phys.*, Vol. 13, No. 39, pp. 17615–17624, 2011.

[13] S. Rotkin and Y. Gogotsi, "Analysis of non-planar graphitic structures: from arched edge planes of graphite crystals to nanotubes," *Mater. Res. Innov.*, Vol. 5, pp. 191–200, 2002.

[14] J. Zhang, J. Xiao, X. Meng, C. Monroe, Y. Huang, and J.-M. Zuo, "Free folding of suspended graphene sheets by random mechanical stimulation.," *Phys. Rev. Lett.*, Vol. 104, No. 16, p. 166805, Apr. 2010.

[15] A. Fasolino, J. H. Los, and M. I. Katsnelson, "Intrinsic ripples in graphene.," *Nat. Mater.*, Vol. 6, No. 11, pp. 858–61, Nov. 2007.

[16] N. Liu, Z. Pan, L. Fu, C. Zhang, B. Dai, and Z. Liu, "The origin of wrinkles on transferred graphene," *Nano Res.*, Vol. 4, No. 10, pp. 996–1004, Jun. 2011.

[17] J. C. Meyer, A. K. Geim, M. I. Katsnelson, K. S. Novoselov, T. J. Booth, and S. Roth, "The structure of suspended graphene sheets.," *Nature*, Vol. 446, No. 7131, pp. 60–3, Mar. 2007.

[18] M. I. Katsnelson and A. K. Geim, "Electron scattering on microscopic corrugations in graphene.," *Philos. Trans. A. Math. Phys. Eng. Sci.*, Vol. 366, No. 1863, pp. 195–204, Jan. 2008.

[19] C. Wang, Y. Liu, L. Lan, and H. Tan, "Graphene wrinkling: formation, evolution and collapse.," *Nanoscale*, Vol. 5, No. 10, pp. 4454–61, May 2013.

[20] P. T. Araujo, M. Terrones, and M. S. Dresselhaus, "Defects and impurities in graphene-like materials," *Mater. Today*, Vol. 15, No. 3, pp. 98–109, 2012.

[21] L. Liu, S. Ryu, M. R. Tomasik, E. Stolyarova, N. Jung, M. S. Hybertsen, M. L. Steigerwald, L. E. Brus, and G. W. Flynn, "Graphene oxidation: thickness-dependent etching and strong chemical doping.," *Nano Lett.*, Vol. 8, No. 7, pp. 1965–70, Jul. 2008.

[22] D. Newton, A. Thorpe, and C. Otter, *Revise A2 chemistry for Salters (OCR)*. Heinemann, 2004.

[23] J. Coates, "Interpretation of Infrared Spectra, A Practical Approach," *Encycl. Anal. Chem.*, pp. 10815–10837, 2000.

[24] X. Jia, J. Campos-Delgado, M. Terrones, V. Meunier, and M. S. Dresselhaus, "Graphene edges: a review of their fabrication and characterization.," *Nanoscale*, Vol. 3, No. 1, pp. 86–95, 2011.

[25] S. Vadahanambi, J.-H. Jung, and I.-K. Oh, "Microwave syntheses of graphene and graphene decorated with metal nanoparticles," *Carbon N. Y.*, Vol. 49, No. 13, pp. 4449–4457, Nov. 2011.

[26] A. Bagri, C. Mattevi, M. Acik, Y. J. Chabal, M. Chhowalla, and V. B. Shenoy, "Structural evolution during the reduction of chemically derived graphene oxide.," *Nat. Chem.*, Vol. 2, No. 7, pp. 581–587, Jul. 2010.

Part One: Conductive Behaviour of Graphene/Carbon Nanotube and Graphene Oxide/ Carbon Nanotube Hybrid Materials

Chapter I-4 Electrical and Magnetic Properties of Graphene/Carbon Nanotube and Graphene Oxide /Carbon Nanotube Hybrid Materials

4.1 Introduction

Recently, hybrid nanostructures have received a great deal of attention in different studies which focused on the graphene-based material. The functionalized hybrid materials can complement the deficiencies of pure graphene films [1]-[3]. Up to now, indium tin oxide (ITO) has usually been used as a transparent electrode (TE) in solar cells, organic light emitting diode panels and touch panels because of its high optical transparency and low sheet resistance. However, sustainability and price concerns give the need to be replaced for new transparent conductive materials with a high mechanical flexible material but low-cost one [4]. Thus, there are daily efforts to fabricate transparent, conductive and flexible graphene-based material electrodes (TEs) and field effect transistor electrodes (FETs) [5]-[8]. For example, graphene and silver or copper nanowire hybrid films attracted enormous interest to be investigated as a possible replacement, in particular, transparent and flexible electrodes [4], [5], [9]. Xu et al. reported the use of graphene/silver nanowire hybrid films as electrodes for transparent and flexible acoustic device, in which the grain boundaries in graphene are bridged by AgNWs and the empty spaces in AgNWs network are filled with graphene [10].

On the other hand, graphene and CNTs hybrid films have been developed with excellent electronic properties to work as electrodes. All studies have focused on the development of graphene/CNT hybrid films to make excellent willing materials which are utilized in different electrical devices. However, the influence of microstructure of the hybrid film on its electrical properties such as conductivity, capacitance and the change of the values with frequency and voltage has never been reported. For the applications of graphene-based hybrid materials as electrodes or electrical devices, the influences are important and must be addressed clearly.

In this chapter, the electrical properties of the graphene/ CNT hybrid films such as conductivity and specific capacitance were discussed. It provides some useful information about the electrical performance of graphene-based hybrid films as electrodes.

4.2 Electrical Properties of Graphene-Based Hybrid Films

Resistance and specific capacitance were measured under scanning voltage and frequency to analyse the electrical properties of the hybrid films. Then, the dielectric constant and resistivity were calculated.

4.2.1 Conductivity for Samples of Size (18mmx18mmx5µm)

The conductivities of all samples were calculated from the measured resistance values using equation (2-2) in chapter I-2. Figure 4-1 shows the electrical conductivity of MWCNTs wt % for G/MWCNT and GO/MWCNT hybrid films. There is a linear relationship of electrical conductivity with CNT content in both GO/MWCNT and GO/MWCNT-OH systems. As seen from figure 4-1 part (a) the conductivity increases as the MWCNT fraction in the film rises. However although the linearity is clear in both systems, the slope with the GO/MWCNT is larger than the one using the GO/MWCNT-OH which resulting in a sharper growth of the conductivity in the GO/MWCNT film. On the other hand, in the G/MWCNT and G/MWCNT-OH systems, a nonlinear relationship of electrical conductivity with CNT content was found. Figure 4-1 part (b) shows clearly in the G/MWCNT film that the conductivity is raised up with increasing the content of the CNT until reaching to a specific value where it started to have an inverse relationship with the content of CNT. This may result from the connection of two nanostructured conductive materials. On the other hand, unlike the G/MWCNT trend, the conductivity of the G/MWCNT-OH film shows a linear relationship with the content of the MWCNT-OH.

Although both G-based MWCNTs and MWCNT-OH hybrid films exhibit similar trends, MWCNTs hybrid thin films show a higher conductivity than the MWCNTs-OH. This can be explained by changing the electrical property of CNT as a result of –OH group presence. This group works as cavities or holes that prevent charges accumulation by reducing the area and dropping the final specific capacity. The –OH groups affect the

material's resistance as well as the percolated network which tends to decrease the overall material conductivity by twisting the CNTs and shorten the conjugated length.

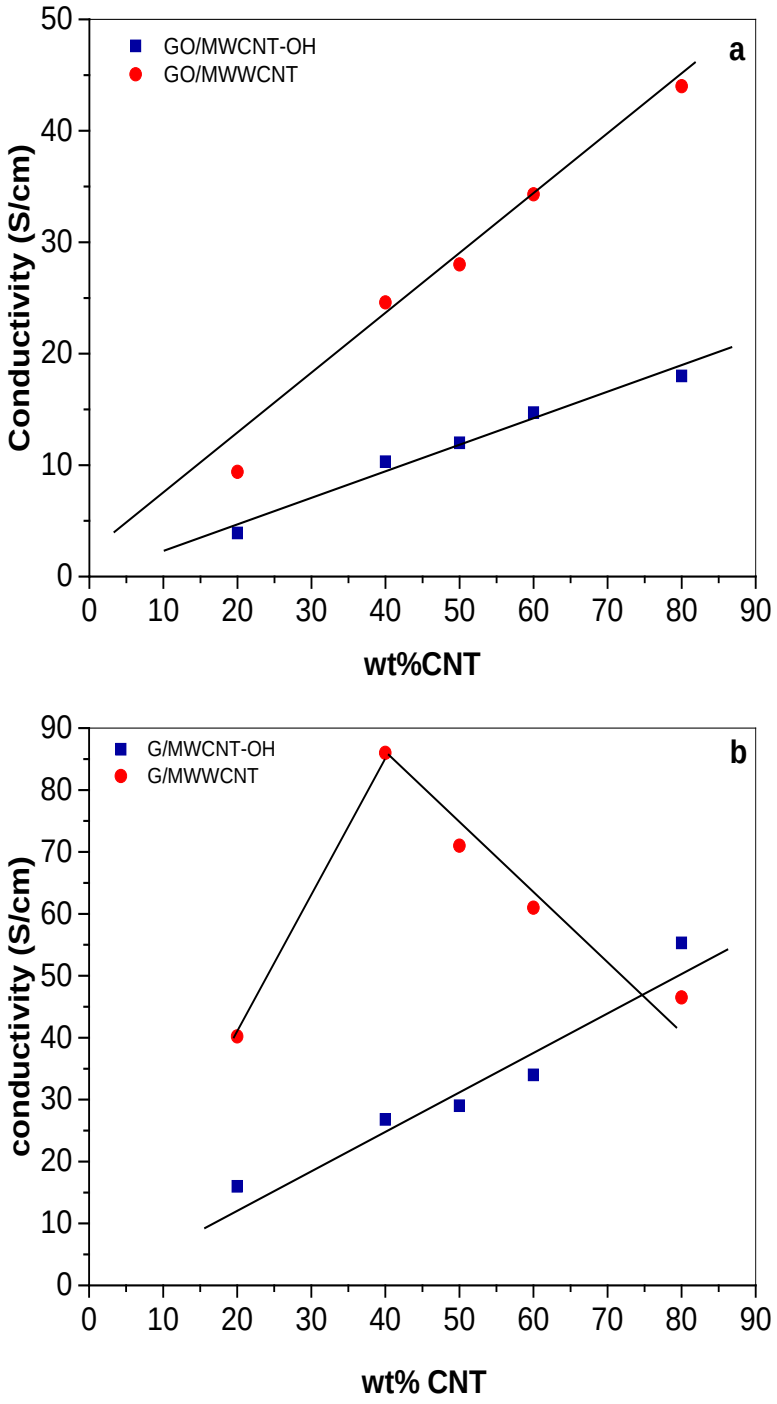

Figure 4-1: Electrical conductivity versus wt% CNTs for (a) GO/MWCNT systems and (b) G/MWCNT systems.

Figure 4-2 illustrates XPS results for MWCNTs and MWCNT-OH which shows the effect of –OH functional group in the MWCNT structure. A noticeable increase of Oxygen content is obviously seen in MWCNT-OH spectrum. The –OH functional group can change the chemical structure of the whole MWCNT as shown in figure 4-3. This influence should be taken into account for a better-percolated network formation.

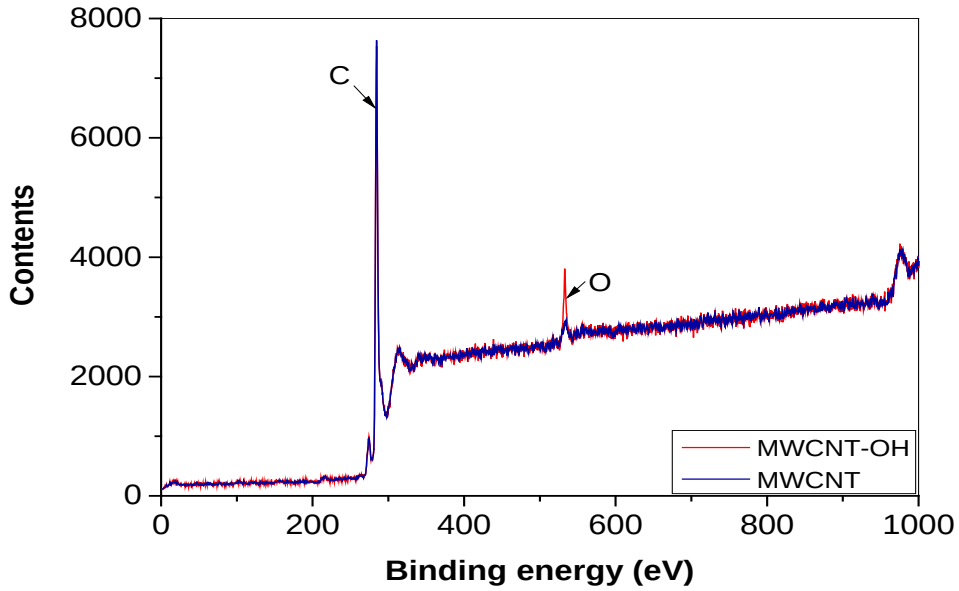

Figure 4-2: XPS results for MWCNTs and MWCNT-OH.

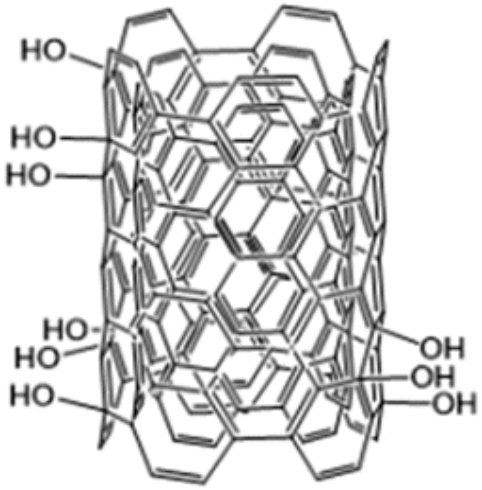

Figure 4-3: MWCNT-OH chemical structure.

On the other side, the G/MWCNT hybrid films have a much higher conductivity comparing with the GO/MWCNT due to both G and CNT are conductive materials. However, the conductivity of the hybrid films with SWCNT in contrast to MWCNT systems is much lower due to the poor dispersion of SWCNT and non-layered structure. The corresponding conductivity of (40wt% G/ 60 wt% SWCNT) and (40wt% GO/ 60 wt% SWCNT) were found to be 15.5 $S.cm^{-1}$and 7.2 $S.cm^{-1}$ respectively, whereas they are 68.0 $S.cm^{-1}$and 34.3 $S.cm^{-1}$ for the same fraction but (40wt% G/ 60 wt% MWCNT) and (40wt% GO/ 60 wt% MWCNT). As well known, generally, SWCNTs are bundled together and very difficult to form a single SWCNT dispersion in solution or in a matrix. Based on these results, it is believed that G/SWCNT or GO/SWCNT systems are not suitable for the development of high-quality electrodes using the simple water casting method.

4.2.2 Capacitance

In this part, the capacitance with frequency from (50 – 10000) Hz for G and GO-based hybrid films were assessed at 2V. As it is known, the specific capacitance highly depends on the frequency loaded, and always decreases as the value of frequency goes up [11]. Refer to the experimental results, generally, these trends can be observed in each film, in which the capacitance was found to decrease down to zero at high frequencies. The highest value of the capacitance was recorded at 50 Hz and rapidly down to zero at about 2000 Hz. But, for several films, capacitance showed a little rise at the beginning of the measurement. It's probably due to the delay of charging at the starting of the process which reduces the capacitance slightly at 50Hz. This rapid falling of capacitance could be because the lower the frequency of the applied voltage, the more time the capacitor needs to be a fully charged. Then, it passes with a zero current state before the voltage reverses its polarity and the capacitor start to discharge. When a higher frequency is applied, the capacitor changes from charging to discharging quicker in its charge curve and it remains further from its fully charged state. The dielectric constant can be calculated from capacitance values of GO and G systems to be plotted against frequency at 2V and presented in figure 4-4 and figure 4-5.

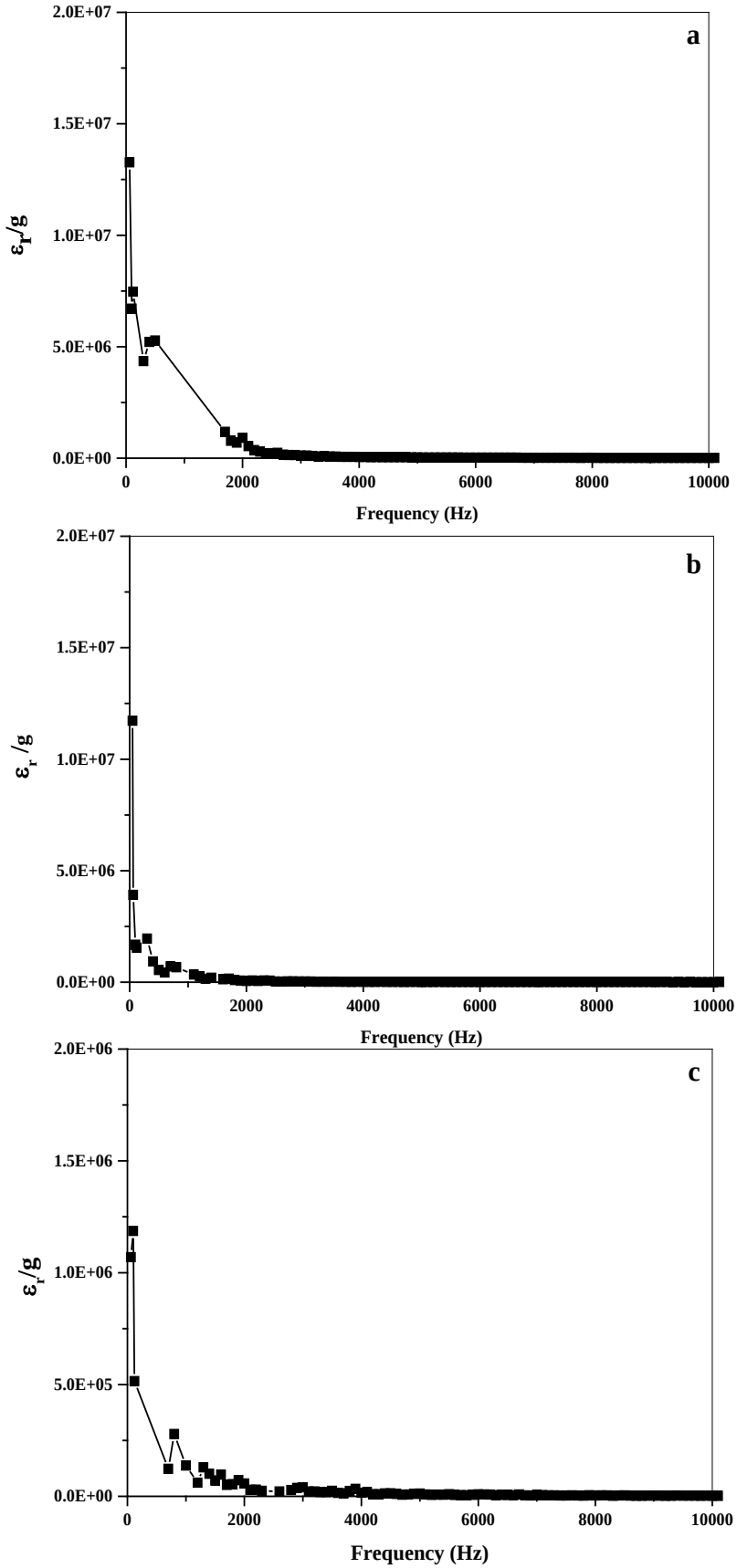

Figure 4-4: a: Plot of dielectric constant versus frequency at 2V of a (GO 40wt %/MWCNT 60 wt %). b: (GO 40wt %/MWCNT-OH60 wt %). C (GO 40wt %/SWCNT 60 wt %).

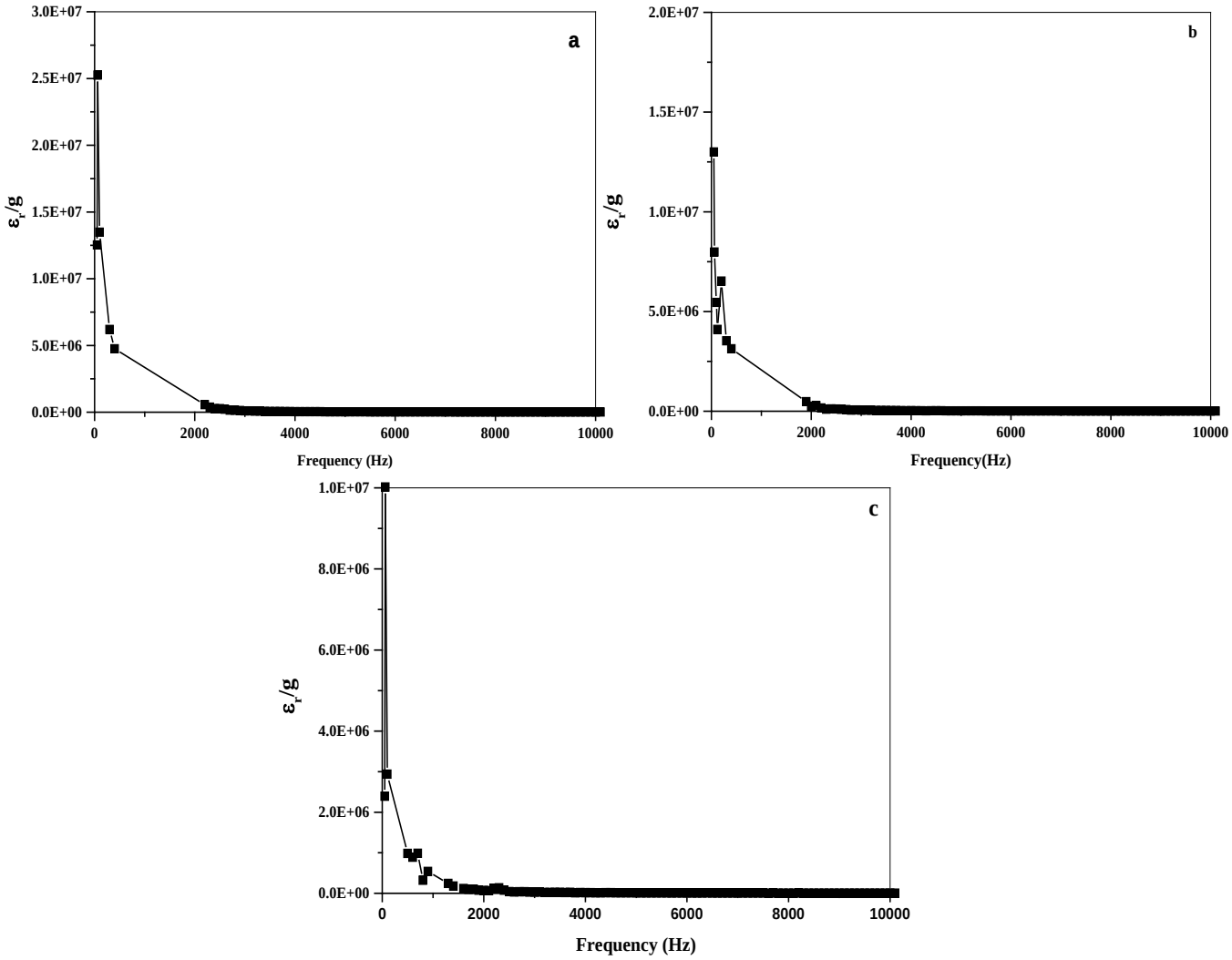

Figure 4-5: a: Plot of dielectric constant versus frequency at 2V of a (G40wt %/MWCNT 60 wt %). b: (G 40wt %/MWCNT-OH 60 wt %). C (G 40wt %/SWCNT 60 wt %)

The dielectric constant of different hybrid films against wt% CNTs at 50Hz with 2V is shown in figure 4-6. Obviously, the trend of dielectric constant versus the content of CNT graph is similar to the conductivity and wt% MCNT trend. Clearly, in part (a) there is an almost linear relationship can be found in each type of GO/MWCNTs film. The dielectric constant is directly proportional to the MWCNTs percentage in the films. Nevertheless, in the G/MWCNT system, the dielectric constant value increased with increasing the CNT content until reaches to the highest at 40wt% MWCNTs for (G/MWCNT) and at 60wt% MWCNT in the G/MWCNT-OH. After this value, the dielectric constant started to be nearly constant. This could be regarded to the influence of the nanostructure in the G/MWCNT systems.

It can be also found that the G/MWCNTs systems act superior to G/MWCNTs-OH systems, exhibiting a higher dielectric constant and lower resistivity. Like the conductivity, the difference in the dielectric constant of the two film types also is resulted from the presence of –OH groups. In G/MWCNTs-OH systems, -OH groups act as 'voids' being incapable of accumulating charge, thus reduced the entire capacitance and so the dielectric constant. Above all, the trend of dielectric constant in figure 4-6 is not only affected by the percolated network, but also the side groups on the carbon nanotubes.

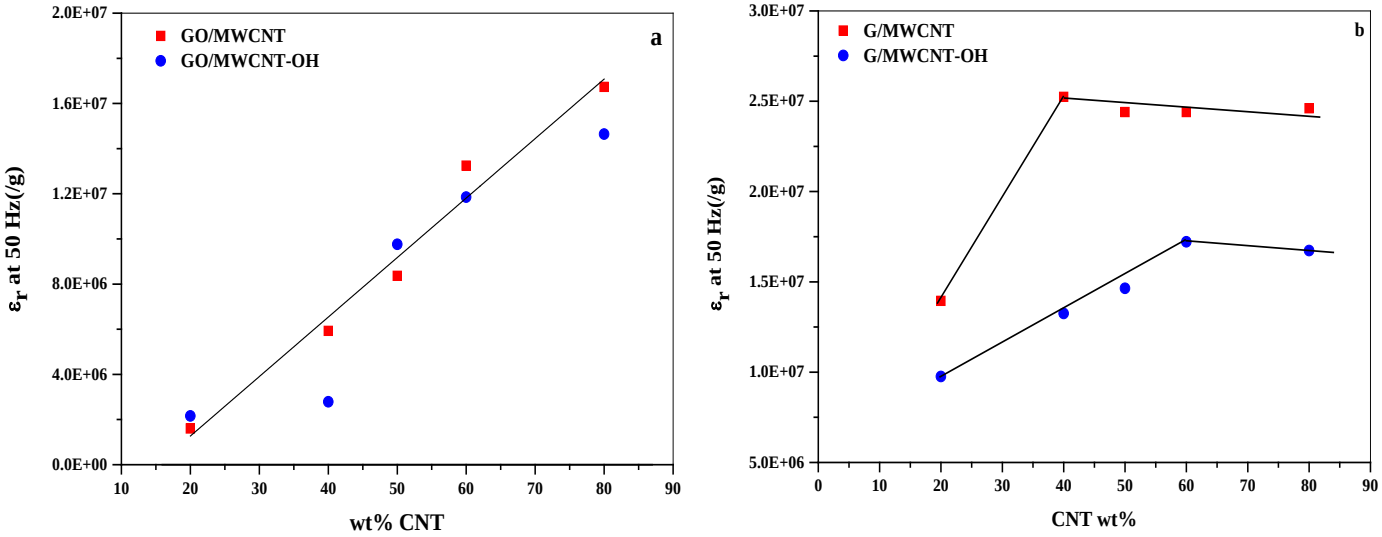

Figure 4-6: Dielectric constant at 50Hz against wt% MWCNTs. (a) GO/MWCNT hybrid films and (b) G/MWCNT hybrid films.

Similar to the conductivity with SWCNT hybrid film content, the dielectric constant was also calculated to be very low in this kind of films. The results of their resistivity at low frequency and the maximal values of dielectric constant are summarized in table 4-1. As mentioned in the discussion of SEM morphology, SWCNT has hardly dispersed in the GO/SWCNT or G/SWCNT mixture even with ultrasonic treatment. No percolated network and layer structure were formed to activate the storage capacity substantially. Accordingly, their resistivity is high and thus the dielectric constant is low.

Table 4-1: dielectric constant and resistivity (at 50Hz) for each hybrid film with SWCNT.

Type of hybrid thin film	G (40wt %) / SWCNT (60wt %)	GO (40wt %) / SWCNT (60wt %)
Dimension	18mmx18mmx5μm	
Maximal specific capacitance F/g	26.7	3.8
ε_r /g	1.5 E+07	1.2 E+07
Resistivity(kΩ.mm)	0.01425	0.0305

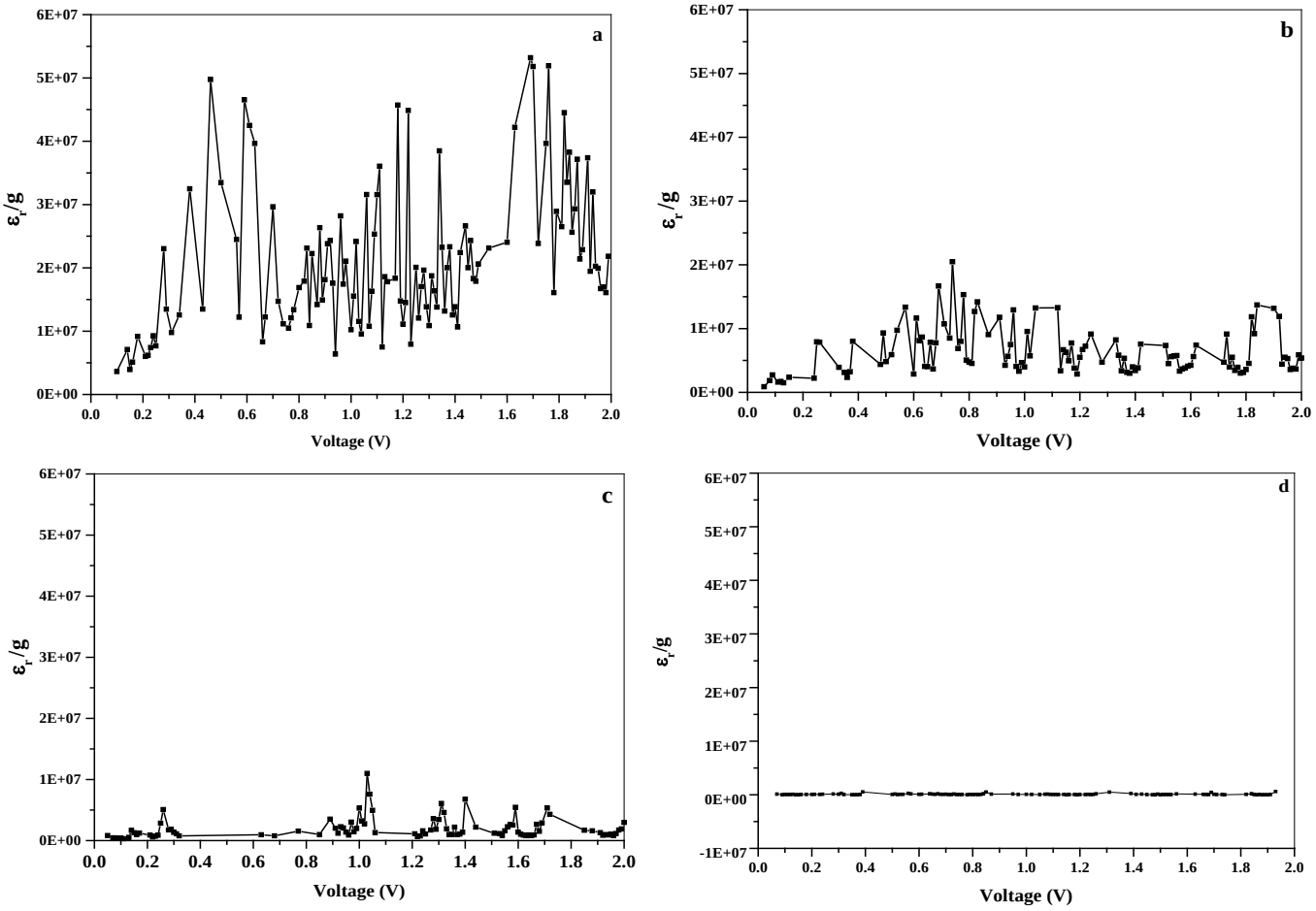

Figure 4-7: Plots of dielectric constant versus scanning voltage at 50Hz. (a) GO (40wt %) /MWCNT (60wt %); (b) GO (40wt %) /MWCNT-OH (60wt %); (c) GO (40wt %) /SWCNT (60wt %); and (d) GO film.

Figure 4-7 illustrates a non-linear behaviour of the dielectric constant during a voltage range from (0-2) V in all hybrid films. Comparing four films with different functional groups but with the same fraction of MWCNT, results came out with the nearly similar finding. Among some voltages, the dielectric constant reaches to maximal values (peak) and at some voltages gets to minimum values (valley). In part (a) of figure 4-7, the dielectric constant value fluctuates between minimum and maximum unexpectedly during (0-2V) scanning voltage for GO (40wt %) /MWCNT (60wt %) hybrid film. The maximal dielectric constant reaches $5.32x10^7$/g and the minimal for around $6.36x10^6$/g. There are some peaks in specific points among this voltage range. Part (b) with GO (40wt %) /MWCNT-OH (60wt %) film has the same trend but with a lower dielectric constant value. The maximal dielectric constant is $2.05x10^7$/g. The peaks are also found in specific voltage which are almost similar to those in part (a). Although, the film of the GO/SWCNT in part (c) has a maximal dielectric constant smaller than previous films, the graph trends still the same with some peaks and valleys in specific voltages. The pure GO film has been also investigated as in part (d) in figure 4-7 to make sure that this influence is not an intrinsic property of the film. As it clear the nonlinearity is missing in this graph and the dielectric constant is nearly constant to 0 /g. This leads to expect that this nonlinear behaviour comes from the junction in the hybrid film. Peaks of voltages in these three hybrid films are summarised in table 4-2:

As it clear from this table, voltage peaks are almost the same or a very close to each other in a specific order.

Table 4-2: Voltage peaks values of (GO (40wt %) /MWCNT (60wt %), GO (40wt %) /MWCNT-OH (60wt %) and GO (40wt %) /SWCNT (60wt %) hybrid films**.**

n	Peak voltage in GO/MWCNT	Peak voltage in GO/MWCNT-OH	Peak voltage in GO/SWCNT
1	0.26	0.25	0.24
2	0.43	0.38	0.34
3	0.5	0.5	0.56
4	0.6	0.61	0.61
5	0.68	0.69	0.69
6	-	0.74	0.73
7	0.79	0.78	-
8	0.89	0.83	0.83
9	0.92	0.91	0.93
10	0.95	0.96	0.99
11	1.01	1.01	1.04
12	1.15	1.17	1.17
13	1.21	1.24	1.24
14	1.38	1.32	1.32
15	1.65	1.62	1.59
16	1.69	1.73	1.74
17	1.83	1.84	1.87

Table 4-3: Voltage peaks values of (G (40wt %) /MWCNT (60wt %), G (40wt %) /MWCNT-OH (60wt %) and G (40wt %) /SWCNT (60wt %) hybrid films

n	Peak voltage in G/MWCNT	Peak voltage in G/MWCNT-OH	Peak voltage in G/SWCNT
1	0.28	0.28	0.28
2	0.33	0.33	0.32
3	0.38	-	-
4	0.46	0.46	-
5	0.52	0.52	0.63
6	0.75	0.78	0.77
7	0.89	0.85	0.89
8	0.92	-	0.93
9	0.99	0.99	1.02
10	1.05	1.04	1.05
11	1.15	1.12	-
12	1.25	1.23	1.22
13	1.31	1.3	1.3
14	1.35	1.35	1.35
15	1.44	1.44	1.44
16	1.55	1.55	1.54
17	1.71	1.7	1.71
18	1.91	1.89	1.88

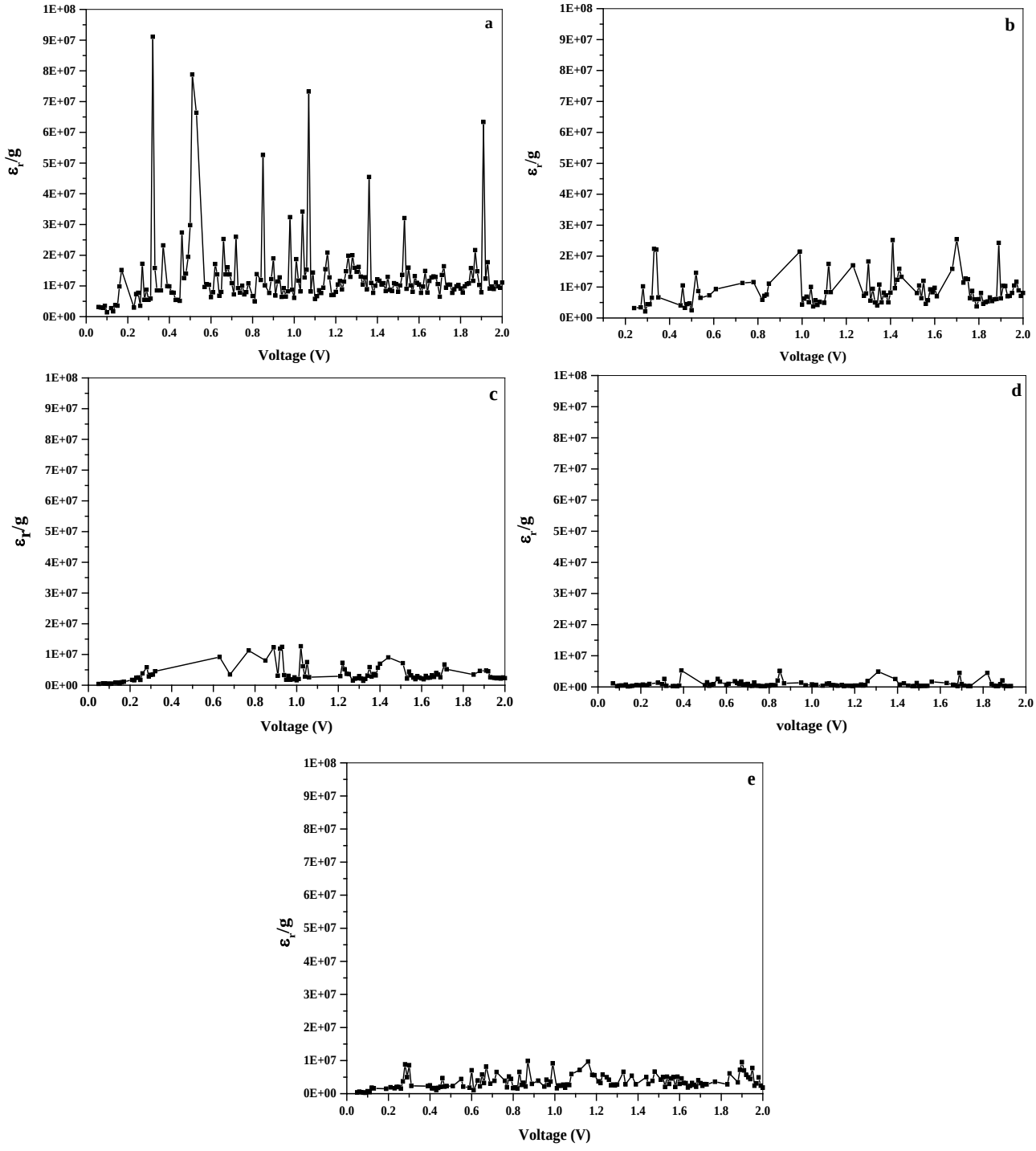

Figure 4-8: Plots of dielectric constant versus scanning voltage at 50Hz. (a) G (40wt %) / MWCNT (60wt %); (b) G (40wt %) /MWCNT-OH (60wt %); (c) G (40wt %) /SWCNT (60wt %); (d) MWCNT film; and (e) graphene film

Figure 4-8, on the other hand, shows the plots of dielectric constant versus scanning voltage from (0-2) V at 50Hz for G/CNT systems which have a trend similar to the GO/CNT one. However, the peaks values are higher than the GO/CNTs system which

reaches $9.21x10^7$/g for GO (40wt %) /MWCNT (60wt %). The peaks of voltages are also in the same position or nearly close to each other as they are summarised in table 4-3.

Pure graphene and pure MWCNT films have been investigated as well to check if any of their intrinsic properties influences this nonlinearity. As it is shown in figure 4-8 (d &e), such behaviour, originally, is found in each pure film but it is very small and rarely noticeable. However, these characteristics are adding up in the hybrid film.

Obviously, the hybrid films GO/CNTs and G/CNTs dielectric constant are voltage loaded dependent. It is possible that nano-junctions formed between G or GO and CNTs when the content of carbon nanotubes is high. The peak values of the dielectric constant appear where the junctions are fully exerted at the relevant voltages. The dielectric constant has been found to be higher in G/CNT than in GO/CNT which is not as expected. GO is an insular which can form a capacitor system with the conductive CNT layers. Conversely, G is a conductive with another CNT conductive material could give a very weak capacitor system. The unexpected results seem that the nanostructure could have significant influences on its performance as electrodes. Generally, the change of the dielectric constant with voltage indicates that the stability of the G/CNT and GO/CNT hybrid films as electrodes is questionable.

The maximal dielectric constant has been found to be $9.91x10^7$/g with the hybrid film (60 wt% G / 40 wt% MWCNT). Principally, this is a promising value referring to the literature value and it would be higher at frequencies that lower than 50Hz.

4.2.3 Nonlinear Behaviour in Graphene-Based Hybrid Film as a Quantum Effect

It's well-known that quantum effect always presents and influences properties of a material when its component is in nano- meter scale. For the CNT-based hybrid films in this project, their capacitance and so the dielectric constant is quite dependent on the voltage loaded. It is delighted to find that both (graphene and graphene oxide)-based hybrid film systems have their peaks in exact position or nearly very close to as it is shown in table 4-2 and table 4-3. When the MWCNT is pure and with a high fraction in the film, the dielectric constant the peak numbers increase and the peak itself become sharper. However, when the CNT is single, functionalised or with a low content, these peak numbers decline and getting smaller. On the other side, it can be seen from these

tables that some of the peaks are missing in some films and some others are sharper in other films. The maximal dielectric constant peaks also are in different voltage position in each graph. This may relate to the nanostructured formed during the preparation stage.

Based on the observed values of voltages developing high dielectric constant in all measured hybrid films with different CNT percentage and functionalized group, the top values of dielectric constant might appear at one of these values: (1.97, 1.71, 1.57, 1.15, 1.02, 0.93, 0.88, 0.74, 0.6, 0.54, 0.46, 0.34 and 0.26) V. These values are of great value that can be referred and chosen to be the rated voltage of the hybrid thin films as capacitors.

4.2.4 Effect of Length and Thickness of the Hybrid Film on Electrical Conductivity and the Maximal Dielectric Constant

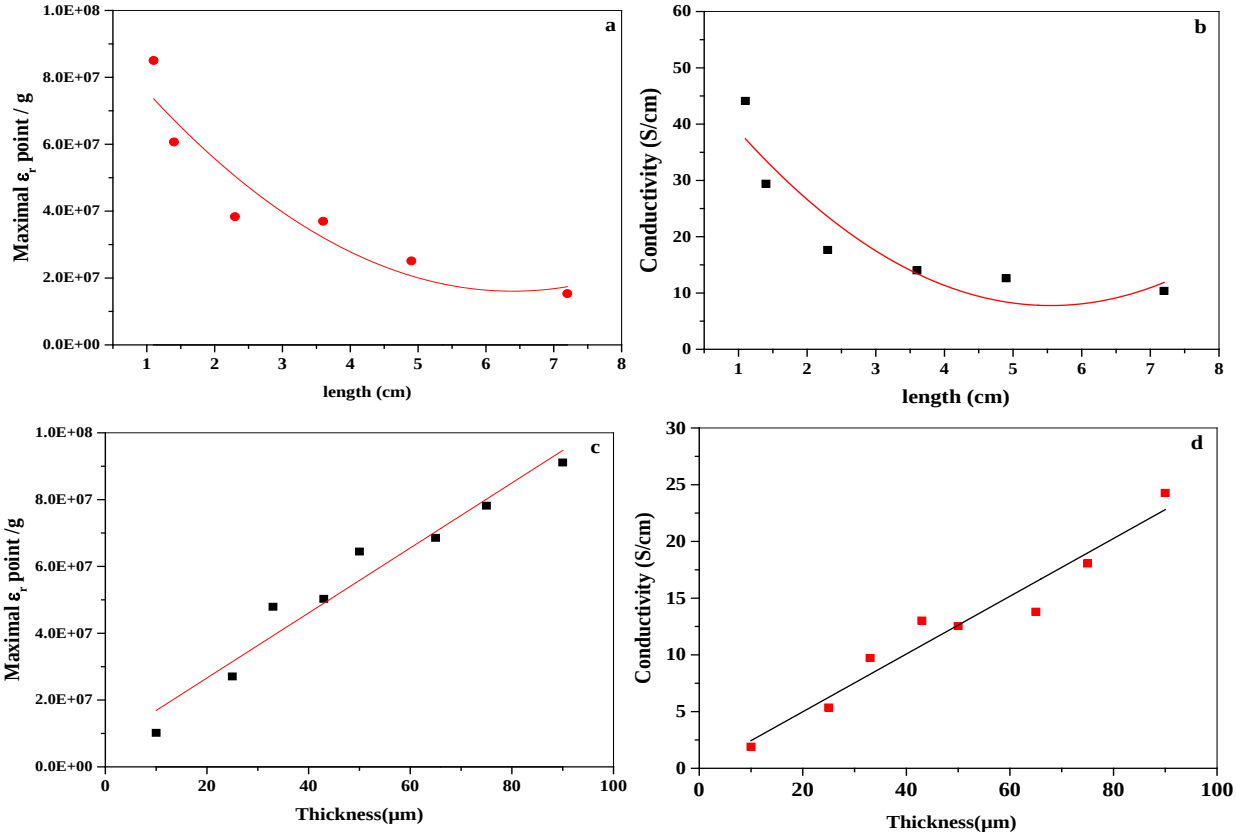

Figure 4-9: Effect of length and thickness of the hybrid film on electrical conductivity and the maximal dielectric constant measured at 50Hz and 0.3V. (a) and (c) G (60wt %) /MWCNT (40wt %); (b) and (d) GO (60wt %)/ MWCNT (40%).

Figure 4-9 presents the relation between the electrical conductivity and the maximal dielectric constant with the length and the thickness of the hybrid films that have measured at 50Hz and 0.3V. The results indicate that the length and thickness of the hybrid film have significant influences on the dielectric constant value. It can be clearly found that as the length of film increases, the maximal dielectric constant and the conductivity of the film decreases rapidly while the resistivity goes up. Trends are shown in figure 4-9 (a and b). Moreover, the dielectric constant and the conductivity in part (c and d) have a directly proportional relation with the thickness of the film. Obviously, they increase with increasing the thickness of the film and decreases with increasing the length.

The effect of length and thickness can be understood by considering layer structures formed as illustrated as an equivalent capacitor circuit for the hybrid film. The stacked layers of the film can be considered as the arrangement of massive series circuits. Each layer consists of sub capacitors that form a parallel circuit as illustrated in figure 4-10.

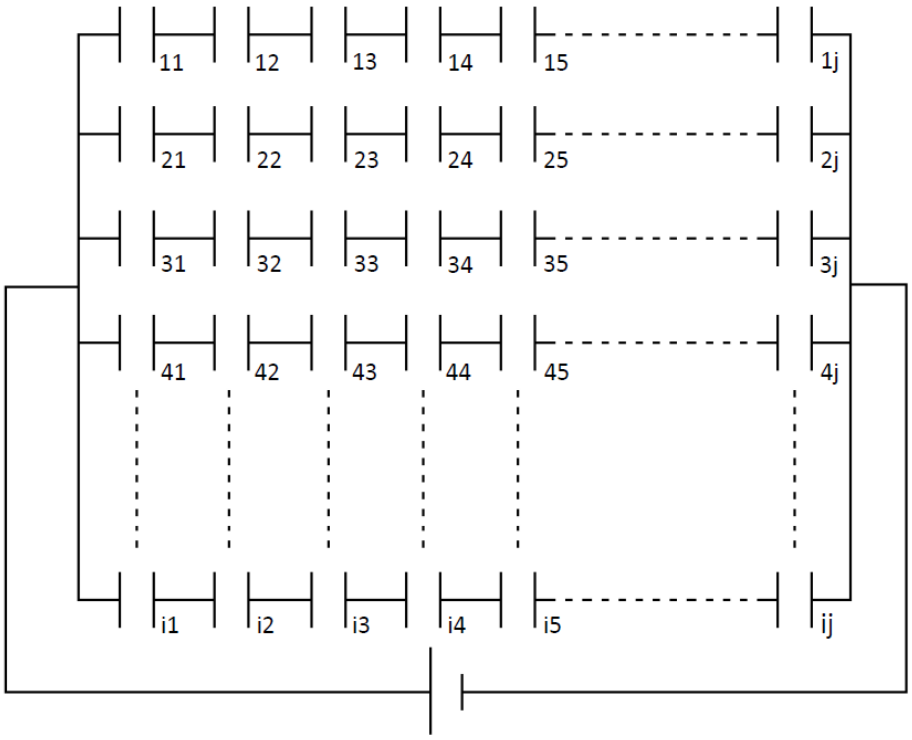

Figure 4-10: Illustration of the equivalent capacitor circuit of the GO/CNTs and G/CNTs hybrid thin films as a capacitor.

The total capacitance will be calculated by summation of all these series sub capacitors in the film first and then the parallel capacitor all over the length. This can be expressed by the following equation.

$$C_t = \sum_1^j \left(\frac{1}{\sum_1^i 1/C_{ij}}\right) \quad (4\text{-}1)$$

C_t is the total capacitance and C_{ij} is the ijth sub-capacitance. Assuming that no essential differences exist between the sub capacitors, each sub capacitor can be regarded as an equal part to the others. Then the total dielectric constant can be calculated from the total capacitance value. The experimental results are in a good agreement with the equation. The high value of a total dielectric constant is always observed in a thicker and shorter film when the length is fixed.

4.3 Magnetic Properties of Graphene-Based Hybrid Films

In this part, a general background about magnetism in materials is first introduced. Then the result of the magnetism experiment finding will be discussed.

4.3.1 Introduction

Magnetic properties of materials depend on the electrons surrounding the atoms. In an atom, both nucleus and electrons motion can produce a magnetic moment. Though, the nucleus magnetic moment has insignificant influence comparing to the electronic contribution. Basically, the spin and the orbital moment are two different types of magnetic moments that are performed as electrons rotate around the nucleus. Thus, the magnetic moment can be calculated as the product of the area described by the current loop of electrons and the current itself [12].

$$\mu_{orbit} = \pi r^2 (ev/2\pi rc)$$

$$= evr/2c \quad (4\text{-}2)$$

μ_{orbit} is the magnetic moment, r is the Bohr atomic radius and v is the electron velocity.

4.3.2 Materials Behaviour in a Magnetic Field

Materials with unpaired electron are called magnetic materials. Conversely, they are termed a non-magnetic or diamagnetic if all electrons are paired. There are two fields to be considered: The magnetic field H which is generated by currents according to Ampère's law (magnetic induction) and the magnetic flux density B. This can be clarified from equations 4-3 and 4-4:

$$B = \mu H \tag{4-3}$$

$$B = \mu_0 H + \mu_0 M \tag{4-4}$$

Where μ: *the permittivity*

B: magnetic flux density

H: magnetic field

M: Magnetization

In free space, $B = \mu_0 H$

However in a material

$$B = \mu_0 (H + M) \tag{4-5}$$

As it is presented in figure 4-11, different material orientation spin can result in different magnetic material structure. The main four types are: (a) Paramagnetic, (b) Ferromagnetic(c) Antiferromagnetic, and (d) Ferrimagnetic materials. Their magnetic behaviours depend on the values of susceptibility (χ), permittivity (μ) and if they are temperature or field dependence or not [13][14].

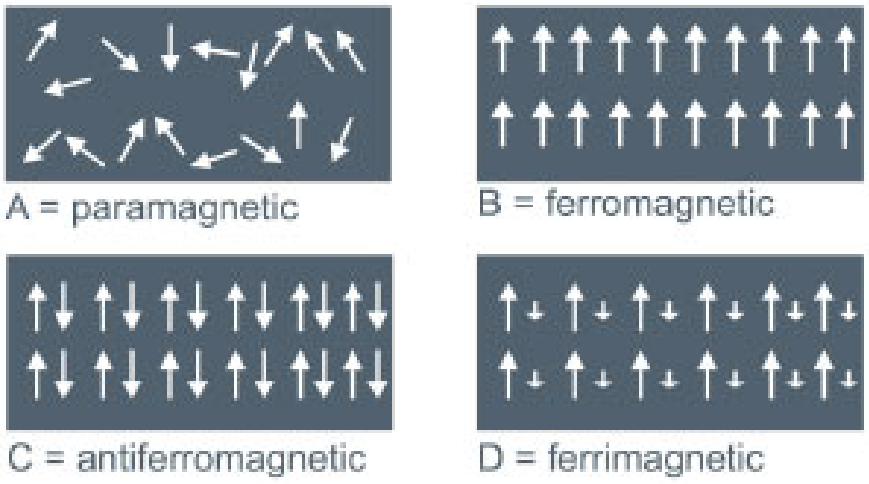

Figure 4-11: Different material spin orientation can lead to different magnetic material structure [14].

4.3.3 Magnetic Properties of Graphene

J. Hong reported that ‘‘Demonstrating the presence of long-range magnetic order in functionalized graphene nanostructures paves the way to realizing the dream of spintronic’’ [15]. When few of the carbon atoms are removed or added, the magnetic properties of graphene appear [16]. Despite the variety of theoretical works in the area, a limited amount of experimental evidences are available. The main focused studies in most of these experiments were in ferromagnetism of graphite, fullerenes and other carbon-based-systems [17], [18]. From an experimental point of view, these studies regarding the presence of ferromagnetism at room temperature in carbon materials [17]-[20] have started to attract the attention of researchers in the past few years. However, these findings have been enclosed with some doubts about the validity of results which attributable to a lack of reproducibility in the experiments and to the underestimated amount of contaminations in the investigated samples.

4.3.4 Challenging of Existence of any Magnetic Order in Graphene

The difficulties of finding a magnetic order in graphene result from different reasons. The first one is the absence of electrons in d and f shells which are responsible for the magnetic coupling in conventional ferromagnets. Although both theory and experiment suggest that a magnetic order can exist in these carbon structures, it still under specific circumstances and conditions. Density Functional Theory (DFT) is the first theoretical

approach that is usually implemented in such a field. Localized electronic states are spin-polarized and occur at the level of Fermi energy can be a source of magnetism. In graphene nanostructures "zig-zag" configuration, the edges of the honeycomb lattice introduce magnetic moments. In contrast, armchair edges result in zero magnetic moments [21]. Figure 3-20 in chapter I-3 shows the armchair and zigzag confirmation of graphene. Secondly, localised states in the presence of point defects such as carbon atom vacancies or additional adding atom in the graphene lattice can originate magnetic moments[22], [23]. Thus, the introduction of defects in graphene can be used as a tool to investigate any existence of such magnetic phenomena.

4.3.5 Graphene-Based Hybrid Film Magnetism

4.3.5.1 Raman Spectra for Different Content of G/ CNT Hybrid Films

Three hybrid films with different functionalized groups (80 wt% GO /20wt % MWCNT), (64 wt%GO/ 33wt%MWCNT) and (20wt% G/80wt%MWCNT-OH) have been investigated first by Raman spectroscopy. As expected, Raman data shows that there are crystal differences between them as shown in figure 4-12

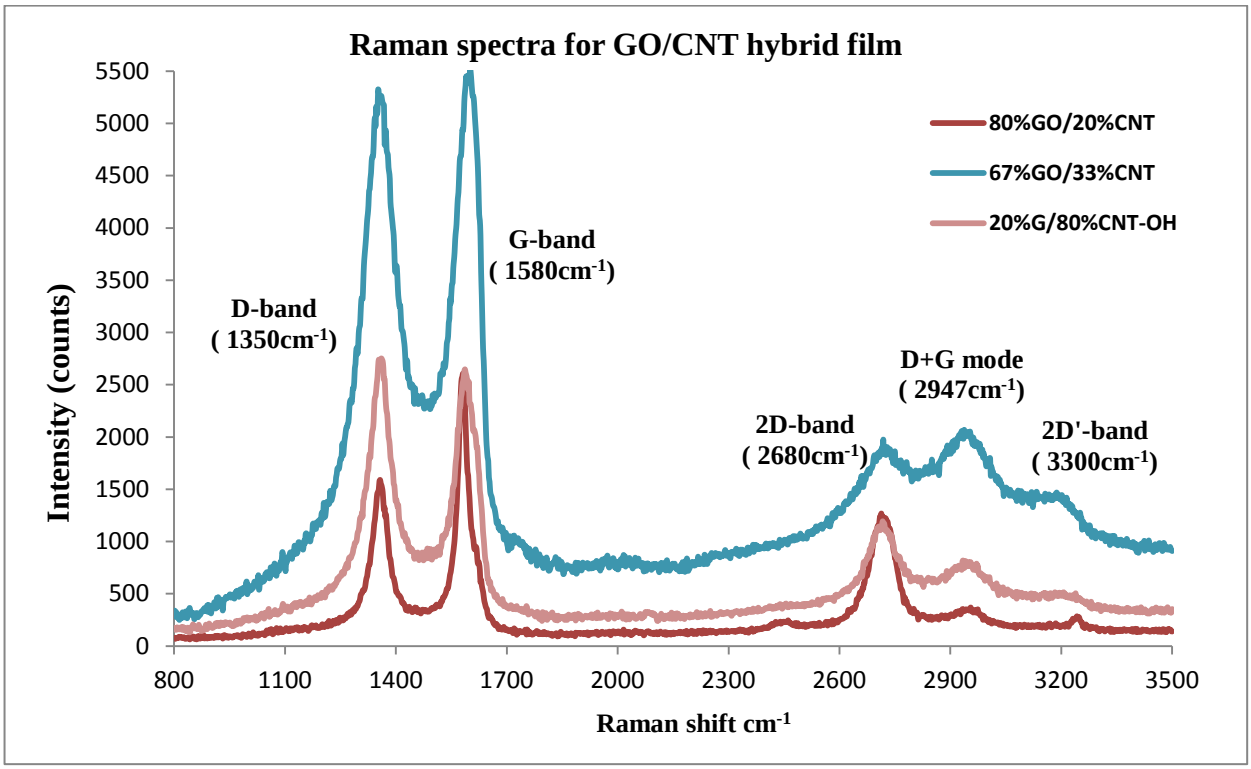

Figure 4-12: Raman spectra for different G/CNT and GO/CNT hybrid film.

As it can be seen in Raman spectra, the film structure is different in each sample. The peaks of G-band of 1580 cm^{-1} and 2D band of 2680 cm^{-1} are clearly identified in the two different spectrums which clarify the spectra of sp^2-hybridized carbon multi-layered system. The D mode at 1350 cm^{-1} raises from the resonance Raman spectra coming from the disordered structure of the graphene. The (D+G) bands appear at 2947 cm^{-1} and the (2D`) band at 3300 cm^{-1} in the (80 wt% GO /20wt % MWCNT) and (64 wt%GO/ 33wt%MWCNT) spectra which are smaller than the 2D. However, they are at a higher intensity in (20wt% G/80wt%MWCNT-OH) spectrum.

4.3.5.2 Magneto Resistance of Graphene Hybrid Film

A small magnetoresistance has been measured in these samples at the room temperature. However, applying a magnetic field to low-temperature measurements to these samples leads to another conclusion. A magnetic field (B) with a direction perpendicular to the surface plane of the sample has been applied to (20 wt% G/80wt% MWCNT-OH) sample. Cooling and warming process have been done from 0K to 300K. The resistivity values have been measured during this period with a magnetic field of B=0T in the first time and then with B=0.65T.

As shown from figure 4-13 to figure 4-14, there is no dependence on the magnetic field found.

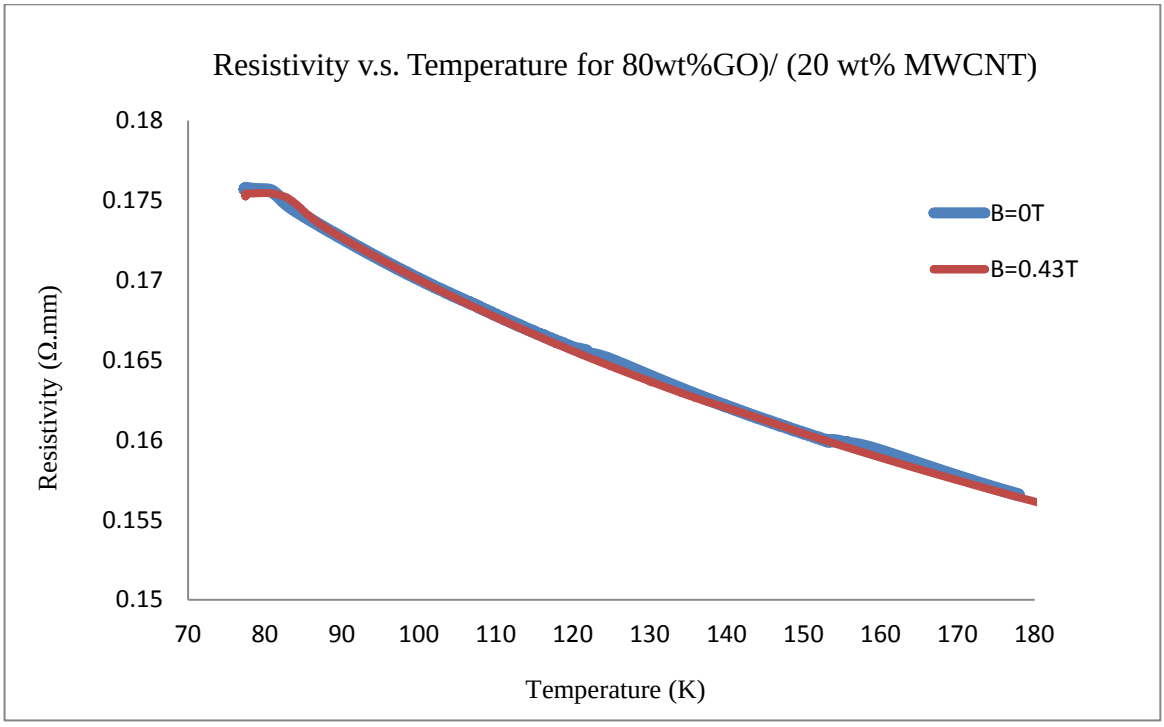

Figure 4-13: Resistivity v.s. Temperature for 80wt%GO/ 20 wt. % MWCNT.

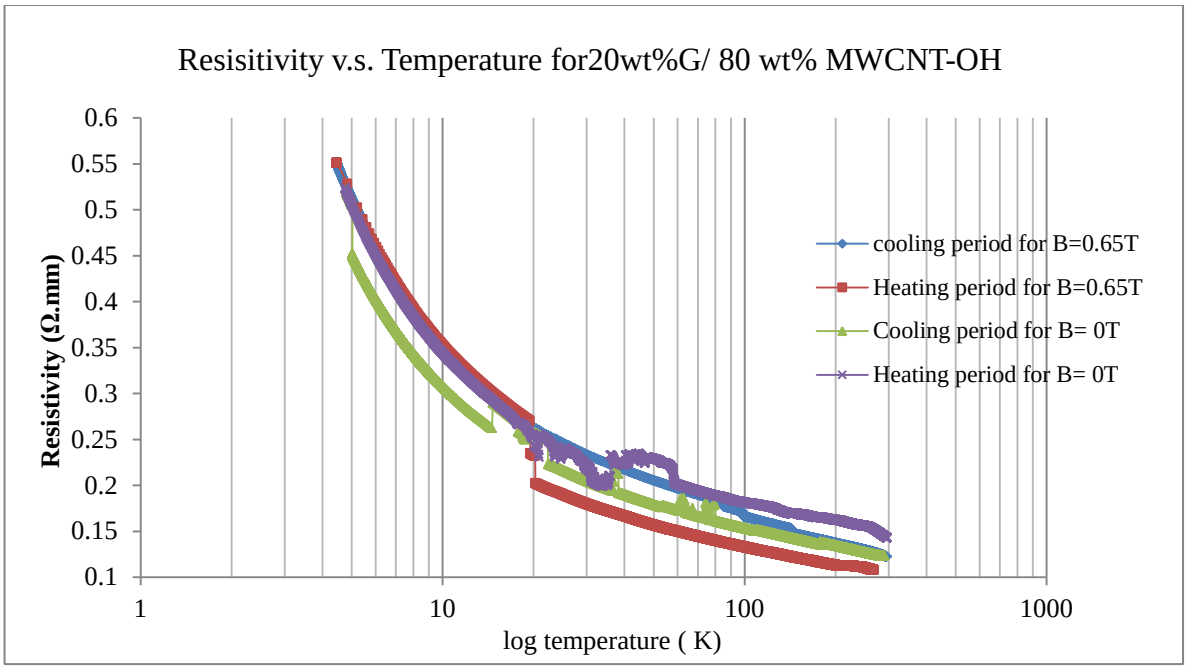

Figure 4-14: Resistivity vs.log temperature for 20wt%G/ 80 wt. % MWCNT-OH.

4.4 Summary

Graphene (G) and graphene oxide (GO)/carbon nanotubes (CNTs) hybrid films were investigated. The finding was as follows:

- With increasing CNT contents, the dielectric constant of the G/MWCNT and GO/MWCNT films have raised almost linearly with wt% MWCNT and their resistivity has reduced.
- G/SWCNT and GO/SWCNT films did not form layered structures leading to a very low dielectric constant.
- Nonlinear behaviour of the dielectric constant with voltage has been observed in the G/MWCNT and GO/MWCNT hybrid films. These results indicate that the length and thickness of the hybrid film have significant influences on the dielectric constant and conductivity of the film.
- The dielectric constant and conductivity rise with increasing film's thickness and decreasing film's length. For the application of graphene/CNT hybrid films as electrodes, this character should be taken into account.
- Moreover, these kinds of hybrid films are found to be independent of any magnetic field.

References

[1] V. Jousseaume, J. Cuzzocrea, N. Bernier, and V. T. Renard, "Few graphene layers/carbon nanotube composites grown at complementary-metal-oxide-semiconductor compatible temperature," *Appl. Phys. Lett.*, Vol. 98, No. 12, p. 123103, 2011.

[2] T. Pei, H. Xu, Z. Zhang, Z. Wang, Y. Liu, Y. Li, S. Wang, and L. M. Peng, "Electronic transport in single-walled carbon nanotube/graphene junction," *Appl. Phys. Lett.*, Vol. 99, No. 11, p. 113102, 2011.

[3] D. H. Lee, J. E. Kim, T. H. Han, W. J. Hwang, S. W. Jeon, S. Y. Choi, S. H. Hong, W. J. Lee, R. S. Ruoff, and S. O. Kim, "Versatile carbon hybrid films composed of vertical carbon nanotubes crown on mechanically compliant graphene films," *Adv. Mater.*, Vol. 22, No. 11, pp. 1247–1252, Mar. 2010.

[4] S. H. Kim, W. Song, M. W. Jung, M. A. Kang, K. Kim, S. J. Chang, S. S. Lee, J. Lim, J. Hwang, S. Myung, and K. S. An, "Carbon nanotube and graphene hybrid thin film for transparent electrodes and field effect transistors," *Adv. Mater.*, Vol. 26, No. 25, pp. 4247–4252, Jul. 2014.

[5] I. N. Kholmanov, S. H. Domingues, H. Chou, X. Wang, C. Tan, J. Y. Kim, H. Li, R. Piner, A. J. G. Zarbin, and R. S. Ruoff, "Reduced graphene oxide/copper nanowire hybrid films as high-performance transparent electrodes," *ACS Nano*, Vol. 7, No. 2, pp. 1811–1816, Feb. 2013.

[6] M. D. Stoller, S. Park, Y. Zhu, J. An, R. S. Ruoff, Z. Yanwu, J. An, R. S. Ruoff, and Y. Zhu, "Graphene-based ultracapacitors.," *Nano Lett.*, Vol. 8, No. 10, pp. 3498–502, Oct. 2008.

[7] S. R. C. Vivekchand, C. S. Rout, K. S. Subrahmanyam, A. Govindaraj, and C. N. R. Rao, "Graphene-based electrochemical supercapacitors," *J. Chem. Sci.*, Vol. 120, No. 1, pp. 9–13, Jan. 2008.

[8] X. Zhao, H. Tian, M. Zhu, K. Tian, J. J. Wang, F. Kang, and R. A. Outlaw, "Carbon nanosheets as the electrode material in supercapacitors," *J. Power*

Sources, Vol. 194, No. 2, pp. 1208–1212, 2009.

[9] W. Hu, X. Niu, L. Li, S. Yun, Z. Yu, and Q. Pei, "Intrinsically stretchable transparent electrodes based on silver-nanowire–crosslinked-polyacrylate composites," *Nanotechnology*, Vol. 23, No. 34, p. 344002, Aug. 2012.

[10] S. Xu, B. Man, S. Jiang, M. Liu, C. Yang, C. Chen, and C. Zhang, "Graphene–silver nanowire hybrid films as electrodes for transparent and flexible loudspeakers," *CrystEngComm*, Vol. 16, No. 17, pp. 3532–3539, 2014.

[11] Richard Fiore, "Effective Capacitance vs Frequency," *Ceramics*, pp. 11746–11746.

[12] B. D. (Bernard D. Cullity and C. D. (Chad D. . Graham, *Introduction to magnetic materials*. IEEE/Wiley, 2009.

[13] E.Y.Tsymbal, "Section 16 : Magnetic properties of materials (continued)," in *The University of Nebraska*, Vol. Physics 92, No. section 16, pp. 1–19.

[14] J. Smit and J. (Jan) 1921-S. E.-I. electronics series vol. 1. Smit, *Magnetic properties of materials*. 1971.

[15] J. Hong, E. Bekyarova, W. A. De Heer, R. C. Haddon, and S. Khizroev, "Chemically engineered graphene-based 2d organic molecular magnet," *ACS Nano*, Vol. 7, No. 11, pp. 10011–10022, Nov. 2013.

[16] M. Sepioni, "Magnetic properties of graphene," The University of Manchester, Manchester, UK, 2012.

[17] J. Červenka, M. I. Katsnelson, and C. F. J. Flipse, "Room-temperature ferromagnetism in graphite driven by two-dimensional networks of point defects," *Nat. Phys.*, Vol. 5, No. 11, pp. 840–844, Oct. 2009.

[18] P. Esquinazi, A. Setzer, R. Höhne, C. Semmelhack, Y. Kopelevich, D. Spemann, T. Butz, B. Kohlstrunk, and M. Lösche, "Ferromagnetism in oriented graphite samples," *Phys. Rev. B*, Vol. 66, No. 2, pp. 1–10, Jul. 2002.

[19] Y. Wang, Y. Hoang, Y. Song, X. Zhang, Y. Ma, J. Liang, and Y. Chen, "Room-temperature ferromagnetism of graphene," *Nano Lett.*, Vol. 9, No. 1, pp. 220–224, Jan. 2009.

[20] T. L. Makarova, B. Sundqvist, R. Höhne, P. Esquinazi, Y. Kopelevich, P. Scharff, V. Davydov, L. S. Kashevarova, and A. V. Rakhmanina, "Retraction: Magnetic carbon," *Nature*, Vol. 440, No. 7084, pp. 707–707, Mar. 2006.

[21] T. Enoki and K. Takai, "The edge state of nanographene and the magnetism of the edge-state spins," *Solid State Commun.*, Vol. 149, No. 27–28, pp. 1144–1150, Jul. 2009.

[22] O. V. Yazyev and L. Helm, "Defect-induced magnetism in graphene," *Phys. Rev. B - Condens. Matter Mater. Phys.*, Vol. 75, No. 12, p. 125408, Mar. 2007.

[23] P. O. Lehtinen, A. S. Foster, Y. Ma, A. V. Krasheninnikov, and R. M. Nieminen, "Irradiation-induced magnetism in graphite: A density functional study," *Phys. Rev. Lett.*, Vol. 93, No. 18, p. 187202, Oct. 2004.

Part One: Conductive Behaviour of Graphene/Carbon Nanotube and Graphene Oxide/ Carbon Nanotube Hybrid Materials

Chapter I-5 Conclusion and Future Work

As graphene plays an essential role in energy storage applications, this part of the project mainly concerns the development of a graphene-based hybrid material as high-performance electrode material using a simple water solution casting method. The investigation of these hybrid film's electrical properties has been proceeded and discussed. In this chapter, a conclusion of the first part of the thesis is given in section 5.1 and future work recommendations follow in section 5.2.

5.1 Conclusion

Considering the fabrication of the graphene-based material hybrid films for an energy storage application propose, the graphene (G) and the graphene oxide (GO) /the carbon nanotubes (CNTs) hybrid films were successfully fabricated as high-performance electrode materials. This has been achieved using a simple water solution casting method, and with the support of a strong ultrasonication process. Different percentages of G, GO, single-wall CNT (SWCNT), multi wall CNT (MWCNT) and MWCNT with a hydroxyl group (MWCNT-OH) were used. To sum up, the finding of the first part are:

1. The hybrid films with MWCNTs have shown well interconnected layered structures at the nanometer scale, where G and GO work as support insulated plates for the MWCNT. G/MWCNTs and GO/MWCNTs film's performance are promising for a capacitor system that would be formed. Numerous of charges are stored in each layer of the conductors which increase the capacitance value and so the dielectric constant.

2. The electrical properties have been studied in an alternating circuit (AC) to find out a linear relationship between the dielectric constant and the CNT weight percent in the film. No matter SWCNT, MWCNTs or MWCNTs-OH incorporated in the film, the energy stored is, in general, directly proportional to the CNT content. Hence, CNTs certainly acted as the conductor assembling charge. Thus, with increasing CNT percentages, the capacitance and so the dielectric constant of the G/MWCNT

and GO/MWCNT films raised up almost linearly and their resistivity reduced. Alternatively, the dielectric constant has found to decline when the frequency went up.

3. Although G/CNT-based hybrid films exhibit a higher dielectric constant and conductivity than GO/CNT-based hybrid thin films, the G/MWCNTs hybrid film is still with a higher dielectric constant and conductivity than G/MWCNT-OH. The (–OH) group in MWCNT-OH with graphene or graphene oxide tends to lower the conductivity and the dielectric constant of the thin film. This can be explained regarding the surface structure of a pure graphene material and materials with functional groups such as –OH group or graphene oxide. The –OH groups influence the material's resistivity as well as the percolated network and decrease the overall material conductivity by twisting the chains of CNTs and shorted the conjugated length. Thus, the resistivity increases until the point of collapsed of the G/MWCNT capacitor around 80% wt CNT. The maximum dielectric constant reached 9.5 x107/g in G (40wt %) / MWCNTs (60wt %).

4. The dispersion of CNTs in the GO or G mixture strongly affects the final quality of the hybrid film that is acting as a capacitor. In compression, GO/SWCNT and G/SWCNT cannot be used in a capacitor system because of their bad dispersion using the water solution casting method. G/SWCNT and GO/SWCNT films have not formed layered structures which lead to having a very low dielectric constant.

5. Thickness and dimension of the film can enhance the capacitor performance and so, the film conductivity will be improved. The dielectric constant and conductivity rise with increasing the thickness of the film and drop with increasing the film length. This character should be taken into account when considering graphene/MWCNT hybrid films for manufacturing electrodes.

6. Some non-linear behaviours of the dielectric constant with a voltage that have been observed in all G/CNT and GO/CNT hybrid films. At some voltages, the dielectric constant reaches the peak or valley. Obviously, the film capacitance is quite dependent on the voltage loaded. Thus, it is possible that nano-junctions have formed between G or GO and CNTs when the content of carbon nanotubes was high. The peak values of the dielectric constant appeared where the junctions are

fully exerted at the relevant voltages.

5.2 Recommends for Future Research

The outcomes of this project part improve the knowledge of the electrical properties of G / CNT-based materials and enhance the fabrication design of G/MWCNT hybrid films. The research on the fabrication and investigation of the electronic and magnetic properties of the G/MWCNT or GOMWCNT hybrid films are still in its early stage. This exciting finding of dielectric constant nonlinear behaviour at this stage leads to digging out for more outcomes. Some of the recommendations for further investigation are as follows.

1. Fabrication and characterisation of real ultracapacitor and battery using GO/MWCNT and G/MWCNT hybrid thin films as electrodes.

2. Analysing and understanding the quantum-like effects of this nonlinear behaviour in different hybrid thin films.

3. Study the dimension effects of the hybrid film in its physical and chemical properties.

Part Two: Carbon Nanotube/Polyethylene Nanocomposites as Strain and Temperature Sensing Materials

Chapter II-1 Literature Review

1.1 Introduction

CNTs have received a lot of attention from scientists during the past two decades, due to their amazing physical properties. Significant efforts in understanding the CNTs physical properties have been made [1], [2]. The one-dimensional (1D) electrical band structure, which gives rise to the unique electrical transport and thermal properties, makes CNTs special candidate for unlimited applications in several fields[1],[2]. Thus, CNT is commonly employed as composite filler -due to the high electrical conductivity- to advance the electrical properties of polymers [3]. This sensitive electronic structure gives CNTs a great potential to develop new strain sensors [4]. This chapter introduces the background of the conductive nanocomposite sensing material. Then, the past progress and on-going efforts on the electronic properties of CNTs and their composites is presented. Section 1.2 gave a general review of nanocomposites. In section 1.3, an overview of conductive polymer nanocomposites, which included a briefly reviewed on the geometric structure of CNTs and the electrical and electronic properties of CNTs, is provided. Sections 1.4 to 1.9 discuss some applications of conductive polymer nanocomposites and the important continuous efforts for developing CNT-based strain and temperature sensors. Lastly, section 1.10 provides some current challenges and difficulties in conductive polymer nanocomposites fabrication.

1.2 General Review of Polymer Nanocomposites

A Composite material is literally two or more chemically distinct materials that differ in shape and chemical composition. They are combined to improve the overall properties of the individual once. It can be a natural composite such as the wood which can be distinguished from a synthesized one like rubber mixed with carbon black. The combination of the composite materials is called (matrix and fiber (filler)). The matrix is usually ductile with low-density material which could be either thermoplastic or thermoset and used to hold the fiber in the desired orientation. The filler, on the other hand, is a substance which is strong but with a low density, such as glass, carbon or particles [5]**.**

Composite material's history was back to early 20th century as the fiberglass was first used to reinforce epoxy in 1940 [6]. Its importance comes from the fact that composites can be a very strong but light material. Also, toughness and fatigue properties are generally greater than common engineering metals. Like steel, corrosion can be also avoided using composites. Moreover, it is possible to achieve combinations of properties which are difficult to find with metals, ceramics or polymers alone [6]. Their implementations are in several industrial branches from aerospace, automotive to sporting goods [7]. However, some drawbacks such as they have anisotropic properties, their properties differ depending on the direction of measurements which may be a disadvantage sometimes as it limits the manufacturing methods. Shaping and manufacturing methods for composite materials are often slow and costly. What is more, many of the polymer-based composites are subject to be attacked by chemicals or solvents which lead to some modification in the composite matrixes [7].

1.3 Conductive Polymer Nanocomposites

Polymers are used in a wide variety of industrial tenders due to their properties like corrosion-resistant and lightweight materials. Although polymers are not good conductors of electricity, electrical conductivity is desired in various polymer applications. Accordingly, production of conductive polymer nanocomposites is essential.

1.3.1 Conductive Nanofillers

Conductive nanofillers are important to make electrical conductive nanocomposites when dispersed into insulating matrices. Conductive powders such as micro-sized metal filings or carbon black can be used as conductive fillers. However, this requires a high loading to mix them well with the matrix. Another way is using the carbon nanofibers which is highly conductive, but a non-uniform dispersion. The nature of conductive nanofillers results in the challenge of a uniform dispersion. In addition, the presence of agglomerates, which is caused by Van der Waals force, in the conductive polymer nanocomposites may compromise the final electrical property. Recent research has suggested that the maximum electrical conductivity of conductive nanocomposites is lower than that of nanofillers by 2 to 4 orders of magnitude because of the tunnelling

resistance [8]. Among all kinds of conductive nanofillers, carbon nanotubes, graphene, and black carbon may draw more attention in recent years.

1.3.1.1 Carbon Nanotube (CNT)

Carbon nanotubes (CNTs) with their outstanding electrical properties became one of the most potential materials that were used as conductive filler in polymer composites since they were reported by Iijima in 1991[9],[10]. They are classified as members of the fullerene structural family, which are allotropes of carbon. The name (carbon nanotubes) has been derived from their size and shape, as their diameter is on the order of a few nanometres, which may reach to several millimeters in length [9].

1.3.1.1.1 Structure and Synthesis of Carbon Nanotubes (CNT)

Carbon nanotubes include two main types: the first one is the single-walled nanotube (SWNT) which is one cylinder (rolled layer) with a diameter between (0.3 and 5.0) nm and length up to (50 to 100) μm [11], [12]. The second one is the multi-walled nanotubes (MWNTs) which consist of multiple rolled layers as presented in figure 1-1. Their production depends on the synthesis process [13]. According to the various arrangements of carbon atoms in their lattice, the geometries of carbon nanotubes can be found as armchair, zigzag or chiral arrangement as shown in figure 1-2. In addition, carbon nanotubes have a high aspect ratio, which can reach to 1000 [14].

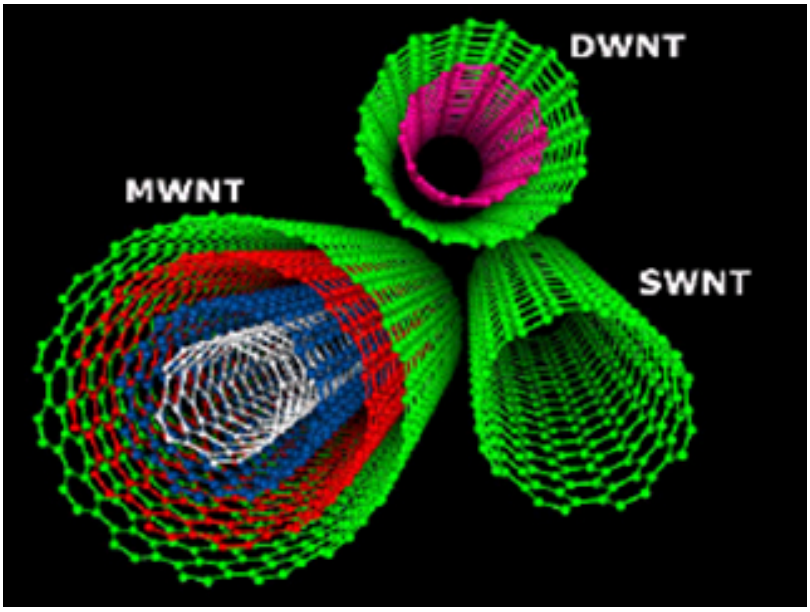

Figure 1-1: Structures of SWNTs and MWNTs[15].

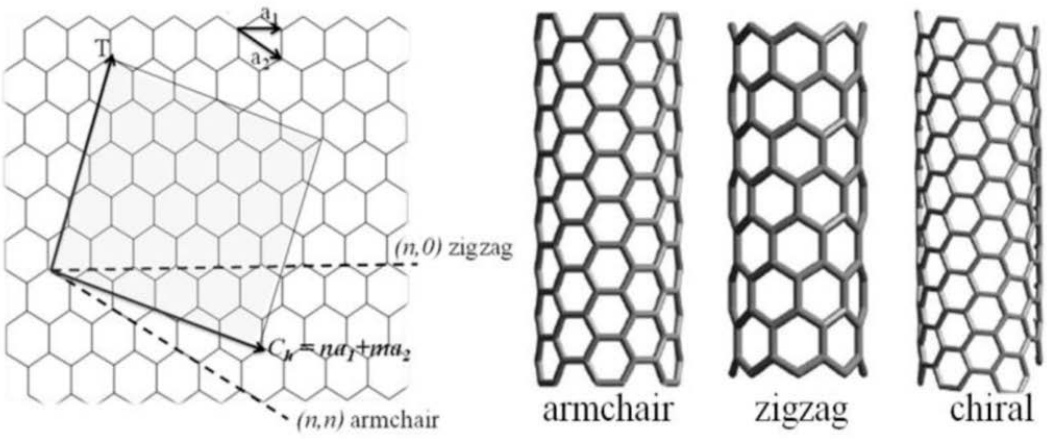

Figure 1-2: The geometries of carbon nanotubes are armchair, zigzag or chiral [16].

1.3.1.1.2 Properties of CNT

1.3.1.1.2.1 Thermal Property

The thermal conductivity of carbon nanotubes is an essential concern, which depends on the temperature and the large phonon mean free paths [17]. At room temperature, measurements show that thermal conductivity of individual MWCNT can reach $3000 Wm^{-1}K^{-1}$. SWNT, as well as MWCNT, has a room-temperature thermal conductivity of about 3500 $W \cdot m^{-1} \cdot K^{-1}$ [18]. Comparing CNTs thermal conductivity to a metal like copper, which is well-known for its good thermal conductivity, 385 $W \cdot m^{-1} \cdot K^{-1}$, CNT is definitely higher [18].

1.3.1.1.2.2 Mechanical property

Apart from the high thermal conductivity, carbon nanotubes have excellent mechanical properties such as high stiffness, modulus and tensile strength due to the stronger sp^2 carbon bonding structure [20]. For example, Young's modulus and tensile strength of MWNTs are respectively in the range of (1.7- 2.4) TPa and (11-63) GPa [21]. Some of CNT's mechanical properties are presented in table 1-1.

Table 1-1: Comparison of CNT mechanical properties [19]

Material	Young's Modulus (TPa)	Tensile Strength (GPa)	Elongation at Break (%)
SWNT	~1 (from 1 to 5)	13–53	16
Armchair SWNT	0.94	126.2	23.1
Zigzag SWNT	0.94	94.5	15.6-17.5
Chiral SWNT	0.92		
MWNT	0.27-0.8--0.95	11-63-150	
Stainless steel	0.186-0.214	0.38-1.55	15-50

1.3.1.1.2.3 Electrical Property

The high thermal conductivity value, the CNT structure, and its greater mechanical properties are the main contributed factors to give the final carbon nanotube electrical properties. CNTs show high electrical conductivity, (1000- 200,000) Scm^{-1} [22], which is influenced by their geometry. Generally, the chirality of the carbon nanotubes, the degree of a twist as well as their diameter have significant influences on the CNT's electrical conductivity which confirm whether the carbon nanotubes are metallic or semiconductor [23]. Hence, SWCNT can be considered as semiconductors, metals or small band-gap semiconductors depending on CNT chirality and tube diameter. Narrow diameter of SWNT can be a strong influence on its electronic excitations [24]. The resistivity of SWCNT is also a temperature dependent, which decreases with temperature in the range of 80K to 350K. Experimentally, at about 200K SWCNT can transfer from non-metallic to weakly metallic material [25]. SWNT's superconductivity has been also observed at low temperature. The transition temperature was found to be 5K for 0.5nm diameter tubes and only 0.55K for 1.4nm diameter [26]. Although the maximum current densities of normal metals are 105 Acm^{-2}, the SWCNT, for example, can carry up to 109Acm^{-2}[27]. Therefore, CNTs is called metallic.

1.3.1.1.3 CNT Fabrication

Carbon nanotubes are synthesized by Chemical Vapour Deposition (CVD) which can be plasma CVD, thermal CVD or vapour phase growth [28], [29], direct-current arc discharge [30] or laser ablation [31]. Image of CNT Synthesis is shown in Figure 1-3.

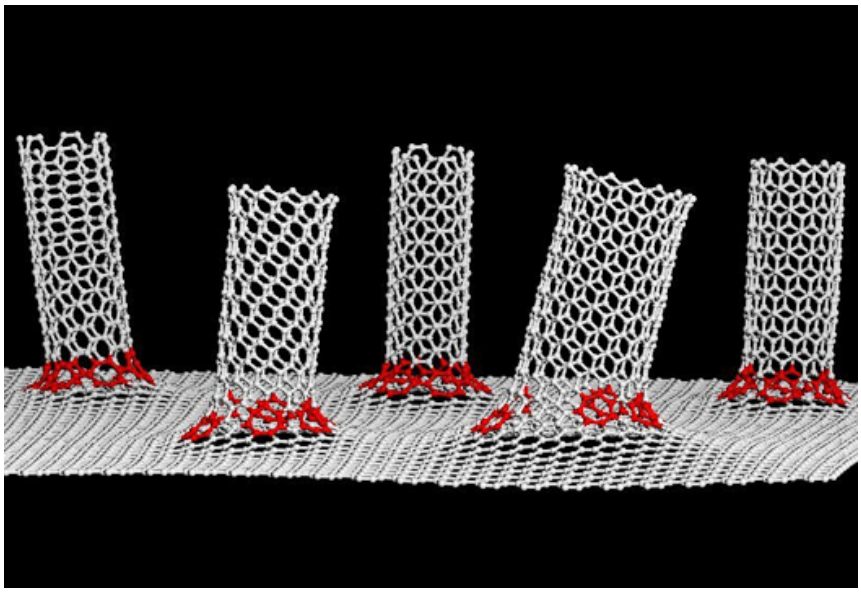

Figure 1-3: Synthesis of carbon nanotubes[32].

A summary of the three types and their advantages and disadvantages are presented in table 1-2.

Table 1-2: Compression of Plasma torch, CVD or Arc discharge method[33][34]

	Plasma Torch	**Arc Discharge Method**	**Chemical Vapour Deposition**
Advantages	Can produce SWNT and MWNTs with few structural defects	Easiest to scale to industrial production; long length	Primarily SWNT with a large diameter range that can be controlled by varying the reaction temperature
Disadvantages	Tubes tend to be short with random sizes and directions	usually MWNTs and often riddled with defects	High cost

1.3.1.1.4 CNT Application

Based on its excellent mechanical, electronic and thermal properties such as high conductivity, ultra-high surface area, good corrosion resistance, high-temperature stability and percolation pore-structure [16-26], great efforts have been made around the world to use CNT in various application systems. It has been utilized in electrochemical energy storage such as capacitors, transistors and hydrogen storage in fuel cells [[35]-[37]. Combined with the particular shape of the electronic band structure of graphene, carbon nanotubes are ideal for quantum wires and biomedical applications as shown in figure 1-4. Moreover, CNT is very useful as probe tips for very high-resolution scanning probe.

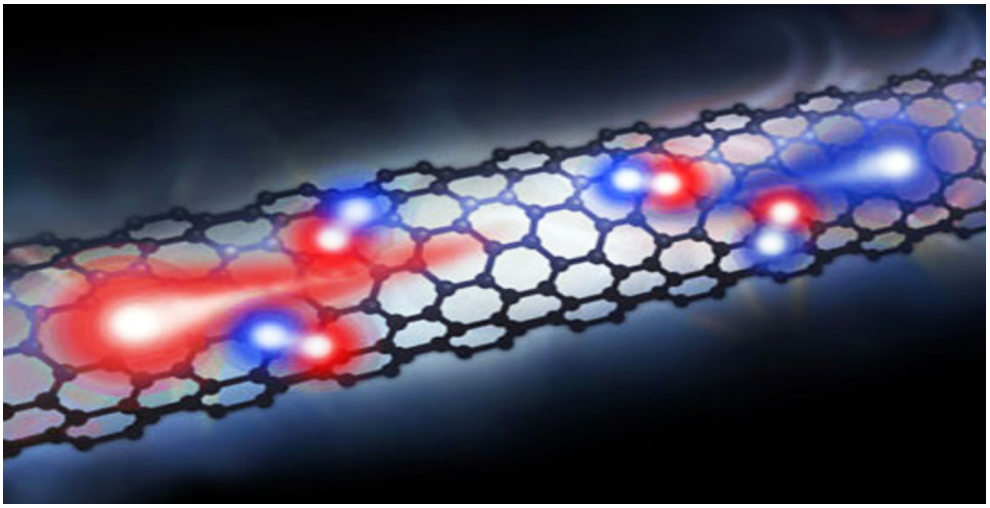

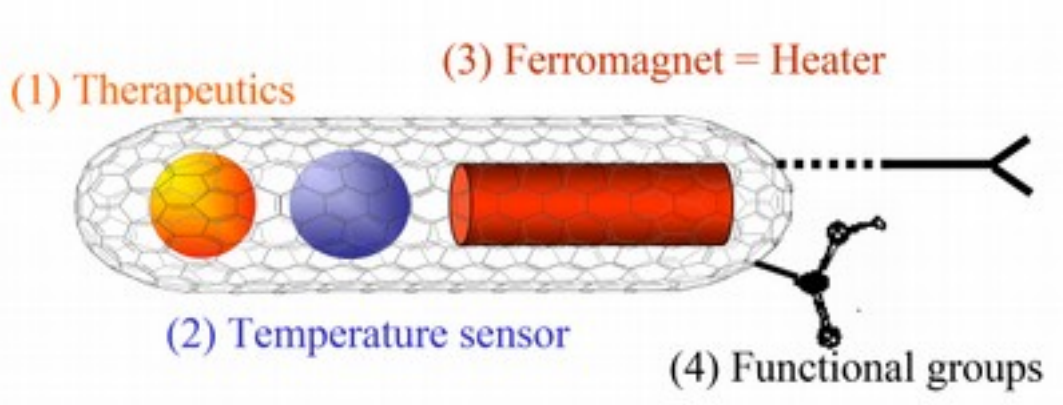

Figure 1-4: Using of carbon nanotubes as drug delivery tools {cancer treatment }[95]**.**

1.3.1.2 Graphene

Graphene literature review has been covered in chapter I-1.

1.3.1.3 Carbon Black

Conductive carbon black is another carbon allotropic that used as filler in polymer nanocomposites. It has a very high void volume which allowing the holding of a carbon network at low filler content [38]. Economic importance and abundant resource make it a good candidate as polymer conductive filler [39]. However, the carbon black surface area is higher than 1000 m^2/g and usually, exists as aggregates of coalesced elemental carbon in the form of colloidal particles rather than individually [40]. The degree of agglomeration affects the final properties of the filled polymer. Carbon black fillers with low surface area and shape factor show a low tendency to agglomerate than carbon black filler with high surface area and shape factor [41].

Generally, carbon black is produced by the incomplete combustion or thermal decomposition of hydrocarbons [41], [42]. Comparing with graphene, the density of the carbon black is much lower. Nevertheless, carbon black shows much higher percolation threshold than carbon nanotube, so the electrical conductivity of the carbon black is lower than the carbon nanotube, especially with lower filler content [43].

1.4 CNTs/ Polymer Nanocomposites

Carbon nanotubes are used to reinforce polymeric matrices such as epoxy, polystyrene, polyurethane, polycarbonate and ultra-high molecular weight polyethylene [44], [45]. This has improved the electrical conductivity of nanocomposites as well as strength, stiffness, thermal conductivity and stability [45]. Enhancement of oxidation stability is another benefit of having CNTs in polymer composite [44], [45]. The very high aspect ratio of some carbon nanotubes may also enable them to be aligned with one axis of the composite which make the fabrication of conducting polymers easier [44].

Deagglomeration and dispersion are two problems which may occur during mixing CNTs with polymers. Therefore, uniform dispersion of nano- sized CNT filler particles can produce an ultra-large interfacial area per volume between the nanoelement and polymer matrices [44].

The matrices can be thermoplastics or thermosetting resin. Nonetheless, the difference in percolation thresholds exists between thermoplastic nanocomposites and thermosetting nanocomposites. Generally, the electrical conductivity of CNTs based thermoplastic nanocomposites is reported to be in the range from 0.2 to 15 wt%, while that of thermosetting nanocomposites lies between 0.1 and 1 wt% [46]. Normally, the electrical conductivity of CNTs reinforced nanocomposites is higher than the based polymer by 8-13 orders of magnitude [46]. The electrical conductivity of common CNTs reinforced polymer nanocomposites is summarized in table 1-3.

Table 1-3: Electrical property of CNTs based polymer nanocomposites[47]

Polymer type	Nanotube type	Percolation threshold (wt%)	CNT content (wt%)	Maximum conductivity (S/m)
Polystyrene	MWNT	0.15–0.2	2	10^3
Polycarbonate	SWNT-functional	0.11	7	4.81×10^2
Polystyrene	SWNT-functional	0.045	7	6.89
Poly(vinyl acetate)	XD grade CNT	–	20	4.8×10^3
Poly(methyl methacrylate)	MWNT	0.3	40	3×10^3
Poly(methyl methacrylate)	SWNT	0.17	10	1.7×10^3
Poly(methyl methacrylate)	$SOCl_2$-doped SWNT	0.17	13.5	10^4
Poly(vinyl alcohol)	MWNT	5–10	60	100
Poly(vinyl acetate)	SWNT	0.04	4	≈15
Epoxy	MWNT	0.0025	1	2

The percolation threshold in table 1-3 is generally in the range from 0.0025 wt% to 10wt%. In addition, Koratkar and co-workers had found that the electrical conductivity of carbon nanotubes reinforced PS nanocomposites is higher than that of graphene/ PS nanocomposites [48].

1.4.1 Fabrication of CNTS/ Polymer Nanocomposites

The first CNTs reinforced nanocomposite was stated by Ajayan and co-workers in 1994 [49]. This result suggested that MWNTs have excellent mechanical properties and their anisotropy can be induced by a flow of such a material. Four years later, in 1998, there were other works published on CNT/polymer composites. Schadler et al. (1998) [50] reported the dispersion of 5 wt% MWNTs in an epoxy resin by an ultrasonic treatment. Although the MWNTs were well separated, they remain poorly distributed.

Recently, polymer /CNT nanocomposite has been prepared by taking epoxy as the polymer matrix and by adding about (1-2) wt% of CNTs to it using the ultra-sonication

route for better dispersion. It has been found that the mechanical strength of a polymer becomes a hundred times better even by the addition of 1% of CNTs [50].

1.5 Graphene/ Polymer Nanocomposites

Graphene-polymer nanocomposites show the outstanding electrical property as well as the good mechanical properties, thermal property and optical property that have been used in a wide range of demanding applications. To date, epoxy, polyurethane, polystyrene, polycarbonate, polyimides, polyethylene terephthalate and poly (methyl methacrylate) have been used as polymeric matrices in graphene reinforced nanocomposites. Generally, the electrical conductivity of graphene /PS nanocomposites is reported to be in the range from 1 Sm^{-1} to 24 Sm^{-1} [51]. The electrical conductivity of common graphene reinforced polymer nanocomposites is summarized in table 1-4. The differences in processing technology, types of polymer matrices and nanofillers may result in different electrical conductivity.

The percolation threshold of the epoxy/graphene nanocomposites, prepared by solution mixing, is only 0.52 wt% which is caused by the high aspect ratio and homogenous dispersion of graphene [52]. PET/graphene nanocomposites, prepared using melt compounding, show high electrical conductivity because the overlaps and the folds in graphene structures result in a high current density [52]. PS/graphene nanocomposites are prepared using either in situ polymerization or solution mixing. The incorporation of graphene in the PS matrix effectively increases the electrical conductivity of pure PS from about 10^{-14} Sm^{-1} to 5.77 Sm^{-1} at 0.38 wt% [52]. The percolation threshold of graphene-based nanocomposites is normally higher than that of carbon nanotubes reinforced polymer nanocomposites, which is about 0.0025 wt% [53].

Table 1-4: Electrical property graphene based polymer nanocomposites[52]

Matrix	Filler	Filler loading (wt.%[a], vol.%[b])	Process	σ (S m^{-1}) of matrix	σ (S m^{-1}) of composite
Epoxy	EG	3.00[a]	Sonication	1E−13	1E−4
	EG	2.50[b]	Solution	1E−15	1E−2
	Graphene	0.52[b]	Solution	1E−10	1E−2
PMMA	NanoG	0.68[b]	*In situ*	1E−13	1E−3
	EG	1.00[a]	Solution	1E−15	1E−3
	EG	10[a]	*In situ*	–	77.65
PS	NanoG	1.00[a]	*In situ*	1E−14	1E−4
	Graphene	0.10[b]	Solution	1E−16	1E−5
	GNS^{C4P}	0.40[b]	Solution	1E−14	1E−5
	GNS^{C4P}	0.10[b]	Solution	1E−14	4
	GNS^{8B}	0.20[b]	Solution	1E−14	1E−5
	GNS^{5D}	0.30[b]	Solution	1E−14	1E−5
	Graphene	–	Solution	1E−16	24
	Graphene	2.0[a]	*In situ*	1E−10	1E−2
	EG	1.50[b]	*In situ*	1E−16	1E−4
	K-GIC	8.20[a]	Solution	NA	–
Nylon-6	EG	1.50[b]	*In situ*	1E−15	0.1
	FG	0.75[b]	*In situ*	1E−15	1E−5
PP	xGnP-1	3.00[b]	Coating	1E−12	0.1
	xGnP-1	3.00[b]	Solution	1E−12	1E−2
	xGnP-15	7.00[b]	Melt	1E−12	1E−3
	xGnP-15	5.00[b]	Coating	1E−12	0.1
	EG	0.67[b]	Solution	1E−16	0.1
HDPE	EG	3.00[a]	Melt	1E−16	1E−8
	UG	5.00[a]	Melt	1E−16	1E−10
PPS	EG	4.0[a]	Melt	1E−12	1E−3
	S-EG	4.0[a]	Melt	1E−12	1E−2
PANI	Graphite	1.5[a]	*In situ*	5.0	3300.3
	GO	–	*In situ*	2.0	1000
PVDF	FGS	2.0[a]	Solution	1E−11	1E−2
	EG	5.0[a]	Solution	1E−11	1E−3
PVA-S	NanoG	0.2[a]	Solution	1E−13	1E−3
PET	Graphene	0.47[b]	Melt	1E−14	7.4E−2
Polycarbonate	FGS	2.0[a]	Melt	1E−14	1E−9
	Graphite	12	Melt	1E−14	6.6E−11

1.6 Carbon Black/ Polymer Nanocomposites

Carbon black is often used as filler in elastomers or plastics to modify the properties of the materials [42]. The fundamental property of the filler used in a filled elastomer is the particle size. This affects the reinforcement of elastomer most strongly. The particle size of carbon black particles varies from (10 to 500) nm. Table 1-5 shows the relation between the particle size and the strength of reinforcement. Normally, carbon black is preferred to be combined with carbon nanotube when used as filler, as the high percolation threshold of the carbon black lowers the mechanical properties of the nanocomposites [41].

Table 1-5: Effect of particle size on reinforcement [41]

Size /mm	Strength
1000-5000	Small reinforcement
<1000	Medium reinforcement
<100	Strong reinforcement

1.7 Applications of Conductive Polymer Nanocomposites (CPNC)

CPNC have been applied in a vast range of industries applications such as automobiles, aerospace [53], constructions, sensors [54], electromagnetic interference materials shielding [55], nano-electric devices [56] and biomedical applications[57],[58]. For instance, polyphenylene oxide (PPO)/ polyamide (PA) blend with CNTs can be used in automotive mirror housings which have been reported to substitute conventional micro-size conductive fillers [59]. Alternatively, Graphene-based nanocomposites have been effectively used for supercapacitors, as complementary devices with batteries [60]. It also utilized with low loadings of graphene as pressure sensors in aerospace and automotive applications [53]. On the other hand, Carbon black based nanocomposites have been involved in gas sensor and the automotive industry. Recently, great interest to develop strain sensors in aerospace using carbon nanotubes reinforced nanocomposites [61]. For this kind of sensors, the direct current (DC) properties of nanocomposites are needed [9]. Compared with conventional sensors, these sensors show the higher sensitivity of electrical conductivity to applied strain, which is related to CNTs addition [62], [63]. Besides, conductive nanocomposites based chemical and biological sensors are widely applied in clinical diagnosis, environmental and food safety monitoring [12]. Nevertheless, the limitation in multidirectional sensibility still exists in the most kinds of sensors [64], [65].

1.8 Polymer Nanotechnology

1.8.1 Preparation, Processing, and Manufacturing of Conductive Polymer Nanocomposites

In order to achieve a good and well dispersion of nanofillers in a polymer matrix, the proper mixing methods are carefully chosen. In-situ polymerization, melt compounding and solution mixing are the conventional methods to synthesize conductive polymer nanocomposites. However, latex technology could be a preferable choice to manufacture the conductive nanocomposites with a uniform dispersion of nanofillers.

1.8.1.1 Conventional Technologies

1.8.1.1.1 In Situ Polymerization

In this method, nanofillers are polymerized from monomers to form nanocomposites. A study of CNTs/ Polyaniline (PANI) nanocomposites that were prepared by using in situ polymerization has been reported [66]. This method offers stronger interactions between the nanofillers and the matrix, which is contributing to better mechanical and electrical properties of final nanocomposites in comparison with other two conventional methods [67]. However, the scale of production is limited by the rise of the electrical energy needed to have a good dispersion of the nanofillers in the matrix [67]. It has been reported that this technique was used to reinforced polyurethane, polyethylene, polystyrene and nylon with MWCNTs [57].

1.8.1.1.2 Solution Mixing Technique

It is a simple and common process in which the nanocomposites are formed in the presence of solvents. The obvious advantage of this method is to prepare the nanocomposites with a good dispersion of nanofillers which resulting in having conductive nanocomposites with low percolation threshold [67]. Using this method, conductive polymer nanocomposites including CNT/PVC (poly (vinyl chloride)), graphene/PVA and CNT/PS (Polystyrene) [57], [68], [69] have been studied. However, solvent removal is still a serious problem which makes the solution-based method is not a common way in industrial manufacturing.

1.8.1.1.3 The Melt Compounding Manner

In this method, nanofillers are mixed with the polymer matrix in the molten state without solvents [52]. This method is quite suitable to prepare thermoplastic nanocomposites. Compared with solution mixing, this method is hard to achieve the uniform dispersion of the nanofillers due to the high viscosity of the thermoplastics [57].

1.8.1.2 Latex Technology

The latest study on conductive polymer nanocomposites has focused on finding better methods to prepare the nanocomposites with uniformly dispersed nanofillers. A new technology, named latex technology, has attracted more interests. A variety of conductive polymer nanocomposites such as CNTs reinforced Isotactic Polypropylene (iPP) and PS have been reported in using latex technology [70], [71]. This technique is mainly to disperse the nanofillers in a surfactant solution first, and then to be mixed with polymer latex [72]. The procedure of using latex technology for the preparation of conductive polymer nanocomposites is described in figure 1-5.

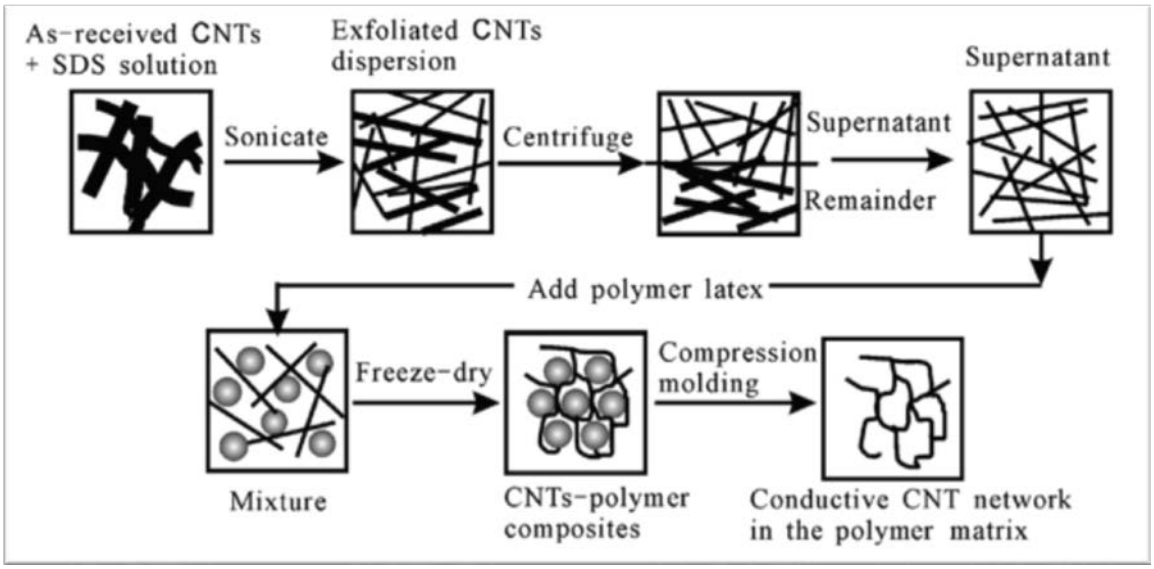

Figure 1-5: Process for the preparation of conductive polymer nanocomposites using latex technology [71]

This method can achieve a homogenous dispersion of nanofillers in the polymeric latex matrix [70]. Also, the final nanocomposites show a very low percolation threshold with the low nanofillers addition [73]. In a recent study, a low percolation threshold of 0.3wt% SWNTs in the PS matrix using latex technology was stated by Grossiord N. [74]. The percolation threshold of 1.5 wt% MWNTs, in PS latex matrix, was reported by Junrong

Yu [71]. Compared with the conventional technologies, the remarkable advantage of latex technology is that it is versatile and most of the polymers that are prepared by emulsion polymerization can be used as matrix [75].

1.9 Characterisation of Conductive Nanocomposite Materials

To study morphology and the properties of conductive polymer nanocomposites, characterisation tools are so important. Different methods and apparatus can be used to study and examine them such as Scanning Electron Microscopy (SEM), Transmission Electron Microscopy (TEM) and X-ray Diffraction (XDR), which are covered in chapterI-1. In addition, SEM, TEM and XRD (both wide-angle X-ray scattering and small-angle X-ray scattering) can be used in studying the nanocomposites morphology. However, a limitation exists in the assessment of the dispersion due to the magnification of the optical microscope. As shown in figure 1-6 (a), no obvious CNT aggregates are found under the optical 1000X, suggesting a good dispersion, while at 30000X in (b); the presence of aggregates found suggests that the dispersion of CNT is not uniform.

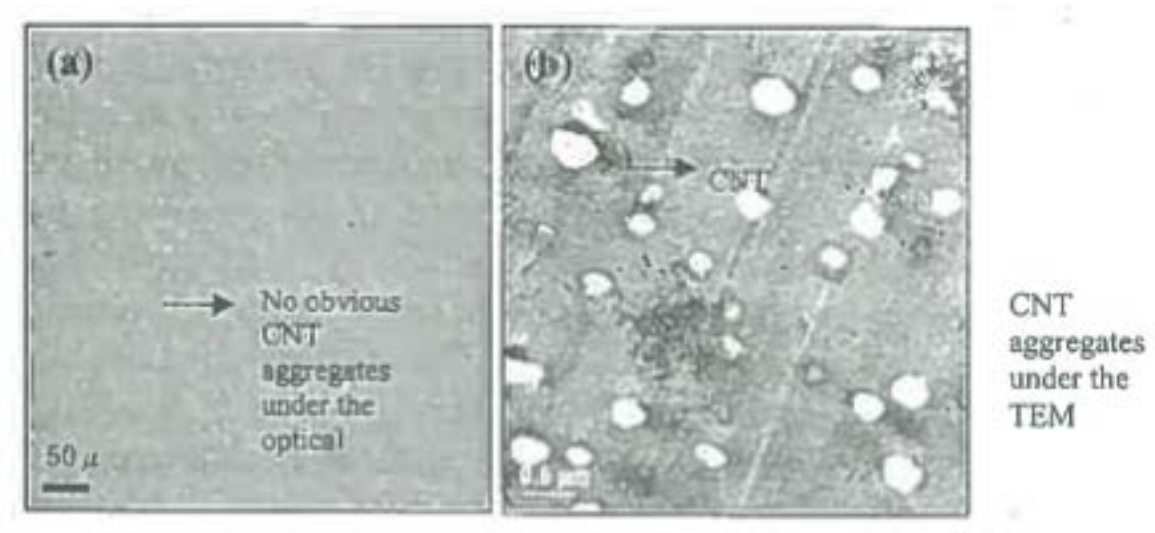

Figure 1-6: (a) TEM image of CNT dispersion at 1000X (b) TEM image of CNT dispersion at 30000X [76].

1.10 Mechanisms and Effects on Electrical Conductivity

1.10.1 Mechanisms of Electrical Conductivity

The main mechanisms of electrical conductivity include quantum tunnelling or electrons hopping and percolation in a conducting network [77]. Recent research pays more

attention to the percolation mechanism, which is defined as the formation of a conductive three-dimensional network of conductive nanofillers in the polymer matrix [78]. The percolation mechanism can be described as follows:

$$\sigma \propto (p - p_c)^{\alpha} \quad (1\text{-}1)$$

Where σ is the conductivity, p is the filler content, α is the critical exponent, and p_c is the percolation threshold characterized by a sharp jump in the electrical conductivity [79]. The effect of conductive nanofillers is to provide percolate pathways for electron transport that makes conductive polymer nanocomposites show electrical conductivity [72].

1.10.2 Effects on Electrical Conductivity

The electrical conductivity of conductive polymer nanocomposite is determined by the number of junction points and the distance between neighbouring nanofillers [80]. Figure 1-7 illustrates the effect of the distance between adjacent nanofillers on their electrical conductivity.

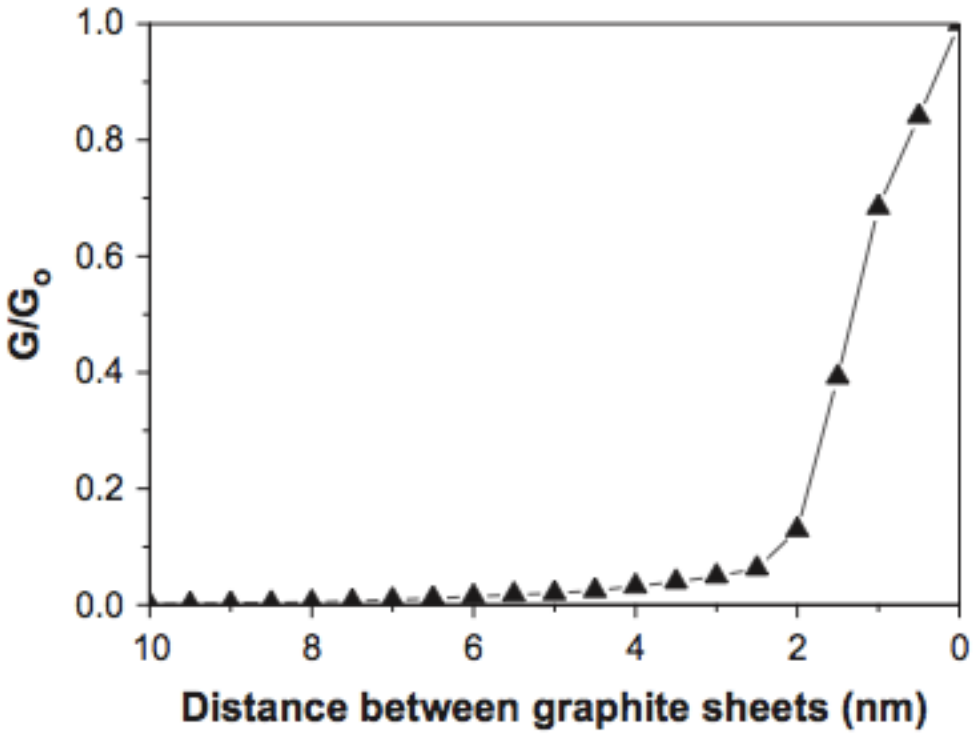

Figure 1-7: Conductance of composites as the function of distance (G is the conductance of the composite, G_0 is the conductance of the filler) [8].

From figure 1-7, there is little change in conductance when the inter-particle distance is less than 5nm, and if the distance is close to 1nm, the conducting pathway is formed. Thus, the inter-particle distance in the range from (1– 5) nm is preferable for the research about the effects on electrical conductivity [8].

Since the formation of conductive three-dimensional networks contributes to the electrical conductivity, the main factors that may interrupt the conductive networks and thus influence the electrical conductivity of nanocomposites to involve the external force or pressure, temperature, the degree of dispersion, alignment and filler content [8].

1.10.2.1 Temperature Influences

The increase of temperature results in the differences of thermal expansion between the conductive nanofillers and the polymer matrix [81]. Normally, the more rapid and larger expansion of the polymer matrix increases the inter-particle gap width which leads to eliminating some conductive pathways [82]. In addition, the expansion of the nanofillers increases the distance between them, leading to a higher resistivity [81]. The temperature dependence of the electrical resistivity is shown in figure 1-8.

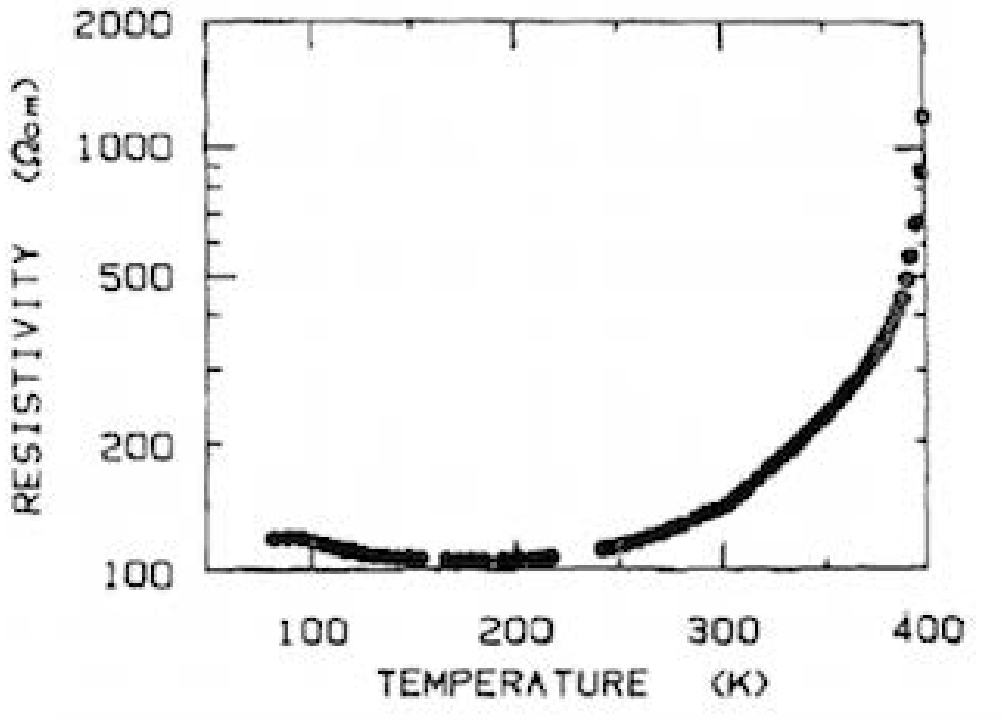

Figure 1-8: Electrical resistivity versus temperature [81]

Figure 1-8 illustrates that as temperature goes up, the electrical resistivity increases and the electrical conductivity correspondingly decreases.

1.10.2.2 Dispersion of CNT

The electrical conductivity of polymer nanocomposites strongly depends on the degree of dispersion. The uniform dispersion of nanofillers helps to form conductive networks. The CNT/PS nanocomposite with good dispersion of nanofillers, prepared using latex technology, has been reported to have a good electrical conductivity [73]. The SEM image of the fracture surface of CNT/PS nanocomposite is shown in figure 1-9.

Nevertheless, conductive nanofillers cannot spontaneously disperse in matrix due to the effect of strong attractive forces [83]. The presence of agglomerates impacts the difficulty of the dispersion. Normally, high shear mixing force needs to break the agglomerates into very small pieces. The effect of dispersion on electrical conductivity is shown in figure 1-10.

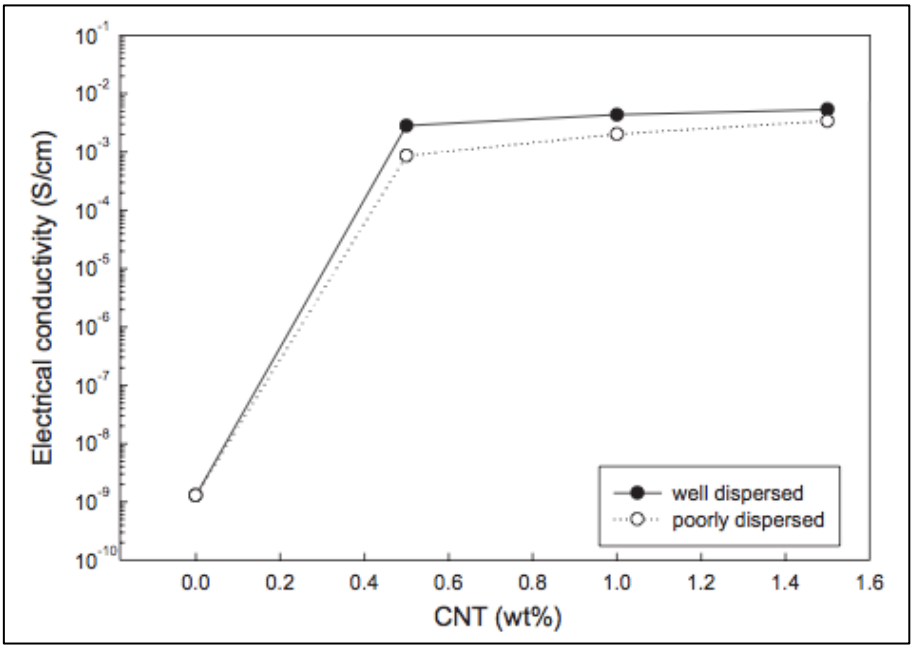

Figure 1-9: SEM image of the fracture surface of CNT/PS nanocomposite [73]

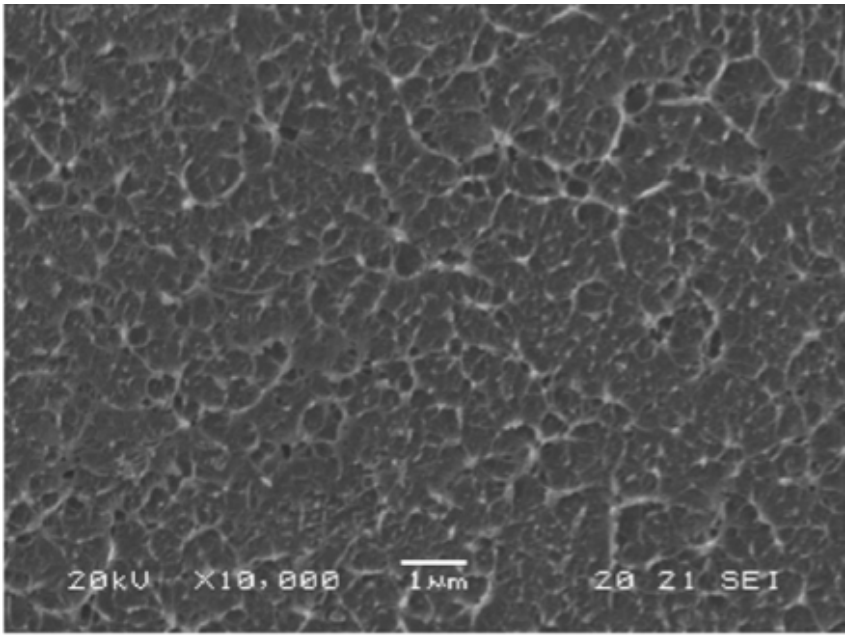

Figure 1-10: The effect of dispersion on electrical conductivity [79]

It is clear from figure 1-10 that the electrical conductivity of the nanocomposites with well-dispersed fillers is higher than with a poor dispersion of fillers. It is due to the high dispersion effectively that reduces the junction points of the nanofillers and so the conductive pathways are easier formed [79]. Nadia Grossiord reported three methods that can improve the dispersion of the nanofillers in the matrix, including direct mixing, modification of the filler and matrix, and the addition of the third component [84].

1.10.2.3 Alignment of CNT

The improvement in the alignment of conductive nanofillers leads to a lower percolation threshold and higher electrical conductivity [59]. Research shows that an increase of 35% in the electrical conductivity has been found for SWNTs/ epoxy nanocomposites with aligned SWNTs comparing to the unaligned one [85]. The reason is that with aligned SWNTs more interactions are created and this provides further percolation pathways [86]. Moreover, orientation and anisotropy also affect the electrical conductivity. Wang et al. found that at the same filler content, the electrical conductivity along the orientation was higher than that perpendicular to it by three orders of magnitude [87]. Electrical conductivity perpendicular to the orientation value is lower than that along the direction at the same level of concentration; consequently, the formation of the conductive networks of nanofillers along the orientation is easier than that perpendicular to it [87].

1.10.2.4 Filler Content

The electrical conductivity strongly depends on the filler content [84]. At lower filler content, the electrical conductivity is also very low. When the percolation threshold is being reached, a little increase in the filler content leads to a dramatic increase in the electrical conductivity of the nanocomposites [84]. With the further incorporation of nanofillers, the rate of increase in the electrical conductivity decreases due to the more generated agglomeration of fillers [88]. According to percolation theory [46], the relationship between resistivity and nanofillers content can be expressed using the equation 1-2:

$$\rho = \rho_0(\upsilon - \upsilon_c)^t \quad (1\text{-}2)$$

Where ρ is the resistivity of nanocomposites, ρ_0 is the resistivity of conductive filler, υ is volume content, υ_c is percolation threshold and t is critical exponent [46].

Furthermore, the relationship between the electrical conductivity and nanofillers content is illustrated in figure 1-11.

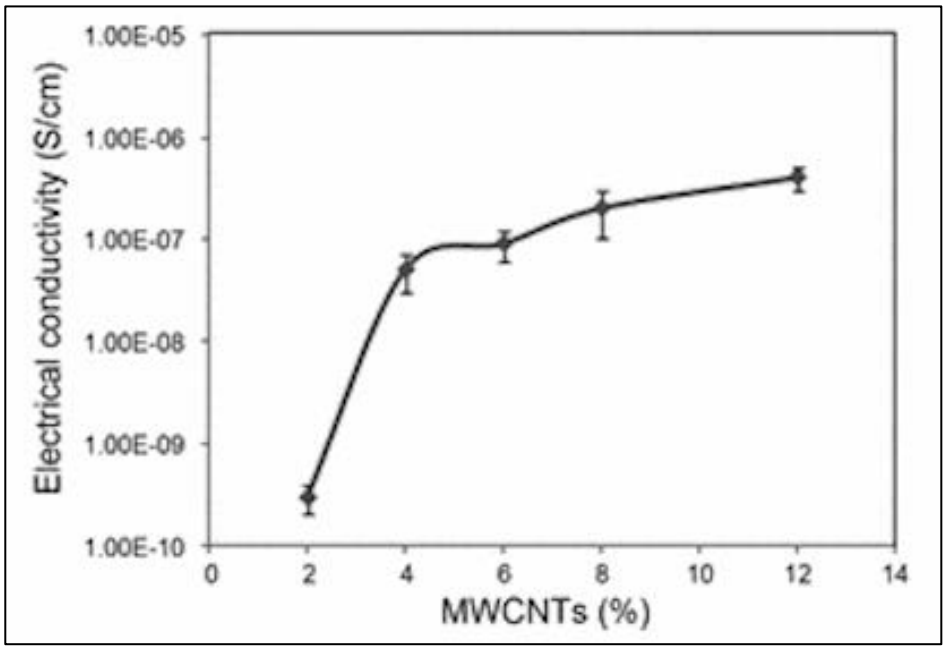

Figure 1-11: Electrical conductivity of MWNTs/PU nanocomposites versus MWNTs content [89].

It is clear that when the MWNTs content increases, the electrical conductivity rise as well. In addition, the electrical conductivity sharply increases in the range of 2-4 wt% of MWNTs, while no improvement on the electrical conductivity is shown when the

MWNTs content is less than 2 wt%. This result is also in a good agreement with Remeo observations of MWNTs/ PCL composites [89].

1.10.2.5 External force

The electrical conductivity of conductive polymer nanocomposites is very sensitive to mechanical deformations [64]. When external force or pressure is applied on the conductive polymer nanocomposites, they tend to deform which makes contact resistance is also changed accordingly [64]. The increase of strain or deformation decreases the electrical conductivity because the deformation widens the distance between the neighbouring nanofillers and causes the disruption of the existing conductive three-dimensional network which reduces of conduction pathways [89]. At low strain, the disruption of the conductive networks occurs, and accordingly, the electrical conductivity decreases, shown in figure 1-12.

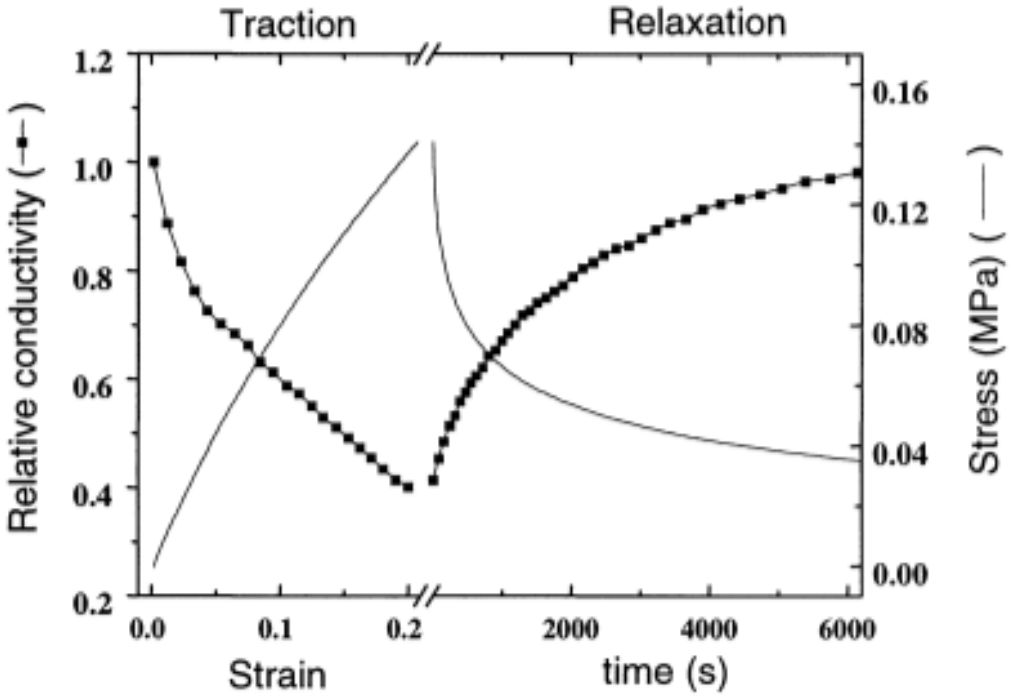

Figure 1-12: The relationship between electrical conductivity and mechanical deformation, and the time-dependent electrical behaviour[90].

It is clear from the same figure that the percolating network is partially recoverable, which means the change of the electrical conductivity is partially reversible [90]. The

mechanism of the electrical conductivity with the change of strain can be explained by figure 1-13.

As shown in figure 1-13 (a), the distances between the particles become larger during the decompression process, resulting in the decline of the electrical conductivity. Part (b) in the same figure, clarify the effective conductive paths are broken during the decompression which leads to the fall of the electrical conductivity. The formation of the effective conductive paths contributes to the increase of the electrical conductivity of the nanocomposite in part (c). (d): Give the explanation of the recovery of the effective conductive paths contributes to the gradual increase of the electrical conductivity of the nanocomposite during the stress relaxation period.

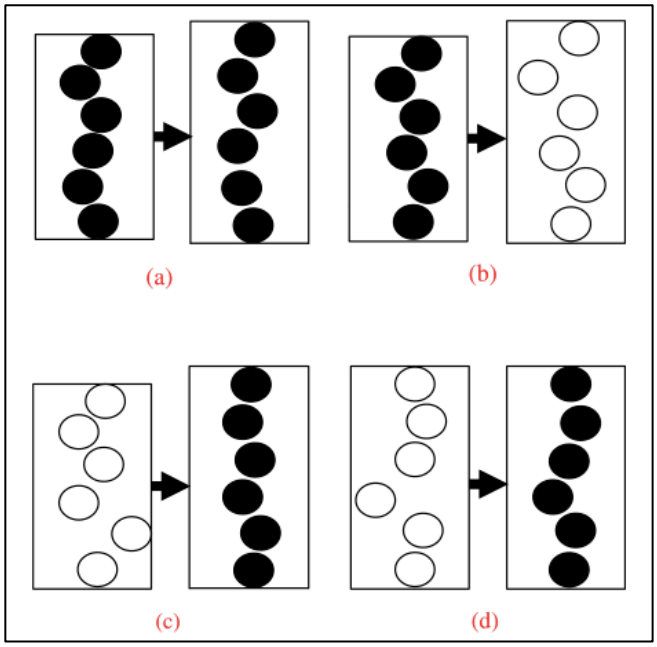

Figure 1-13: Sketch of the changes in the effective conductive paths during the period of decompression and relaxation. (a) Change of distance between particles during decompression (b) Effective conductive path destruction (c) Effective conductive path formation (d) Recovery of the effective conductive path [91].

1.10.2.6 Other Factors

Apart from the previously mentioned factors, aspect ratio, filler or polymer types and processing methods can also affect the electrical conductivity of the nanocomposites. Generally, the higher the aspect ratio is, the lower the percolation thresholds are and the higher the electrical conductivity is [9]. Higher aspect ratio means lower excluded

volume; hence, the conducting pathways are formed at relatively low filler content, resulting in the high electrical conductivity [88].

1.10.3 Current Challenges

Although conductive polymer nanocomposites have been successfully applied in many industrial areas such as construction, automobile, and aerospace, they still face several challenges that may limit their potential applications. The first is the high cost of conductive nanofillers which restricts their scales of production [92].

Secondly, as discussed earlier, the success in the processing of conductive polymer nanocomposites depends on the degree of the nanofillers dispersion. Generally, the conductive polymer nanocomposites with uniformly dispersed nanofillers would show optimum conductive performance. However, if the dispersion of nanofillers is not well uniform, aggregates may generate, which are detrimental to the performance of nanocomposites [93]. Current techniques are insufficient to make nano-size conductive polymer composites with a high degree of nanofillers dispersion [93].

Thirdly, adhesion between nanofillers and polymers is also considered as a challenge in polymer nanotechnology. Poor adhesion would compromise all nanocomposites properties.

Finally, the reproducibility of conductive polymer nanocomposites is difficult to be obtained [94]. Since the electrical conductivity, as well as mechanical properties, is highly influenced by the degree of dispersion and processing conditions, such as temperature and external force, the electrical behaviour is partial re-coverable.

1.11 Conclusions

In this chapter, the fundamentals of the conductive nanocomposite sensing material were reviewed. The past progress and on-going efforts on the electronic properties of CNTs and their composites were covered. Some applications of conductive polymer nanocomposites and the important continuous efforts for developing CNT-based strain and temperature sensors were discussed.

References

[1] R. Saito, G. Dresselhaus, and M. S. Dresselhaus, Physical Properties of Carbon Nanotubes. PUBLISHED BY IMPERIAL COLLEGE PRESS AND DISTRIBUTED BY WORLD SCIENTIFIC PUBLISHING CO., 1998.

[2] R. H. Baughman, A. A. Zakhidov, and W. A. de Heer, "Carbon nanotubes--the route toward applications.," *Science*, Vol. 297, No. 5582, pp. 787–92, Aug. 2002.

[3] E. Kymakis, I. Alexandou, and G. A. . Amaratunga, "Single-walled carbon nanotube–polymer composites: electrical, optical and structural investigation," *Synth. Met.*, Vol. 127, No. 1–3, pp. 59–62, Mar. 2002.

[4] P. Dharap, Z. Li, S. Nagarajaiah, and E. V Barrera, "Nanotube film based on single-wall carbon nanotubes for strain sensing," *Nanotechnology*, Vol. 15, No. 3, pp. 379–382, Mar. 2004.

[5] D. F. Adams, "Engineering composite materials," *Composites*, Vol. 18, No. 3, p. 261, 1987.

[6] R.-M. Wang, S.-R. Zheng, and Y.-P. Zheng, "Polymer Matrix Composites and Technology," *Polym. Matrix Compos. Technol.*, pp. 101–548, 2011.

[7] M. A. Masuelli, *Fiber Reinforced Polymers - The Technology Applied for Concrete Repair*. InTech, 2013.

[8] J. Jin, Y. Lin, M. Song, C. Gui, and S. Leesirisan, "Enhancing the electrical conductivity of polymer composites," *Eur. Polym. J.*, Vol. 49, No. 5, pp. 1066–1072, May 2013.

[9] S. Iijima, "Helical microtubules of graphitic carbon," *Nature*, Vol. 354, No. 6348, pp. 56–58, Nov. 1991.

[10] K. P. Yung, J. Wei, Z. F. Wang, and B. K. Tay, "Carbon Nanotubes (CNTs) as conductive filler for polymer composite," in *2008 2nd IEEE International Nanoelectronics Conference*, 2008, pp. 1198–1201.

[11] A. Eftekhari, Ed., *Nanostructured Conductive Polymers*. Chichester, UK: John

Wiley & Sons, Ltd, 2010.

[12] T. Ahuja and D. Kumar, “Recent progress in the development of nano-structured conducting polymers/nanocomposites for sensor applications,” *Sensors Actuators B Chem.*, Vol. 136, No. 1, pp. 275–286, Feb. 2009.

[13] J. Wang and M. Musameh, “Carbon Nanotube / Teflon Composite Electrochemical Sensors and Biosensors,” *Anal. Chem.*, Vol. 75, No. 9, pp. 2075–2079, May 2003.

[14] J. Sandler, M. S. . Shaffer, T. Prasse, W. Bauhofer, K. Schulte, and A. . Windle, “Development of a dispersion process for carbon nanotubes in an epoxy matrix and the resulting electrical properties,” *Polymer (Guildf).*, Vol. 40, No. 21, pp. 5967–5971, Oct. 1999.

[15] “Carbon Nanotube Enhanced Epoxy - FinalProjects.” [Online]. Available: http://voitlab.com/courses/thermodynamics/index.php?title=Carbon_Nanotube_Enhanced_Epoxy. [Accessed: 10-Sep-2015].

[16] O. Kanoun, C. Müller, A. Benchirouf, A. Sanli, T. N. Dinh, A. Al-Hamry, L. Bu, C. Gerlach, and A. Bouhamed, “Flexible carbon nanotube films for high performance strain sensors.,” *Sensors (Basel).*, Vol. 14, No. 6, pp. 10042–71, Jun. 2014.

[17] Z. Han and A. Fina, “Thermal conductivity of carbon nanotubes and their polymer nanocomposites: A review,” *Prog. Polym. Sci.*, Vol. 36, No. 7, pp. 914–944, 2011.

[18] F. Wu, X. He, Y. Zeng, and H.-M. Cheng, “Thermal transport enhancement of multi-walled carbon nanotubes/ high-density polyethylene composites,” *Appl. Phys. A*, Vol. 85, No. 1, pp. 25–28, Jul. 2006.

[19] S. Bellucci, *Carbon nanotubes: physics and applications*,Vol. 2, No. 1. 2005.

[20] P.-C. Ma, N. A. Siddiqui, G. Marom, and J.-K. Kim, “Dispersion and functionalization of carbon nanotubes for polymer-based nanocomposites: A review,” *Compos. Part A Appl. Sci. Manuf.*, Vol. 41, No. 10, pp. 1345–1367, Oct. 2010.

[21] M.-F. Yu, “Fundamental Mechanical Properties of Carbon Nanotubes: Current Understanding and the Related Experimental Studies,” *J. Eng. Mater. Technol.*, Vol. 126, No. 3, p. 271, Jul. 2004.

[22] T. W. Ebbesen, H. J. Lezec, H. Hiura, J. W. Bennett, H. F. Ghaemi, and T. Thio, “Electrical conductivity of individual carbon nanotubes,” *Nature*, Vol. 382, No. 6586, pp. 54–56, Jul. 1996.

[23] E. T. Thostenson, Z. Ren, and T.-W. Chou, “Advances in the science and technology of carbon nanotubes and their composites: a review,” *Compos. Sci. Technol.*, Vol. 61, No. 13, pp. 1899–1912, Oct. 2001.

[24] P. Avouris, M. Freitag, and V. Perebeinos, “Carbon-nanotube photonics and optoelectronics,” *Nat. Photonics*, Vol. 2, No. 6, pp. 341–350, 2008.

[25] J. Mahmoud, V. Majid, M. Momhamad, and H. Abazar, “Investigation of thermal conductivity of single-wall carbon nanotubes,” *Therm. Sci.*, Vol. 15, No. 2, pp. 565–570, 2011.

[26] Z. K. Tang, N. Wang, X. X. Zhang, J. N. Wang, and C. T. Chan, “Novel properties of 0 . 4 nm single-walled carbon nanotubes templated in the channels of AlPO 4 -5,” *New J. Phys.*, Vol. 5, p. 146.1-146.29, 2003.

[27] A. Javey, P. Qi, Q. Wang, and H. Dai, “Ten- to 50-nm-long quasi-ballistic carbon nanotube devices obtained without complex lithography.,” *Proc. Natl. Acad. Sci. U. S. A.*, Vol. 101, No. 37, pp. 13408–13410, 2004.

[28] A. Szabó, C. Perri, A. Csató, G. Giordano, D. Vuono, and J. B. Nagy, “Synthesis methods of carbon nanotubes and related materials,” *Materials (Basel).*, Vol. 3, No. 5, pp. 3092–3140, 2010.

[29] S. Huang, M. Woodson, R. Smalley, and J. Liu, “Growth Mechanism of Oriented Long Single Walled Carbon Nanotubes Using ‘Fast-Heating’ Chemical Vapor Deposition Process,” *Nano Lett.*, Vol. 4, No. 6, pp. 1025–1028, Jun. 2004.

[30] S. Iijima and T. Ichihashi, “Single-shell carbon nanotubes of 1-nm diameter,” *Nature*, Vol. 363, No. 6430, pp. 603–605, Jun. 1993.

[31] T. Guo, T. Guo, P. Nikolaev, P. Nikolaev, a Thess, a Thess, D. T. Colbert, D. T. Colbert, R. E. Smalley, and R. E. Smalley, "Catalytic growth of single -walled nanotubes by laser vaporization," *Chem. Phys. Lett*, Vol. 243, No. September, pp. 49–54, 1995.

[32] "Growing Carbon Nano-Tubes and the Space Elevator ... - Science Llama." [Online]. Available: http://the-science-llama.tumblr.com/post/38237617452/growing-carbon-nano-tubes-and-the-space-elevator. [Accessed: 14-Sep-2015].

[33] A. Eatemadi, H. Daraee, H. Karimkhanloo, M. Kouhi, N. Zarghami, A. Akbarzadeh, M. Abasi, Y. Hanifehpour, and S. W. Joo, "Carbon nanotubes: properties, synthesis, purification, and medical applications.," *Nanoscale Res. Lett.*, Vol. 9, No. 1, p. 393, Jan. 2014.

[34] T. Guo, P. Nikolaev, A. Thess, D. T. Colbert, and R. E. Smalley, "Catalytic growth of single-walled manotubes by laser vaporization," *Chem. Phys. Lett.*, Vol. 243, No. 1–2, pp. 49–54, Sep. 1995.

[35] K. H. An, W. S. Kim, Y. S. Park, Y. C. Choi, S. M. Lee, D. C. Chung, D. J. Bae, S. C. Lim, and Y. H. Lee, "Supercapacitors Using Single-Walled Carbon Nanotube Electrodes," *Adv. Mater.*, Vol. 13, No. 7, pp. 497–500, Apr. 2001.

[36] C. Du and N. Pan, "High power density supercapacitor electrodes of carbon nanotube films by electrophoretic deposition," *Nanotechnology*, Vol. 17, No. 21, pp. 5314–5318, Nov. 2006.

[37] B. Gao, A. Kleinhammes, X. P. Tang, C. Bower, L. Fleming, Y. Wu, and O. Zhou, "Electrochemical intercalation of single-walled carbon nanotubes with lithium," *Chem. Phys. Lett.*, Vol. 307, No. 3–4, pp. 153–157, Jul. 1999.

[38] TIMCAL Graphite and Carbon, "Carbon Additives for Polymer Compounds," pp. 4–10, 2012.

[39] J.-C. Huang, "Carbon black filled conducting polymers and polymer blends," *Adv. Polym. Technol.*, Vol. 21, No. 4, pp. 299–313, 2002.

[40] E. Llobet, “Gas sensors using carbon nanomaterials: A review,” *Sensors Actuators B Chem.*, Vol. 179, pp. 32–45, Mar. 2013.

[41] V. Jha, “Carbon Black Filler Reinforcement of Elastomers,” no. October, p. 229, 2008.

[42] J. WANG, J. VINCENT, and C. A. QUARLES, “Review of positron annihilation spectroscopy studies of rubber with carbon black filler,” *Nucl. Instrum. Methods Phys. Res. B.*, Vol. 241, No. 1–4, pp. 271–275.

[43] O. Meincke, D. Kaempfer, H. Weickmann, C. Friedrich, M. Vathauer, and H. Warth, “Mechanical properties and electrical conductivity of carbon-nanotube filled polyamide-6 and its blends with acrylonitrile/butadiene/styrene,” *Polymer (Guildf).*, Vol. 45, No. 3, pp. 739–748, Feb. 2004.

[44] S. Bal and S. S. Samal, “Carbon nanotube reinforced polymer composites—A state of the art,” *Bull. Mater. Sci.*, Vol. 30, No. 4, pp. 379–386, 2007.

[45] C. Kingston, R. Zepp, A. Andrady, D. Boverhof, R. Fehir, D. Hawkins, J. Roberts, P. Sayre, B. Shelton, Y. Sultan, V. Vejins, and W. Wohlleben, “Release characteristics of selected carbon nanotube polymer composites,” *Carbon N. Y.*, Vol. 68, pp. 33–57, Mar. 2014.

[46] C. Min, X. Shen, Z. Shi, L. Chen, and Z. Xu, “The Electrical Properties and Conducting Mechanisms of Carbon Nanotube/Polymer Nanocomposites: A Review,” *Polym. Plast. Technol. Eng.*, Vol. 49, No. 12, pp. 1172–1181, Sep. 2010.

[47] N. G. Sahoo, S. Rana, J. W. Cho, L. Li, and S. H. Chan, “Polymer nanocomposites based on functionalized carbon nanotubes,” *Prog. Polym. Sci.*, Vol. 35, No. 7, pp. 837–867, Jul. 2010.

[48] X.-Y. Qi, D. Yan, Z. Jiang, Y.-K. Cao, Z.-Z. Yu, F. Yavari, and N. Koratkar, “Enhanced electrical conductivity in polystyrene nanocomposites at ultra-low graphene content.,” *ACS Appl. Mater. Interfaces*, Vol. 3, No. 8, pp. 3130–3, Aug. 2011.

[49] P. M. Ajayan, O. Stephan, C. Colliex, and D. Trauth, “Aligned carbon nanotube

arrays formed by cutting a polymer resin--nanotube composite.," *Science*, Vol. 265, No. 5176, pp. 1212–4, Aug. 1994.

[50] S. Bal and Y. Nayak, "Archived in Dspace @ NITR Proceedings of Indian Science Congress Association , Jan 3-7 2006 Hyderabad This paper was awarded the Best Poster Presentation Award Influence of nanomodification on physical properties of polymer nanocomposites," 2006.

[51] S. Stankovich, D. a Dikin, G. H. B. Dommett, K. M. Kohlhaas, E. J. Zimney, E. a Stach, R. D. Piner, S. T. Nguyen, and R. S. Ruoff, "Graphene-based composite materials.," *Nature*, Vol. 442, No. 7100, pp. 282–286, Jul. 2006.

[52] T. Kuilla, S. Bhadra, D. Yao, N. H. Kim, S. Bose, and J. H. Lee, "Recent advances in graphene based polymer composites," *Prog. Polym. Sci.*, Vol. 35, No. 11, pp. 1350–1375, Nov. 2010.

[53] J. R. Potts, D. R. Dreyer, C. W. Bielawski, and R. S. Ruoff, "Graphene-based polymer nanocomposites," *Polymer (Guildf).*, Vol. 52, No. 1, pp. 5–25, Jan. 2011.

[54] S. Frank, "Carbon Nanotube Quantum Resistors," *Science (80-.).*, Vol. 280, No. 5370, pp. 1744–1746, Jun. 1998.

[55] Alamusi, N. Hu, H. Fukunaga, S. Atobe, Y. Liu, and J. Li, "Piezoresistive strain sensors made from carbon nanotubes based polymer nanocomposites.," *Sensors (Basel).*, Vol. 11, No. 11, pp. 10691–723, Jan. 2011.

[56] P. Thori, P. Sharma, and M. Bhargava, "an Approach of Composite Materials in Industrial Machinery : Advantages , Disadvantages and Applications," pp. 350–355, 2013.

[57] G. Mittal, V. Dhand, K. Y. Rhee, H.-J. Kim, and D. H. Jung, "Carbon nanotubes synthesis using diffusion and premixed flame methods: a review," *Carbon Lett.*, Vol. 16, No. 1, pp. 1–10, Jan. 2015.

[58] S. Li, M. Meng Lin, M. S. Toprak, D. K. Kim, and M. Muhammed, "Nanocomposites of polymer and inorganic nanoparticles for optical and magnetic applications.," *Nano Rev.*, Vol. 1, Jan. 2010.

[59] Y.-W. Mai, X. Xie, and X.-P. Zhou, “Dispersion and alignment of carbon nanotubes in polymer matrix: A review,” 2005.

[60] A. K. Mishra and S. Ramaprabhu, “Functionalized Graphene-Based Nanocomposites for Supercapacitor Application,” *J. Phys. Chem. C*, Vol. 115, No. 29, pp. 14006–14013, Jul. 2011.

[61] N. Hu, Y. Karube, M. Arai, T. Watanabe, C. Yan, Y. Li, Y. Liu, and H. Fukunaga, “Investigation on sensitivity of a polymer/carbon nanotube composite strain sensor,” *Carbon N. Y.*, Vol. 48, No. 3, pp. 680–687, Mar. 2010.

[62] W. Zhang, J. Suhr, and N. Koratkar, “Carbon Nanotube/Polycarbonate Composites as Multifunctional Strain Sensors,” *J. Nanosci. Nanotechnol.*, Vol. 6, No. 4, pp. 960–964, Apr. 2006.

[63] N. Hu, Y. Karube, C. Yan, Z. Masuda, and H. Fukunaga, “Tunneling effect in a polymer/carbon nanotube nanocompositestrain sensor,” *Acta Materialia*. Elsevier, 01-Aug-2008.

[64] M. S. Xinxin Sun, “Conductive Behaviour of Carbon Nanotube Based Composites,” *Dr. thesis Loughbrgh. Univ.*, 2009.

[65] Jin Hyunjong, “Carbon nanotube strain sensors with wide dynamic range fabricated on flexible substrates by novel processing techniques,” 2009.

[66] Y. Zhou, B. He, W. Zhou, J. Huang, X. Li, B. Wu, and H. Li, “Electrochemical capacitance of well-coated single-walled carbon nanotube with polyaniline composites,” *Electrochim. Acta*, Vol. 49, No. 2, pp. 257–262, Jan. 2004.

[67] R. Sengupta, M. Bhattacharya, S. Bandyopadhyay, and A. K. Bhowmick, “A review on the mechanical and electrical properties of graphite and modified graphite reinforced polymer composites,” *Prog. Polym. Sci.*, Vol. 36, No. 5, pp. 638–670, May 2011.

[68] M. Zammarano, M. Franceschi, S. Bellayer, J. W. Gilman, and S. Meriani, “Preparation and flame resistance properties of revolutionary self-extinguishing epoxy nanocomposites based on layered double hydroxides,” *Polymer (Guildf).*,

Vol. 46, No. 22, pp. 9314–9328, Oct. 2005.

[69] J. Liang, Y. Huang, L. Zhang, Y. Wang, Y. Ma, T. Guo, and Y. Chen, "Molecular-Level Dispersion of Graphene into Poly(vinyl alcohol) and Effective Reinforcement of their Nanocomposites," *Adv. Funct. Mater.*, Vol. 19, No. 14, pp. 2297–2302, Jul. 2009.

[70] K. Lu, N. Grossiord, C. E. Koning, H. E. Miltner, B. van Mele, and J. Loos, "Carbon Nanotube/Isotactic Polypropylene Composites Prepared by Latex Technology: Morphology Analysis of CNT-Induced Nucleation," *Macromolecules*, Vol. 41, No. 21, pp. 8081–8085, Nov. 2008.

[71] J. Yu, K. Lu, E. Sourty, N. Grossiord, C. E. Koning, and J. Loos, "Characterization of conductive multiwall carbon nanotube/polystyrene composites prepared by latex technology," *Carbon N. Y.*, Vol. 45, No. 15, pp. 2897–2903, Dec. 2007.

[72] P. Mukhopadhyay, *Graphite, graphene, and their polymer nanocomposites*. Boca Raton [etc.]: CRC Press/Taylor & Francis Group, 2013.

[73] M. H. Kang and S. J. Lee, "Rheological and electrical properties of polystyrene/multi-walled carbon nanotube nanocomposites prepared by latex technology," *Korea-Australia Rheol. J.*, Vol. 24, No. 2, pp. 97–103, Jul. 2012.

[74] N. Grossiord, J. Loos, and C. E. Koning, "Strategies for dispersing carbon nanotubes in highly viscous polymers," *J. Mater. Chem.*, Vol. 15, No. 24, p. 2349, Jun. 2005.

[75] N. Grossiord, M. E. L. Wouters, H. E. Miltner, K. Lu, J. Loos, B. Van Mele, and C. E. Koning, "Isotactic polypropylene/carbon nanotube composites prepared by latex technology: Electrical conductivity study," *Eur. Polym. J.*, Vol. 46, pp. 1833–43, 2010.

[76] S. Advani, *Processing and properties of nanocomposites*. 2007.

[77] N. Jović, D. Dudić, A. Montone, and M. Antisari, "Temperature dependence of the electrical conductivity of epoxy/expanded graphite nanosheet composites,"

Scr. Mater., 2008.

[78] X. Sun and M. Song, "Highly conductive carbon nanotube/polymer nanocomposites achievable?," *Macromol. Theory Simulations*, 2009.

[79] Y. Song and J. Youn, "Influence of dispersion states of carbon nanotubes on physical properties of epoxy nanocomposites," *Carbon N. Y.*, 2005.

[80] G. T. Pham, Y.-B. Park, Z. Liang, C. Zhang, and B. Wang, "Processing and modeling of conductive thermoplastic/carbon nanotube films for strain sensing," *Compos. Part B Eng.*, Vol. 39, No. 1, pp. 209–216, Jan. 2008.

[81] B. Lundberg and B. Sundqvist, "Resistivity of a composite conducting polymer as a function of temperature, pressure, and environment: Applications as a pressure and gas concentration transducer," *J. Appl. Phys.*, Vol. 60, No. 3, p. 1074, Aug. 1986.

[82] C. Zhang, C.-A. Ma, P. Wang, and M. Sumita, "Temperature dependence of electrical resistivity for carbon black filled ultra-high molecular weight polyethylene composites prepared by hot compaction," *Carbon N. Y.*, Vol. 43, No. 12, pp. 2544–2553, 2005.

[83] S. Rana, R. Alagirusamy, and M. Joshi, "A review on carbon epoxy nanocomposites," *J. Reinf. Plast.* …, 2008.

[84] N. Grossiord, J. Loos, O. Regev, and C. Koning, "Toolbox for dispersing carbon nanotubes into polymers to get conductive nanocomposites," *Chem. Mater.*, 2006.

[85] E. Choi, J. Brooks, and D. Eaton, "Enhancement of thermal and electrical properties of carbon nanotube polymer composites by magnetic field processing," *J. Appl.* …, 2003.

[86] F. Du, J. Fischer, and K. Winey, "Effect of nanotube alignment on percolation conductivity in carbon nanotube/polymer composites," *Phys. Rev. B*, 2005.

[87] Q. Wang, J. Dai, W. Li, Z. Wei, and J. Jiang, "The effects of CNT alignment on electrical conductivity and mechanical properties of SWNT/epoxy nanocomposites," *Compos. Sci. Technol.*, 2008.

[88] M. R. Ayatollahi, S. Shadlou, M. M. Shokrieh, and M. Chitsazzadeh, “Effect of multi-walled carbon nanotube aspect ratio on mechanical and electrical properties of epoxy-based nanocomposites,” *Polym. Test.*, Vol. 30, No. 5, pp. 548–556, Aug. 2011.

[89] S. Mojtaba Alizadeh Darbandi, M. Nouri, and J. Mokhtari, “Electrospun nanostructures based on polyurethane/MWCNTs for strain sensing applications,” *Fibers Polym.*, Vol. 13, No. 9, pp. 1126–1131, Nov. 2012.

[90] L. Flandin, Y. Bréchet, and J.-Y. Cavaillé, “Electrically conductive polymer nanocomposites as deformation sensors,” *Compos. Sci. Technol.*, Vol. 61, No. 6, pp. 895–901, May 2001.

[91] L. Wang, T. Ding, and P. Wang, “Research on stress and electrical resistance of skin-sensing silicone rubber/carbon black nanocomposite during decompressive stress relaxation,” *Smart Mater. Struct.*, Vol. 18, No. 6, p. 65002, Jun. 2009.

[92] J. Li, M. Sham, J. Kim, and G. Marom, “Morphology and properties of UV/ozone treated graphite nanoplatelet/epoxy nanocomposites,” *Compos. Sci. Technol.*, 2007.

[93] S. Jana and S. Jain, “Dispersion of nanofillers in high performance polymers using reactive solvents as processing aids,” *Polymer (Guildf).*, 2001.

[94] N. Das, T. Chaki, and D. Khastgir, “Effect of processing parameters, applied pressure and temperature on the electrical resistivity of rubber-based conductive composites,” *Carbon N. Y.*, 2002.

[95] “Research — Carbio.” [Online]. Available: http://www.carbio.eu/research.html. [Accessed: 15-Sep-2015].

Part Two: Carbon Nanotube/Polyethylene Nanocomposites as Strain and Temperature Sensing Materials

Chapter II-2 Experimental

2.1 Introduction

Electrically conductive polymer nanocomposites have been widely used in electromagnetic interference (EMI), shielding, nano-electric devices, strain sensors and temperature sensors. Conducting filler in the development of conductive polymer composites has received some intensive effort in the materials application in recent years. MWCNT is considering as conductive nanofillers due to the high electrical conductivity as well as good mechanical and thermal properties which are expected to improve the electrical conductivity of polymers. Thus, CNT/polymer composite is one of the promising fields of CNT future application. The important two concerns in the success of CNT/polymer nanocomposite fabricating with excellent properties are the good dispersion of CNTs in polymer and their strong interfacial adhesion with a polymer surface [1],[2]. Although numerous investigations have been made to the electrical properties of CNT/polymer composites, there are still some gaps that need to be filled. The intent of this chapter is to give the details of the preparation of materials that used to prepare CNT/polymer composites.

This chapter is organized to be as following: section 2.2 gives some details about the materials that used in the experiments. Section 2.3 presents the sample preparation and fabrication of MWCNT and MWCNT/HDPE. Section 2.5 provides the characterization methods of the samples. The measurements are presented in section 2.6. Lastly, a brief summary was given in section 2.7.

2.2 Materials

The main materials used in this study were multi-walled carbon nanotubes (MWCNTs) and high-density polyethylene (HDPE). MWCNTs with a purity rating of 95% were purchased from Chengdu Institute of Organic Chemistry, Chinese Academy of Sciences. The length of the MWCNTs was 20-50μm; the average outer diameter was 10-20nm. HDPE matrix with (Density: 0.98gcm^{-3}, MFI: 4.0g/10min) powder with a particle size on average 850μm in length was supplied by Exxon Mobil Corporation, UK. All the materials were used as received.

2.3 Sample Preparation

2.3.1 Preparation of MWCNT Suspensions

Starting with 100mg MWCNTs immersed into 20ml distilled water, which then was treated by ultrasound for 30 minutes. The sonic dismembrator (Fisher Scientific Model 500, 300 W) was used to get better dispersion by this ultra-sonication.

2.3.2 Preparation of MWCNT/HDPE Nanocomposites

MWCNT/HDPE nanocomposites were prepared by dispersed the MWCNTs in the (HDPE) polymer matrix using patented method [3][4] which allowed CNT particles to be coated on the surface of the individual polymer powder particles without any change to the morphology of the particle. The MWCNT added to the HDPE particles with constantly and rapidly manual stirring after dilution. Then, the MWCNT/HDPE nanocomposites were dried at 80°C for 24 hours to remove residual water, which was the last step for the preparation of the MWCNT/HDPE composites as shown in figure 2-1. The MWCNT/HDPE nanocomposites with MWCNTs weight fractions of 0.1wt%, 0.5wt%, and 1.0wt% were produced in this study.

Figure 2-1: The MWCNT/HDPE nanocomposites with MWCNTs weight fractions of 0.1wt%.

2.4 2 Fabrication of MWCNT/HDPE

The MWCNT/HDPE nanocomposite films were prepared using the melt mixing and hot pressing. For starters: MWCNT/HDPE nanocomposite powders were compressed into sheets with the diameter of 50mm and the thickness of 1mm at 135°C using hot compression moulding. These sheets are for investigation the relationship between the temperature and the electrical conductivity. In addition, to study the relationship between the strain and the electrical conductivity, the MWCNT/HDPE nanocomposite powders were compressed into 5 mm thick samples with the size of 100mm×15mm at 135°C. The pressure of compression moulding for the two different sizes of samples was set at 18 tons. The whole procedure for preparing MWCNT/polymer nanocomposites is shown in figure 2-2.

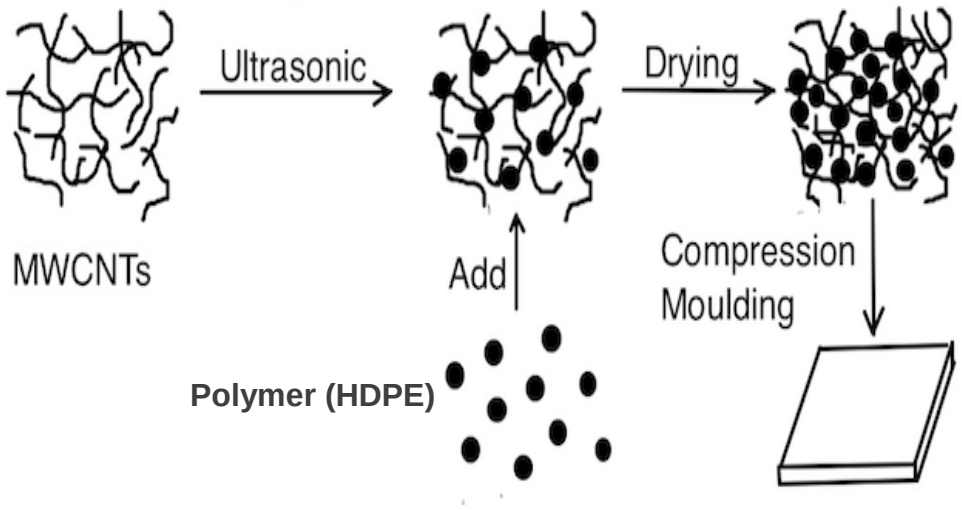

Figure 2-2: Schematic procedure for preparation of MWCNT/polymer nanocomposites.

2.5 Characterization

2.5.1 Scanning Electron Microscopy (SEM)

The morphology and the dispersion of MWCNT fillers for both nanocomposite powders and fracture surfaces were studied by using a field emission gun scanning electron microscopy (FEGSEM) LEO 1530VP instrument at a voltage of 5kV. The samples after compression moulding were fractured in liquid nitrogen. Both the nanocomposite powders and the fracture surfaces were coated with gold before SEM measurements.

2.6 Measurements

2.6.1 Modulated Differential Scanning Calorimetry (MDSC) Measurements

The thermal behaviour of pure HDPE was investigated by using a TA Instruments 2920 MDSC. The sample was weighted (about 10mg) and sealed in an aluminum pan and was heated from room temperature to 200°C at a heating rate of 10°C/min.

2.6.2 Electrical Conductivity Measurements

2.6.2.1 Electrical Conductivity-Temperature

The Fluke PM6306 Programmable Automatic RCL Meter was used to measure the electrical resistances of all samples. The samples with the diameter of 50mm and the thickness of 1mm were coated with the silver paint to ensure a good electrical contact and connect to the automatic RCL meter. Then, they were placed into an oven where the temperature could be adjusted and controlled. The electrical conductivity was recorded with a rise of 20°C from 20°C (room temperature) to 100°C and then recorded with the decrease of 20°C in the temperature from 100°C to 20°. The heating and cooling processes were repeated twice for each sample. After the two times of heating and cooling, half of the samples were left for three days and then were repeated the process of heating and cooling with the record of the electrical conductivity. Another half of the samples were then put in the oven, at a temperature of 80°C, for twelve hours. After that, the process of heating and cooling were repeated to samples with recorded conductivity.

2.6.2.2 Electrical Conductivity-Stress

In a strain with electrical conductivity measurements, the samples with the size of 100mm×15mm×5mm were tested at room temperature using three points bending rigs and timers from W.E.S. Plastics Pty Ltd. The samples were placed on the three points bending machine and subjected to a constant load of approximate 39.2N. The electrical conductivity and strain were measured at various times up to 60 minutes and recorded. Another recording was done when the samples were unloaded. Each test was repeated twice. For all the electrical conductivity measurements, each reported conductivity data was the average value of three measurements, and all values of resistance were recorded as the values of direct current (DC) resistance. The stress and the resistivity are then calculated from the measured force and resistance values.

2.7 Conclusions

A melt processing method has been used to prepare MWCNT/HDPE nanocomposites with different filler loading between 0.1, 0.5 and 1.0 wt% of MWCNT. The MWCNTs were dispersed into the host HDPE matrix by manually stirring. The presence of MWCNT in polymer matrix HDPE is clearly observed even at low loadings of MWCNTs.

References

[1] G. L. G. L. Hwang, Y.-T. Y. T. Shieh, and K. C. K. C. Hwang, “Efficient load transfer to polymer-grafted multiwalled carbon nanotubes in polymer composites,” *Adv. Funct. Mater.*, Vol. 14, No. 5, pp. 487–491, May 2004.

[2] A. Schönhals, H. Goering, F. R. Costa, U. Wagenknecht, and G. Heinrich, “Dielectric Properties of Nanocomposites Based on Polyethylene and Layered Double Hydroxide,” *Macromolecules*, Vol. 42, No. 12, pp. 4165–4174, 2009.

[3] M. S. Dongyu Cai, Jie Jin, “Process,” 2008.

[4] J. Bai, R. D. Goodridge, R. J. M. Hague, and M. Song, “Improving the mechanical properties of laser-sintered polyamide 12 through incorporation of carbon nanotubes,” *Polym. Eng. Sci.*, Vol. 53, No. 9, pp. 1937–1946, Sep. 2013.

Part Two: Carbon Nanotube/Polyethylene Nanocomposites as Strain and Temperature Sensing Materials

Chapter II-3 Characterization of Carbon Nanotube/ Polyethylene Composites

3.1 Introduction

Besides, CNT/polymer nanocomposite is one of the most promising fields for CNT applications, polyethylene (PE) also is one of the most commonly material used as a thermoplastic. High-density polyethylene (HDPE) is a frequently preferred among other PE types due to the high degree of crystalline structure with a higher tensile strength which can effectively resist corrosions of most of the chemical solvents at room temperature [1]-[3]. Moreover, HDPE resin is ideal for orthopedic implants and distribution pipes and other applications because of its low cost and minimum processing energy consumption [2]

In this chapter, results of the characterization of MWCNT/ (HDPE) composite as powder and films are discussed. Then, the quality of these thin films and the dispersions of MWCNTs in the HDPE matrices are investigated.

3.2 Results and Discussion

3.2.1 HDPE and MWCNT Powder Morphology

Figure 3-1 (a) and (b) shows the SEM images of HDPE and MWCNT respectively in the powder state.

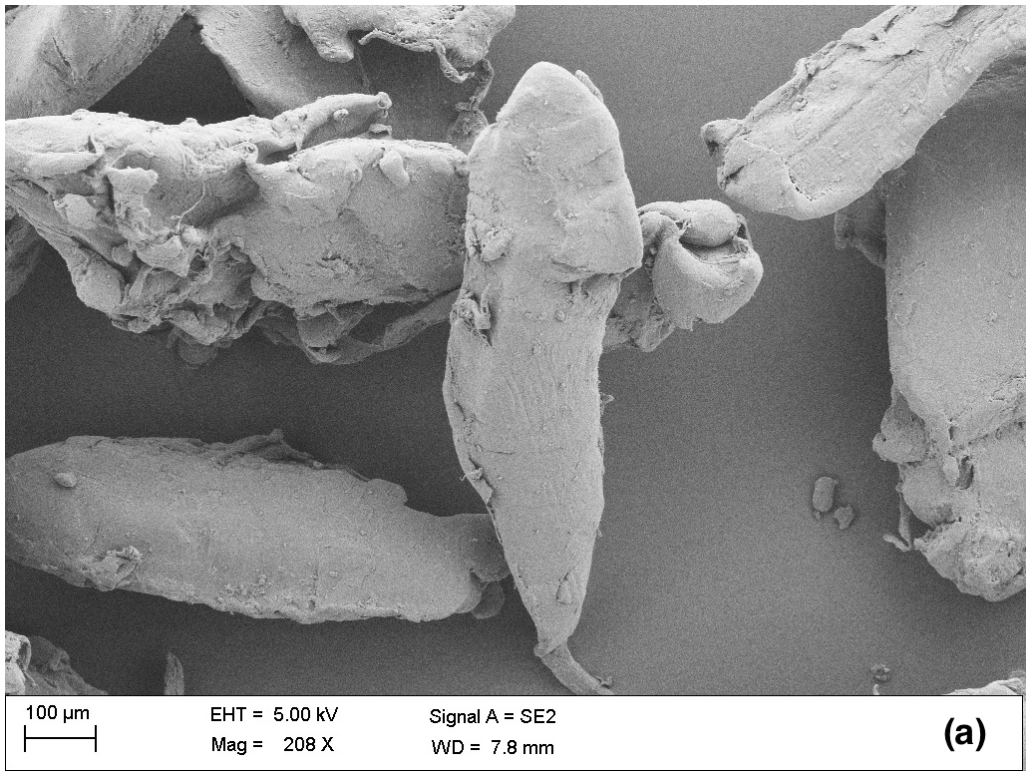

Figure 3-1: SEM images of HDPE and MWCNT powders micrographs.

As it can be seen from figure 3-1, the morphology of HDPE powder (shown in part (a)) shows an irregular microstructure which may weaken the reinforcement [4]. However, the bamboo-shaped MWNTs are clear in part (b).

3.2.2 MWCNT/HDPE Nanocomposites (powder)

Figure 3-2 illustrates the SEM images of the matrix of MWCNT/HDPE nanocomposite in powder state with MWCNTs weight of 0.1wt%, 0.5wt%, and 1.0wt% respectively. In these images, the MWCNTs can be easily observed as white strands which almost covered the whole surfaces of the HDPE powder particles with only 1.0wt% of MWCNT. In addition, nanofillers usually tend to accumulate very easily, which can affect and weaken the mechanical properties of the final nanocomposites part. However, the dispersions of the MWCNTs were uniform, although a few agglomerates could be detected.

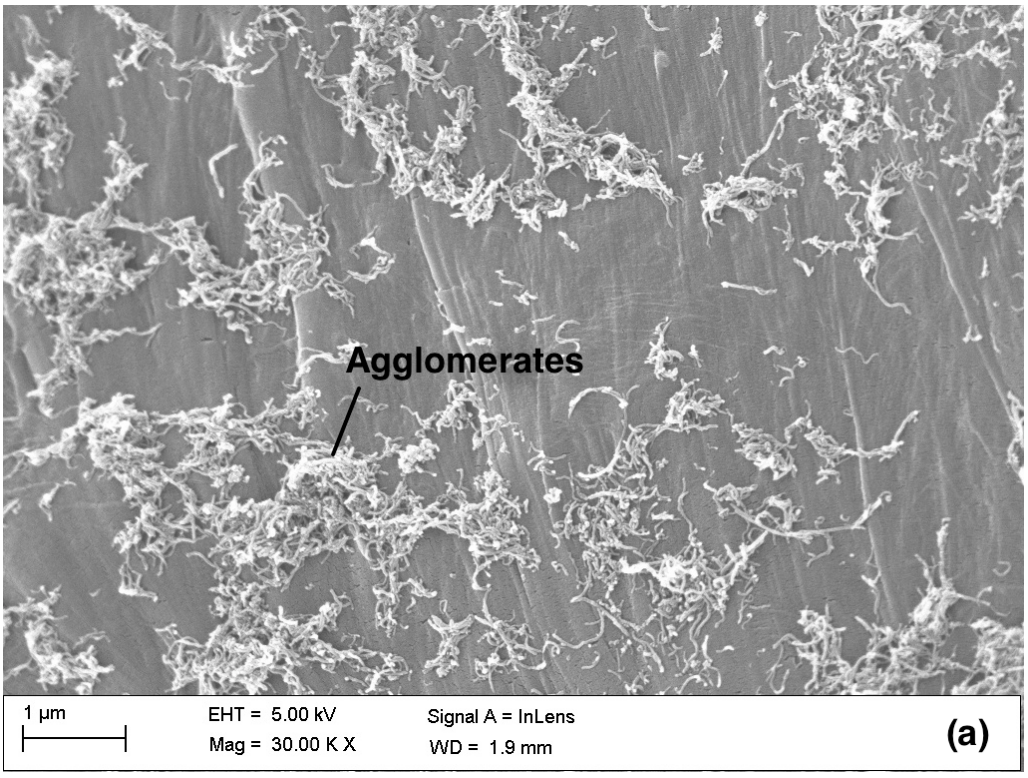

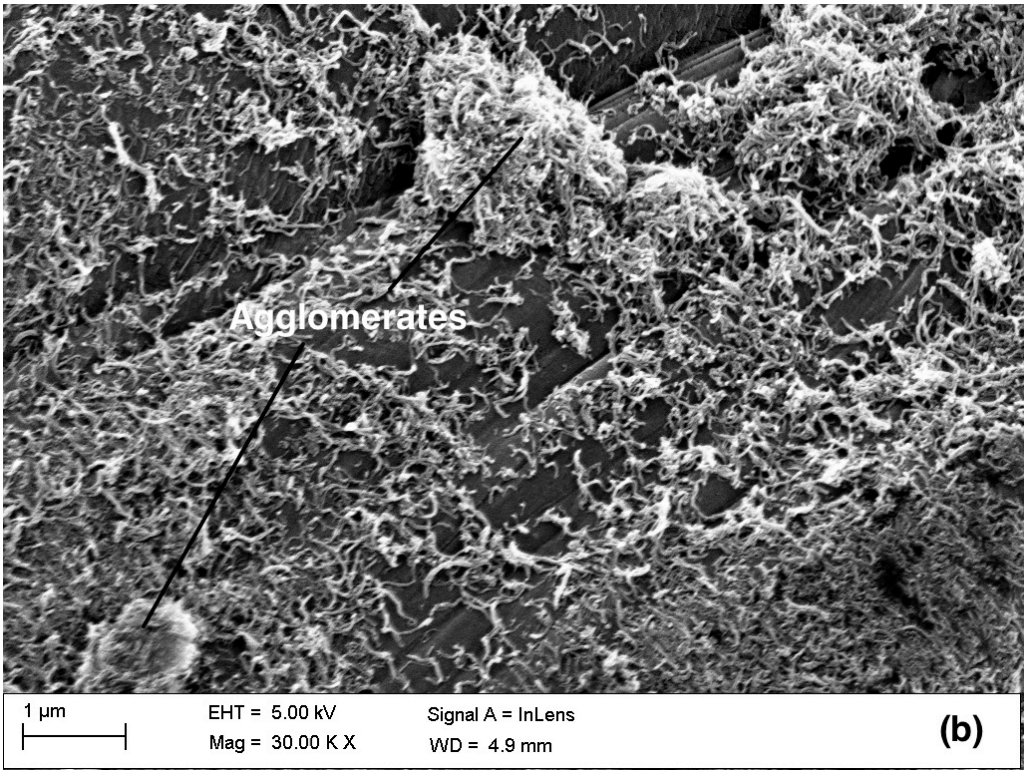

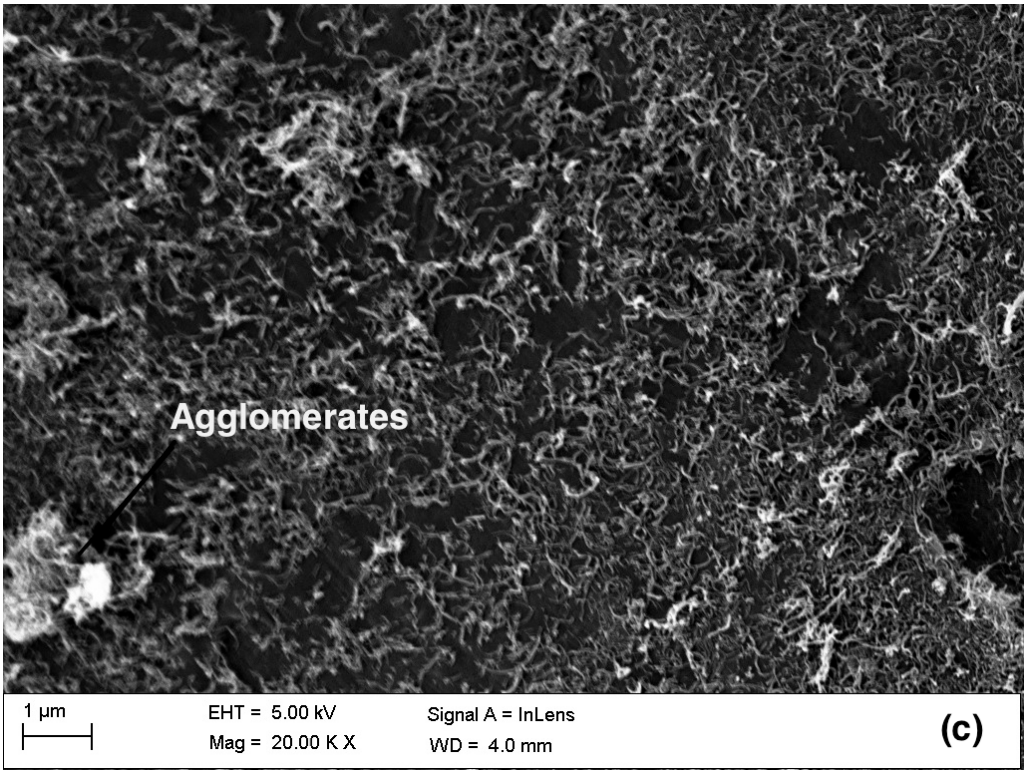

Figure 3-2: SEM images of (a) 0.1 wt% MWCNT/HDPE nanocomposite powders (b) 0.5 wt% MWCNT/HDPE nanocomposite powders (c) 1.0 wt% MWCNT/HDPE nanocomposite powders.

It is clear that as the content of MWCNT increases the averaged area with MWCNT increased. And the agglomeration of the MWCNT becomes more noticeable. However, these agglomerates form conductive three-dimensional networks during the next stage of compression moulding. That is because of the hot pressing which may improve the connections between adjacent agglomerates [5]. As mentioned before, the successful preparation of polymer nanocomposites strongly depends on the uniform dispersion of nanofillers in the polymer matrix. In this project, MWCNT/polymer nanocomposite powders were prepared by coating the MWCNTs on the surface of HDPE which results in this uniform dispersion of the CNT in a different part of HDPE surface.

3.2.3 MWCNT/HDPE Nanocomposites sheets

The prepared nanocomposite powders were compressed into sheets at 135°C. The chosen temperatures were around the melting points of the polymer, which is in the range of 130°C to 137°C for HDPE [6]. At these temperatures, the nanocomposite powders are not totally molten, which is good for forming conductive networks. The procedure of the fabrication of nanocomposite powders is shown in Figure 3-3.

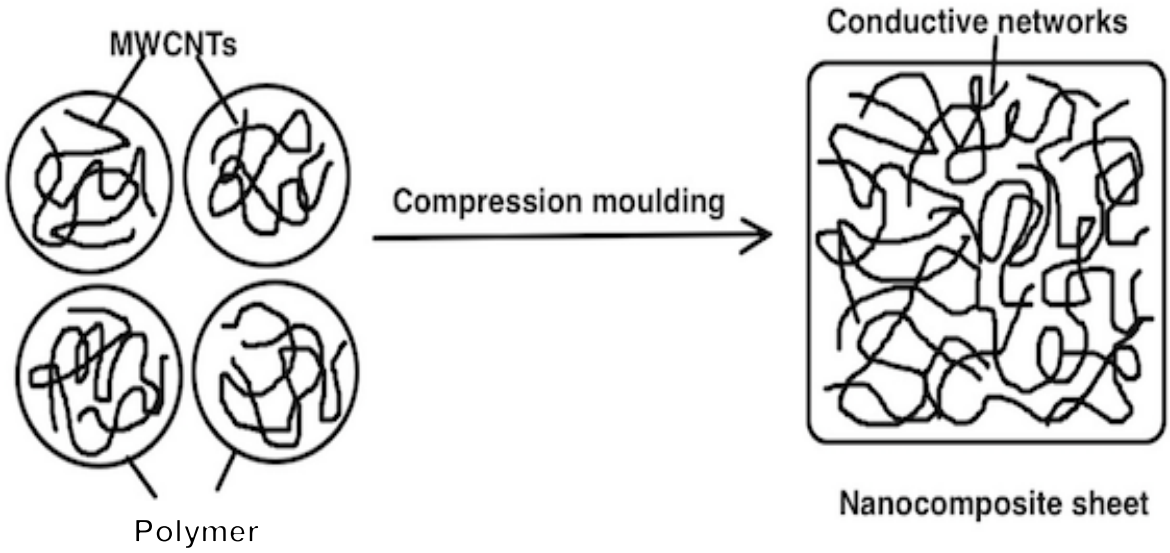

Figure 3-3: Schematic procedure for preparation of MWCNT/polymer nanocomposite sheet

Figure 3-4 shows the SEM images of a surface fracture from MWCNT/ HDPE nanocomposite sheets with the MWCNTs weight fractions of 0.1 wt%, 0.5 wt%, and 1.0 wt%. It is clear that from (a) to (c) the content of the MWCNT increases which result in forming a network of this connected MWCNT. This network becomes denser with a higher fraction of MWCNT.

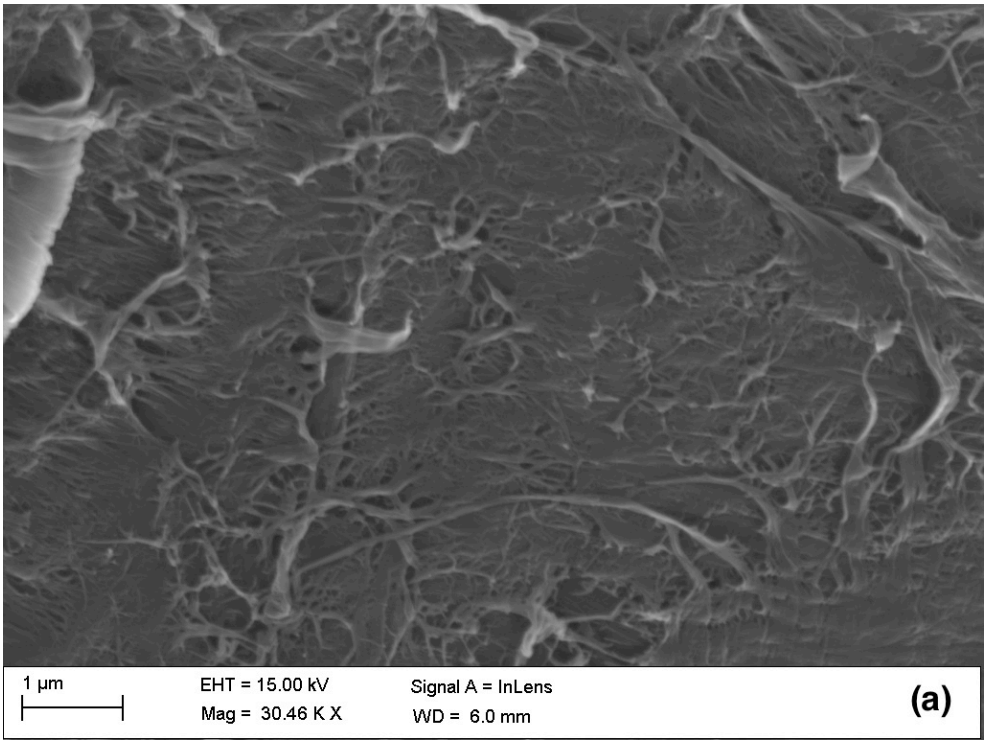

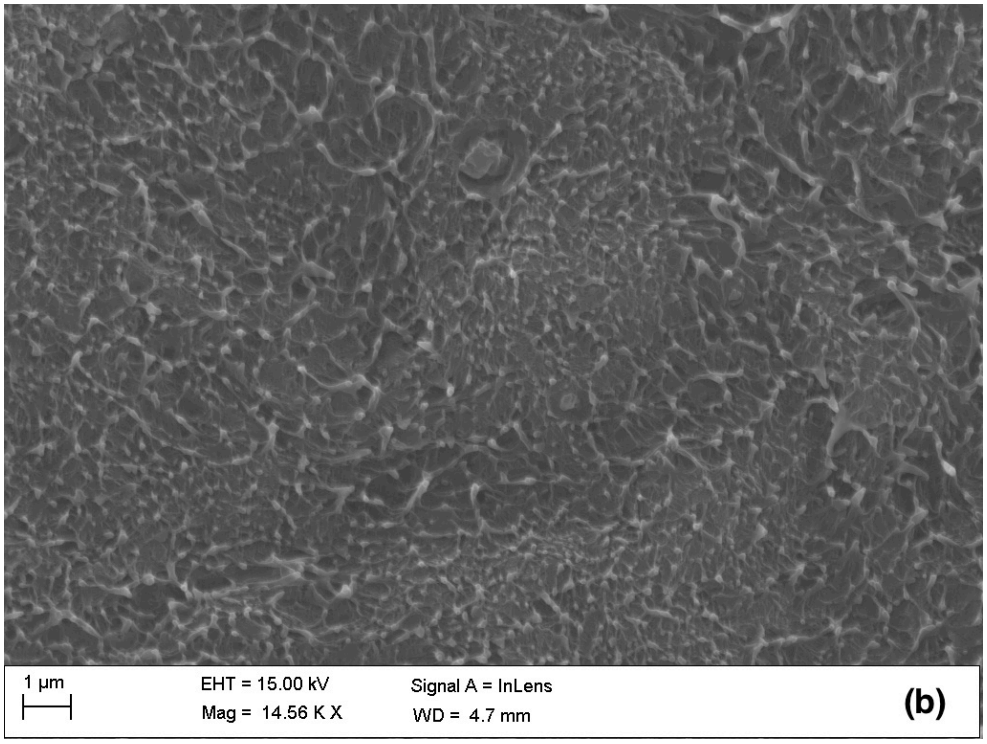

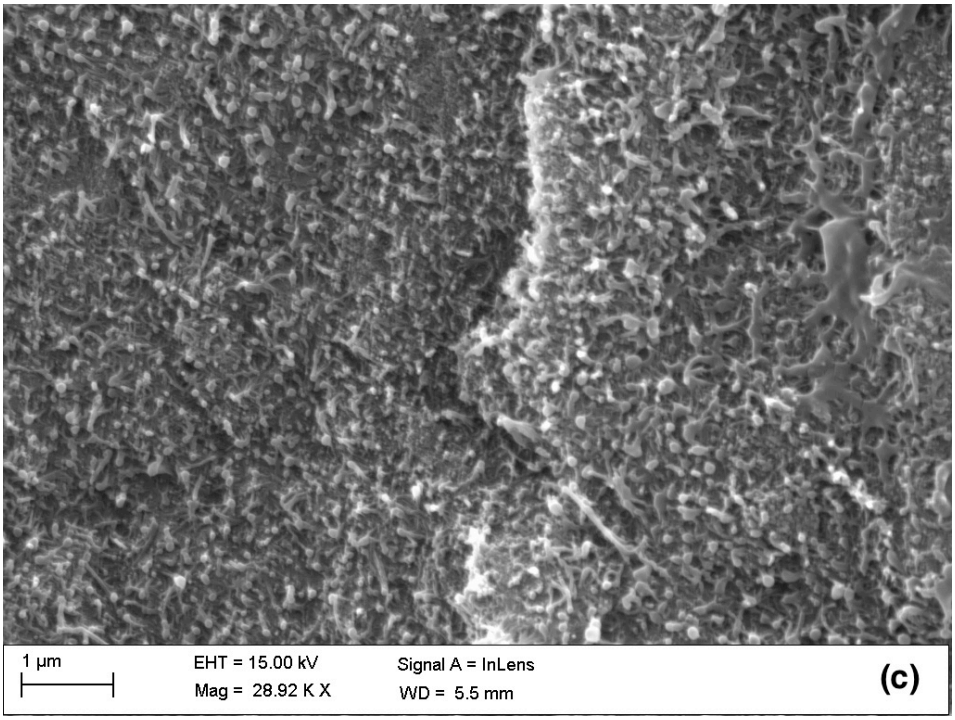

Figure 3-4: SEM images of surfaces fracture of (a) 0.1 wt% MWCNT/HDPE nanocomposite sheet (b) 0.5 wt% MWCNT/HDPE nanocomposite sheet (c) 1.0 wt% MWCNT/HDPE nanocomposite sheet.

3.2.4 Conductivity of the MWCNT/HDPE Sheets

To check the conductivity of these networks, the initial electrical resistivity of the MWCNT/HDPE nanocomposites with each concentration of MWCNTs were calculated and illustrated in table 3-1.

Table 3-1: The initial electrical resistivity of MWCNT/HDPE nanocomposites

Weight fraction of MWCNTs	Resistivity (kΩ.mm)	Standard deviation (%)
0.1 wt%	792.6375	±5.77
0.5 wt%	111.6675	±0.96
1.0 wt%	9.9525	±0.06

Thus, table 3-1 and figure 3-4 (b) and (c) present the conductive networks with 0.5 wt% and 1.0 wt% MWCNT/HDPE nanocomposites throughout the whole sample. However, the resistivity of the composite has found to decreases until 9.95 kΩ.mm as MWCNT reaches 1.0wt%. Although the conductive networks in 0.1 wt% MWCNT/HDPE

nanocomposite are not observable in the SEM image (see figure 3-4 (a)), the electrical resistivity of about 792.6 kΩ.mm with 0.1 wt% MWCNT/HDPE nanocomposite is detected. The invisible and conductive networks in the SEM image of the 0.1 wt% MWCNT/HDPE nanocomposite are probably because most of the MWCNTs are enclosed into the HDPE matrix [7].

Figure 3-5 shows the electrical resistivity of MWCNT/HDPE nanocomposites with different MWCNTs content. In this figure, the percolation threshold was difficult to be identified for only three different fractions of MWCNT. Though, it is clear from the slope that the decreasing rate in electrical resistivity is higher from 0.1 wt% to 0.5 wt% than from 0.5 wt % to 1.0 wt % in MWCNT/HDPE nanocomposite. The change in electrical resistivity becomes nearly remained stable from 0.9 wt% to 1.0 wt%. Thus, comparing the nanocomposites resistivity of 0.1 wt% and 0.5 wt% and 1.0 wt% MWCNTs, the nanocomposite with the 1.0 wt% MWCNTs was closer to the percolation threshold.

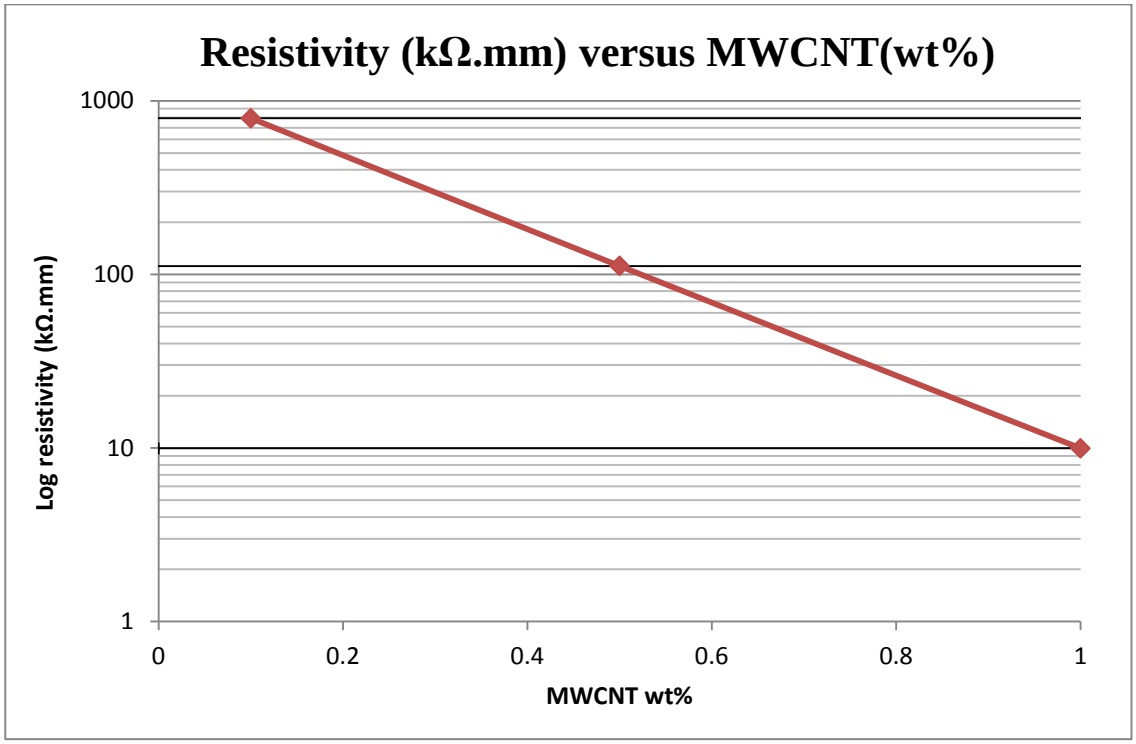

Figure 3-5: Log resistivity of MWCNT/HDPE nanocomposites with different MWCNTs contents.

In addition, the standard deviation of resistivity is quite small for the nanocomposite with 1.0 wt% MWCNTs which differs from other fractions as present in table 3-1. This comes with a good agreement with the sensitivity of the electrical signal which altered for different nanotube contents and the greater electrical stability was shown in the nanocomposites with CNT contents around the percolation threshold [8].

3.3 Conclusion

The SEM was used to characterize the powder and sheets of MWCNT/HDPE nanocomposite. The powder of HDPE had an irregular morphology structures which are connected to a conductive network with the MWCNT. The 1.0 wt% MWCNT/HDPE nanocomposite sheet showed the best electrical conductivity and the lowest standard deviation which indicate the greatest electrical stability among other two fractions.

References

[1] I. Grigoriadou, K. M. Paraskevopoulos, K. Chrissafis, E. Pavlidou, T. G. Stamkopoulos, and D. Bikiaris, "Effect of different nanoparticles on HDPE UV stability," *Polym. Degrad. Stab.*,Vol. 96, No. 1, pp. 151–163, 2011.

[2] K. Jeon, L. Lumata, T. Tokumoto, E. Steven, J. Brooks, and R. G. Alamo, "Low electrical conductivity threshold and crystalline morphology of single-walled carbon nanotubes - high density polyethylene nanocomposites characterized by SEM, Raman spectroscopy and AFM," *Polymer (Guildf).*, Vol. 48, No. 16, pp. 4751–4764, 2007.

[3] J. Kim, S. Kwak, S. M. Hong, J. R. Lee, A. Takahara, and Y. Seo, "Nonisothermal crystallization behaviors of nanocomposites prepared by in situ polymerizations of high-density polyethylene on multiwalled carbon nanotubes," *Macromolecules*, Vol. 43, No. 24, pp. 10545–10553, 2010.

[4] J. Bai, R. D. Goodridge, R. J. M. M. Hague, M. Song, and M. Okamoto, "Influence of carbon nanotubes on the rheology and dynamic mechanical properties of polyamide-12 for laser sintering," *Polym. Test.*, Vol. 36, pp. 95–100, 2014.

[5] M. O. Lisunova, Y. P. Mamunya, N. I. Lebovka, and A. V. Melezhyk, "Percolation behaviour of ultra high molecular weight polyethylene/multi-walled carbon nanotubes composites," *Eur. Polym. J.*, Vol. 43, No. 3, pp. 949–958, Mar. 2007.

[6] A. Domard, M. Domard, and S. Dumitriu, "Polymeric biomaterials," p. 1168, 2002.

[7] J. Bai, R. D. Goodridge, R. J. M. Hague, and M. Song, "Improving the mechanical properties of laser-sintered polyamide 12 through incorporation of carbon nanotubes," *Polym. Eng. Sci.*, Vol. 53, No. 9, pp. 1937–1946, Sep. 2013.

[8] F. Mai, Y. Habibi, J. M. Raquez, P. Dubois, J. F. Feller, T. Peijs, and E. Bilotti, "Poly(lactic acid)/carbon nanotube nanocomposites with integrated degradation sensing," *Polym. (United Kingdom)*, Vol. 54, No. 25, pp. 6818–6823, 2013.

Part Two: Carbon Nanotube/Polyethylene Nanocomposites as Strain and Temperature Sensing Materials

Chapter II-4 Temperature-Conductivity Behaviour in Carbon Nanotube/ Polyethylene Composites

4.1 Introduction

Carbon nanotubes (CNTs) play a diverse two roles in composites. First, the CNT/polymer structural composites; the amazing mechanical properties of the CNTs are used to obtain structural materials with high elastic modulus and tensile, stiffness, compressive strength and lightweight. Secondly, CNT/polymer functional composites, in which other interesting properties like the high electrical and thermal conductivity, are utilized to develop functional chemical sensing materials, electrical and thermal conducting materials and energy storage performances [1]. There are a number of reports on the nanocomposite's thermal and electrical conductivity using different fillers and polymer matrices with changes in filler loadings [2]. The most current issues that related to nanocomposite fabrication with CNT filler are the dispersion of CNT in the polymer host are the CNT-polymer interaction, the nature of this interface, and the alignment of CNT in a polymer matrix. All of these issues are believed to be directly related to the electrical, mechanical and thermal performance of nanocomposites [3]- [5].

Among this chapter, the effects of the temperature on the electrical conductivity of the MWCNT/ high-density polyethylene nanocomposites will be investigated. Although many efforts have contributed to this field, the knowledge of the reproducibility of the conductive polymer nanocomposites is still limited. Therefore, the aim of this chapter is to study the reproducibility of the MWCNTs based nanocomposites prepared by a coating method.

4.2 Temperature-Dependent Electrical Conductivity

In the temperature-electrical conductivity measurements, the MWCNT/HDPE nanocomposite sheets with the size of 50mm×50mm×1mm were fabricated and tested. There are three to four samples for each CNT fraction of the MWCNT/HDPE nanocomposite sheets. One sheet from each fraction has been tested to check its reproducibility. Figure 4-1 illustrates the graphs of resistivity versus temperature for the

MWCNT/HDPE nanocomposites with three different percentages (1.0 wt%, 0.5 wt%, and 0.1 wt %) of MWCNT in three measurement steps. Graph (a, c and e) without any heat treatment but graph (b, d and f) has the last measurement steps after 12 hours of heat treatment at 80°C.

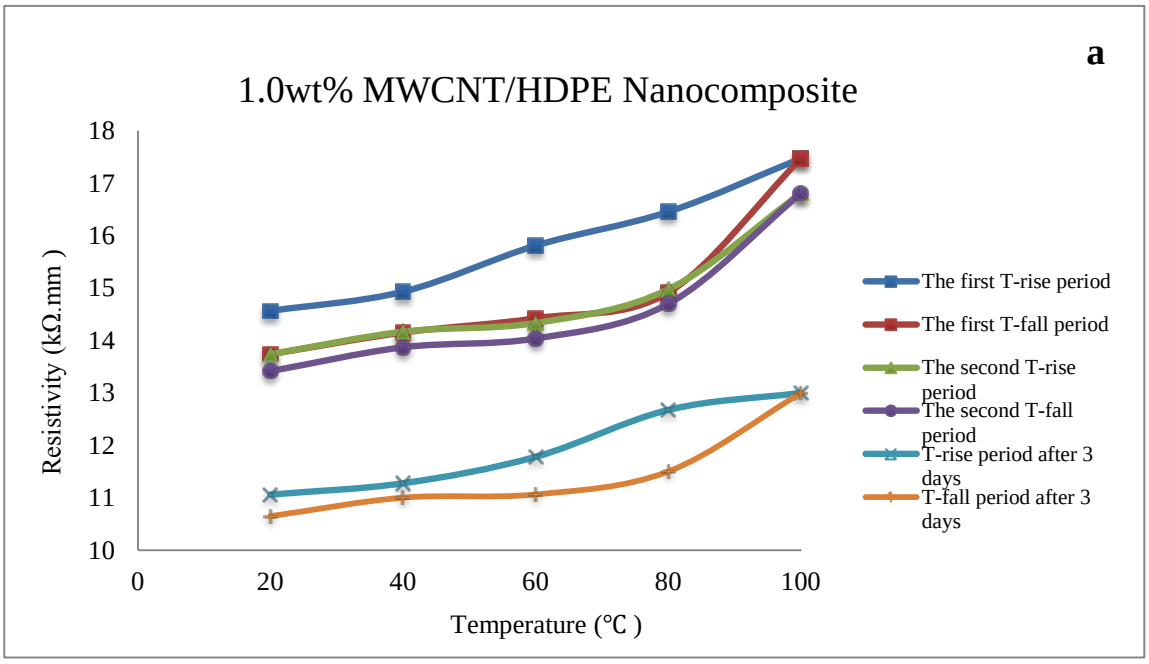

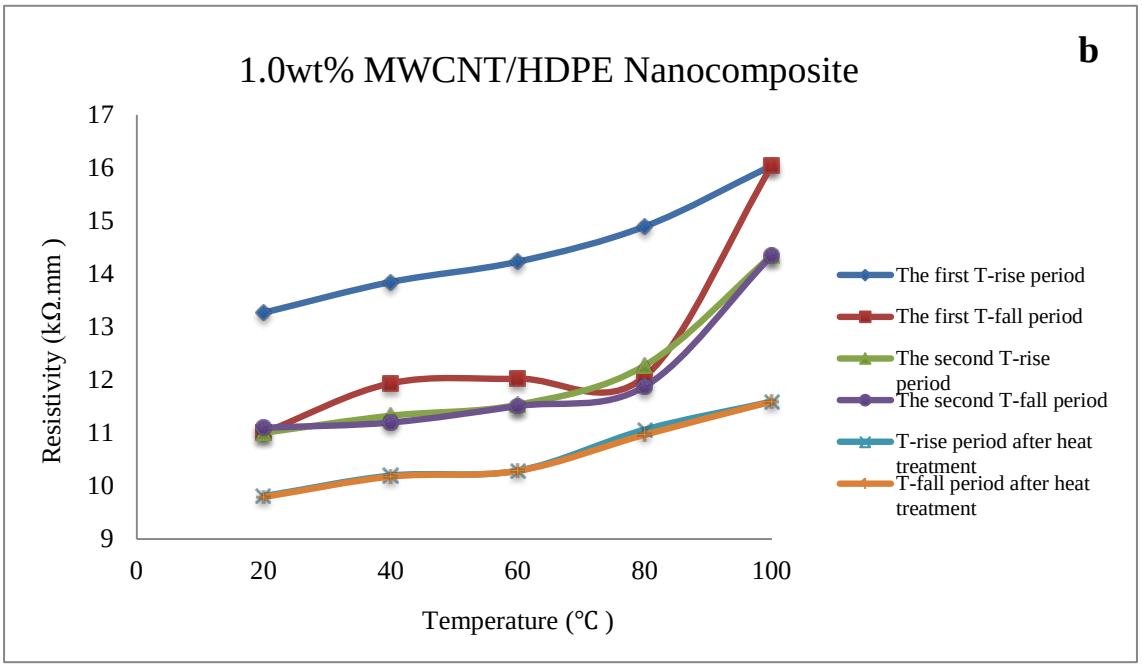

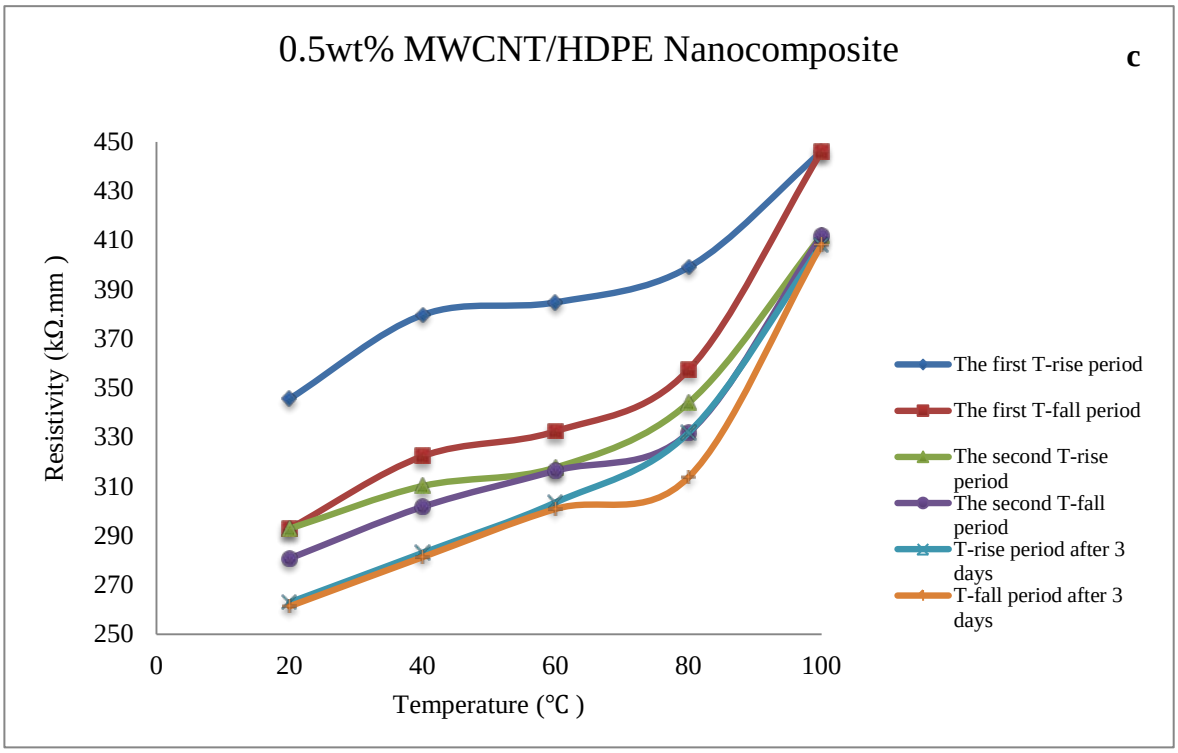
0.5wt% MWCNT/HDPE Nanocomposite
c
Resistivity (kΩ.mm)
450
430
410
390
370
350
330
310
290
270
250
0
20
40
60
80
100
Temperature (℃)
The first T-rise period
The first T-fall period
The second T-rise period
The second T-fall period
T-rise period after 3 days
T-fall period after 3 days

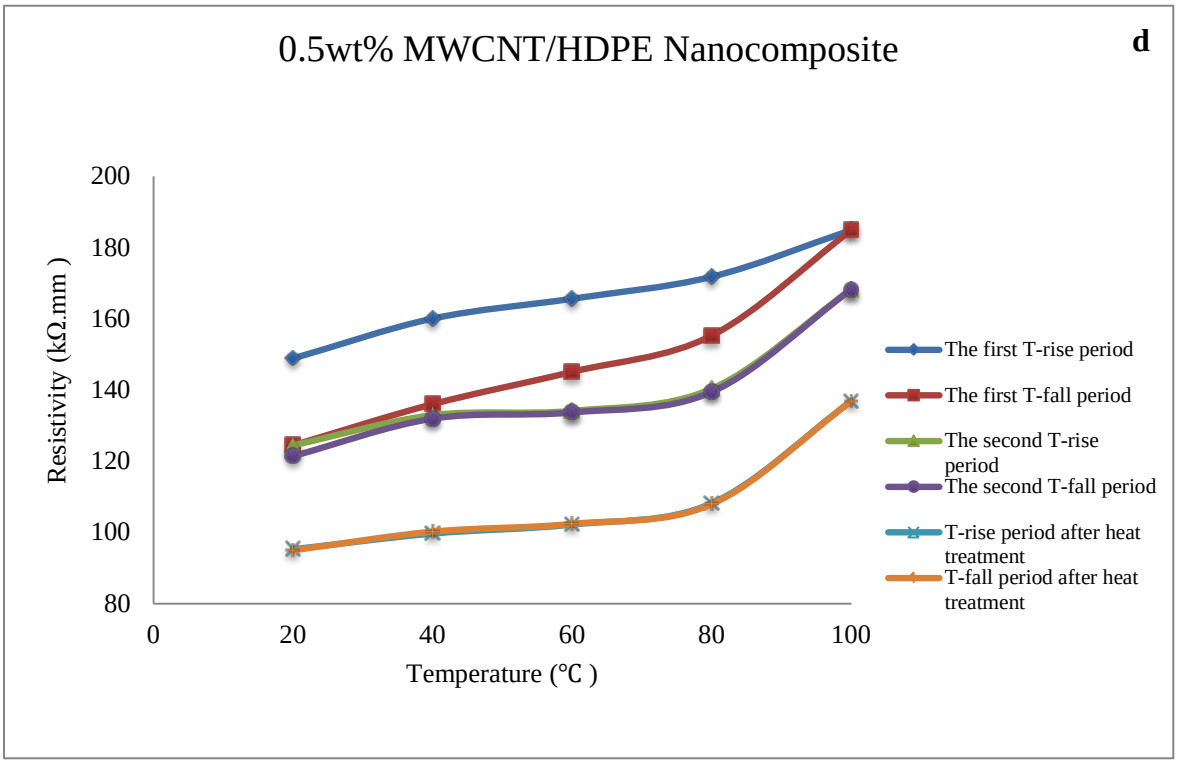
0.5wt% MWCNT/HDPE Nanocomposite
d
Resistivity (kΩ.mm)
200
180
160
140
120
100
80
0
20
40
60
80
100
Temperature (℃)
The first T-rise period
The first T-fall period
The second T-rise period
The second T-fall period
T-rise period after heat treatment
T-fall period after heat treatment

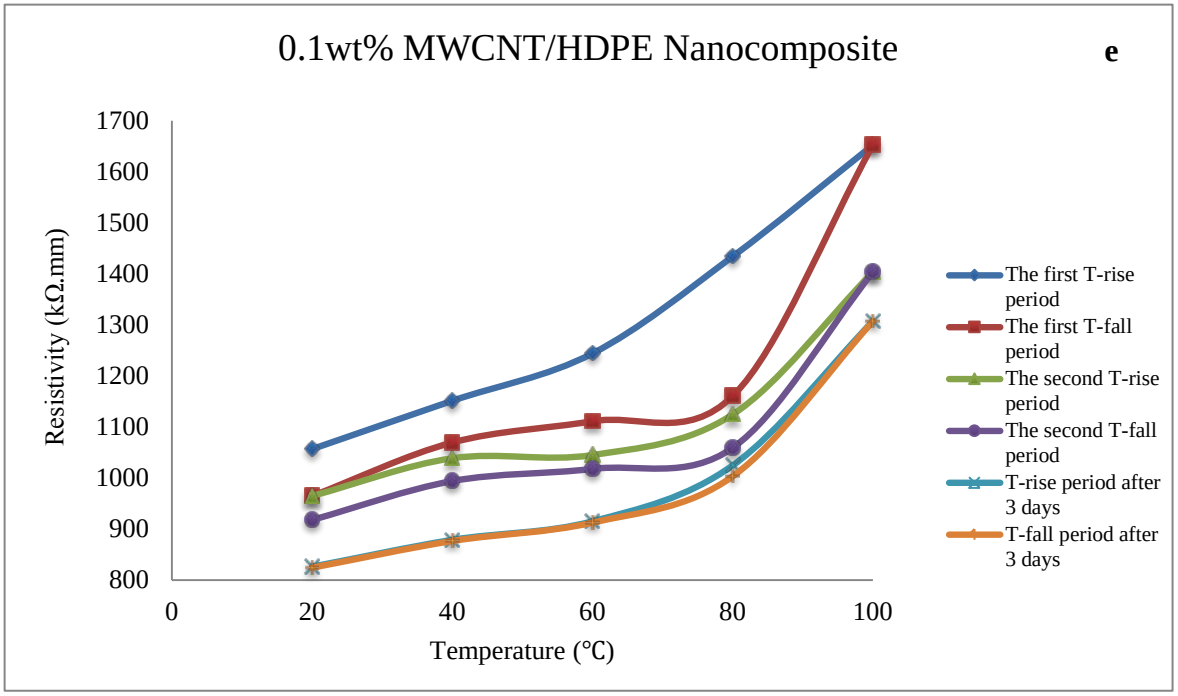

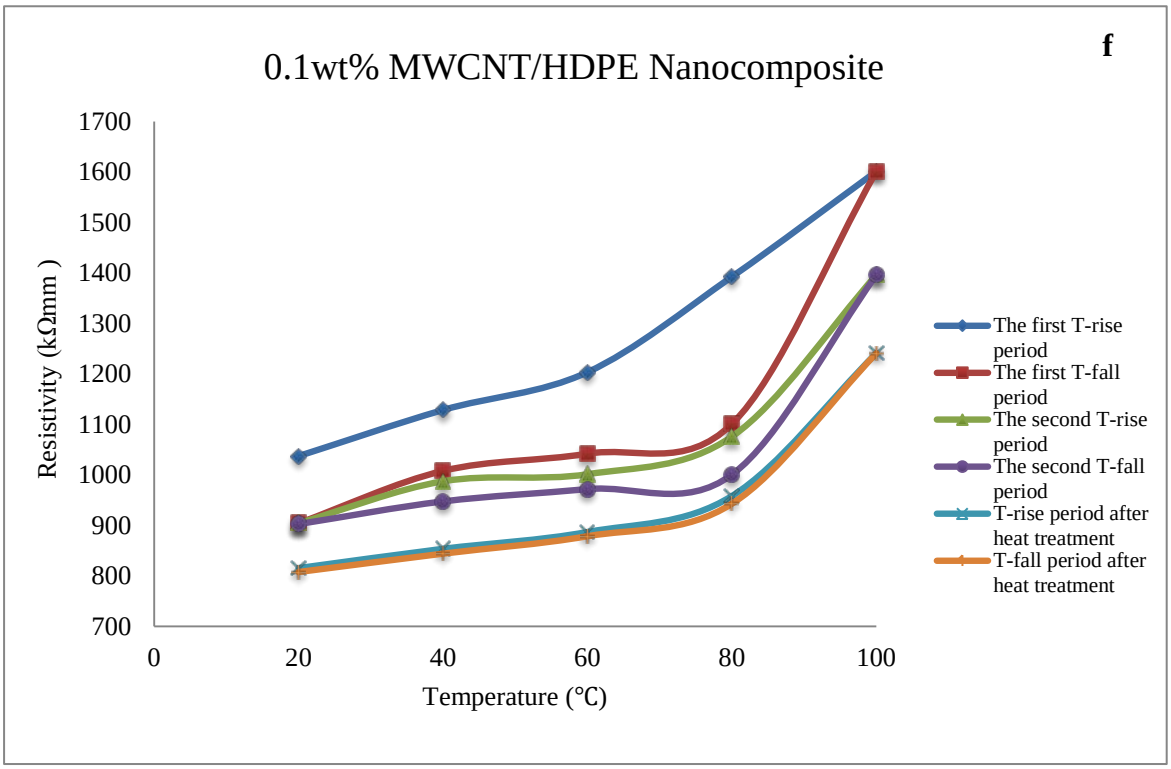

Figure 4-1: Plots of resistivity versus temperature for the MWCNT/HDPE nanocomposites with the MWCNT contents of (a) 0.1 wt% without heat treatment (b) 0.1 wt% after 12h of heat treatment (c) 0.5 wt% without heat treatment (d) 0.5 wt% after 12h of heat treatment (e).

From figure 4-1, there is a directly proportional relation between the resistivity and the temperature in each single sheet as expected [6]. The resistivity has a steady increase as the temperature rises from 20^{o}C to 100^{o}C and vice versa. However, the initial electrical resistivity for each MWCNT/HDPE nanocomposite sheet with the same filler fraction was found to be different before and after the heat treatment, which can be summarized in table 4-1.

Table 4-1: Initial electrical resistivity of the MWCNT/HDPE nanocomposites with different filler contents.

Heat treatment	**Nanocomposites initial electrical resistivity (kΩ.mm)**		
	with 0.1 wt% MWCNT	with 0.5 wt% MWCNT	with 1.0 wt% MWCNT
Before	1056.9	345.6	14.6
After	1037.6	148.9	13.3

As it is seen from the table above, the initial electrical resistivity values for each MWCNT/HDPE nanocomposites with the same filler contents is smaller after the heat treatment. This can be related to the heat influence on the nanocomposite structure which makes it much more homogenous and rebonded the conductive nanofillers paths which decrease the resistivity of the whole sheet.

As shown in figure 4-1, when the temperature increases, the electrical resistivity of the MWCNT/HDPE nanocomposite with different filler contents is rising dramatically. This is because the increase in temperature causes the distance between the conductive nanofillers to be larger which leads to the increase of the electrical resistivity. Similarly, when the temperature decreases, the distance between the conductive nanofillers has accordingly reduced which is resulting in the reduction of the electrical resistivity.

During these tests, each sample was experienced two processes of heating and cooling. From figure 4-1, it was interesting that the electrical resistivity of the MWCNT/HDPE nanocomposites during each process of cooling were smaller than that during the same process of heating. This indicates that the electrical conductivity during the process of cooling was better than the same process of heating. During the cooling process, the conductive nanofillers retain to its original structure very slowly. Thus, the bonds can be formed slowly and strongly. In another word, the distances between the conductive

nanofillers are adjusted to be smaller, leading to better electrical conductivities during the process of cooling.

Additionally, for all MWCNT/HDPE nanocomposites samples, the electrical resistivity for the second process of heating and cooling were smaller than that for the first process of heating and cooling. These results are most likely because of the heating induces some movement of polymer chains which result in a rearrangement of the conductive nanofillers in the first process which results in having a smaller resistivity in the next measurements.

Furthermore, for the MWCNT/HDPE nanocomposites with the MWCNT contents of 0.1 wt%, 0.5 wt% and 1.0 wt%, the fitting of the electrical resistivity graphs between the first process of heating and cooling was smaller than that between the second process of heating and cooling, which indicated that the reproducibility of the electrical conductivity of the second process of heating and cooling was better than that of the first process.

For the MWCNT/HDPE nanocomposite sheets used in this project, which were made from nanocomposite powders, there are probably some cavities left inside the samples after the compression moulding. These voids lead to increase the distances between the conductive nanofillers, and further, make the electrical conductivity decreased. Thus, each process of heating can decrease these size and number of the voids. The effect of the voids on the electrical conductivity can be gradually excluded with each process of heating, which results in the improvement of the reproducibility. These are the reasons why the reproducibility of the electrical conductivity of the second process of heating and cooling was better than that for the first process. Based on the conductive tunnelling mechanics, as the temperature increases, the distances between the conductive nanofillers increases consequently, which lead to a drop of the electrical conductivity.

Figure 4-2 shows the MDSC curve of pure HDPE which indicates that the melting point of pure HDPE can be identified as 133.57°C. Thus, the heat treatment temperature of 80°C can be suggested as a “safe-side” chosen temperature, because, at 80°C, the nanocomposites cannot further fuse, so no new distribution of the MWCNTs can establish itself [7]

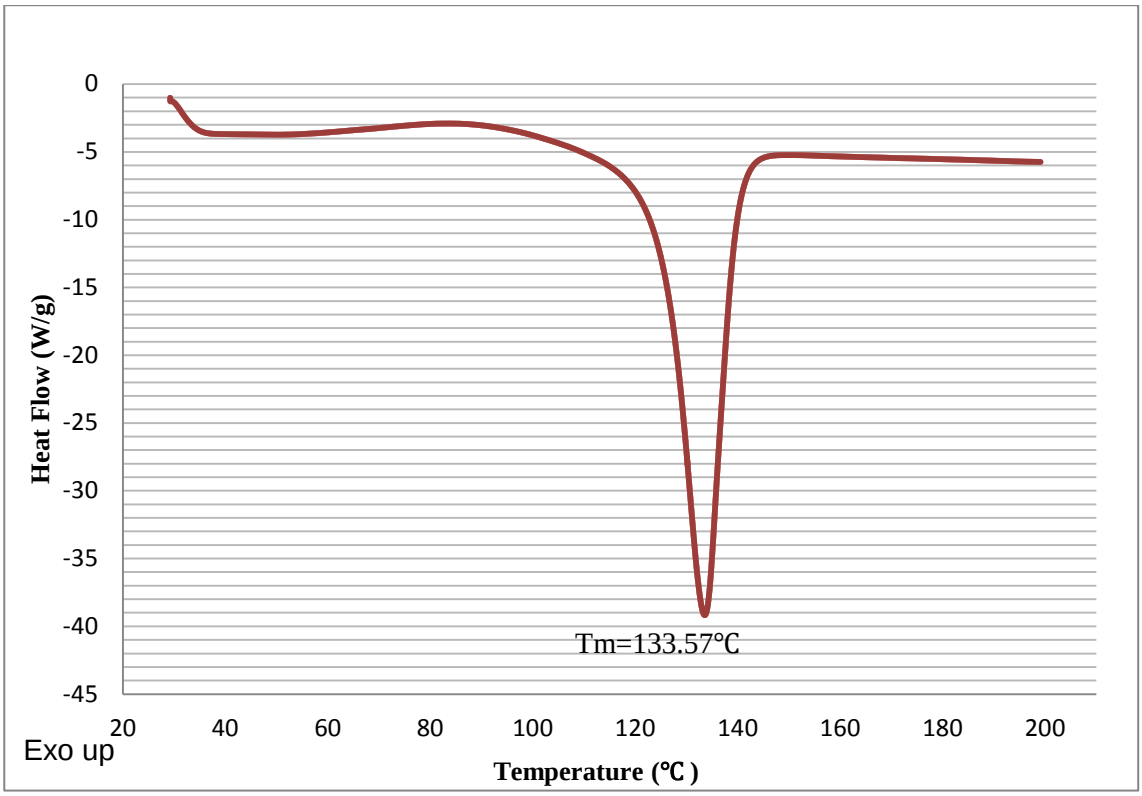

Figure 4-2: MDSC curve of pure HDPE

As for the reproducibility of the MWCNT/HDPE nanocomposites, from figure 4-1 (e) and (f), the heat treatment did not have the obvious effect on the reproducibility for the MWCNT/HDPE nanocomposite with the MWCNT content of 0.1 wt%. This is probably due to the little conductive filler content in the MWCNT/HDPE nanocomposites. The two processes of heating before the heat treatment have made the voids in the nanocomposite sheets be excluded which leave the treatment heating without any further influence in the nanocomposite structure. Besides, the conductive nanofillers rearrangement is almost completed during the two processes of heating and cooling. Therefore, the heat treatment has only a little effect on the reproducibility.

Apart from the 0.1 wt% MWCNT/HDPE nanocomposite, the heat treatment had apparent effects on the reproducibility for the rest of the tested fractions of the nanocomposites; especially for the 1.0 wt% MWCNT/HDPE nanocomposites (figure 4-1 (a)-(d)). Without using the heat treatment, there was still a large gap in the electrical resistivity path between the process of heating and cooling after three days, shown in figure 4-1 (a). However, figure 4-1 (b) indicates that heat treatment results in significant

decreasing on this gap between the electrical resistivity of the heating and cooling process paths, and effectively improved the reproducibility.

As shown in figure 4-3 and figure 4-4, another temperature-electrical conductivity measurement has been taken for (100mm x15mm x 5mm) samples in return path after 2 weeks of heat treatment. Clearly, from these results, although the resistivity increases as the temperature rise up, it is noticeable that there is a different starting resistivity value with each sample even if they are with the same MWCNT fraction.

The difference in the electrical resistivity of each MWCNT/HDPE nanocomposites sheet with the same filler fraction possibly lies in the inhomogeneous heating of the samples, which induces different melt viscosity throughout the whole samples. Thus, the dispersion of the conductive nanofillers in each nanocomposite sheet is different, resulting in the variation of the whole volume resistivity.

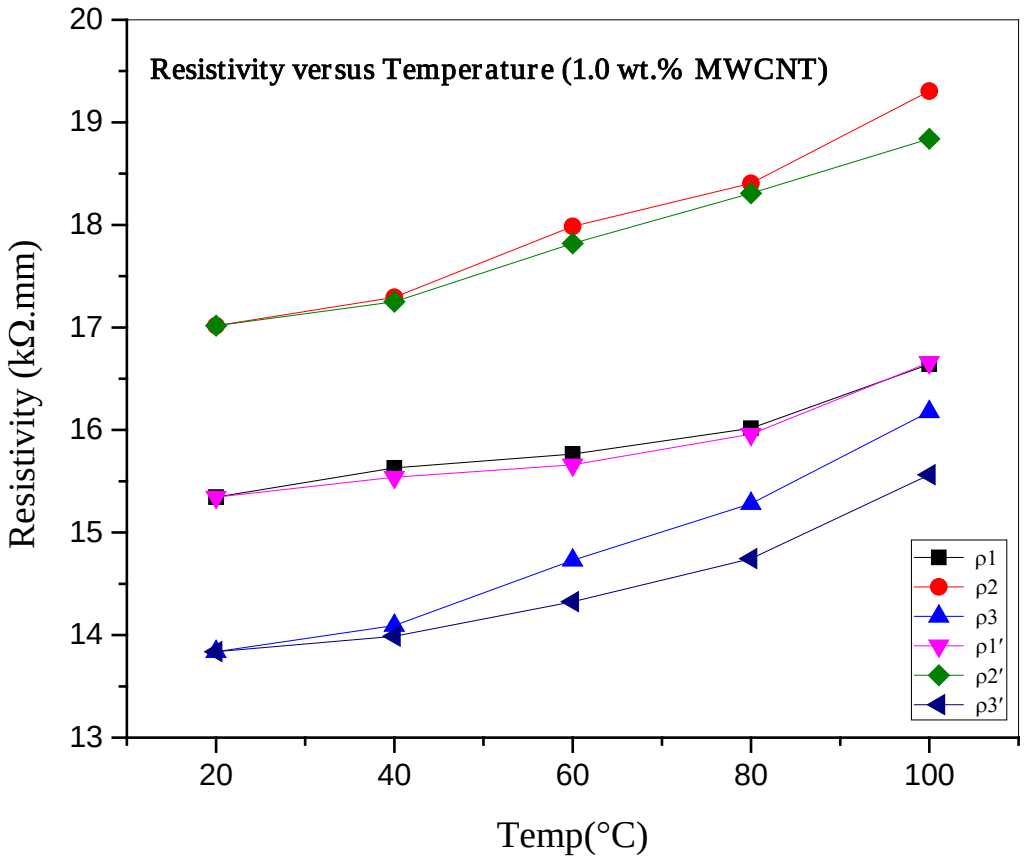

Figure 4-3: Plots of resistivity versus temperature from 20°C to 100°C and vice versa for two samples of MWCNT/HDPE nanocomposites with the MWCNT contents of 1.0 wt%.

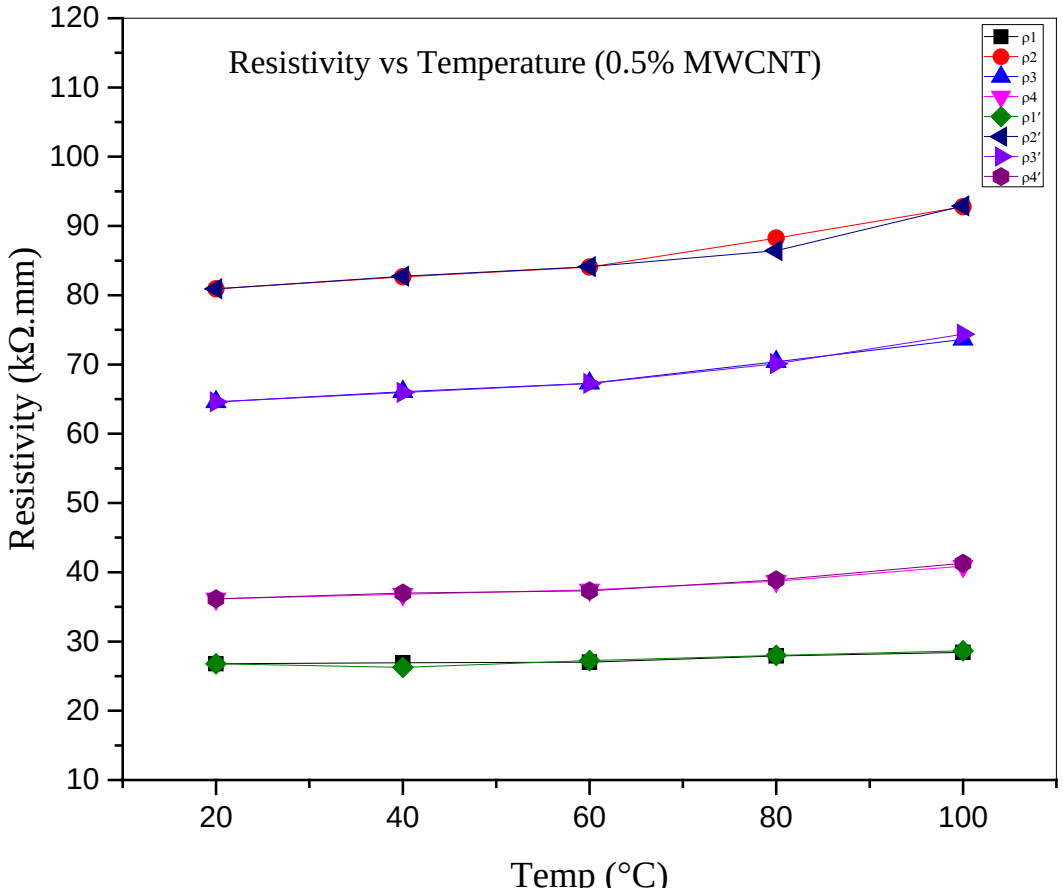

Figure 4-4: Plots of resistivity versus temperature for four samples of MWCNT/HDPE nanocomposites with the MWCNT contents of 0.5 wt%.

4.3 Conclusion

In this chapter, the effects of the temperature on the electrical conductivity of the MWCNTs based nanocomposites were considered. Average electrical resistivity decreased as MWCNT wt% increased from 0.1 to 1% wt. This indicates to an increase in the electrical conductivity in samples. 1.0 wt% MWCNT/HDPE nanocomposite has shown the best reproducibility of the electrical conductivity to temperature. Moreover, It was found that the reproducibility was improved by preheating treatment before each test. On the other hand, the difference in the initial electrical resistivity during the temperature-electrical conductivity measurements of the nanocomposites with the same filler contents inevitably affects the study of the heat treatment effects on the reproducibility. Thus, the fabrication of the nanocomposites with almost the same initial electrical resistivity with the same filler contents is crucial.

References

[1] J. H. Du, J. Bai, and H. M. Cheng, "The present status and key problems of carbon nanotube based polymer composites," *Express Polym. Lett.*, Vol. 1, No. 5, pp. 253–273, 2007.

[2] R. Haggenmueller, C. Guthy, J. R. Lukes, J. E. Fischer, K. I. Winey, † Reto Haggenmueller, † Csaba Guthy, ‡ Jennifer R. Lukes, † and John E. Fischer, and † Karen I. Winey*, "Single wall carbon nanotube/polyethylene nanocomposites: Thermal and electrical conductivity," *Macromolecules*, Vol. 40, No. 7, pp. 2417–2421, 2007.

[3] W. E. Jones, J. Chiguma, E. Johnson, A. Pachamuthu, and D. Santos, "Electrically and thermally conducting nanocomposites for electronic applications," *Materials*, Vol. 3, No. 2. Molecular Diversity Preservation International, pp. 1478–1496, 25-Feb-2010.

[4] M. O. O. Lisunova, Y. P. P. Mamunya, N. I. I. Lebovka, and A. V. V. Melezhyk, "Percolation behaviour of ultrahigh molecular weight polyethylene/multi-walled carbon nanotubes composites," *Eur. Polym. J.*, Vol. 43, No. 3, pp. 949–958, Mar. 2007.

[5] F. Chouit, O. Guellati, S. Boukhezar, A. Harat, M. Guerioune, and N. Badi, "Synthesis and characterization of HDPE/N-MWNT nanocomposite films.," *Nanoscale Res. Lett.*, Vol. 9, No. 1, p. 288, 2014.

[6] C. Kingston, R. Zepp, A. Andrady, D. Boverhof, R. Fehir, D. Hawkins, J. Roberts, P. Sayre, B. Shelton, Y. Sultan, V. Vejins, and W. Wohlleben, "Release characteristics of selected carbon nanotube polymer composites," *Carbon*, Vol. 68. pp. 33–57, 2014.

[7] N. Grossiord, P. J. J. J. Kivit, J. Loos, J. Meuldijk, A. V. Kyrylyuk, P. van der Schoot, and C. E. Koning, "On the influence of the processing conditions on the performance of electrically conductive carbon nanotube/polymer nanocomposites," *Polymer (Guildf).*, Vol. 49, No. 12, pp. 2866–2872, Jun. 2008.

Part Two: Carbon Nanotube/Polyethylene Nanocomposites as Strain and Temperature Sensing Materials

Chapter II-5 : Strain-Conductivity Behaviour in Carbon Nanotube/ High-Density Polyethylene Composites.

5.1 Introduction

The strain sensor is one of the important concerns in science fields. Although current strain sensors have excellent performances in terms of time and sensitivity, they still have to be related to signal acquisition equipment and power sources [1]. These limitations prevent the existing strain sensors from being embedded at material or atom levels to monitor the moving structures. Significant improvements and understanding have been made in this field, but many challenges still need to be overcome. Recently, a developing strain sensor from optical fiber was employed to be embedded into material level [2]. Nonetheless, the high cost of the required expensive equipment for acquiring strain information is still a limitation of the optical fiber based strain sensor [2]. Therefore, to overcome these difficulties, a new strain sensor is needed.

Nanotechnology science has the potential to develop an innovative way for measuring the motion in the micro to nano-scale size [3]-[5]. Carbon nanotubes have received a great interest due to their unique electronic structure as viewed in chapter II-1. Thus, they offer an alternative new strain sensor by integrating CNTs into polymers which have currently attracted researcher interest [5],[6].

In this chapter, the study of the stress effects and mechanical deformation (strain) on the electrical conductivity of the MWCNT/ high-density polyethylene nanocomposites in room temperature will be discussed. The reproducibility and the strain sensing behaviours investigation of the MWCNTs based nanocomposites will be considered.

5.2 Strain-Dependent Electrical Conductivity in MWCNT/HDPE Nanocomposite

During the strain-electrical conductivity measurements, fabricated sheets of the MWCNT/HDPE nanocomposite with the size of (100mm×15mm×5mm) and (0.5 wt% and 1.0 wt %) percentage of MWCNTs were used. All the measurements were conducted at room temperature. The three points bending test was carried out in this part as it is a British slandered method for small deformation measurements BS 2782-10. Stress of 0.0065 N/mm^2, 0.013 N/mm^2, 0.019 N/mm^2, and 0.026 N/mm^{2}were applied on these samples respectively. The resulted strain had only a slight influence or even no change in electrical conductivities with the increase of the deformation happened. This outcome is probably because the samples with the thickness of 5mm are somehow thick and so, the electrical conductivity is not sensitive to that deformation shift. The relationships among the stress, the strain and the initial electrical conductivities for 0.5 wt% MWCNT/HDPE nanocomposites are shown in table 5-1 and figure 5-1.

Table 5-1: Results of the stress, strain, resistance and resistivity for 0.5 wt% MWCNT/HDPE nanocomposite

stress (N/mm2)	Strain (mm)	Resistance (kΩ)	Resistivity (kΩ.mm)
0	0	136.44	102.33
0.0065	0.37	136.50	102.375
0.013	0.82	136.56	102.42
0.019	1.28	136.66	102.495
0.026	1.81	136.93	102.6975

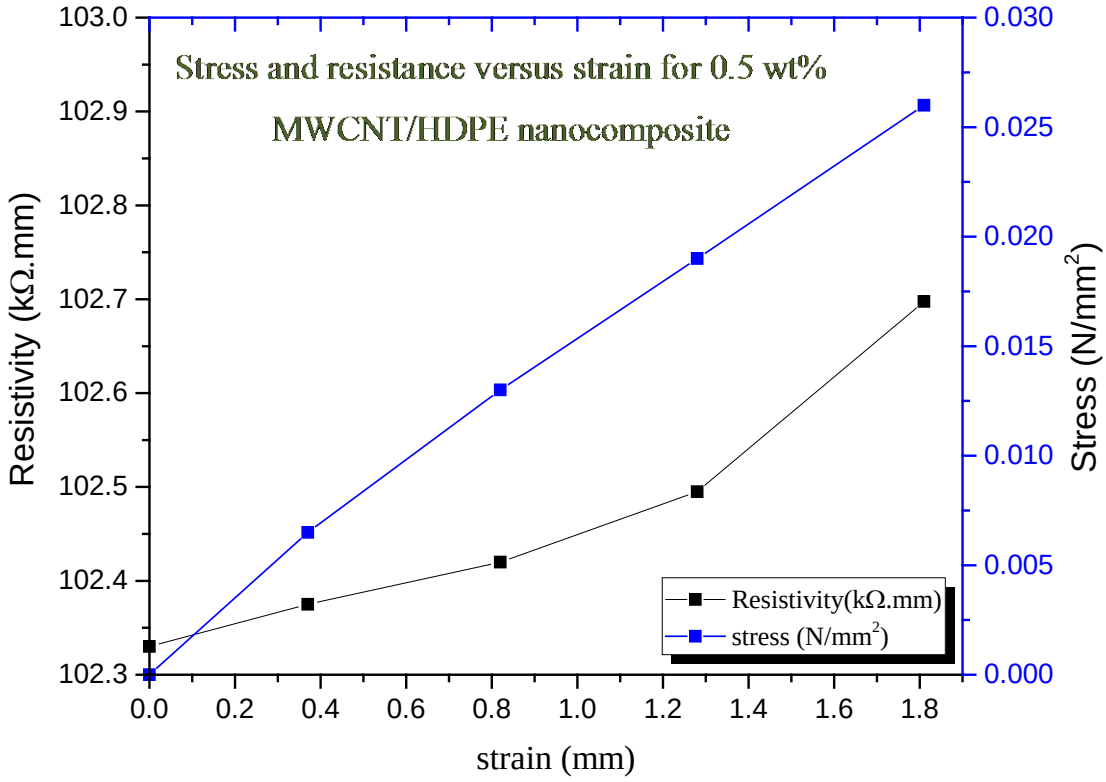

Figure 5-1: Plot of stress and resistivity versus strain for 0.5 wt% MWCNT/HDPE nanocomposite

There is a linear relation between each of applied stress, resistivity, and the strain. When the applied stress increases, the strain rise up and the resistivity does so. What actually happened is that as the stress is applied on the samples, the strain becomes larger and thus the distances between the conductive nanofillers enlarge leading to a drop in electrical conductivity [7].

The relationship between resistivity and strain for 0.5wt% MWCNT/HDPE nanocomposite is shown in figure 5-2.

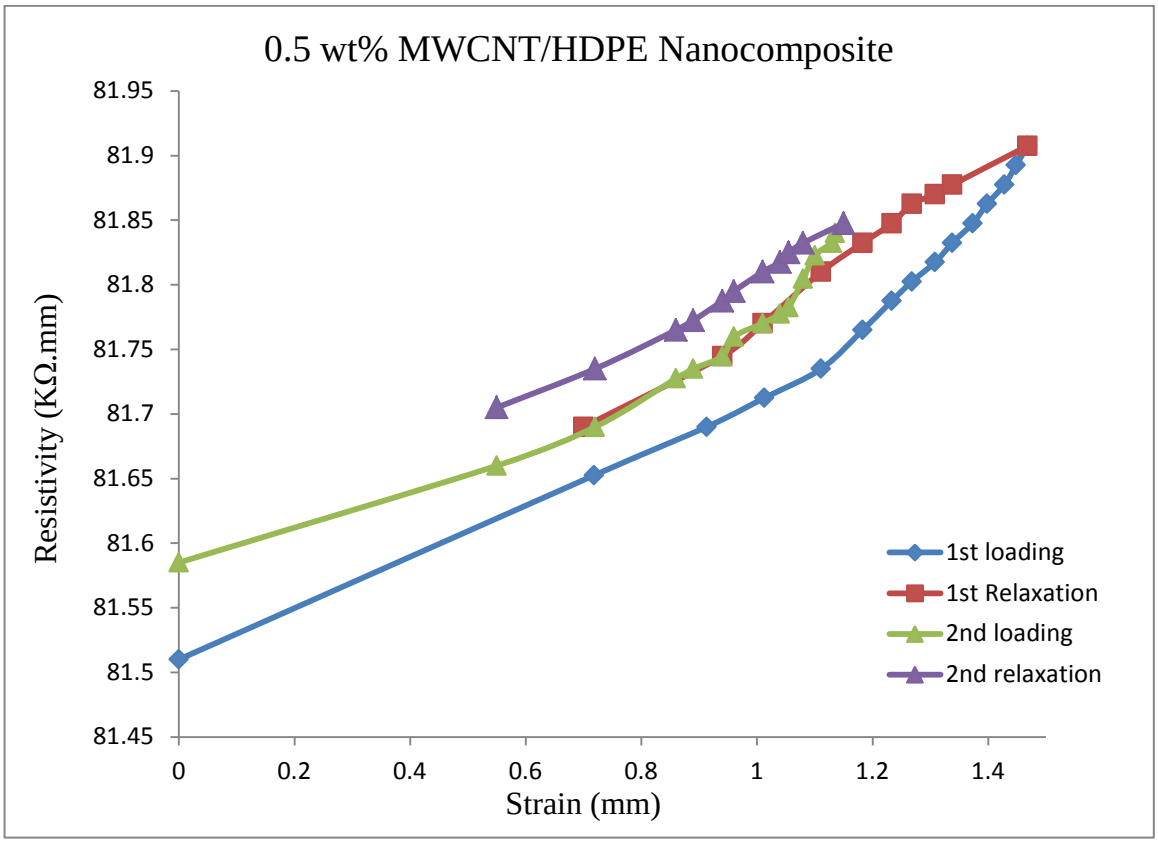

Figure 5-2: Plot of resistivity versus strain for 0.5 wt% MWCNT/HDPE nanocomposite.

From figure 5-2, when a 4kg loading was firstly applied on the sample gradually, the resistivity increased from 81.511 kΩ.mm to 81.910 kΩ.mm with the rising up of the strain. Then, the resistivity decreased down to 81.692 kΩ.mm during the process of unloading. The resistivity, as well as the strain, is not able to go back to the original state. Similarly, in the second time, once 4kg was loading, the resistivity also increased from 81.585 kΩ.mm to 81.848 kΩ.mm with the increase of the strain and then they decreased during the unloading process. The resistivity reached to 81.705 kΩ.mm. Again, the resistivity and the strain, could not totally recover. It was interesting that from this figure that the initial resistivity for the second period of loading, which was 81.585 kΩ.mm, was larger than that for the first period of loading, which was 81.51 kΩ.mm.

The relationship between resistivity and strain for 1.0wt% MWCNT/HDPE nanocomposite is shown in figure 5-3.

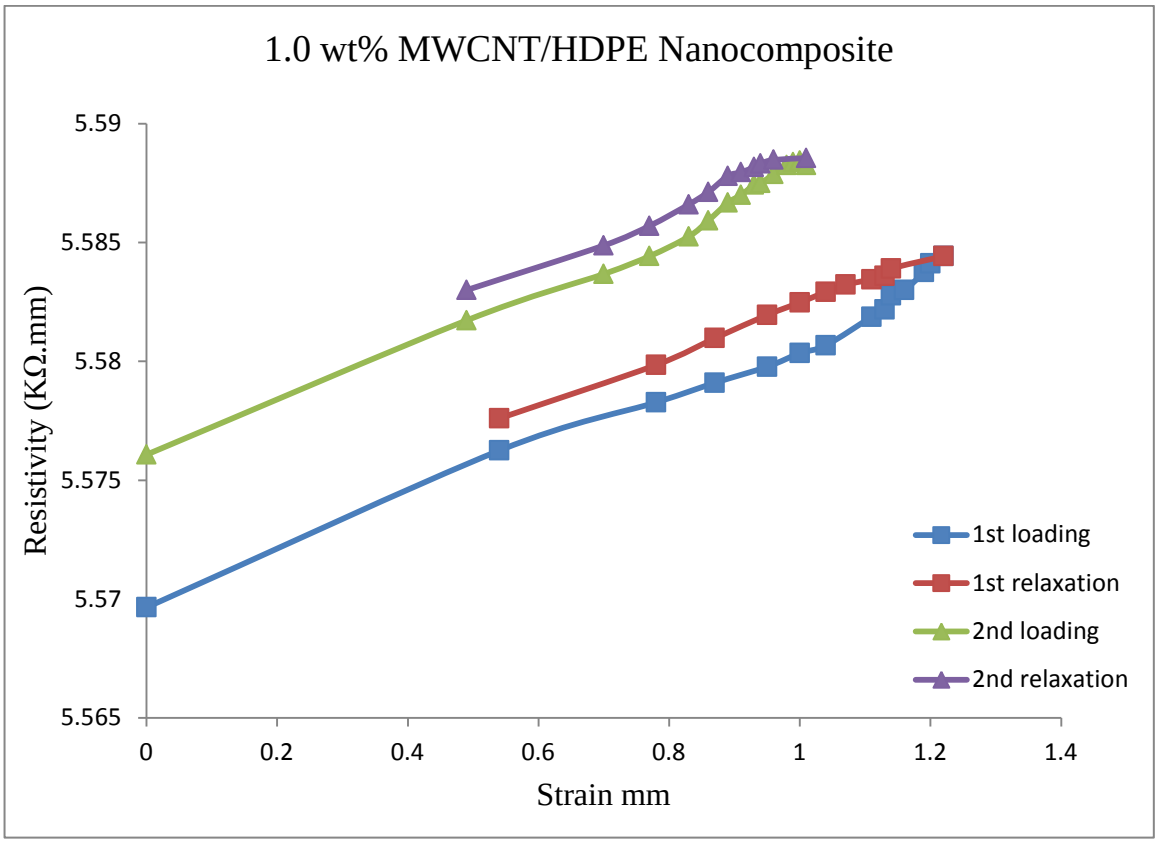

Figure 5-3: Plot of resistivity versus strain for 1.0 wt% MWCNT/HDPE nanocomposite

Similar to the 0.5 wt% MWCNT/HDPE nanocomposite, when 4kg loading was firstly applied on the sample, the resistivity increased (from 5.569kΩ.mm to 5.584kΩ.mm) with the increase of the strain, and then went down during the process of unloading, as shown in figure 5-3. As 4kg loading was secondly applied to the sample, the resistivity also went up from (5.576kΩ.mm to 5.588 kΩ.mm) with the rise of the strain and decreased to only 5.583 kΩ.mm during the relaxation period. In both the first and the second period of loading/unloading, the resistivity besides the strain, could not reveal their original state. In addition, the initial resistivity for the first period of loading was smaller than that for the second period. This result was the same as the result of 0.5 wt% MWCNT/HDPE nanocomposite.

During the loading and unloading processes, the MWCNT/HDPE nanocomposites experience elongation and relaxation periods which can move the polymer segments induces the change of the conductive networks, resulting in the change of the electrical resistivity. The mechanism of the loading and unloading process can be concluded in that: An applied force on an area (stress) can induce a deformation (strain) in the

nanocomposites which lead to destruction in the conductive networks. The distances between the conductive nanofillers enlarged, and accordingly the electrical resistivity increased [8]. Consequently, in this project, the electrical resistivity of both MWCNT/HDPE nanocomposites with the MWCNT fillings of 0.5 wt% and 1.0 wt% increased during the process of loading and then decreased during the process of unloading.

5.3 Electrical Recovery Behaviour in MWCNT/HDPE Nanocomposite

The first process of loading and unloading that are shown in figure 5-2 and figure 5-3 had finished in about 2 days for both nanocomposites. The resulted electrical resistivity values of both of them were larger than the initial electrical resistivity of the first loading period.

These results are possible because of the electrical recovery that is concerned with the viscoelastic behaviour of the nanocomposite. The electrical resistivity cannot totally recover during the relaxation [9]. Voigt-Kelvin model has been used to describe the electrical recovery behaviour by a previous group researcher. The following formula was used to describe the relation of the original resistivity and the new electrical resistivity [9]:

$$R(t) = R_m(\varepsilon) + R_d exp\left(-\frac{t}{\tau}\right) \quad (5\text{-}1)$$

Where: $R_m(\varepsilon)$ *is the un-recoverable resistivity,*

R_d *: The original resistivity of the deformed sample,*

τ *: a constant at the given strain*

As clearly seen in these tests, when the loading was removed and the nanocomposites with the thickness of 5mm have experienced the relaxation for two days. The electrical resistance and so the resistivity could not recover to a zero-deformation (strain) value that was found in the beginning of the first loading. This is due to the viscoelastic electrical response which based on the “viscoelastic” behaviour of the electrical recovery.

From equation (5-1), the electrical recovery can be expressed as a time-dependent behaviour. The initial electrical resistivity for the second process of loading was smaller than last resistivity point for the first process of unloading because the resistivity tended to recover within the two days. Therefore, it seems that, although the electrical resistivity cannot totally go back to the original state, it is possible that when nanocomposites experience quite a long period of relaxation. The electrical conductivity can be quite close to the initial conductivity of the first process of loading. This hypothesis needs to be proved by further works.

5.4 Reproducibility of MWCNT/HDPE Nanocomposites with Stress

In the 0.5 wt% MWCNT/HDPE nanocomposite, the zero-deformation value of resistivity for the first period of loading was 81.51 kΩ.mm but, the measured electrical resistivity after the two times of loading and unloading was 81.705kΩ.mm.

Thus, the degree of the electrical recovery could be calculated as:

$$1 - \frac{81.705 - 81.51}{81.51} \times 100\% = 99.76\%$$

Similarly, for the 1.0 wt% MWCNT/HDPE nanocomposite, the zero-deformation value of resistivity for the first period of loading was 5.5696 kΩ,.mm and electrical resistivity measured after the two times of loading and unloading was 5.583 kΩ..mm. Therefore, the degree of the electrical recovery was calculated to be 99.76%, which was basically equivalent to the 0.5 wt% MWCNT/HDPE nanocomposites.

Table 5-2 and table 5-3 demonstrate the degree of the electrical recovery at each deformation (strain) measured for the 0.5 wt% and the 1.0 wt% MWCNT/HDPE nanocomposites respectively. Both nanocomposites have the degrees of the electrical recovery at each deformation during the second process of relaxation higher than the first process of relaxation. This result was with a good agreement with the gaps in the electrical resistivity between the loadings and unloading process which were smaller for the second process than that for the first one (see table 5-2 and Table 5-3). Consequently, the reproducibility of the second process of loading and unloading was better than that of the first process.

Table 5-2: Degree of the electrical recovery at each strain for the 0.5 wt% MWCNT/HDPE nanocomposite**.**

First Relaxation		**Second Relaxation**	
Strain (mm)	Degree of electrical recovery (%)	Strain (mm)	Degree of electrical recovery (%)
0.718	99.95	0.550	99.95
0.913	99.94	0.720	99.95
1.013	99.93	0.860	99.96
1.111	99.92	0.890	99.95
1.183	99.92	0.940	99.95
1.233	99.93	0.960	99.96
1.268	99.93	1.010	99.95
1.308	99.94	1.040	99.95
1.338	99.95	1.055	99.95

Table 5-3: Degree of the electrical recovery at each strain for the 1.0 wt%MWCNT/HDPE nanocomposite

First Relaxation		**Second Relaxation**	
Strain (mm)	Degree of electrical recovery (%)	Strain (mm)	Degree of electrical recovery (%)
0.540	99.97	0.490	99.97
0.780	99.97	0.700	99.98
0.870	99.96	0.770	99.98
0.950	99.96	0.830	99.98
1.000	99.96	0.860	99.98
1.040	99.96	0.890	99.98
1.070	99.96	0.910	99.98
1.110	99.97	0.930	99.99
1.130	99.97	0.940	99.99
1.140	99.98	0.960	99.99

Moreover, the strain of the 1.0 wt% MWCNT/HDPE nanocomposites was smaller than that of the 0.5 wt% MWCNT/HDPE nanocomposite. In addition, as shown table 5-2 and table 5-3, the degree of the electrical recovery at each strain for the 1.0 wt% MWCNT/HDPE nanocomposite was higher than that for the 0.5 wt% MWCNT/HDPE nanocomposite. Although the ultimate degree of the electrical recovery, 99.76%, for the 0.5 wt% MWCNT/HDPE nanocomposite approximately equalled to that for the 1.0 wt% MWCNT/HDPE nanocomposite, the reproducibility of the 1.0 wt% MWCNT/HDPE nanocomposite was better than that of the 0.5 wt% MWCNT/HDPE nanocomposite during each process of loading and unloading. Essentially, for the whole process of unloading, the resistance relaxation is due to the recovery of the effective conductive paths induced by the disorientation of the polymer chains [10].

5.5 Conclusion

The results of the strain-electrical conductivity measurements revealed that the initial electrical resistivity for the MWCNT/HDPE nanocomposites increased with the increasing of the applied stress because the distances between the conductive nanofillers increased and some conductive networks were destroyed. It was found that the MWCNT/HDPE nanocomposite sheets exhibited “viscoelastic” behaviour of the electrical recovery which causes the electrical resistivity could not totally recover during the relaxation. In addition, 1.0 wt% MWCNT/HDPE nanocomposite showed the best reproducibility of the electrical conductivity against stress. In conclusion, as increasing strain leads to damage the conductive networks and so decrease the electrical conductivity, these nanocomposites may consider as stress sensing materials for the development of strain sensors for engineering applications.

References

[1] L. Ristić, *Sensor technology and devices*. Artech House, 1994.

[2] K. T. V. Grattan and B. T. Meggitt, "Optical Fibre Sensor Technologies," 1999.

[3] Y. Li, X. Qiu, F. Yang, X.-S. Wang, and Y. Yin, "Ultra-high sensitivity of super carbon-nanotube-based mass and strain sensors.," *Nanotechnology*, Vol. 19, No. 16, p. 165502, Apr. 2008.

[4] J. Zhou, Y. Gu, Y. Hu, W. Mai, P. H. Yeh, G. Bao, A. K. Sood, D. L. Polla, and Z. L. Wang, "Gigantic enhancement in response and reset time of ZnO UV nanosensor by utilizing Schottky contact and surface functionalization," *Appl. Phys. Lett.*, Vol. 94, No. 19, p. 191103, May 2009.

[5] Q. Zhao, M. D. Frogley, and H. D. Wagner, "Direction-sensitive strain-mapping with carbon nanotube sensors," *Compos. Sci. Technol.*, Vol. 62, No. 1, pp. 147–150, 2002.

[6] N. Muto, Y. Arai, S. G. Shin, H. Matsubara, H. Yanagida, M. Sugita, and T. Nakatsuji, "Hybrid composites with self-diagnosing function for preventing fatal fracture," *Compos. Sci. Technol.*, Vol. 61, No. 6, pp. 875–883, 2001.

[7] J. Jin, Y. Lin, M. Song, C. Gui, and S. Leesirisan, "Enhancing the electrical conductivity of polymer composites," *Eur. Polym. J.*, Vol. 49, No. 5, pp. 1066–1072, May 2013.

[8] L. Flandin, Y. Brechet, and J. Y. Cavaille, "Electrically conductive polymer nanocomposites as deformation sensors," *Compos. Sci. Technol.*, Vol. 61, No. 6, pp. 895–901, 2001.

[9] X. Sun, "Conductive behaviour of carbon nanotube based composites," 2009.

[10] L. Wang, T. Ding, and P. Wang, "Research on stress and electrical resistance of skin-sensing silicone rubber/carbon black nanocomposite during decompressive stress relaxation," *Smart Mater. Struct.*, Vol. 18, No. 6, p. 65002, Jun. 2009.

Part Two: Carbon Nanotube/Polyethylene Nanocomposites as Strain and Temperature Sensing Materials

Chapter II-6 Conclusions and Future Work

As it is clear, the properties of materials can be also determined by the dimension of the material not only by its chemical bonding and composition. As the dimension of any material system decreases to the nano-meter-scale, different and special chemical and physical characteristics arise. To improve polymer's conductivity, strength and other attributes, nanomaterials such as multi-walled carbon nanotubes (MWCNTs) are frequently used in polymer preparations

Although extensive efforts have been made to develop a CNT-based temperature or strain sensors, reproducibility of the sensors, which can keep their electrical conductivity for long-term use, are still being challenged. Thus, in the aspect of the conductive CNT/polymer composites reproducibility, the results of this research part (strain and temperature sensing materials nanocomposites) revealed some points which will be summarized in this chapter.

This chapter introduces a summary of the second part (Carbon nanotube/polyethylene nanocomposites as strain and temperature sensing materials) of the thesis, which is given in section 6.1 and a future work plan is followed in section 6.2.

6.1 Conclusions

To summarize: Well-dispersed MWCNT/HDPE nanocomposite powder was successfully prepared by coating the MWCNTs on the surface of the matrix particles (HDPE). The volume resistivity of the nanocomposites was investigated related to the temperature and stress influence. Besides, the reproducibility of the nanocomposites was studied in this project. Several conclusions could be drawn.

Firstly, the prepared MWCNT/HDPE nanocomposite powders had an irregular morphology, which affects the final MWCNT/HDPE nanocomposite sheet properties. Secondly, the average electrical resistivity for the MWCNT/HDPE nanocomposite sheets with the MWCNT contents of 0.1 wt%, 0.5 wt%, and 1.0 wt% were 792.64 kΩ.mm, 111.67 kΩ.mm, and 9.953 kΩ.mm respectively which indicate that the 1.0 wt%

MWCNT/HDPE nanocomposite sheet showed the best electrical conductivity. In addition, 0.1 wt% MWCNT/HDPE nanocomposite had the highest standard deviation of the electrical resistivity, while 1.0 wt% MWCNT/HDPE nanocomposite showed the lowest one. This indicates that the MWCNT/HDPE nanocomposite with the MWCNT content of 1.0 wt% had the greatest electrical stability in this project.

Furthermore, the results of the temperature-electrical conductivity measurements revealed that the initial electrical resistivity for the MWCNT/HDPE nanocomposites with the same filler contents were different, because of the different dispersions of the MWCNTs in each nanocomposite sheet induced by the inhomogeneous heating of the samples. It was found that with the rise of the temperature, the electrical resistivity for the MWCNT/HDPE nanocomposites increased due to the increase of the distances between the conductive nanofillers.

The electrical conductivities of the MWCNT/HDPE nanocomposites during each process of cooling were better than the same process of heating due to the rearrangement of the conductive CNT that was induced by heating. In addition, the heat treatment could effectively improve the reproducibility of the MWCNT/HDPE nanocomposites, especially the nanocomposite with the MWCNT content of 1.0 wt%, because the voids in the nanocomposite sheets were excluded during the heat treatment.

Moreover, the results of the strain-electrical conductivity measurements reveal that the initial electrical resistivity for the MWCNT/HDPE nanocomposites increases with the increase of the applied stress because the distances between the conductive nanofillers increased and some conductive networks were damaged. In addition, the reproducibility of the 1.0 wt% MWCNT/HDPE nanocomposite was better than the 0.5 wt% MWCNT/HDPE nanocomposite. It was found that the MWCNT/HDPE nanocomposite sheets exhibited “viscoelastic” behaviour of the electrical recovery. The electrical resistivity cannot totally recover during the relaxation. This could be useful in designing CNT/ polymer composite strain sensors in the future.

For all the MWCNT/HDPE nanocomposite sheets, the electrical recovery was larger than 99% during each process of elongation and reduction.

The increasing temperature from 20 to 100ºC and strain amount influence the composite structure leading the CNTs separation increases gradually. The gap between CNTs becomes larger which finally reaches to a value where the conductance vanishes. For a sensing material development, the conductivity sensitivity can make a significant challenge in controlling the sensors fabrication process. In another word, making a stress or temperature sensors from CNT/PE nanocomposites needs to have the length of the separation between CNTs in control. This research could provide practical assistance in the developed electrical conductive composites for desirable future sensing devices

6.2 Future Research

This project has improved the knowledge of the electrical conductivity of MWCNT/HDPE nanocomposites. Progress has been made in the study of the electrical reproducibility of conductive polymer nanocomposites, and heat treatment has been put forward to improve the electrical reproducibility in this project. However, current research on the electrical reproducibility is still in the early stage and some limitation still needed to be overcome:

1. The results of the project reveal that the electrical reproducibility of the MWCNT/HDPE nanocomposites is not promising without heat treatment. In order to develop reliable carbon nanotubes based temperature sensors, further works could focus on the reproducibility of the CNT sensors only after the heat treatment stage.

2. The strain-dependent electrical reproducibility of the MWCNT/HDPE nanocomposites indicates that the electrical conductivity is not very sensitive to the changes of stress, leading to the difficulty in the study of the electrical reproducibility. In order to overcome this difficulty, thinner nanocomposites sheets could be used in the future research.

3. More conductive nanofillers and matrices are needed to be dug out for the development of electrical reproducible sensors.

6.3 List of Publications

6.3.1 Journal Publications

- *S. Alsawafi, X. Wang, J. Jin, and M. Song, "An experimental study of nonlinear behaviour of capacitance in graphene/carbon nanotube hybrid films," EPJ Appl. Phys., vol. 74, no. 3, p. 30401, Jun. 2016.*

- *S. Alsawafi and M. Song, "Polymer/ Carbon nanotube nanocomposites as strain and temperature sensing materials'' To be submitted this December.*

6.3.2 Conference Papers

- *S. Alsawafi, and M. Song., 2015. Electrical properties of graphene / CNT hybrid films. Presented at: ANM 2015 International conference on graphene technology, Aveiro, Portugal, 20-22 July 2015.*

- *X. Wang, Y. Ren, M. Song. S. Alsawafi and J.Jin., 2016. Preparation and characterisation of graphene oxide/ carbon nanotubes films. Presented at: 2016 IEEE International Conference on Manipulation, Manufacturing, and Measurement on the Nanoscale (3M-NANO).*